

Estimation and Tracking of Rapidly Time-Varying Broadband Acoustic Communication Channels

by

Weichang Li

B.S., Acoustic and Electronic Engineering, Harbin Engineering University (1993)

S.M., Acoustics, Harbin Engineering University (1996)

S.M., Electrical Engineering and Computer Science and Ocean Engineering,
Massachusetts Institute of Technology (2002)

Submitted in partial fulfillment of the
requirements for the degree of

Doctor of Philosophy

at the

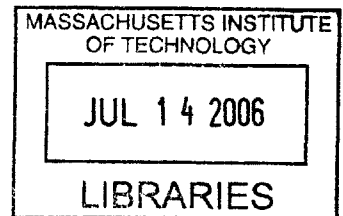
MASSACHUSETTS INSTITUTE OF TECHNOLOGY

and the

WOODS HOLE OCEANOGRAPHIC INSTITUTION

February 2006

©2006 Weichang Li. All rights reserved.




The author hereby grants to the United States Government, MIT and WHOI
permission to reproduce and to distribute copies of this thesis
document in whole or in part.

BARKER


Signature of Author_____

Joint Program in Oceanography / Applied Ocean Science and Engineering
Massachusetts Institute of Technology
and Woods Hole Oceanographic Institution
December 22, 2005

Certified by_____

 James C. Preisig, Thesis Supervisor
Associate Scientist, Woods Hole Oceanographic Institution

Accepted by_____

 Henrik Schmidt
Chairman, Joint Committee for Applied Ocean Science and Engineering
Massachusetts Institute of Technology/Woods Hole Oceanographic Institution

Estimation and Tracking of Rapidly Time-Varying Broadband Acoustic Communication Channels

by

Weichang Li

Submitted to the MIT Department of Mechanical Engineering
and to the WHOI Department of Applied Ocean Science and Engineering
on December 22, 2005 in partial fulfillment of the
Requirements for the degree of Doctor of Philosophy

Abstract

This thesis develops methods for estimating wideband shallow-water acoustic communication channels. The very shallow water wideband channel has three distinct features: large dimension caused by extensive delay spread; limited number of degrees of freedom (DOF) due to resolvable paths and inter-path correlations; and rapid fluctuations induced by scattering from the moving sea surface. Traditional LS estimation techniques often fail to reconcile the rapid fluctuations with the large dimensionality. Subspace based approaches with DOF reduction are confronted with unstable subspace structure subject to significant changes over a short period of time.

Based on state-space channel modeling, the first part of this thesis develops algorithms that jointly estimate the channel as well as its dynamics. Algorithms based on the Extended Kalman Filter (EKF) and the Expectation Maximization (EM) approach respectively are developed. Analysis shows conceptual parallels, including an identical second-order innovation form shared by the EKF modification and the suboptimal EM, and the shared issue of parameter identifiability due to channel structure, reflected as parameter unobservability in EKF and insufficient excitation in EM. Modifications of both algorithms, including a two-model based EKF and a subspace EM algorithm which selectively track dominant taps and reduce prediction error, are proposed to overcome the identifiability issue. The second part of the thesis develops algorithms that explicitly find the sparse estimate of the delay-Doppler spread function.

The study contributes to a better understanding of the channel physical constraints on algorithm design and potential performance improvement. It may also be generalized to other applications where dimensionality and variability collide.

Thesis Supervisor: James C. Preisig
Associate Scientist, Woods Hole Oceanographic Institution

Acknowledgements

My sincerest thanks to my thesis supervisor, Dr. James Preisig, for his encouragement and guidance throughout this thesis research and my graduate study in the MIT-WHOI joint program. Jim's devotion to students, enthusiasm and thoroughness for his work was an inspiration. His insistence on out-of-box thinking and intuitive reasoning had a great impact on this thesis work. The privilege of working with him closely in the past four and half years means a great deal to me both professionally and personally.

I am extremely grateful to my thesis committee members Prof. Arthur Baggeroer and Prof. Sanjoy Mitter, for sharing thoughtful comments and valuable suggestions. The stimulating discussions I had with both of them over many occasions greatly helped shaping the thesis development. The opportunity of working with Prof. Baggeroer as a teaching assistant was a great learning experience. It would be a privilege for me to continue working with both of them in the future.

I am also thankful to Prof. Henrik Schmidt for being on my thesis qualify exam committee and chairing the thesis defense.

I want to thank Dr. Müjdat Çetin for fruitful discussions on sparse estimation and providing Matlab codes for L_p norm constrained estimation, which greatly helped my understanding of the subject. Also thanks to Dr. Yongmin Jiang from University of Victoria for help proof-reading the first two chapters of the thesis.

Thanks to all the members of the WHOI Ocean Acoustic Lab. for providing helps too numerous to mention individually. Especially I would like to thank Dr. Jim Lynch, Dr. Tim Stanton and Dr. Ying-Tsong Lin for offering thoughtful suggestions to the thesis presentation, Dr. Dezhong Chu for many interesting discussions and Dr. Andone Lavery for great helps on many occasions.

I am especially grateful to my academic advisor, Prof. Jerome Milgram, for offering me the chance to come to MIT and work on the fantastic digital holography project. I also want to thank Dr. Sandy Williams for many stimulating discussions and the collaboration on applications of signal processing techniques to current measurements while tolerating my initial request of being excused from his course.

I would like to thank MIT OE and later ME administration offices and the WHOI academic program office for providing numerous helps during this work.

In the course of graduate study at MIT, I have profited considerably from discussions with several friends and colleagues on several problems, although not necessarily related to this thesis. Special thanks to Yile Li, Guanyu Wu, Manish Bhardwaj and Raj Rao.

None of this would have been possible without the lifetime support and love from my parents and the sacrifice they've made. Finally, I want to thank my wife, Hua, for her love, patience and support over these years. Also I want to thank our daughter, Jada, for all the joys and wonders she has brought to us.

Financial support for this thesis research was provided by the Office of Naval Research and the WHOI Academic Program Office.

Contents

Table of Contents	4
List of Figures	7
1 Introduction	12
1.1 The Problem	12
1.2 Previous Work	17
1.2.1 Adaptive Algorithms for Channel Estimation	17
1.2.2 Dynamic Channel Tracking	21
1.2.3 Sparse Channel Estimation	23
1.3 Approaches of this Thesis	25
1.4 Summary of Contributions	26
2 Surface Channel Physics and Modeling	28
2.1 Characteristics of Surface Scattering Channel	28
2.1.1 Acoustic Surface Scattering	29
2.1.2 A Wideband Surf-Zone Channel Example	31
2.2 Channel Modeling	43
2.2.1 LTV and WSSUS Channels	43
2.2.2 State-Space Channel Model	47
2.3 Concluding Remarks	59

3	EKF based Channel Impulse Response Estimation	60
3.1	Introduction	61
3.2	EKF Joint Channel State and Parameter Estimation	64
3.2.1	The EKF Procedure	66
3.2.2	EKF Channel Estimation Error	68
3.2.3	EKF vs. MMSE and ML Estimation	73
3.3	Parameter Observability and Detectability	78
3.4	Two-Model EKF Parameter Estimation	86
3.4.1	Two-Model Parameter Estimation	88
3.5	Concluding Remarks	98
4	EM based Channel Impulse Response Estimation	101
4.1	Introduction	102
4.2	EM Joint Channel State and Parameter Estimation	104
4.3	Fast Recursion of Sums of the Second-Order Smoothed State Moments	109
4.4	Suboptimal Algorithms	113
4.4.1	The Derivation of the Suboptimal Algorithm	114
4.4.2	Special Cases	116
4.4.3	A General Parameter Recursion	117
4.4.4	A Numerical Example	118
4.5	Properties of the Suboptimal Algorithm	120
4.5.1	The Innovation Form of the Parameter Recursion	120
4.5.2	The Extended Persistent Excitation Condition	123
4.5.3	Convergence of the Parameter Recursion	126
4.6	EM Parameter Estimation Within Subspace	127
4.7	Concluding Remarks	130
5	Sparse Estimation of the Delay-Doppler Spread Function	132
5.1	Introduction	132

5.2	Explicit Sparse Channel Estimation	135
5.2.1	Basis Pursuit With L_1 Norm Constraint	136
5.2.2	Matching Pursuit (MP)	137
5.2.3	Sensitivity to Channel Time-Variations	141
5.3	Sequential Least Squares Matching Pursuit	143
5.4	Sparse Estimation of the Delay-Doppler Spread Function	155
5.4.1	Suboptimal Two-Stage Sparse Estimation Algorithms	156
5.5	Experimental Results	157
5.6	Concluding Remarks	157
6	Summary and Future Work	160
6.1	Summary	160
6.2	Future Work	162
A	EKF Channel Estimation	164
A.1	The Extended Kalman Filter Channel Estimation Algorithm	164
A.2	Special Cases: Diagonal and Tridiagonal State Transition Matrix	168
B	EM Channel Estimation	172
B.1	Derivation of the smoothed state correlation equations	172
B.2	Kalman smoothing formula	174
B.2.1	Fixed-point Kalman smoothing	174
B.2.2	Fixed-interval Kalman smoothing	175
B.3	Derivation of the new vector form recursions	176
B.4	Proof of the stability of the new vector form recursions	179
B.5	Some Proofs for Section 4.5	180
B.5.1	Derivation of (4.32)	180
B.5.2	Derivation of (4.35)	182
B.6	$\ \Pi_{i=n}^{n+m-1}(\mathbf{I} - \mathbf{S}_i \mathbf{b}_i \mathbf{b}_i^h)\ $	186

C The Kronecker Product **193**
C.1 The *Vec*(\cdot) Operator 193
C.2 The Kronecker Product and Its Properties 194

List of Figures

1-1	Acoustic communications in surf-zone channel	15
1-2	Channel estimate based equalization	15
1-3	Diagram of the state-space channel model	15
2-1	Wavefronts II experiment top view	32
2-2	Wavefronts II experiment side view	32
2-3	Channel Impulse Response Estimate	35
2-4	Time-varying scattering function estimate sequence I	38
2-5	Time-varying scattering function estimate sequence II	39
2-6	Signal prediction error using the RLS algorithm	42
3-1	Parameter undetectability, a numerical example	87
3-2	Two-Model EKF, Plain EKF and RLS	94
3-3	Doppler Estimates Using the Two-Model EKF algorithm	96
3-4	Doppler Estimates Using the Plain EKF algorithm	97
3-5	Channel Impulse Response Estimates Using the Two-Model EKF algorithm	97
3-6	The Scattering Function Estimate at $t = 20.05747$ seconds	98
3-7	Doppler Estimates Using the Two-Model EKF algorithm, faster parameter convergence.	99
4-1	EM parameter estimation with Kalman state smoother	108
4-2	Diagram for the new vector form recursions.	112

4-3	EM algorithm based on the new recursion form	113
4-4	Diagram of the suboptimal EM algorithm	116
4-5	Parameter convergence of the suboptimal EM algorithms	120
4-6	Steady-state channel prediction errors of Suboptimal EM algorithm .	121
5-1	A constant sparse channel	143
5-2	Tap identification of a constant sparse channel	144
5-3	MSE of sparse estimation of a constant sparse channel	144
5-4	A sparse channel with fixed tap delays and varying gains	145
5-5	Tap Identification of a sparse channel with fixed tap delays and varying gains	145
5-6	MSE of sparse estimation of a sparse channel with fixed tap delays and varying gains	146
5-7	A sparse channel with varying tap delays and fixed gains	146
5-8	Tap Identification of a sparse channel with varying tap delays and fixed gains	147
5-9	MSE of sparse estimation of a sparse channel with varying tap delays and fixed gains	147
5-10	Comparison of Matching Pursuit algorithms, A simple Example . . .	148
5-11	Sparse estimation of the discrete delay-Doppler spread function . . .	158
5-12	Delay-Doppler spread function estimate via the SLSMP algorithm . .	159
B-1	Singular values of $\Pi_{i=n}^{n+m-1}(\mathbf{I} - \mathbf{Sb}_i\mathbf{b}_i^h)$, $\frac{\lambda_{max}}{\lambda_{min}}(\mathbf{S}) = 10$	190
B-2	Singular values of $\Pi_{i=n}^{n+m-1}(\mathbf{I} - \mathbf{Sb}_i\mathbf{b}_i^h)$, $\frac{\lambda_{max}}{\lambda_{min}}(\mathbf{S}) = 10^4$	190
B-3	Singular and eigen values of $\Pi_{i=n}^{n+m-1}(\mathbf{I} - \mathbf{Sb}_i\mathbf{b}_i^h)$, $\frac{\lambda_{max}}{\lambda_{min}}(\mathbf{S}) = 10$	191
B-4	Singular and eigen values of $\Pi_{i=n}^{n+m-1}(\mathbf{I} - \mathbf{Sb}_i\mathbf{b}_i^h)$, $\frac{\lambda_{max}}{\lambda_{min}}(\mathbf{S}) = 10^4$	192

Abbreviations

LTI	linear time invariant
LTV	linear time-varying
WSSUS	wide-sense stationary and uncorrelated scattering
DFE	decision feedback equalizer
SVD	singular value decomposition
MSE	mean square error
MMSE	minimum mean square error
MAE	minimum achievable error
ML	maximum likelihood
MAP	maximum a posteriori
LMS	least mean square
RLS	recursive least squares
KF	Kalman filter
EKF	Extended Kalman Filter
EM	Expectation Maximization
BMP	basic matching pursuit
OMP	orthogonal matching pursuit
SLSMP	sequential least squares matching pursuit
BP	basis pursuit
PE	persistent excitation
EPE	extended persistent excitation
DOF	degrees of freedom

Notation for thesis

The following notation is used throughout the whole thesis, unless otherwise stated:

a, b, \dots	lower case letters denote scalars
$\mathbf{a}, \mathbf{b}, \dots$	bold face lower case letters denote column vectors
$\mathbf{A}, \mathbf{B}, \dots$	bold face upper case letters denote matrices
\mathbf{A}^t	transpose of \mathbf{A}
\mathbf{A}^*	complex conjugate of \mathbf{A}
\mathbf{A}^h	Hermitian (complex conjugate transpose) of \mathbf{A}
\mathbf{A}^{-1}	inverse of \mathbf{A}
\mathbf{A}^\dagger	psuedo-inverse of \mathbf{A}
$\lambda_i(\mathbf{A})$	i th eigenvalue of \mathbf{A}
$\lambda_{max}(\mathbf{A})$	maximum eigenvalue of \mathbf{A}
\mathbf{I}_N	$N \times N$ identity matrix
$\ \mathbf{a}\ $	L_2 norm of vector \mathbf{a}
$\ \mathbf{A}\ $	the L_2 induced norm of \mathbf{A}
$det(\mathbf{A})$	determinant of \mathbf{A}
$Vec(\mathbf{A})$	long vector obtained by stacking all columns of \mathbf{A}
$Mat_L(\mathbf{a})$	matrix whose columns are the consecutive L segments of \mathbf{a} , the inverse operator of $Vec(\cdot)$
$Diag(\mathbf{a})$	diagonal matrix whose diagonal elements are \mathbf{a}
$diag(\mathbf{A})$	column vector consists of the diagonal elements of \mathbf{A}
\otimes	Kronecker product
\odot	Hadamard (or Schur) product, elementwise product
\mathbb{C}^M	the space of $M \times 1$ complex vectors

Chapter 1

Introduction

This introductory chapter presents a discussion of the main problem studied by the thesis, a review of previous work relevant to the problem and an outline of the thesis itself, including its approaches and contributions.

1.1 The Problem

Underwater acoustic communication has experienced significant progress over the last two decades [Kil00] [Sto96] [Bag84] [Bag81]. Technological feasibility has allowed advanced developments such as underwater acoustic networks [Pro01b]. However, the complex underwater acoustic environment still remains one of the most challenging type of channels for information transmission. As research and applications push towards even shallower and more extreme environments, understanding the physical constraints of the channel and developing signal processing techniques based on these constraints becomes even more crucial to system design and performance evaluation.

The chief concern in the thesis is with channel estimation for wideband acoustic communications in very shallow-water environments.

The very shallow-water short-range wideband channel often has the following distinct features: large channel dimension due to an extensive delay spread; limited

number of degrees of freedom (DOF) due to resolvable multipath arrivals and inter-path correlations; and rapid channel fluctuations due to scattering from the moving sea surface, as elaborated below.

As illustrated in Figure 1-1, surface waves are the dominant factor contributing to the dynamics of the rapidly varying channel in shallow-water environment. While traveling through the channel, the transmitted signal experiences severe distortions induced by multipath propagation. Multiple scatterings from both the surface and bottom, with relatively small propagation attenuation over short range, can yield a delay spread well over a hundred symbols. Within that delay spread the resolvable arrivals compose a fairly sparse multipath structure, given a sufficiently wide bandwidth. Due to the surface time-variability, the surface scattered arrivals have migrating propagation delays and large, time-varying Doppler spread and shifts. Scattered by different surface patches at variable angles, surface scattered arrivals may have very different fluctuating rates among themselves and from the non-surface scattered arrivals. On the other hand, large scale smoothness of the surface motion may contribute to correlations among macropath fluctuations and scattering from the same surface patch causes correlated micropath fluctuations. The direct arrival and bottom scattered arrival usually have little surface induced variations and are more stable. Channels with such rapid time-variabilities and the inter-path correlations mentioned above would be difficult to assume as wide-sense stationary uncorrelated scattering (WSSUS) (the concept of WSSUS channel is introduced in [Bel63] and also explained in section 2.2.1).

While other aspects of the channel physics, such as attenuation and scattering by bubbles created by breaking waves, transient caustics due to acoustic focusing by wave crest curvature, may also contribute to the fluctuations of the channel [Pre04], the factors mentioned above, highlighting a well structured multipath image that is over-extended in delay with inhomogeneously fluctuating arrivals, contribute to significant challenges to acoustic communications.

Phase coherent demodulation relies, explicitly or implicitly, on accurate estimation of channel impulse response. Imperfect channel estimation directly causes performance degradation of a channel estimate based equalizer [Pre05] [Sto95]. For time-varying channels, it has been shown in [Shu91] that channel estimate based equalizer (see Figure 1-2) has superior performance over the directly adapted linear equalizer (LE) or decision feedback equalizer (DFE).

The channel properties mentioned previously, combined, pose significant challenges to the accurate estimation of the channel impulse response. The specific question this thesis addresses is how to estimate accurately and track the channel impulse response or other transfer functions under these physical conditions.

Without an appropriate dynamic model, traditional estimation techniques such as the RLS algorithm often fail to reconcile the rapid fluctuations with the large dimensionality. It has been observed [Pre05] [Li,05] that for the type of environments considered here LS channel estimation leads to significant errors. This inadequacy is due to the assumption held by these algorithms that the channel is constant or slowly varying over a time scale proportional to the channel dimension, which becomes invalid when the channel fluctuates rapidly and even the dynamics of the fluctuations vary over time. The time scale over which the channel may be assumed stationary becomes much shorter than $2 \sim 3$ times of the channel dimension, the rule of thumb value required to maintain the stability of the RLS algorithm.

Also, efforts to reduce the number of DOF based on subspace decomposition are confronted with unstable subspace structure due to significant changes in arrival delays and Doppler phases over a short period of time. Frequent updating of subspaces will not improve the situation greatly, as it is still limited by the minimum time scale required to extract the dominant subspace directions. If over this time scale the channel changes significantly, then the obtained subspace directions may not be a good basis with which to represent the channel at the next sample.

Clearly the dynamics of the channel fluctuations as well as the variations of these

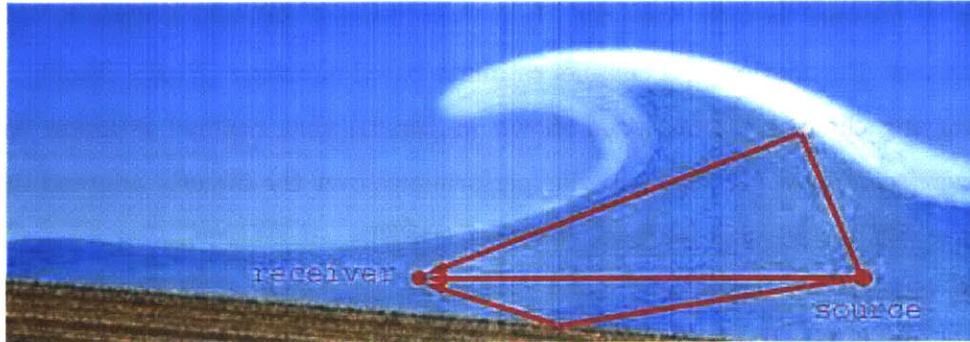


Figure 1-1: Acoustic Communications in Surf-Zone Channel. *Surface waves are the dominant factor causing channel dynamics.*

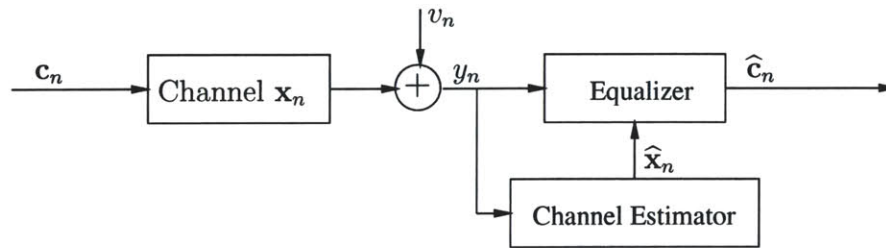


Figure 1-2: Channel Estimate based Equalization. *n is the time index, c_n is the sequence of transmitted symbols, x_n is the channel impulse response, v_n is the additive ambient noise and y_n is the received signal.*

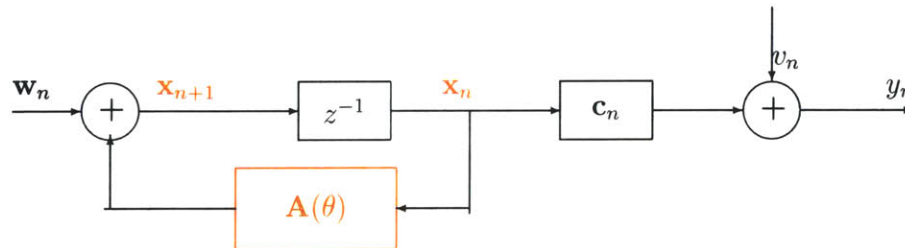


Figure 1-3: Diagram of the State-Space Channel Model, *red marks unknowns.*

dynamics have to be accounted for in order to successfully estimate and track this type of channel. In the first part of the thesis, this is done through dynamic modeling. A state-space model modeling the variation of channel taps as first-order AR process is adopted due to its analytical tractability and the wealth of theory associated with it. Although it may not closely match acoustic scattering models for time-varying random rough surface, it is still found to be a good approximation for wideband transmissions as shown in Chapter 2. A more accurate acoustic model for wideband scattering from time-varying random rough surface would be too cumbersome to be directly usable and its development is itself still an unsolved problem.

Channel estimation with dynamic modeling is essentially a system identification problem. Within this framework, the channel impulse response is the state vector and its dynamics are specified by a set of unknown parameters. In reality neither the channel impulse response nor how it evolves over time is known. Both the state and the parameters need to be estimated jointly from the received signals. More explicitly, given a state-space channel model (as will be derived rigorously in Chapter 2),

$$\begin{cases} \mathbf{x}_{i+1} = \mathbf{A}_i \mathbf{x}_i + \mathbf{w}_i & (1.1a) \\ y_i = \mathbf{c}_i \mathbf{x}_i + v_i & (1.1b) \end{cases}$$

where \mathbf{x}_i , \mathbf{c}_i and y_i are the channel state, the transmitted symbol sequence and the received signal, respectively, the problem is to estimate \mathbf{x}_i and the unknown model parameters based on y_i . Figure 1-3 depicts the block diagram of the state-space model (1.1). Both \mathbf{x}_i and y_i are complex. \mathbf{w}_i and v_i are a zero-mean, circularly Gaussian complex random vector and variable respectively. For the channel to be asymptotically wide-sense stationary, it is necessary and sufficient to have $\lambda(\mathbf{A}_i) < 1$. For the channel to be characterized as uncorrelated scattering, it would require that \mathbf{A}_i be diagonal.

Throughout the thesis it is assumed that the transmitted symbol sequence \mathbf{c}_i is perfectly known, as would be the case in the training period where the channel

is probed using symbols known to the receiver, or in a decision direct mode where the previously detected symbols are used as known, neglecting the error propagating effects.

The second part of the thesis finds the explicit sparse estimation of the channel delay-Doppler spread function [Bel63]. The channel time variability is accounted for via the assumed Doppler for each component and the channel structure is explored using sparse estimation.

The development in this thesis draws concepts and results from several areas, including adaptive filtering, linear system theory, system identification and digital communications, as reviewed in the next section.

1.2 Previous Work

In this section, previous work relevant to the thesis from various aspects is reviewed.

1.2.1 Adaptive Algorithms for Channel Estimation

Adaptive filters have been extensively used for channel equalization and estimation [Hay96]. This section reviews several basic concepts, commonly used analysis approaches and results of these algorithms. A general form, from which each individual algorithm may be derived, provides the basis for the presentation. The goal is to provide conceptual parallels to later algorithm analysis developed in this thesis. Comprehensive coverage of these topics can be found, for instance, in [Hay96],[Guo95a] [Lju90] and [Ben87].

Consider the following linear regression model:

$$z_i = \mathbf{w}_i^h \mathbf{u}_i + v_i \tag{1.2}$$

where the output z_i and the regressor \mathbf{u}_i are both known, \mathbf{w}_i is to be estimated.¹

Several well-known adaptive filter algorithms include least mean squares (LMS), recursive least squares (RLS) and adaptive Kalman filter (AKF)², can all be derived as special cases from the following general form:

$$\widehat{\mathbf{w}}_{i+1} = \widehat{\mathbf{w}}_i + \mu \mathbf{k}_i e_i^* \quad (1.3)$$

where $e_i = y_i - \widehat{\mathbf{w}}_i^h \mathbf{u}_i$ is the prediction error. The adapting gain vector often has the form $\mathbf{k}_i = \mu \mathbf{R}_i^{-1} \mathbf{u}_i$ for some $0 < \mu < 1$ and non-negative \mathbf{R}_i . \mathbf{k}_i and μ reflect the adaptation direction and rate respectively. \mathbf{R}_i is often called the information matrix. Its inverse $\mathbf{P}_i \triangleq \mathbf{R}_i^{-1}$ plays the role similar to the state error covariance matrix in the Kalman Filter (KF).

Various algorithms can be obtained from (1.3) by taking special values of μ and \mathbf{R}_i or \mathbf{P}_i , see, for instance, [Guo95a]. A stochastic linear difference equation governing the channel estimation error propagation is very important. Denoting $\boldsymbol{\epsilon}_i \triangleq \mathbf{w}_i - \widehat{\mathbf{w}}_i$, then

$$\boldsymbol{\epsilon}_{i+1} = (\mathbf{I} - \mu \mathbf{R}_i^{-1} \mathbf{u}_i \mathbf{u}_i^h) \boldsymbol{\epsilon}_i - \mu \mathbf{R}_i^{-1} \mathbf{u}_i v_i + (\mathbf{w}_{i+1} - \mathbf{w}_i) \quad (1.4)$$

which is often used in tracking analysis. The algorithm stability is determined by the largest singular value magnitude of the matrix $(\mathbf{I} - \mu \mathbf{R}_i^{-1} \mathbf{u}_i \mathbf{u}_i^h)$, The second term and the last term on the right hand side of (1.4) are associated with noise and the time variations of \mathbf{w}_i , hence are often called as the *noise error* term and *lag error* term of $\boldsymbol{\epsilon}_{i+1}$ respectively. It can be shown that increasing the adapting gain will have opposite effects on the *noise error* and the *lag error* contributions to the channel estimation error.

Error analysis of adaptive algorithms based on (1.4) have been extensively stud-

¹A note about notation. (1.2) is often adopted in adaptive filtering for linear regression models. By letting $\mathbf{c}_i = \mathbf{u}_i^h$, $\mathbf{x}_i = \mathbf{w}_i$ and $y_i = z_i^*$, this can be converted into the observation equation in state-space model, *i.e.* $y_i = \mathbf{c}_i \mathbf{x}_i + v_i^*$

²AKF is essentially a Kalman filter based on random walk state model with *ad hoc* noise covariances.

ied, see, for instance, [Mac86], [Say03] for LMS, and [Ele86], [Nie91] for RLS. The above error ϵ_i is often split into the *minimum achievable error* (MAE) associated with the optimal Wiener filter, and the *excess error* that above MAE. Similarly follows the terms *excess lag error* and *excess noise error*.

Three important properties of an adaptive algorithm are its *tracking capability*, *stability* and *convergence rate*.

1. Tracking Capability

Tracking capability is a steady-state concept. When $\lim_{i \rightarrow \infty} \mathbf{k}_i \rightarrow \mathbf{0}$ in (1.3), in steady-state the estimate will not be alert to any changes. Thus the algorithm is said to stop tracking. Therefore to maintain tracking capability \mathbf{k}_i should be kept away from zero, or equivalently, \mathbf{P}_i bounded from below and \mathbf{R}_i bounded from above. In RLS, this is done by either exponentially weighting or finite windowing. In AKF, a positive definite process noise \mathbf{Q} ensures that tracking capability will not be lost. Intuitively, in either case the algorithm attains some finite bandwidth to keep from allowing no change.

Discussion of tracking capability can be found in [Hag85], [Ben87], [Par92], [Nie91] for RLS and [Lju90] in a general form, just to name a few.

2. Stability

Stability of an algorithm is often associated with the step size as well as the so-called Persistent Excitation condition which essentially requires that \mathbf{R}_i bounded from below, or equivalently, \mathbf{P}_i bounded from above. The Persistent Excitation condition usually requires that \mathbf{u}_i span the whole space, deterministically or stochastically. Under this condition new information is acquired (as excited by the regression vector as a probe) to update $\hat{\mathbf{w}}_i$ in all directions. Insufficient excitation will cause the algorithm to diverge since \mathbf{P}_i hence the adapting gain \mathbf{k}_i would increase unbounded. The step size is usually chosen such that the largest singular value magnitude of the matrix $(\mathbf{I} - \mu \mathbf{R}_i^{-1} \mathbf{u}_i \mathbf{u}_i^h)$

is less than one.

Later in Chapter 4 this concept is extended for parameter estimation in linear dynamic models. From the system identifiability perspective, the PE condition is closely related to the observability/detectability of a state-space model. This is discussed in Chapter 3.

The condition of persistent excitation and its requirement on the regression vector is covered for instance in [Bit84] [Cam94] and recently in [Cao00]. Cao, *et al.* [Cao00] proposed a directional forgetting RLS algorithm to ease this problem by updating only the excited subspace, or forgetting information in the excited directions, based on the subspace decomposition of \mathbf{R}_i .

3. Convergence Rate

By convergence rate here it refers to the learning speed of the algorithm hence is a transient performance measure. From (1.4) it follows that the convergence speed is closely related to the eigen-structure (modes and singular values) of the matrix $(\mathbf{I} - \mu\mathbf{R}_i^{-1}\mathbf{u}_i\mathbf{u}_i^h)$. In Chapter 4, similar results are developed for a suboptimal EM algorithm.

The adapting gain, the boundedness of \mathbf{R}_i , or equivalently, \mathbf{P}_i , as well as the degree of excitation of \mathbf{u}_i and the eigen-structure of $\mathbf{I} - \mu\mathbf{R}_i^{-1}\mathbf{u}_i\mathbf{u}_i^h$ are the key factors governing the performance of an adaptive algorithm, *i.e.* maintaining tracking ability while staying stable, trading noise error with lag error, balancing convergence rate with steady-state error, etc. Many of these results will find analogy in the analysis in Chapter 3 and Chapter 4.

Although these adaptive algorithms have been successfully applied for many tracking problems, they are still quite inadequate in dealing with rapidly varying systems, due to the general assumption that the parameter is constant or as a simple random walk process. For RLS this is generally limited by the minimum effective window length that it requires to maintain stability. Even in the case of random

walk model, effects such as phasor rotation caused by Doppler would not be captured effectively.

1.2.2 Dynamic Channel Tracking

When the channel fluctuates rapidly, often due to environmental changes or platform motions, more effective tracking can be achieved via dynamic modeling and model based channel estimation. This is especially true in underwater acoustic environments.

In the context of underwater acoustic communication, the work by Eggen et al. [Egg00, Egg01] precedes and closely relates to the current development in this thesis. While addressing channels mainly suffering from severe Doppler spread, Eggen, *et al.* propose to estimate explicitly the channel scattering function (the concept of channel scattering function is introduced in section 2.2.1) and then track the channel impulse response using a state space model derived from the estimated scattering function. This approach significantly improves the performance of channel estimate based equalizers in such environments. However, this technique is limited by the requirement that the channel scattering function remain constant for a period of time sufficiently long to initialize and run a model based tracking algorithm. Unfortunately, as later demonstrated in Chapter 2, the scattering function of some surface scattered paths can change as rapidly as the channel impulse response itself. Thus, techniques requiring a constant or slowly varying channel scattering function such as that proposed by Eggen would fail in this type of channel.

In estimating the scattering function of underwater acoustic channels, Kay [Kay03] extended the 2D autoregressive (AR) spectrum estimation method and applied to nonstationary channels with limited data length. For channels with limited spread in delay and Doppler, hence of small dimension, this method would be very appealing, although it does not directly provide the channel impulse response. When the scattering function has a sparse structure that is both severely spread and time-varying,

this method will quickly become overwhelmed due to the large channel dimension, the necessary large AR order and the need to keep track of the time variations.

The work by Iltis ([Ilt90] pertains to underwater acoustic channels and [Ilt91, Ilt94, Ilt01] mainly for wireless channels) is based on explicitly modeling of the parameters associated with the multipath arrivals for single user channel, including the complex arrival gain, the delay and Doppler shift. Extended Kalman filter (EKF) algorithm is then applied to estimate those parameters due to the nonlinearity introduced by this modeling. Iltis' scheme is largely limited by two factors. First, only the bulk delay and bulk Doppler are modeled and estimated. This implicitly assumes that all arrivals fluctuate uniformly, which is generally not the case for surface scattering channels. As shown in Chapter 2, the surface scattered and non-surface scattered arrivals have very different fluctuation rates. Even among surface scattered arrivals, fluctuation rates may vary due to interactions with different patches at variable angles, and possibly with multiple times of scattering. Secondly, the dynamics of those arrival gain, bulk delay and Doppler, are assumed by Iltis as known and constant. Similar to the reason mentioned early, it is unrealistic to make such assumptions when the dynamics of the channel fluctuation also vary rapidly with time.

More recently, in [Tsa05] and [Gao03], dynamic channel estimation algorithms in the context of multi-user direct-sequence spread-spectrum (DSSS) transmission are developed, based on the Extended Kalman filter (EKF) and the Expectation Maximization (EM) algorithms respectively. In both cases the single user channel is assumed flat fading and modeled as lower-order AR process. Joint estimation of the tap gain as well as its AR coefficients are obtained using the EKF or the EM algorithm. The line of thinking would be very close to this thesis, except that in both cases the authors are more focused on the analysis of the EKF and EM algorithms themselves, which are fairly well-developed topics, see for instances, [Lju79] for EKF and [Shu82] for EM respectively, without paying any attention to the physical properties of the channel being estimated. The distinction between the work in this thesis

and those of [Tsa05] and [Gao03] is that the fundamental assumptions held by the existing general theory and analysis results of either EKF or EM algorithms may be violated due to certain physical conditions of the interested channel; hence, the results of those general analysis can not be applied or become marginally important. For instance, as demonstrated in Chapter 2, wideband underwater acoustic channels are generally sparse which leads to unobservable parameters. Without appropriate modeling to account for this sparseness, direct application of the standard EKF and EM algorithms will diverge when applied to such sparse channels. The plausible solution would be to actively track the occupied delay-Doppler cells only.

1.2.3 Sparse Channel Estimation

In wideband transmission with sufficiently large bandwidth, the delay spread of each multipath arrival is small. As a result, different multipath arrivals are resolvable in delay. This gives rise to a sparse channel impulse response where within the overall delay span, there are clusters of energetic taps ³ associated with strong arrivals as well as large silent regions in between, occupied by quiescent taps that have little energy.

Inclusion of those quiescent taps for adaptive estimation, whether or not it is model based, will cause channel overparameterization and risk increased noise sensitivity. Dynamic tracking of these quiescent taps without an appropriate model, as shown in Chapter 3 and Chapter 4, would even cause algorithm to diverge. Often it is with the motivation of reducing noise sensitivity and potentially improving tracking performance that various sparse estimation techniques have been developed, most of which are based on least squares formulation thus divergence due to the sparseness is of a less concern.

The idea of channel sparsing is to reduce the number of taps of the channel

³By tap, it refers to a discretized delay sample, *i.e.* an element of a uniformly sampled channel impulse response.

impulse response that are tracked. Applied to a sparsing processed channel, the tracking algorithm have a reduced computational complexity and memory, and more importantly, the rate of channel fluctuations that it can track increases [Sto99][Stoed].

A majority of sparsing techniques can be classified into two different categories.

The first group include approximation algorithms that try to solve the nonlinear optimization problem of minimizing the squared prediction residual error as a function of the gain and the delay location of all the dominant taps, among which are the sparse DFE [Ron05], the adaptive delay filter [Che89], the adaptive echo canceller[Yip90], the thresholding RLS algorithm [Stoed] [Koc95] [Sto99] [Oze02]. The common strategy of these algorithms is to break down the original optimization problem over the whole gains-delays space into a sequence of optimization problems with smaller parameter spaces. In [Ron05] this is done by optimizing over the gains first and then find the optimal delays. The adaptive delay filter [Che89] approximates the original problem by sequentially optimizing over the gain/delay of each tap. The adaptive echo canceller [Yip90] and the threshold RLS are similar, in the sense that a full-tap adaptive filter is used as an auxiliary filter to provide tap location and then transfer the detected delay locations to a set of lower order filters to adapt the gains of those identified taps. The adaptive echo canceller uses a combination of various criteria to pick the dominant taps while the threshold RLS uses simple energy criterion.

The second group include algorithms that find the sparsest representation of the received signal, using the transmitted symbol sequence as basis vectors (often called as dictionary as they may not be orthogonal). Explicit sparse estimation mainly includes L_p norm regularized method [Don03] [Mal03][Fuc00] and "greedy" method such as the Matching Pursuit (MP) algorithm [Mal93]. The MP algorithm is computationally more efficient, yet, until the recent work by Tropp [Tro04], has been analytically less tractable. These methods originate from the signal representation problem where the dictionary subset providing the most compact signal represen-

tation is sought after. Recently, some of these sparse techniques, mostly the MP and its orthogonalized variant, have been increasingly applied for sparse channel estimation and equalization, see for instance [Cot00, Cot02] [Kar04] [Cet05]. Note that some of these works are developed for the high definition television (HDTV) terrestrial broadcast channel which, similar to wideband acoustic channel, has very sparse structure.

Comparison between these algorithms has not been done extensively, especially in the context of channel estimation. It has been pointed out in [Cot01] based on simulation results that the thresholding RLS method does not perform as well compared with explicit sparse estimation methods such as the MP algorithms for time-varying channels.⁴

Yet the main limitation of these sparsing methods, is that they require the sparse structure of the channel is stable over a certain time scale, which could be easily violated for the type of channel considered in this thesis as illustrated in the next chapter.

1.3 Approaches of this Thesis

The approaches taken in this thesis are directly motivated by the three dominant features of wideband shallow-water acoustic channels mentioned in section 1.1, namely, large channel dimension due to an extensive delay spread; limited number of degrees of freedom (DOF) due to resolvable multipath arrivals and inter-path correlations; and rapid channel fluctuations due to scattering from the moving sea surface.

To account for channel fluctuations, two different approaches have been taken. The first is to model explicitly the channel dynamics using a state-space channel model (derived in Chapter 2) based on which both the channel state and its dynamic model parameters are jointly estimated using the EKF (Chapter 3) or the

⁴Cotter's result on RLS may not be reliable due to the rather large forgetting factor he used which causes his results to show that the RLS is significantly slower than the LMS to converge.

EM approach (Chapter 4) with necessary modifications. The second approach is to represent the channel by its discrete delay-Doppler spread function (Chapter 5) which models channel variations through populating its components uniformly along the Doppler axis.

To deal with the sparse channel structure, soft constrained methods are first developed for the dynamic model based channel estimators, including a two-model based EKF algorithm (Chapter 3) and the subspace EM algorithm (Chapter 4). Both selectively track the dominant channel components by adaptively changing the model parameters, while also avoid the divergence problem. Secondly, explicit sparse algorithms such as the MP algorithm and its variants are applied to find sparse estimate of the delay-Doppler spread function (Chapter 5).

1.4 Summary of Contributions

The main contributions of this thesis consists of the following:

1. The derivation of a state-space model for communication channels consisting of clusters of moving point scatterers. The dependency of the model parameter, specifically the state transition matrix, on the Doppler associated with each scatterer and the equivalent shaping filter, is explicitly derived;
2. The development and analysis of the EKF channel estimation algorithm under the wideband rapidly varying sparse channel condition; The constraint of channel sparseness upon the EKF algorithm is identified in terms of parameter observability and detectability. It is shown that channel sparseness may lead to potential divergence in dynamics parameter estimation if the parameters are not modeled appropriately; The development and analysis of a separate parameter model based EKF algorithm which selectively tracks active taps while circumventing the parameter identifiability issue. A 2 ~ 3 dB reduction

in signal prediction error is achieved using the Two-model EKF algorithm on experimental data that involves significant channel dynamics.

3. The development and analysis of the EM channel estimation algorithm; The derivation of a fast recursive algorithm for computing the cumulative second-order smoothed state moments and its stability analysis; The development and analysis of a class of suboptimal EM algorithms, including the derivation of a second-order innovation form for the parameter recursion. The establishment of the extended Persistent Excitation (EPE) condition which indicates successful dynamic tracking requires fully exciting channel estimate sequence as well as transmitted symbol sequence. The development of the subspace EM algorithm.
4. The derivation of a sequential least squares matching pursuit (SLSMP) algorithm for sparse processing with nonorthogonal dictionaries. The development of sparse algorithms estimating the channel delay-Doppler spread function, including the SLSMP algorithm and two-stage sparse estimation algorithms. A uniform 2 ~ 3 dB reduction in signal prediction error is achieved using sparse estimation of the channel delay-Doppler spread function.
5. The thesis presents a relatively systematic, albeit preliminary, study of dynamic channel estimation and tracking based on state-space model, with an emphasis on application. Performance gain in terms of signal prediction residual error reduction is demonstrated through a set of surf-zone wideband experimental data. Within this framework, channel physical features and constraints are transformed, through modeling, into concepts well known in system and filtering theory which then provide guidance and insights for algorithm design. The overall development may be viewed as a first step towards the development of a general framework within which one could effectively cope with realistic situations where rapid time variations, large dimensionality and limited numbers of freedom are all combined, as typical in many applications.

Chapter 2

Surface Channel Physics and Modeling

This chapter discusses channel characteristics and modeling. Characteristics of time-varying surface scattering channel are presented through examining a set of experimental data obtained from a surf-zone channel, following a brief review of acoustic surface scattering theory and results. Linear time-varying (LTV) filter and wide-sense stationary uncorrelated scattering (WSSUS) channel representations are briefly reviewed. A state-space model is derived for wideband channel consisting of clusters of moving point scatterers, which provides the model framework for the development in Chapter 3 and Chapter 4.

2.1 Characteristics of Surface Scattering Channel

Surface forward scattering plays an important role in shallow-water acoustic communication channels. The sea surface by nature is a time-varying and randomly rough interface. It also generates bubble sublayers via wave breaking. Consequently signals scattered from the surface experience a great deal of fluctuations, including Doppler spread/shift, variations in amplitude, propagation time as well as arrival

angle. These fluctuations are time-varying and random as well.

A brief review of acoustic scattering from sea surface is given in section 2.1.1, followed by an examination of a set of surf-zone experimental data in section 2.1.2. It is found that the general results obtained from acoustic surface scattering theory only provide fairly limited information for wideband shallow-water short-range channel due to the various assumptions upon which the theory is based. Furthermore, experimental data analysis in section 2.1.2 as well as previous study [Pre04], reveal that many aspects of the channel dynamics, although not captured by the general acoustic scattering theory, have significant impacts on acoustic communication performance.

2.1.1 Acoustic Surface Scattering

The problem of scattering from sea surface has been extensively studied, resulting an abundant literature including general theory [Bec63] [Ogi1] [Bre1] [Vor9]; various numerical approximation methods such as the Kirchhoff Approximation [Eck53] [Tho88], the Small Perturbation Method [Tho89] and the Small Slope Approximation [Vor9][Tho95][Bro97]; and a few experimental studies such as [Med70][Spi72][Bro74], and more recently [Dah01][Dah99][Dah96]. Review of early work may be found in [For70]. Although these theoretical and experimental studies provide basic understandings of the mechanism of acoustic surface scattering and certain second-order statistics and sometimes characteristic scales of the acoustic scattering field, many of these results are limited to narrowband scattering and are either too detailed to be useful for robust design or too simplistic to provide any realistic guidance for algorithm design. For wideband very shallow-water short-range channels considered in this thesis, however, these studies fail to capture the most salient channel features, hence their results provide little valuable information germane to coherent wideband communications.

Most previous studies of surface scattering focuses the dependency of the mean scattering field, the second order statistics (such as the power spectra as well as

the spatial and temporal coherence), or the characteristic scales (such as the delay, Doppler and angle spread) on the grazing geometry and the surface conditions such as the wave spectrum and roughness scale (*e.g.* the Rayleigh roughness). As important are these results, however, they do not provide a dynamic picture of the scattered field, *i.e.* the variations of these statistics and scales, which are evident in the example channel shown in section 2.1.2. The channel dynamics are the main factor limiting the performance of channel estimation and equalization for this type of channel. In statistical channel modeling, previous efforts have also been made to tie the statistical properties of the scattering field with explicit channel representations, such as [Ven71] for time-varying transfer function modeling, [Spi72] with impulse response measurements, [McD75] for scattering function representation, and [Zio82a, Zio82b] for both the time-varying transfer function and the scattering function. Although efforts in [Zio82a, Zio82b] made the important connection from the acoustic scattering mechanism to the LTV filter channel representation which is more accessible to communications applications, they had not been transformed into any significant conceptual impact on either surface scattering or stochastic channel modeling.

The inadequacy is mainly due to the surface assumptions upon which these studies are generally based. With rare exception the surface is usually portrayed as spatially homogeneous and temporally stationary random processes (or deterministic periodic gratings) specified by a wavenumber spectrum. For shoaling surface waves homogeneity and stationarity are often not good assumptions as the waves become more directional and nonstationary. The stationary assumption is a concept largely dependent on the relative scales of the problem which is determined by the surface wave period, the acoustic wavelength, the propagation range and the water depths of the source and receiver. For low frequency, long distance, deep water transmission, stationarity in general is a good approximation. Yet, for high-frequency short-range shallow water channels the surface is in general highly nonstationary as the relative surface scale increases. A key factor in channel estimation is the required adaptation

rate which is intimately related with the stationary scale. In dealing with time-variations of the surface, some recent work substitutes the traveling surface with a series of instantaneously frozen surfaces [Mil03][Ros99]. That essentially neglects the effect of surface motions, both vertically and horizontally, during its interaction with the acoustic signal. As a result, the resulting Doppler prediction could be severely underestimated.

Most of the theoretical and approximation based studies are carried out earlier for monochromatic waves. Result for wideband scattering of a pulse from a time-varying rough surface is understandably scarce considering the complexity of the problem.

2.1.2 A Wideband Surf-Zone Channel Example

To illustrate the characteristics of wideband short range shallow-water channels, this section exams such an example taken during the Wavefronts II experiment.

The Wavefronts II Experiment

A detailed description of the Wavefronts II experiment can be found in [Pre04]. The Wavefronts II experiment took place in the surf zone with approximately 6 m deep water, 30 m north of Scripps Pier in December 2000. Figure 2-1 and Figure 2-2 show the top and side views of the experiment geometry. As shown in Figure 2-2, the source transducer is fixed at 2 m above the seafloor. Broadband signals with center frequencies ranging from 12 to 26 kHz were transmitted 38 m inshore to a vertical array of 3 hydrophones spaced 0.5 m apart, with the bottom hydrophone 1.51 m above the seafloor. A reference hydrophone, used to monitor the source signal level, was deployed at the same depth as and 0.71 m shoreward of the source. The experiment geometry was designed to allow surface reflected arrivals to be resolved from other paths in delay with the source bandwidth. Shoaling surface gravity waves were monitored simultaneously with the acoustic transmissions by an array of 8 pressure sensors deployed just above the seafloor along the acoustic propagation path. The

seafloor had an almost constant slope of 2.0° along the propagation path. The sea surface corresponds to an actual surface gravity wave profile measured during the time of the transmissions, and illustrates the fact that generally only one wave crest was found between the source and the receive array. The sound speed during the experiment was measured to be 1503 m/s. The density and sound speed of the seafloor is calculated as 2048 kg/m^3 and 1757 m/s respectively, corresponding to a critical angle in the seafloor of 31.2° and an absorption of 0.85 dB per wavelength.

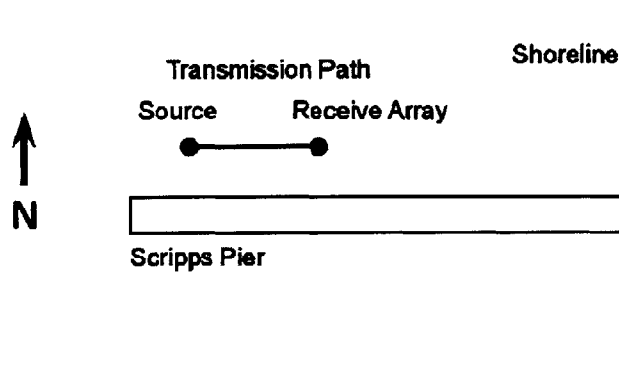


Figure 2-1: Wavefronts II Experiment Top View [Pre04]

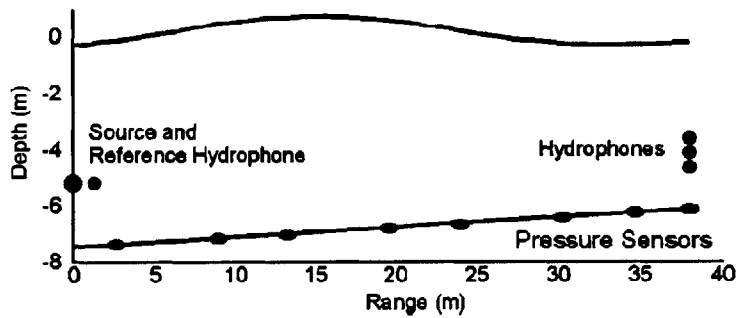


Figure 2-2: Wavefronts II Experiment Side View [Pre04]

For the data analyzed and presented below, the transmit and receive signals were both sampled at 96 kHz. Transmit signals were generated with center frequencies of 18 kHz, and were prefiltered to provide an approximately flat system frequency response over a bandwidth of the inverse of the pulse or symbol duration around the

center frequency of the signal. The signal format is binary phase shift keyed (BPSK) signal modulated by continuous repetitions of a 4095 point maximum length shift register sequence (M-sequence). The symbol rate is 24000 symbols per second.

Channel Characteristics

The time-varying channel impulse response (or the input-delay spread function), estimated from the received signal via a simple exponentially weighted RLS algorithm with a forgetting factor $\lambda = 0.998$ assuming perfectly known transmitted symbols, is shown in Figure 2-3 for a time span of approximately 60 seconds. The effective averaging window of the RLS algorithm used is 250 symbols, or 10.4 ms. As Figure 2-3 (a) shows, the channel has a delay spread (vertical axis) of approximately 7 ms, or equivalently 336 samples at a fractional sample rate of 2 samples per symbol. The multipath arrivals are resolved from each other in delay. As labeled in Figure 2-3 (a), counting upwards from the bottom of the plot are the directly arrival (DA), the bottom reflected arrival (BA), the surface reflected arrival (SA), the surface reflected and then bottom reflected arrival (SB), the bottom reflected and then surface reflected arrival (BS) and the bottom reflected, surface reflected and then bottom reflected arrival (BSB). Above BSB are arrivals have multiple surface interactions. The overall multipath structure is very sparse, in the sense that between those discrete multipath arrivals, the channel impulse response does not have significant energy.

On the very top of Figure 2-3 (a) is the surface gravity wave profile measured during the same time span. It is the pressure sensor measurement obtained at the nominal specular point after spatial and temporal interpolation. A cross-section of Figure 2-3 (a) at each particular time corresponds to the channel impulse response at that time. It can be observed that as time progresses, the channel impulse response changes significantly, as reflected in Figure 2-3 (a) by both the intensity fluctuations and the delay migrations of those surface scattered arrivals. The Doppler associated with these variations, although not shown in Figure 2-3 (a), can be expected to be

large. The direct and bottom reflected arrivals are relatively stable. It is evident that the channel fluctuations are closely coupled with that of the surface. Note that due to the fact that the pressure sensors are deployed just above the seafloor, the small scale surface features are lost.

According to the surface wave time series plotted on top of Figure 2-3 (a), a large wave crest ran over the nominal specular point in the time period of 19.5 seconds and 21.5 seconds. A segment of the time-varying channel impulse response covering the first two surface scattered arrivals over that time period is shown enlarged in Figure 2-3 (b). The zoomed plot shows 'butterfly' shaped structure for both surface arrivals, and the appearance of a strong transient arrival in the first surface scattered arrival at about 20.5 second. The bifurcation of a single arrival into two 'butterfly' wings moving at opposite directions is caused by the splitting of a single specular reflecting point (or rather a surface patch) into two moving specular reflecting patches within the surface wave crest as the surface curvature increases. The strong transient arrival is a result of surface focusing. Detailed explanation for the physical mechanisms behind these processes as well as comparison with model predictions are can be found in [Pre04]. From Figure 2-3 (b), it is shown that the delay-advancing 'butterfly wing' of the first surface arrival migrated over 0.6 ms in delay within approximately 1.5 seconds, corresponding to about 7.2 Hz Doppler calculated according to the center frequency 18 KHz. Considering that the other 'butterfly wing' is moving in opposition at approximately equal velocity, this leads to a Doppler spread of about 14 Hz. The second surface scattered arrival, also shown in Figure 2-3 (b), has even faster moving rate hence can be expected to have a larger Doppler spread. This is reflected more clearly in the channel scattering function plots shown in Figure 2-4 and Figure 2-5.

The time-varying scattering function was estimated using the Matched Filter (see, for instance [Egg97][Van71]) with an effective averaging window of 8190 symbols, or 341 ms, corresponding to Doppler resolution around 2.9 Hz. A sequence of 12 such estimates were obtained between 19.852 seconds and 22.582 seconds, an

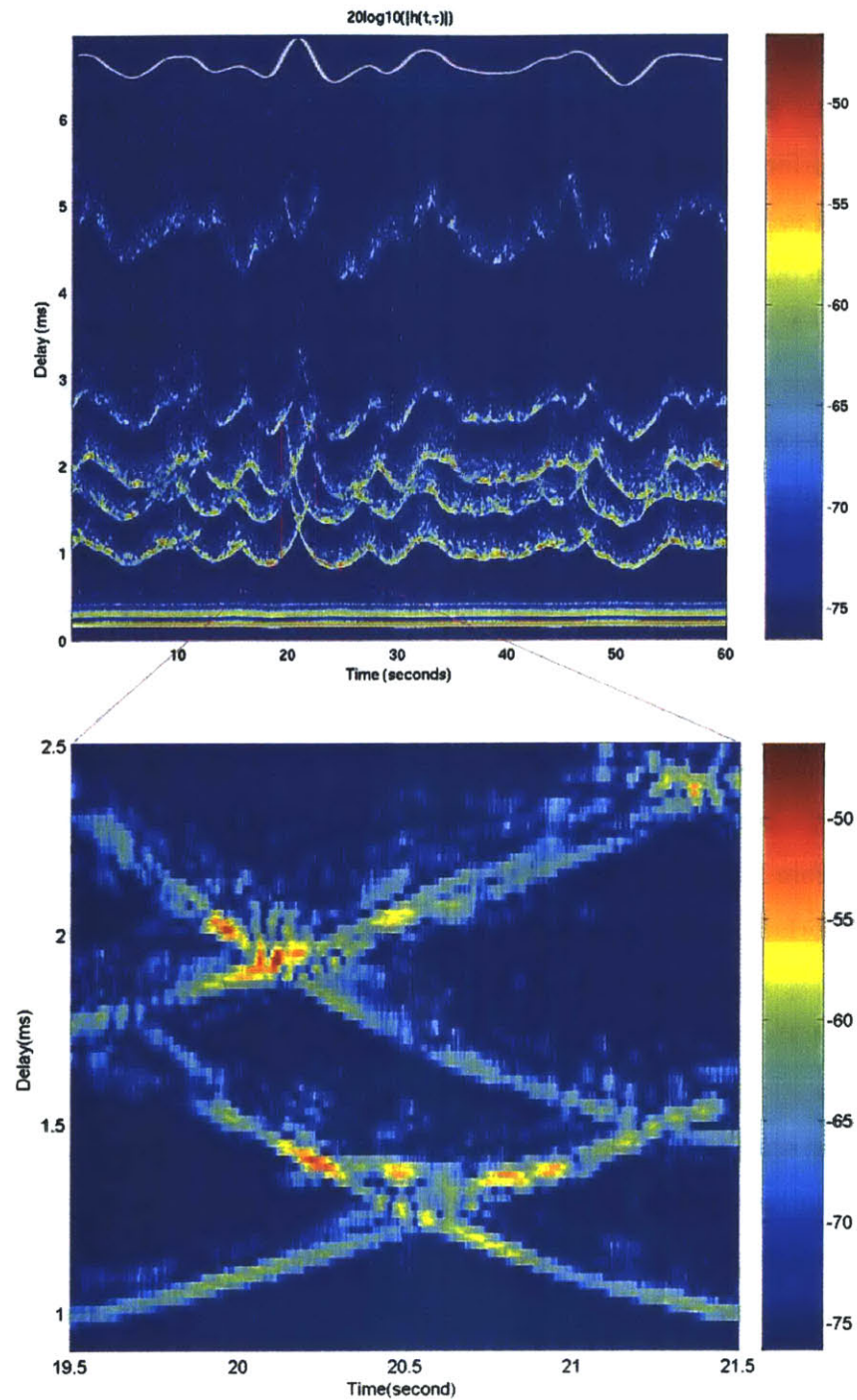


Figure 2-3: Channel Impulse Response Estimate. In the upper plot (a) the horizontal axis is time in second and the vertical axis is delay in ms. On the very top of (a) is the smoothed surface wave height time series³⁵ measured at the specular point. The lower plot (b) is an enlarged plot of the delay-time region [0.8 ms, 2.5 ms, 19.5 s, 21.5 s] of (a)

approximately 3 second period, at a time step 273 ms (or 6552 symbols). Only the Doppler-delay region ($[-20 \text{ Hz } 20 \text{ Hz } 0.8 \text{ ms } 3 \text{ ms}]$), covering the first four surface scattered arrivals, is shown in Figures 2-4 and 2-5. For each plot the horizontal axis is Doppler in Hz and the vertical axis is delay in ms. The order of each plot in the sequence is labeled at its lower left corner, from 1 to 12. The whole sequence covers from the onset of the large surface wave till it completely leaves the nominal specular reflecting region.

The channel dynamics induced by scattering from this traveling wave can be observed through the movement of those energetic delay-Doppler components, the emergence and the disappearance of the 'butterfly' wings with opposite Doppler and transient arrivals with little Doppler.

As shown in Figure 2-4 (1), in the beginning all surface arrivals have negative Doppler as they start to retreat in delay when the surface level rises. As the wave crest moves close to the nominal specular reflection region, the birth process of the opposite 'butterfly wing' for the first two surface arrivals can be readily observed from Figure 2-4 (2) to (4) where they gradually develop into very strong arrivals. The positive Dopplers associated with those newly born arrivals indicate that they are moving in the opposite direction, since the original arrivals still maintain negative Dopplers. In Figure 2-4 (4) to (6), these arrivals start to develop significant intensity and move closer towards each other in delay, effectively caused by the progressing of the wave crest into the nominal specular reflection region. A strong stable arrival with zero Doppler emerges in Figure 2-4 (5). During the wave onset period, the formation of the 'butterfly' patterns in delay-time domain observed in Figure 2-3 assumes a different dynamic appearance on the delay-Doppler domain: All arrivals follow a clockwise nearly circular motion: the original arrivals retreat in delay with negative Dopplers whose magnitudes increase; the newly emerged arrivals (the 'butterfly wings moving in opposite direction) advance in delay with positive Dopplers that reduce magnitude gradually. The increasing negative Doppler and the reducing positive Doppler are

both associated with changes of the surface slope at the scattering patches as the wave crest moves. This circular motion continues as the wave crest moves on, until the original arrivals are replaced by the arrivals newly developed during the onset of the wave crest, as shown from Figure 2-4 (7) to (8). The channel resumes a stable condition after the wave crest moves away. The remaining arrivals have positive Dopplers due to the lowering of the surface level.

During the whole process, maximum Doppler spread of approximately 25 Hz (Figure 2-4 (5) and (6)) , 30 Hz (Figure 2-4 (4) and (5)) and 35Hz (Figure 2-5 (9) and (10)) are observed for the first, second and third surface arrivals, respectively. Another important observation is that the scattering function has a very sparse structure, in the sense that the energy clusters around several dominant components that are well separated, the large area between them has little energy.

The most dominant feature of the example channel is its highly dynamic behavior. Judging either from the time-varying channel impulse response estimate or the time-varying scattering function estimate, the channel cannot be assumed as stationary. The circular rotation of the delay-Doppler components and the butterfly pattern bifurcation of multipath arrivals characterize a type of channels that could not be appropriately modeled using the general acoustic surface scattering theory mentioned early.

Implications on Channel Estimation

The observed channel characteristics pose significant challenges for the problem of channel estimation, mainly due to the following competing requirements:

1. The rapid channel fluctuations as well as the variations of the dynamics of those fluctuations would keep algorithms with long averaging window from accurately tracking the channel; While on the other hand the extensive delay spread multipath structure implies a proportionally long averaging time window is necessary;

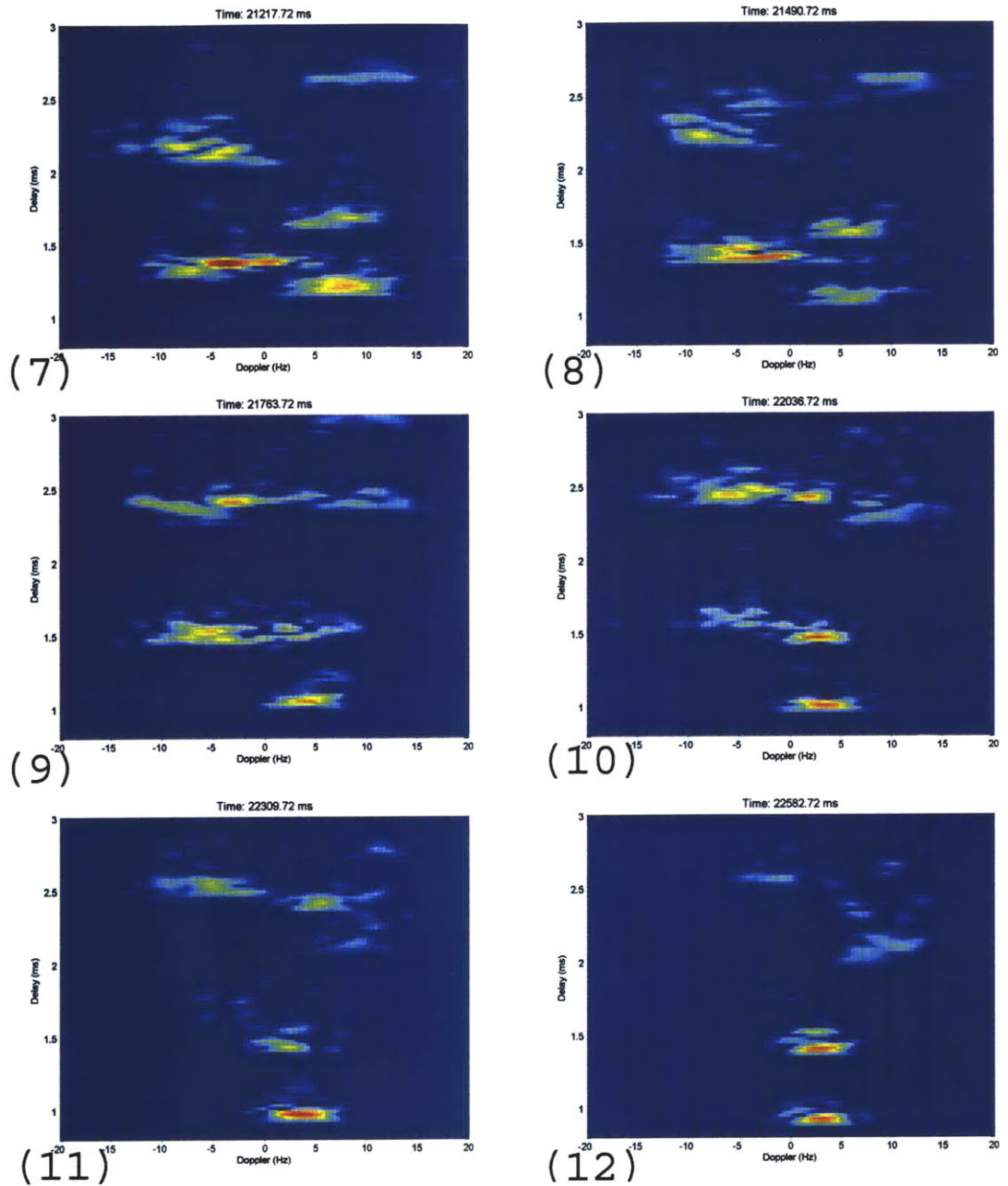


Figure 2-5: Time-Varying Scattering Function Sequence II, Each plot shows the Doppler-delay region $[-20 \text{ Hz } 20 \text{ Hz } 0.8 \text{ ms } 3 \text{ ms}]$. Adjacent plots are approximately 273 ms (or 6552 symbols) apart. Plots (1)-(6) cover 21.217 – 22.582 seconds.

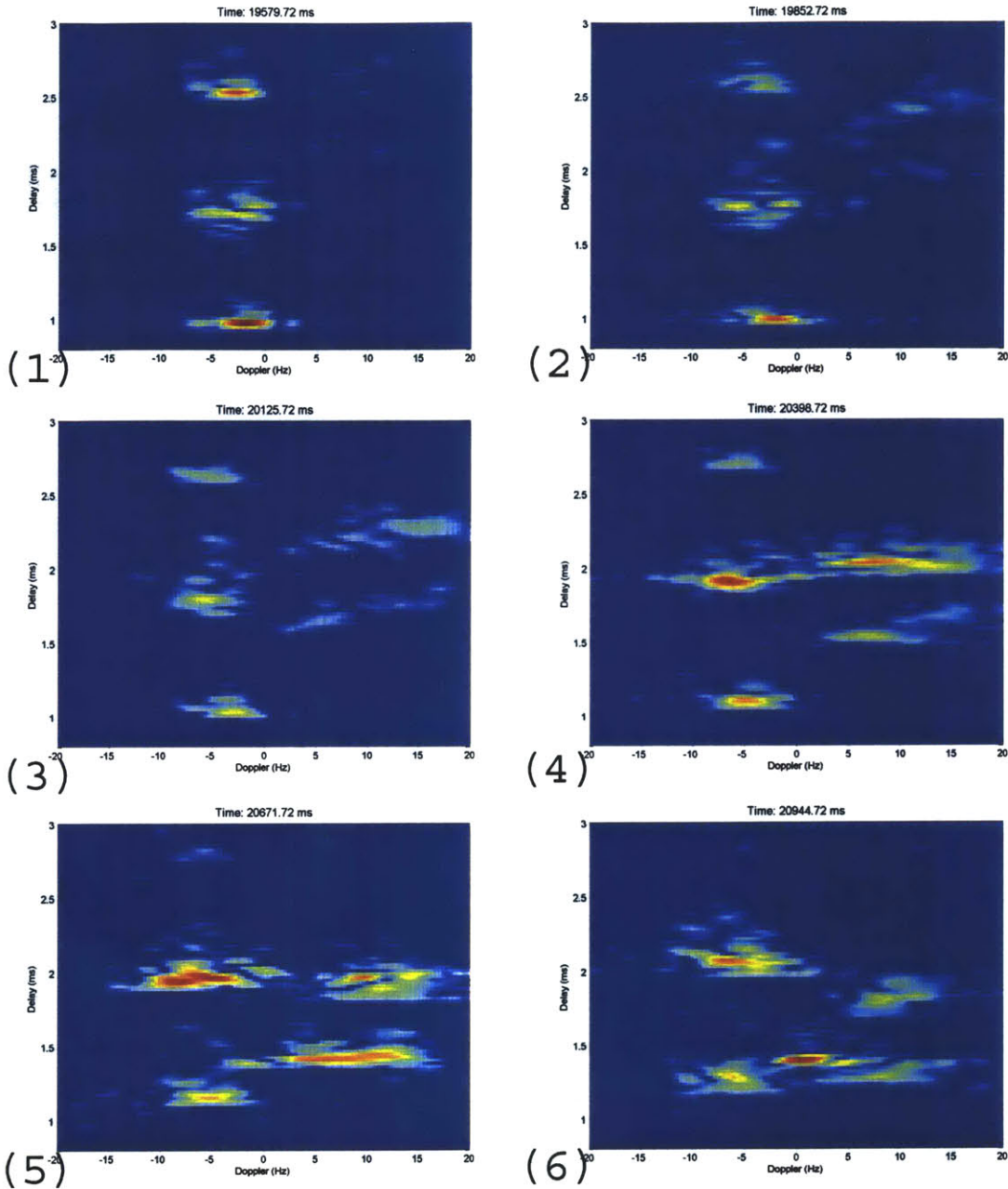


Figure 2-4: Time-Varying Scattering Function Sequence I. Each plot shows the Doppler-delay region $[-20 \text{ Hz} \ 20 \text{ Hz} \ 0.8 \text{ ms} \ 3 \text{ ms}]$. Adjacent plots are approximately 273 ms (or 6552 symbols) apart. Plots (1)-(6) cover 19.852 – 20.944 seconds.

2. The highly structured channel impulse response and delay-Doppler spread function, either being explicitly sparse or having inter-path correlations, prompt consideration for sparse processing which usually requires such structures to be stable over a period of time proportional to the channel dimension; On the other hand, the multipath structure is rapidly time-varying;
3. The migration of arrivals over delay effectively makes the uniformly sampled channel impulse response a physically less meaningful representation; However, arrival based estimation approaches are confronted with the time-varying and sometimes unstable arrival tracks, not to mention the nonlinearity that would arise in estimating the propagation delay of each arrival.

Other factors such as the emergence and disappearance of strong transient arrivals, the crossing of arrivals, all make the tasks of channel estimation and subsequent equalization more difficult.

Note that the Doppler spread observed above at a scale of 30 Hz, which probably would seem less harmful to wireless applications, has a more severe effect due to the significantly slower symbol rate typical in acoustic communications. For the example above, the Doppler spread 30Hz, at symbol rate 24000 symbols per second, contributes to a phase rotation of π in only 400 symbols, a scale comparable to the channel dimension. This means significant phase smearing if an averaging based algorithm is used without accounting for these Doppler effects. The problem is further complicated by the fact that arrivals fluctuate at different rates. Hence the bulk Doppler or bulk delay models together with the approaches based on that, such as Doppler and delay correction using Phase-Lock Loop and Delay-Lock Loop, becomes inadequate.

Yet much of these complications can be attributed to the single factor of channel dynamics. To see the problem more concretely, in the following a simple exponentially weighted RLS algorithm is applied to estimate the example channel mentioned early. Figure 2-6 shows the performance of RLS with different effective averaging

window length. The performance is evaluated in terms of the signal prediction residual error

$$e_k \triangleq y_k - \hat{y}_{k|k-1} = y_k - \mathbf{c}_k \hat{\mathbf{x}}_{k|k-1} \quad (2.1)$$

where y_k and $\hat{y}_{k|k-1}$ are the received signal at time k and its prediction based on previously received signals. \mathbf{c}_k is the transmitted symbols, a row vector. $\hat{\mathbf{x}}_{k|k-1}$ is the one-step channel prediction. That is, the estimate of the channel at time k using data up to time $k - 1$.

Figure 2-6 (a) shows in a dB scale the total received signal energy (the blue curve on the top), the squared signal prediction residual error $|e_k|^2$ for RLS with $\lambda = 0.96, 0.98, 0.998$ respectively. The curves are all smoothed over one second. λ is related to the effective averaging window length approximately as below [Hay96]:

$$N \propto \frac{1}{1 - \lambda} \quad (2.2)$$

Hence larger λ means longer averaging window.

As shown in Figure 2-6 (a), the overall $|e_k|^2$ reduces significantly as λ increases towards 1, or, effectively the length of the averaging window increases towards infinity. This is mainly due to noise suppression by longer averaging. However, this trend is reversed around 20 second when the channel becomes highly dynamic due to the passage of the surface wave event. As shown enlarged in Figure 2-6 (b) (the averaging window is 1/6 seconds), $|e_k|^2$ increases when λ increases from 0.98 to 0.998, and is only about 2dB smaller than the total energy (note this is still a smoothed result. result prior to smoothing has sharper spikes and indicates even smaller difference between the total energy and the residual error), which means that the channel is probably not being tracked at all during these dynamic events.

This simple example is a good indication of the limitation of the often used *ad hoc* tracking mechanism, namely, to bound the information matrix from above (with $\lambda < 1$), without explicitly modeling the dynamics of the time variation. For the

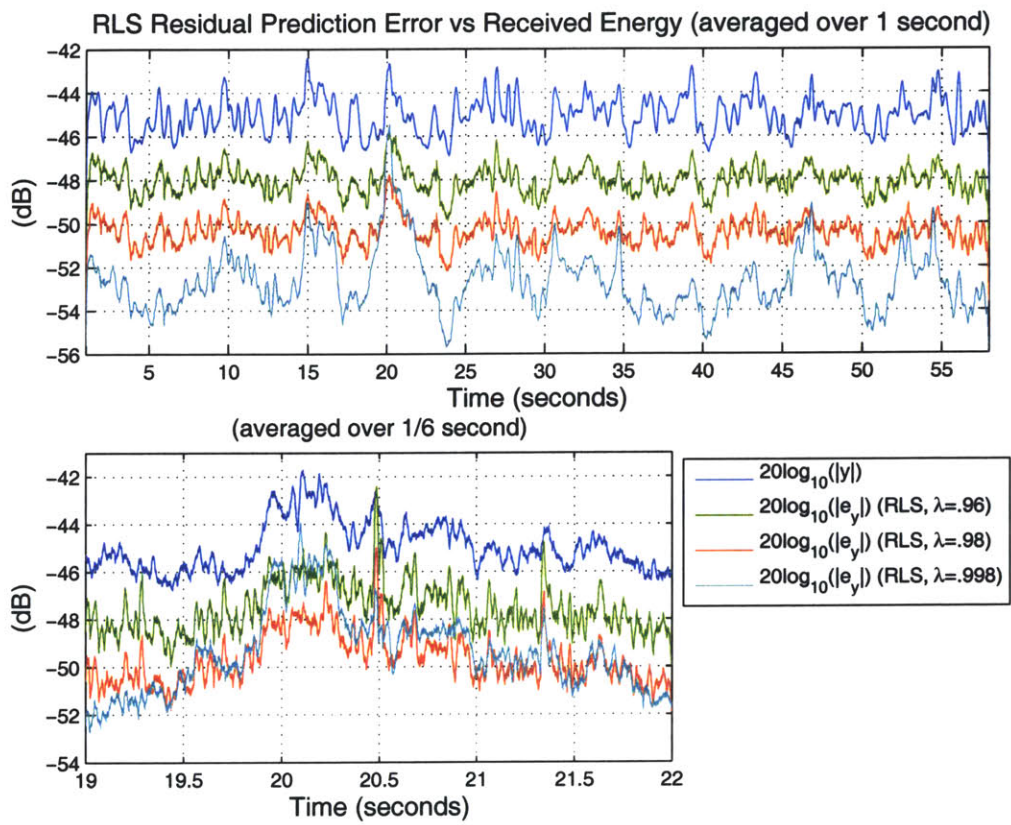


Figure 2-6: Signal Prediction Error Using the RLS algorithm

type channel considered in this thesis, it indicates that these simple techniques are inadequate.

2.2 Channel Modeling

This section discusses channel modeling. A concise review on various aspects of channel modeling for general underwater acoustic communications can be found in [Kil00]. First, in section 2.2.1 results from the well-known theory of linear time-varying (LTV) filter channel model [Pri58] [Kai59] [Bel63] [Ken68] [Van71] and the wide sense stationary uncorrelated scattering (WSSUS) channel model [Bel63] [Ken68][Van71] are briefly reviewed, as some of the concepts will be used throughout the thesis. Secondly, a state-space channel model is derived in section 2.2.2, directly based on a simplified channel model that consists of clusters of moving pointer scatterers. The state-space dynamic model is motivated by the observation and analysis made in the previous section, and most importantly, will be the foundation for the development of dynamic model based channel estimation and tracking algorithms in Chapter 3 and Chapter 4.

2.2.1 LTV and WSSUS Channels

Modeling communication channels as linear time-varying (LTV) filter has been a well-developed topic as nicely summarized in [Bel63]. The channel is represented by a set of system functions that are inter-connected via Fourier transformation over two pairs of dual domains: time vs Doppler and delay vs frequency. These system functions not only provide mathematical channel descriptions, but also lead to a physical picture of channel consisting of scatterers [Van71]. Since conceptually these system functions are equivalent, it is not necessary to repeat them all here. Instead, the two most popularly used functions, the so-called *input delay-spread function* and the *delay-Doppler spread function*, are reviewed as they will be heavily used

throughout the thesis.

The *input-delay spread function* (later it will be used interchangeably with the name *time-varying channel impulse response*), denoted by $g(t, \tau)$ is defined as follows [Bel63]:

$$r(t) = \int g(t, \tau) z(t - \tau) d\tau \quad (2.3)$$

where $r(t)$ and $z(t)$ are the received signal and the transmitted signal respectively. Hence $g(t, \tau)$ is the current channel response to a unit impulse input τ seconds earlier. Should the channel be time-invariant, $g(t, \tau)$ simply degenerates into the channel impulse response.

In discrete-time, a vector form may be used

$$r_i = \mathbf{g}_i^t \mathbf{z}_i \quad (2.4)$$

where $r_i = r(i\delta t)$, $\mathbf{g}_i = [g(i\delta t, \tau_0) \ g(i\delta t, \tau_0 + \delta\tau) \ \cdots \ g(i\delta t, \tau_0 + M\delta\tau)]^t$ and $\mathbf{z}_i = [z(i\delta t - \tau_0) \ z(i\delta t - \tau_0 - \delta\tau) \ \cdots \ z(i\delta t - \tau_0 - M\delta\tau)]^t$. τ_0 is the reference delay, δt and $\delta\tau$ are the sample interval in time and delay respectively and M is the number of delay-taps, *i.e.* the channel dimension.

The delay-Doppler spread function, denoted by $u(\nu, \tau)$, is defined as follows:

$$r(t) = \int u(\nu, \tau) e^{j2\pi\nu t} z(t - \tau) d\tau d\nu \quad (2.5)$$

which represents the output as a sum of delayed and Doppler shifted elements.

In discrete-time,

$$r_i = \mathbf{u}_i^t (\mathbf{z}_i \otimes \boldsymbol{\phi}_i) \quad (2.6)$$

where r_i and \mathbf{z}_i are defined the same as previously, \otimes is the Kronecker product,

$$\begin{aligned} \mathbf{u}_i = & [u(\nu_0, \tau_0) u(\nu_0 + \delta\nu, \tau_0) \cdots u(\nu_0 + P\delta\nu, \tau_0) \\ & u(\nu_0, \tau_0 + \delta\tau) u(\nu_0 + \delta\nu, \tau_0 + \delta\tau) \cdots u(\nu_0 + P\delta\nu, \tau_0 + \delta\tau) \\ & \dots\dots\dots \\ & u(\nu_0, \tau_0 + M\delta\tau) u(\nu_0 + \delta\nu, \tau_0 + M\delta\tau) \cdots u(\nu_0 + P\delta\nu, \tau_0 + M\delta\tau)]^t \end{aligned} \quad (2.7)$$

$$\phi_i = [e^{j2\pi\nu_0 i\delta t} \ e^{j2\pi(\nu_0 + \delta\nu) i\delta t} \ \dots \ e^{j2\pi(\nu_0 + P\delta\nu) i\delta t}]^t \quad (2.8)$$

$u(\nu, \tau)$ is related to $g(t, \tau)$ via the Fourier transformation between t and ν :

$$u(\nu, \tau) = \int g(t, \tau) e^{-j2\pi\nu t} dt \quad (2.9)$$

It is clear that $u(\nu, \tau)$ explicitly models the channel time-variation in terms of Doppler shifts. When dealing with rapidly varying channels, the assumption that the delay-Doppler spread function remains constant for a certain period of time is less strict than assuming the channel impulse response to be constant.

Both $g(t, \tau)$ and $u(\nu, \tau)$ are deterministic channel representations. In general channels are random processes, hence so are $g(t, \tau)$ and $u(\nu, \tau)$. The second-order moments of $g(t, \tau)$, denoted by $R_g(t_1, t_2; \tau_1, \tau_2)$, is defined as follows:

$$R_g(t_1, t_2; \tau_1, \tau_2) = E\{g(t_1, \tau_1)g^*(t_2, \tau_2)\} \quad (2.10)$$

Two important assumptions that will significantly simplify the problem and in most cases thought to be valid, are the wide-sense stationary and the uncorrelated scattering assumptions. Reflected on $R_g(t_1, t_2; \tau_1, \tau_2)$, that means

$$R_g(t_1, t_2; \tau_1, \tau_2) = R_g(t_2 - t_1, \tau_1)\delta(\tau_1 - \tau_2) \quad (2.11)$$

Consequently, the scattering function, denoted as $S(\nu, \tau)$, is given by

$$S(\nu, \tau) = \int R_g(\Delta t, \tau) e^{-j2\pi\nu\Delta t} d\Delta t \quad (2.12)$$

which is essentially the delay-Doppler power spectrum.

The wide-sense stationary assumption implies that the first and second-order moments are invariant to shift in time, or equivalently white in Doppler domain. That is, elements associated with different Doppler shifts are uncorrelated. Combined with uncorrelated scattering assumption, it essentially relates the channel to a set of scatterers with different delay and Doppler and are uncorrelated. For most cases when the scale of the surface time-varying roughness is relatively small, the wide-sense stationary assumption would be a good approximation. However, as discussed early, it is not so for wideband shallow-water short-range channels where the relative surface scale is large. Also, the assumption that elements with different delays are uncorrelated may not hold. Scattering from a common random surface patch, multipath arrivals may be correlated. Large scale surface motion and wave traveling may introduce correlation among the macropaths.

The scattering function represents the average distribution of energy over the delay-Doppler plane, from which several important characteristic scales can be derived, including the delay spread, Doppler spread, and coherence time and coherence bandwidth [Bel63][Ken68]. Without repeating these concepts, it is worth pointing out here that the notions of overspread and underspread sometimes can be misleading. In the example channel above, the delay spread L_τ is about 7ms and a maximum Doppler spread L_ν is less than 40Hz. As a result, the product $L_\tau L_\nu \leq 0.28 < 1$. This channel would be claimed as underspread [Ken68] [Bel69]. On the other hand, as argued previously, phase smearing can be pretty severe even within a time window comparable to the channel dimension, hence the channel may not be measurable using a LS method which contradicts the results in [Bel69].

2.2.2 State-Space Channel Model

In this section a state-space channel model is derived directly based on the assumption that the channel consists of clusters of moving pointer scatterers. Finite dimensional state-space model has been previously used for communication channels, see, for instance [Van71] where the optimal receiver is also derived based on the state-space channel model. However, it has not been shown, even for the simplest cases, that finite-dimensional state-space models are good channel models based on certain criteria. In fact, as explained later, a state-space formulation is generally not as natural as the tapped delay line model, except for a few rare cases.

The derivation starts with a single point scatterer channel and then consider the multiple pointer scatterer case. The derivation follows the notation of [Van71].

Single Point Scatterer Channel

Consider the case where the channel consists of only a single moving point scatterer, denoted as P . Suppose the following signal is being transmitted over a communication channel:

$$s(t) = \sqrt{2}E_t \text{Re}\{\bar{s}(t)e^{j2\pi f_c t}\} \quad (2.13)$$

where $\bar{s}(t)$ and E_t are the baseband signal and its power; and f_c is the carrier frequency.

Denote the signal propagation path length by $R(t)$. Neglecting additive noise the received signal is given by

$$\begin{aligned} y(t) &= \sqrt{2}E_t \text{Re}\left\{b(t)\tilde{p}\left(t - \frac{R(t)}{C}\right)e^{j2\pi f_c\left(t - \frac{R(t)}{C}\right)}\right\} \\ &\triangleq \sqrt{2}E_t \text{Re}\{\tilde{y}(t)e^{j2\pi f_c t}\} \end{aligned} \quad (2.14)$$

The equivalent baseband received signal $\tilde{y}(t)$ is given by

$$\tilde{y}(t) = b(t)\tilde{p}\left(t - \frac{R(t)}{C}\right)e^{j2\pi f_c\left(-\frac{R(t)}{C}\right)} \quad (2.15)$$

where $b(t)$ denotes the scattering cross section, C is the speed of sound; $\tilde{p}(t)$ is the equivalent matched filter output, and may be represented by the convolution of the input $\tilde{s}(t)$ with a continuously differentiable shaping filter $f(t)$ [Pro01a]:

$$\tilde{p}(t) = \int \tilde{s}(\tau)f(t - \tau)d\tau \quad (2.16)$$

The baseband channel output $\tilde{y}(t)$ and the baseband transmitted signal $\tilde{s}(t)$ can be related via the baseband *input delay-spread function* as follows:

$$\tilde{y}(t) = \int g(t, \tau)\tilde{s}(t - \tau)d\tau \quad (2.17)$$

and

$$g(t, \tau) = b(t)f\left(\tau - \frac{R(t)}{C}\right)e^{-j2\pi f_c\frac{R(t)}{C}} \quad (2.18)$$

In [Van71] (Chapter 9), it is pointed out that the scatterer velocity, denoted as V , causes both Doppler shift and time scale compression/dilation of the complex envelope in the received signal; Furthermore a upper limit for the signal bandwidth-pulse width product (BT product) is established under which the time scale compression/dilation of the complex envelope may be neglected:

$$BT \ll \frac{C}{2V} \quad (2.19)$$

where B and T are the signal bandwidth and pulse duration respectively. The factor of 2 is related with the monostatic scattering.

In the current development such requirement is not needed. In fact, the time scale compression/dilation is preserved, which is necessary for wideband transmissions

considered in this thesis. According to (2.15) the time scale variation of the complex envelope is caused by the time-varying propagation delay associated with the moving scatterer. Equation (2.18) indicates that this can be represented by the delay shift of $g(t, \tau)$ over time. In the state-space channel model to be developed later this is represented quite conveniently using a diagonally banded state transition matrix.

Continuing the consideration of channel dynamics caused by the scatterer motion. After some small time interval δt ,

$$\begin{aligned}
g(t + \delta t, \tau') &= b(t + \delta t) f\left(\tau' - \frac{R(t + \delta t)}{C}\right) e^{-j2\pi f_c \frac{R(t + \delta t)}{C}} \\
&= b(t + \delta t) f\left(\tau' - \frac{R(t)}{C} - \frac{R(t + \delta t) - R(t)}{C}\right) e^{-j2\pi f_c \left(\frac{R(t)}{C} + \frac{R(t + \delta t) - R(t)}{C}\right)} \\
&= b(t + \delta t) f\left(\tau' - \frac{R(t)}{C} - \frac{\delta R(t)}{C}\right) e^{-j2\pi f_c \left(\frac{R(t)}{C} + \frac{\delta R(t)}{C}\right)} \tag{2.20}
\end{aligned}$$

where $\delta R(t) = R(t + \delta t) - R(t)$.

Applying change of variable $\tau' = \tau + \frac{\delta R(t)}{C}$, the following equation is obtained connecting $g(t + \delta t, \tau)$ with $g(t, \tau)$:

$$g(t + \delta t, \tau) = \underbrace{\frac{b(t + \delta t)}{b(t)}}_{(1)} \underbrace{g\left(t, \tau - \frac{\delta R(t)}{C}\right)}_{(2)} \underbrace{e^{-j2\pi f_c \frac{\delta R(t)}{C}}}_{(3)} \tag{2.21}$$

where the first factor is due to the change of scattering cross section over the time interval δt , the second factor reflects the path length change, and the third factor is a phase component associated with Doppler shift. Note that the expression in the first term runs into trouble in the presence of scintillation, *i.e.*, $b(t)$ becomes very small or close to zero. This is an inherent limitation of dynamic modeling and will cause the estimation of the channel dynamics a mathematically ill-defined problem as shown later. Equation (2.21) essentially describes the time-evolution of the baseband channel *input delay-spread function* following the scatterer trajectory. This evolution could appear very different when observed through fixed delays, *i.e.*

from the perspective of the uniformly sample channel impulse response. To see that, expanding the second term in (2.21) using the first order Taylor series of $f(\cdot)$, it yields

$$\begin{aligned}
g(t, \tau - \frac{\delta R(t)}{C}) &= b(t)f(\tau - \frac{R(t)}{C} - \frac{\delta R(t)}{C})e^{-j2\pi f_c \frac{R(t)}{C}} \\
&\approx b(t)[f(\tau - \frac{R(t)}{C}) - f'(\tau - \frac{R(t)}{C})\frac{\delta R(t)}{C}]e^{-j2\pi f_c \frac{R(t)}{C}} \\
&= g(t, \tau) - b(t)f'(\tau - \frac{R(t)}{C})\frac{\delta R(t)}{C}e^{-j2\pi f_c \frac{R(t)}{C}} \\
&\triangleq \gamma_f(t, \tau)g(t, \tau)
\end{aligned} \tag{2.22}$$

where $\gamma_f(t, \tau) = 1 - [f'(\tau - \frac{R(t)}{C})\frac{\delta R(t)}{C}/f(\tau - \frac{R(t)}{C})]$; and $f'(\tau - \frac{R(t)}{C})$ is the first-order derivative of $f(\cdot)$ taken at $\tau - \frac{R(t)}{C}$. It is clear that the significance of the second term of $\gamma_f(t)$ depends on $f'(\tau - \frac{R(t)}{C})$ as well as $\frac{\delta R(t)}{C}$.

Note that the above approximation requires $\delta R(t)/C$ to be small compared to the pulse duration. Consider the case where the pulse has a Gaussian shape. If $\delta R(t)/C$ is larger than the pulse duration, denoted as T_f , then $f(\tau - \frac{R(t+1)}{C})_{\tau=R(t)/C} = 0$ even though $f(\tau - \frac{R(t)}{C})_{\tau=R(t)/C}$ can be fairly large. The first-order approximation breaks down since $f'(\tau - \frac{R(t)}{C})_{\tau=R(t)/C} = 0$. More specifically, let V be the scatterer velocity, B as the signal bandwidth hence, the symbol interval is $dt = 1/B$, then the above requirement becomes

$$\frac{V dt}{C} < T_f \tag{2.23}$$

equivalently,

$$BT_f > \frac{V}{C} \tag{2.24}$$

As $T_f \geq dt$ hence $BT_f \geq 1$, (2.24) is generally satisfied since $V < C$. Considering the example channel mentioned previously, $B = 24000$ Hz, $C = 1500$ m/s, assuming $V = 2$ m/s, then (2.24) requires that the delay spread of each multipath arrival $T_f > \frac{2}{24000 \cdot 1500} \approx 5.6 \times 10^{-5}$ ms, which is easily satisfied. (2.24) can also be interpreted as requiring that the scatterer has a relatively smooth migration from tap to tap for

a given BT_f product, which is usually a reasonable assumption for surface scattering channels.

Substituting (2.22) back into (2.21) yields

$$\begin{aligned}
g(t + \delta t, \tau) &= \frac{b(t + \delta t)}{b(t)} e^{-j2\pi f_c \frac{\delta R(t)}{c}} \left[g(t, \tau) - b(t) f' \left(\tau - \frac{R(t)}{C} \right) \frac{\delta R(t)}{C} e^{-j2\pi f_c \frac{R(t)}{C}} \right] \\
&= \frac{b(t + \delta t)}{b(t)} e^{-j2\pi f_c \frac{\delta R(t)}{c}} \gamma_f(t, \tau) g(t, \tau) \\
&\triangleq \alpha(t, \tau) g(t, \tau)
\end{aligned} \tag{2.25}$$

where $\alpha(t, \tau) \triangleq \frac{b(t + \delta t)}{b(t)} e^{-j2\pi f_c \frac{\delta R(t)}{c}} \gamma_f(t, \tau)$. (2.25) describes the time evolution of the channel tap gain along the fixed delay τ , while (2.21) governs the evolution of the tap gains along the trajectory of the scatterer. Another difference is that (2.25) only applies for differentiable pulse shape $f(\cdot)$, since otherwise $\gamma_f(t)$ is ill-defined. On the other hand, (2.21) always holds regardless the choice of $f(\cdot)$. Again (2.25) becomes ill-defined for scatterers with strong scintillation or weaker scatterers as $b(t) \rightarrow 0$.

Channel with Multiple Point Scatterers

Now assume that a channel consists of a cluster of point scatterers and the second-order multiple scattering among the scatterers is neglected. Then the input delay-spread function is the sum of contributions from all scatterers:

$$\begin{aligned}
g(t, \tau) &= \sum_{k=1}^K g_k(t, \tau) \\
&= \sum_{k=1}^K b_k(t) f_k \left(\tau - \frac{R_k(t)}{C} \right) e^{-j2\pi f_c \frac{R_k(t)}{C}}
\end{aligned} \tag{2.26}$$

where the subscript k is used to indicate the variables' association with the k th scatterer. For simplicity, here it is assumed that the number of scatterers, K , is fixed. In many real situations due to the emergence and disappearance of scatterers, K often varies over time.

Now suppose that the input delay-spread function is sampled along the delay axis uniformly with interval $\delta\tau$, *i.e.* $\tau_m = \tau_0 + m\delta\tau$, for $m = 0, \dots, M-1$. Here τ_0 is the bulk delay and M is the total number of delay taps. The sampled input delay-spread function is then represented by a vector $\mathbf{g}(t)$:

$$\mathbf{g}(t) = [g(t, \tau_0), g(t, \tau_1), \dots, g(t, \tau_{M-1})]^t \quad (2.27)$$

From (2.26), it follows

$$\mathbf{g}(t) = \mathbf{F}(t)\mathbf{b}(t) \quad (2.28)$$

where

$$\mathbf{b}(t) \triangleq [b_1(t)e^{-j2\pi f_c(R_1(t)/C)} \quad b_2(t)e^{-j2\pi f_c(R_2(t)/C)} \quad \dots \quad b_K(t)e^{-j2\pi f_c(R_K(t)/C)}]^t \quad (2.29)$$

$$\mathbf{F}(t) \triangleq \begin{bmatrix} f_1(\tau_0 - \frac{R_1(t)}{C}) & f_2(\tau_0 - \frac{R_2(t)}{C}) & \dots & f_K(\tau_0 - \frac{R_K(t)}{C}) \\ f_1(\tau_1 - \frac{R_1(t)}{C}) & f_2(\tau_1 - \frac{R_2(t)}{C}) & \dots & f_K(\tau_1 - \frac{R_K(t)}{C}) \\ \vdots & \vdots & \vdots & \vdots \\ f_1(\tau_{M-1} - \frac{R_1(t)}{C}) & f_2(\tau_{M-1} - \frac{R_2(t)}{C}) & \dots & f_K(\tau_{M-1} - \frac{R_K(t)}{C}) \end{bmatrix} \quad (2.30)$$

Remarks:

1. The matrix $\mathbf{F}(t)$ contains all the delay information. Columns of $\mathbf{F}(t)$ are associated with different scatterers and rows of $\mathbf{F}(t)$ are associated with fixed delay taps. The vector $\mathbf{b}(t)$ bears information on the scattering gain variation, and more importantly, the Doppler associated with each point scatterer. The latter can be better seen using the simple linearly moving scatterer model $R_k(t) = r_k + v_k(t)t$. In that case,

$$\begin{aligned} \mathbf{b}(t) &= [\tilde{b}_1(t)e^{-j2\pi(f_c v_1(t)/C)t} \quad \tilde{b}_2(t)e^{-j2\pi(f_c v_2(t)/C)t} \quad \dots \quad \tilde{b}_K(t)e^{-j2\pi(f_c v_K(t)/C)t}]^t \\ &= [\tilde{b}_1(t)e^{-j2\pi f_{d,1}(t)t} \quad \tilde{b}_2(t)e^{-j2\pi f_{d,2}(t)t} \quad \dots \quad \tilde{b}_K(t)e^{-j2\pi f_{d,K}(t)t}]^t \end{aligned} \quad (2.31)$$

where $\tilde{b}_k(t) = b_k(t)e^{-j2\pi f_c(r_k/C)}$, for $k = 1, \dots, K$; and the Dopplers $f_{d,k}(t) =$

$f_c v(t)/C$.

2. In the case of wideband transmission, the pulses $f_k(\cdot)$ typically have narrow width. This leads to a block diagonal structure in the matrix $\mathbf{F}(t)$. Suppose at time t , $\tau_{m_1} = m_1 \delta \tau$ is the delay tap closest to $R_1(t)/C$. Then due to the finite support of $f_1(\cdot)$, the first column of $\mathbf{F}(t)$ will concentrate near its m_1 th element, with spread proportional to the pulse width. The same argument affects the remaining columns.
3. Further decomposition of the channel into subspaces may be carried out based on this representation, in terms of $\mathbf{F}(t)$ and $\mathbf{b}(t)$, *i.e.* delay subspace, Doppler subspace.

If the signal bandwidth is sufficiently large, the paths associated with different scatterers may become resolvable in delay. Reflected in $\mathbf{F}(t)$, different columns will span distinct row segments. This requires that $(T_k + T_j)/2 < [R_k(t) - R_j(t)]/C$ for all k, j . Here T_k and T_j are pulse width associated with k th and j th scatterers.

Consider after a small time interval δt ,

$$\begin{aligned} g(t + \delta t, \tau) &= \sum_{k=1}^K g_k(t + \delta t, \tau) \\ &= \sum_{k=1}^K b_k(t + \delta t) f_k\left(\tau - \frac{R_k(t + \delta t)}{C}\right) e^{-j2\pi f_c \frac{R_k(t + \delta t)}{C}} \end{aligned} \quad (2.32)$$

In vector notation,

$$\mathbf{g}(t + \delta t) = \mathbf{F}(t + \delta t) \mathbf{b}(t + \delta t) \quad (2.33)$$

Using the first-order Taylor series expansion,

$$\mathbf{F}(t + \delta t) \approx \mathbf{F}(t) + \mathbf{F}'(t) \Delta \mathbf{T}(t) \quad (2.34)$$

$$\Delta \mathbf{T}(t) \triangleq \text{diag}([\delta R_1(t) \quad \delta R_2(t) \quad \cdots \quad \delta R_K(t)]) / C \quad (2.35)$$

where $\delta R_i(t) = R_i(t + \delta t) - R_i(t)$; and $\mathbf{F}'(t)$ is an matrix whose entries are $f'_k(m\delta\tau - R_k(t)/C)$.

In addition,

$$\mathbf{b}(t + \delta t) = \mathbf{\Lambda}(t)\mathbf{b}(t) \quad (2.36)$$

where

$$\mathbf{\Lambda}(t) \triangleq \text{diag}\left(\left[\frac{b_1(t + \delta t)}{b_1(t)} e^{-j2\pi f_c \delta R_1/C} \quad \frac{b_2(t + \delta t)}{b_2(t)} e^{-j2\pi f_c \delta R_2/C} \quad \dots \quad \frac{b_K(t + \delta t)}{b_K(t)} e^{-j2\pi f_c \delta R_K/C}\right]\right) \quad (2.37)$$

Substituting (2.34)-(2.36) into (2.33) yields

$$\begin{aligned} \mathbf{g}(t + \delta t) &= [\mathbf{F}(t) + \mathbf{F}'(t)\mathbf{\Delta T}(t)]\mathbf{\Lambda}(t)\mathbf{b}(t) \\ &= [\mathbf{I} + \mathbf{F}'(t)\mathbf{\Delta T}(t)\mathbf{F}^\dagger(t)]\mathbf{F}(t)\mathbf{\Lambda}(t)\mathbf{b}(t) \end{aligned} \quad (2.38)$$

where $\mathbf{F}^\dagger(t) = [\mathbf{F}^h(t)\mathbf{F}(t)]^{-1}\mathbf{F}^h(t)$ is the pseudo-inverse of $\mathbf{F}(t)$, *i.e.* $\mathbf{F}^\dagger(t)\mathbf{F}(t) = \mathbf{I}$. Here $\mathbf{F}^h(t)$ is the Hermitian of $\mathbf{F}(t)$.

Let $\mathbf{M}(t) \triangleq \mathbf{F}(t)\mathbf{\Lambda}(t)\mathbf{F}^\dagger(t)$, it yields $\mathbf{F}(t)\mathbf{\Lambda}(t) = \mathbf{M}(t)\mathbf{F}(t)$. Therefore

$$\begin{aligned} \mathbf{g}(t + \delta t) &= [\mathbf{I} + \mathbf{F}'(t)\mathbf{\Delta T}(t)\mathbf{F}^\dagger(t)]\mathbf{M}(t)\mathbf{F}(t)\mathbf{b}(t) \\ &= [\mathbf{I} + \mathbf{F}'(t)\mathbf{\Delta T}(t)\mathbf{F}^\dagger(t)]\mathbf{M}(t)\mathbf{g}(t) \\ &\triangleq \mathbf{\Gamma}(t)\mathbf{g}(t) \end{aligned} \quad (2.39)$$

where $\mathbf{\Gamma}(t) \triangleq [\mathbf{I} + \mathbf{F}'(t)\mathbf{\Delta T}(t)\mathbf{F}^\dagger(t)]\mathbf{M}(t) = [\mathbf{I} + \mathbf{F}'(t)\mathbf{\Delta T}(t)\mathbf{F}^\dagger(t)]\mathbf{F}(t)\mathbf{\Lambda}(t)\mathbf{F}^\dagger(t)$.

While the form of equation (2.39) is simple, the transition matrix $\mathbf{\Gamma}(t)$ is unfortunately a complicated function of $\mathbf{F}(t)$, $\mathbf{F}^\dagger(t)$, $\mathbf{F}'(t)$, $\mathbf{\Delta T}(t)$ as well as $\mathbf{\Lambda}(t)$.

In general the transition matrix $\mathbf{\Gamma}(t)$ in equation (2.39) does not have a simple dependency on channel parameters such as Doppler and delay, as in the single point scattering case. One exception is when the signal bandwidth is sufficiently large. As shown in the following, for wideband transmission, a block diagonal structure can

be obtained for the transition matrix and explicit dependency on Doppler and delay can be derived.

Wideband Channel Model

As mentioned early, when the transmitted signal has sufficiently wide band, the arrival signals from different scatterers are resolvable in delay which means that each column of $\mathbf{F}(t)$ has narrow nonzero span and these spans do not overlap. For a two-scatterer channel, this yields:

$$\mathbf{F}(t) = \begin{bmatrix} \mathbf{f}_1(t) & \mathbf{0} \\ \mathbf{0} & \mathbf{f}_2(t) \end{bmatrix} \quad (2.40)$$

where $\mathbf{f}_1(t)$ and $\mathbf{f}_2(t)$ are column vectors that cover the nonzero support regions of scatterer 1 and 2, respectively. $\mathbf{F}'(t)$ has the same block structure. $\mathbf{F}^\dagger(t)$ is given by

$$\mathbf{F}^\dagger(t) = \begin{bmatrix} \|\mathbf{f}_1(t)\|^{-2} \mathbf{f}_1^h(t) & \mathbf{0}^t \\ \mathbf{0}^t & \|\mathbf{f}_2(t)\|^{-2} \mathbf{f}_2^h(t) \end{bmatrix} \quad (2.41)$$

is also well structured.

Accordingly, for this two-scatterer channel (2.35) and (2.37) become:

$$\mathbf{\Lambda}(t) = \begin{bmatrix} \frac{b_1(t+\delta t)}{b_1(t)} e^{-j2\pi f_c \delta R_1/C} & 0 \\ 0 & \frac{b_2(t+\delta t)}{b_2(t)} e^{-j2\pi f_c \delta R_2/C} \end{bmatrix} \quad (2.42)$$

$$\mathbf{\Delta T}(t) = \begin{bmatrix} \delta R_1(t)/C & 0 \\ 0 & \delta R_2(t)/C \end{bmatrix} \quad (2.43)$$

Consequently, following (2.39) it yields:

$$\mathbf{M}(t) = \begin{bmatrix} \frac{b_1(t+\delta t)}{b_1(t)} e^{-j2\pi f_c \delta R_1/C} \mathbf{f}_1(t) \mathbf{f}_1^h(t) & \mathbf{0} \\ \mathbf{0} & \frac{b_2(t+\delta t)}{b_2(t)} e^{-j2\pi f_c \delta R_2/C} \mathbf{f}_2(t) \mathbf{f}_2^h(t) \end{bmatrix} \quad (2.44)$$

$$\begin{aligned} \Gamma(t) &= \left(\mathbf{I} + \begin{bmatrix} \mathbf{f}'_1(t) & \mathbf{0} \\ \mathbf{0} & \mathbf{f}'_2(t) \end{bmatrix} \begin{bmatrix} \delta R_1/C & 0 \\ 0 & \delta R_2/C \end{bmatrix} \begin{bmatrix} \|\mathbf{f}_1(t)\|^{-2} \mathbf{f}_1^h(t) & \mathbf{0}^t \\ \mathbf{0}^t & \|\mathbf{f}_2(t)\|^{-2} \mathbf{f}_2^h(t) \end{bmatrix} \right) \mathbf{M}(t) \\ &\triangleq \begin{bmatrix} \Gamma_1(t) & \mathbf{0} \\ \mathbf{0} & \Gamma_2(t) \end{bmatrix} \end{aligned} \quad (2.45)$$

where for $i = 1, 2$,

$$\Gamma_i(t) \triangleq \frac{b_i(t+\delta t)}{b_i(t)} e^{-j2\pi f_c \delta R_i/C} \left[\mathbf{f}_i(t) + \mathbf{f}'_i(t) \delta R_i/C \right] \mathbf{f}_i^h(t) \quad (2.46)$$

where the term inside the bracket is the first order Taylor expansion of $\mathbf{f}_i(t + \delta R_i/C)$.

Further expanding the scattering cross section:

$$b_i(t + \delta t) \approx b_i(t) + b'_i(t) \delta t \quad (2.47)$$

it follows that

$$\Gamma_i(t) \approx \left[1 + \frac{b'_i(t) \delta t}{b_i(t)} \right] \left[\mathbf{f}_i(t) + \mathbf{f}'_i(t) \delta R_i/C \right] \mathbf{f}_i^h(t) e^{-j2\pi f_c \delta R_i/C} \quad (2.48)$$

In summary, (2.45), (2.46) and (2.48) give a block diagonal transition matrix for a wideband channel that consists of moving scatterers. They also explicitly gives the dependency of the transition matrix on the Doppler associated with each individual scatterer.

Based on this dynamic formulation, the following discrete-time state-space model

can be proposed for the uniformly sampled channel impulse response:

$$\begin{cases} \mathbf{x}_{i+1} = \mathbf{A}_i \mathbf{x}_i + \mathbf{w}_i & (2.49a) \\ y_i = \mathbf{c}_i \mathbf{x}_i + v_i & (2.49b) \end{cases}$$

where $\mathbf{x}_i \triangleq \mathbf{g}(i\delta t)$, $y_i \triangleq y(i\delta t)$, $\mathbf{A}_i \triangleq \Gamma(i\delta t)$ are the sampled channel impulse response, the sampled received signal and the channel state transition matrix, respectively. \mathbf{c}_i is the sequence of transmitted symbols.

The derivation of (2.45), (2.46), (2.48) and (2.49) does not rely on explicit assumptions regarding the signal bandwidth. The signal BT product upper bound (2.19) is not necessary as the time-scale compression or dilation in the complex envelope is preserved and its effect is represented conveniently using the off-diagonal elements of the matrix \mathbf{A}_i in (2.49a). The lower bound for the product BT_f , the signal bandwidth and the delay spread of multipath arrivals, is not an issue typically. However, as will be shown later, estimation of the channel dynamic parameters, i.e. the unknown elements of \mathbf{A}_i in (2.49a), does require that the multipath arrivals energize the corresponding delay taps throughout the averaging window within which the parameter estimation is operated. Otherwise, it'll lead to the problem of parameter unobservability in Chapter 3 and insufficient excitation in Chapter 4.

All modeling attempts involve approximations and the point is usually to highlight the dominant aspects of the problem while simplifying others under identifiable conditions. The same is true in this case. The state-space model proposed above is based on deterministic dynamical arguments, as motivated by the previous observations of significant channel dynamics. The derivation does not involve statistical properties of the channel. For instance, the process noise \mathbf{w}_i is largely unspecified, although the observation noise v_i can be added on without any conceptual confusion. However, this does not imply that the statistical channel properties are not important, rather it is hoped that (2.49), assuming a general state-space formulation, would account for a fairly broad range of statistical cases.

A more rigorous development of statistical channel properties of a channel, under the assumption that the channel consists of clusters of point scatterers, can potentially be considered based on statistical as well as dynamical properties of i) the scattering gain $b_k(t)$ which is a random process and ii) the motion, or velocity of those scatterers. It is certainly an interesting direction for further development based on stochastic modeling of b_k and their motions, for which results derived from acoustic surface scattering may then be used.

For the purpose of dynamic channel estimation, (2.49) provides a good justification for developing channel tracking algorithms. As it is generally unrealistic to assume that one could possibly have perfect knowledge of model parameters for any real channel, for the purpose of channel estimation or equalization, the common practice is either to estimate these parameters from received signals or simply consider them as tweaking parameters of the estimation algorithm.

Thus here and throughout the remaining part of the thesis, it is simply assumed that both \mathbf{w}_i and v_i are zero-mean Gaussian white processes, with covariances \mathbf{Q}_w and variance σ_v^2 , respectively. They are mutually and temporally independent, and independent from the initial state \mathbf{x}_0 . That assumed, one can connect the noise covariance \mathbf{Q}_w and the transition matrix \mathbf{A}_i with the steady-state tap gain energy via the state-space equation provided the model is stable. The Doppler shift/spread associated with channel taps are specified by \mathbf{A}_i as derived in (2.46).

It is well known that finite-dimensional state-space model has a rational spectrum, hence the model (2.49) may be viewed as approximating the channel with one having rational spectrum. Due to the simplistic assumption of single scattering from point scatterers, the model (2.49) is essentially of first-order and would not be suitable for channels that have multiple Doppler shifts at a single tap, or equivalently, multiple poles. However, extension towards high-order cases are straightforward based on the development above.

2.3 Concluding Remarks

The characteristics of wideband shallow-water surface scattering acoustic channels are presented via a set of surf-zone communication experimental data. Examination of both the channel impulse response and the time-varying scattering function highlights that the channel is rapidly fluctuating with a fast-changing dynamics; it also has a very sparse channel structure that spreads extensively over both propagation delay and Doppler. All these features are not captured by the previous acoustic surface scattering theory and results.

A general state-space channel model is derived, based on the assumption that the channel consists of clusters of moving pointer scatterers. Explicit dependency of the state transition matrix on the Doppler and the signal parameters is given for the wideband case.

The presented channel characteristics and the established state-space channel model provide, respectively, the physical constraints and the model theoretical basis for the development of channel estimation methods in the forthcoming chapters.

Chapter 3

EKF based Channel Impulse Response Estimation

Dynamic model based channel estimation approaches are developed in this chapter and Chapter 4. This chapter covers the extended Kalman Filter (EKF) based approaches. The Expectation Maximization (EM) based approaches are discussed in Chapter 4. The primary goal is to obtain accurate one-step prediction of the rapidly time-varying channel impulse response which can then be used for channel estimate based equalization. The major issue is that in reality neither the channel nor how it evolves over time is known. Based on the state-space channel model developed in Chapter 2, both the EKF and the EM based approaches jointly estimate the state and the model parameters from the received signal. Hence, it is essentially a system identification problem.

In this chapter the EKF algorithm for joint channel state and parameter estimation is derived. Tracking error analysis of the EKF as an adaptive filter is presented. Second-order innovation corrections of the EKF are proposed based on the comparison between the EKF and stochastic descent algorithms minimizing the mean squared prediction error (MSE) and the negative log-likelihood function (ML). More importantly, it is shown that due to the structure of the wideband channel

impulse response, the dynamic parameters associated with those quiescent taps or the unexcited tap subspace are unobservable and if not modeled properly, become undetectable. A two-model based EKF algorithm is then proposed to address the parameter detectability issue. It is effectively a soft constraint based approach to actively track the dominant taps while maintaining modest adapting gain for those quiescent taps.

3.1 Introduction

It is well known that the EKF can be applied for joint state and parameter estimation [Jaz70][Lju79][And79]. By augmenting the original state with the unknown model coefficients, it applies the standard Kalman Filter (KF) to the augmented state space system linearized around the current estimates. The resulting estimates are suboptimal solutions to the nonlinear estimation problem. The EKF can also be viewed as an adaptive filter rather than a suboptimal approximation to the Kalman filter. In reality it is rarely the case that one would know the noise covariances while not knowing the model coefficients. The inaccuracy in the assumed noise covariances could disqualify any optimality claims of the EKF. Although one could estimate those noise covariances directly from data, which is a well-studied topic and dates back to early 70s, see, for instance Mehra[Meh70][Meh72], Jazwinski [Jaz70] and Belanger[Bel74], and more recently, Bunn [Bun81], the number of unknowns in the process noise covariance that can be estimated is found to be limited [Meh72]. Furthermore, all the approaches, which are based on the correlation properties of either the innovation or the observation sequence, assume that model coefficients are perfectly known. With joint estimation of the model coefficients, noise covariances and the states, the algorithm will likely run into the issue of overparameterization, not to mention the amount of computation involved. A more practical and robust approach would be to choose the noise covariances in an *ad hoc* manner to accomplish

some desired filter properties rather than seeking the exact match with the ground truth (which is often model dependent). Effectively these covariances become tuning parameters of the EKF as an adaptive algorithm.

Despite the extensive use of the EKF algorithm in numerous applications, rigorous analysis of its transient as well as steady-state performance has been scarce. A well cited work on that aspect is by Ljung [Lju79]. In addition to pointing out that parameter bias is mainly caused by inaccuracy in the assumed noise covariance matrices, Ljung [Lju79] proposed two modifications of EKF to improve steady-state convergence based on the comparison between EKF and the stochastic descent algorithms that minimize either the mean squared prediction error or the negative log-likelihood function. The analysis is based on the assumption that the model parameterization is both detectable and stabilizable.

In the context of dynamic model based channel estimation using EKF, there have been several developments that may be connected with this chapter on various aspects.

In a series of papers [Ilt90, Ilt91, Ilt94, Ilt01], Iltis has developed several EKF based algorithms for joint estimation of multipath gain, delay and/or Doppler in direct-sequence (DS) spread-spectrum systems. In all cases the channel for a single user ([Ilt01] considers multiple access formulation) is modeled such that only the bulk delay and/or the bulk Doppler shift need to be estimated. Furthermore, the dynamics of the delay, Doppler and multipath gains are assumed known. These assumptions significantly simplify the problem but are ill-suited for the wideband rapidly varying multipath channel considered in this thesis. The multipath arrival structure and their dynamics considered here cannot be adequately represented by bulk delay or Doppler since the arrivals have inhomogeneous fluctuation rates. Furthermore, compared to the tap-based model 2.49, Iltis uses arrival based channel model which leads to an observation equation that is nonlinear in delay. The paper by Lakhzouri, *et al.* [Lak03] may be considered as an extension of the work by Iltis, in the sense that

instead of modeling a bulk delay, the delays of all the multipath arrivals are modeled and estimated. Again the dynamic parameters of delay fluctuations are assumed perfectly known. This assumption of known channel dynamics is unrealistic for the type of channel considered in this thesis because not only the channel fluctuates rapidly, but the dynamics of these fluctuations vary over time as well.

In terms of application context, closely related to this chapter is the recent work by Tsai, *et al.* [Tsa05] where in the context of multi-user DSSS transmission, the single user channel is assumed flat fading and modeled as a low-order AR process. The tap gain and its AR coefficients are then jointly estimated from the received signal. The authors focus on the asymptotic analysis of the algorithm, such as bias correction and convergence improvement by comparing with ML estimation, which may be viewed as a straightforward application of Ljung's work [Lju79]. No attention was paid to the potential impact of channel properties on the performance of the channel estimator.

In the context of channel estimation, however, the performance of the EKF algorithm is affected inevitably by the physical properties of the channel. A fundamental issue concerning joint state and parameter estimation is that the assumption of model detectability and stabilizability of [Lju79] may not hold for some wideband multipath channels, thus the analysis results of [Lju79] will not be applicable. This connection from channel physics to the performance of the EKF channel estimation algorithm is not exploited in any of the work mentioned above. Yet understanding the implications of the channel physical characteristics, through system theoretic properties of the model, upon channel estimation and tracking is essential to algorithm design and performance analysis. Especially in the case of wideband transmission, the channel impulse response or delay-Doppler spread function generally has very sparse structure. As a result direct application of the EKF algorithm to a state-space model of channel taps runs into parameter identifiability issues and eventually cause algorithm divergence.

In this chapter, the EKF algorithm for joint channel state and dynamic parameter estimation is derived, the performance issues related with channel sparseness are identified and modified algorithms based on system theoretic arguments are proposed. The content is organized as follows: Section 3.2 presents a brief account of the EKF algorithm for joint channel state and parameter estimation (its derivation details and specialization to cases with diagonal and tridiagonal state transition matrix are provided in Appendix A) which is followed by a tracking error analysis of EKF channel estimation and a discussion of the EKF vs MSE and ML parameter estimation. Parameter observability and detectability within the linearized system model is analyzed in Section 3.3; and a two model based EKF algorithm is presented in Sections 3.4 . Separate models for parameters associated with active taps and inactive taps are proposed in Section 3.4 to avoid the algorithm divergence due to parameter undetectability, and also as a soft constraint based approach to actively tracking the dominant taps while maintain a modest adapting gain for those quiescent taps.

3.2 EKF Joint Channel State and Parameter Estimation

Restate the state space channel model from Section 2.2.2:

$$\begin{cases} \mathbf{x}_{i+1} = \mathbf{A}_i \mathbf{x}_i + \mathbf{w}_i & (3.1a) \\ y_i = \mathbf{c}_i \mathbf{x}_i + v_i & (3.1b) \end{cases}$$

where $\mathbf{x}_i \in \mathbb{C}^M$ denotes the channel impulse response state, $\mathbf{A}_i \in \mathbb{C}^{M \times M}$ is the state transition matrix, y_i is the scalar observation and the row vector \mathbf{c}_i consists of the transmitted symbol sequence at time i . Both \mathbf{w}_i and v_i are zero-mean circularly Gaussian complex white processes, with covariances \mathbf{Q}_w and variance σ_v^2 , respectively. They are mutually and temporally independent, and independent from the initial state \mathbf{x}_0 .

The model parameters including \mathbf{A}_i , \mathbf{Q}_w and σ_v^2 are not known in general. The transmitted symbols \mathbf{c}_i here are perfectly known, assuming the system works in training mode, or in decision directed mode with the error propagation effect neglected.

The goal then is to estimate the state process \mathbf{x}_i based on the observation sequence $\mathcal{Y}_i = \{y_1, \dots, y_i\}$. To do so the parameter set θ_i , which consists of \mathbf{A}_i , \mathbf{Q}_w and σ_v^2 , also needs to be estimated. Therefore, the problem is one of joint state and parameter estimation.

Note that it might be tempting to estimate all the unknown parameters, including \mathbf{A}_i , \mathbf{Q}_w and σ_v^2 , jointly with the state vector from the data. Doing so has several disadvantages. First, the number of unknown parameters becomes prohibitively large, $\mathcal{O}(M^2)$ given \mathbf{x}_i is $M \times 1$. That raises problems including algorithm instability and extra noise errors due to overparameterization. Secondly, it potentially causes large tracking errors if these parameters are actually time-varying due to the very long processing window needed. Despite the existence of noise estimation approaches mentioned in the previous section (they assume known model coefficients though and may not really apply), these approaches will not be pursued that in the current development. Instead, both \mathbf{Q}_w and σ_v^2 are treated as tuning parameters for the algorithm and only estimate \mathbf{A}_i jointly with the state. This work will focus on the priority issue, that is, the rapid channel variations. The effect of the choices of \mathbf{Q}_w and σ_v^2 on the steady-state tracking performance of EKF algorithm will be discussed later.

3.2.1 The EKF Procedure

Assume a random walk model for the parameters θ_i which contains the unknowns in \mathbf{A}_i only. Then, (3.1) becomes

$$\begin{cases} \boldsymbol{\theta}_{i+1} = \boldsymbol{\theta}_i + \mathbf{u}_i & (3.2a) \\ \mathbf{x}_{i+1} = \mathbf{A}(\boldsymbol{\theta}_i)\mathbf{x}_i + \mathbf{w}_i & (3.2b) \\ y_i = \mathbf{c}_i\mathbf{x}_i + v_i & (3.2c) \end{cases}$$

where \mathbf{u}_i , the process noise of $\boldsymbol{\theta}_i$, is i.i.d. zero-mean complex circularly Gaussian with covariance \mathbf{Q}_u , and independent from \mathbf{w}_i , v_i , \mathbf{x}_0 and $\boldsymbol{\theta}_0$.

Without any prior knowledge about the structure of \mathbf{A}_i , all elements of \mathbf{A}_i are assumed unknown, *i.e.* $\boldsymbol{\theta}_i = \mathbf{a}_i \triangleq \text{Vec}(\mathbf{A}_i)$. \mathbf{a}_i is an $M^2 \times 1$ column vector formed by stacking orderly all columns of the matrix \mathbf{A}_i . Special cases where some elements of \mathbf{A}_i are known to be zero can significantly reduce the number of unknown and the amount of computation.

The EKF procedure basically consists of i) state augmentation, ii) linearization and iii) applying the Kalman filter to the linearized model [Jaz70, And79, Lju79]. Appendix A contains the derivation of the EKF algorithm for (3.2), for general \mathbf{A}_i as well as diagonal and tridiagonal \mathbf{A}_i .

For reference the linearized model (c.f. (A.7) and (A.9)) and the time and measurement update steps for the general case(c.f. Table A.1) are restated here:

$$\begin{cases} \begin{bmatrix} \mathbf{a}_{i+1} \\ \mathbf{x}_{i+1} \end{bmatrix} \approx \begin{bmatrix} \mathbf{I}_{M^2} & \mathbf{0}_{M^2 \times M} \\ \hat{\mathbf{X}}_{i|i} & \hat{\mathbf{A}}_{i|i} \end{bmatrix} \begin{bmatrix} \mathbf{a}_i \\ \mathbf{x}_i \end{bmatrix} + \begin{bmatrix} \mathbf{u}_i \\ \mathbf{w}_i \end{bmatrix} + \mathbf{d}_i & (3.3a) \\ y_i = [0 \quad \mathbf{c}_i] \begin{bmatrix} \mathbf{a}_i \\ \mathbf{x}_i \end{bmatrix} + v_i & (3.3b) \end{cases}$$

where $\mathbf{X}_i \triangleq \mathbf{x}_i^t \otimes \mathbf{I}_M$ and \mathbf{d}_i is assumed deterministic as given in Appendix A.

$$\text{Time} \quad \hat{\mathbf{a}}_{i+1|i} = \hat{\mathbf{a}}_{i|i} \quad (3.4)$$

$$\text{Update:} \quad \hat{\mathbf{x}}_{i+1|i} = \hat{\mathbf{A}}_{i|i} \hat{\mathbf{x}}_{i|i} = \hat{\mathbf{X}}_{i|i} \hat{\mathbf{a}}_{i|i} \quad (3.5)$$

$$\mathbf{P}_{a,i+1|i} = \mathbf{P}_{a,i|i} + \mathbf{Q}_{u,i} \quad (3.6)$$

$$\begin{aligned} \mathbf{P}_{x,i+1|i} &= \hat{\mathbf{X}}_{i|i} \mathbf{P}_{a,i|i} \hat{\mathbf{X}}_{i|i}^h + \hat{\mathbf{A}}_{i|i} \mathbf{P}_{x,i|i} \hat{\mathbf{A}}_{i|i}^h \\ &\quad + \hat{\mathbf{X}}_{i|i} \mathbf{P}_{ax,i|i} \hat{\mathbf{A}}_{i|i}^h + \hat{\mathbf{A}}_{i|i} \mathbf{P}_{ax,i|i}^h \hat{\mathbf{X}}_{i|i}^h + \mathbf{Q}_{w,i} \end{aligned} \quad (3.7)$$

$$\mathbf{P}_{ax,i+1|i} = \mathbf{P}_{a,i|i} \hat{\mathbf{X}}_{i|i}^h + \mathbf{P}_{ax,i|i} \hat{\mathbf{A}}_{i|i}^h \quad (3.8)$$

$$\text{Measurement} \quad e_i = y_i - \mathbf{c}_i \hat{\mathbf{x}}_{i|i-1} \quad (3.9)$$

$$\text{Update:} \quad R_{e,i} = \mathbf{c}_i \mathbf{P}_{x,i|i-1} \mathbf{c}_i^h + \sigma_{v,i}^2 \quad (3.10)$$

$$\hat{\mathbf{a}}_{i|i} = \hat{\mathbf{a}}_{i|i-1} + \mathbf{k}_{a,i} e_i \quad (3.11)$$

$$\hat{\mathbf{x}}_{i|i} = \hat{\mathbf{x}}_{i|i-1} + \mathbf{k}_{x,i} e_i \quad (3.12)$$

$$\mathbf{P}_{a,i|i} = \mathbf{P}_{a,i|i-1} - \mathbf{k}_{a,i} R_{e,i} \mathbf{k}_{a,i}^h \quad (3.13)$$

$$\mathbf{P}_{x,i|i} = \mathbf{P}_{x,i|i-1} - \mathbf{k}_{x,i} R_{e,i} \mathbf{k}_{x,i}^h \quad (3.14)$$

$$\mathbf{P}_{ax,i|i} = \mathbf{P}_{ax,i|i-1} - \mathbf{k}_{a,i} R_{e,i} \mathbf{k}_{x,i}^h \quad (3.15)$$

where $\mathbf{k}_{a,i} \triangleq \mathbf{P}_{ax,i|i-1} \mathbf{c}_i^h R_{e,i}^{-1}$ and $\mathbf{k}_{x,i} \triangleq \mathbf{P}_{x,i|i-1} \mathbf{c}_i^h R_{e,i}^{-1}$ are the Kalman gains for the parameter and state estimates, respectively.

The key step in EKF is the linearization of the augmented state equation around the current state and parameter estimates. The coefficients of the resulting linear model and the Kalman gains thus become data dependent. This data-dependency constitutes the important difference between EKF and the standard Kalman filter. In the latter the state error covariance and Kalman gain do not depend on the observed data and can actually be calculated offline [And79]. This difference has fundamental impact on the algorithm behavior and properties such as the asymptotic stability, steady-state tracking capability, etc.

In the context of channel estimation, the off-diagonal elements of the \mathbf{A}_i specify

the coupling between channel tap fluctuations. In general strong cross-tap coupling is confined within a small neighborhood. Hence the elements in \mathbf{A}_i becomes less significant as they move further away from the main diagonal. These further off-diagonal elements of \mathbf{A} may thus be neglected (*i.e.* assumed to be equal to zero) without causing large estimation error. When the coupling is time varying, as occur in scenarios where the multipath arrivals change their drifting directions in delay, it is also desirable to dynamically populate the elements of \mathbf{A}_i to reflect this type of variations.

3.2.2 EKF Channel Estimation Error

From an adaptive tracking point of view, error analysis is often carried out in terms of the so-called *lag error* (associated with channel variations) and *noise error* (associated with observation noise). The asymptotic bounds for the mean squares of these error components are often sought to quantify the performance of particular algorithms, see, for instance, [Mac86] for LMS, [Ele86] for RLS, [Lju90] and [Guo95b] for a general framework that includes LMS, RLS and adaptive Kalman filter with random walk state model as special cases, and more recently [Pre05] for RLS applied to a state-space channel model. In [Ele86], the analysis is explicitly done in terms of the *excess error*, that is, the error above the MSE of the optimal Wiener solution, while others consider the total error. A common tool to facilitate this type of analysis is the so-called *direct averaging method* which was originally proposed in [Kus78].

This analysis methodology is applied to the EKF algorithm (3.4)-(3.15) in this section. First the decomposition of the total estimation error is carried out and the recursion for the *lag error* and the *noise error* are derived. Then similar to [Ele86], a decomposition of the *excess error* is derived and recursion forms for the *excess lag* and *noise errors* are given. The *excess error* in this case becomes the error above the MSE of the optimal Kalman solution assuming full model knowledge, compared to the Wiener solution as in [Ele86]. This is a natural result of the state-space

formulation. The steady-state MSE of the optimal Kalman estimate is specified by the solution of the associated steady-state Ricatti equation.

Due to the state-space formulation, the analysis becomes more challenging. Although previous efforts of analyzing the Kalman filter have been reported in [Lju90] and [Guo95b], the formulation does not include a full state-space model. Instead, a random walk model is assumed to simplify the analysis. The presence of a state transition matrix that is not an identity matrix complicates the error propagation equation and the *direct averaging method* becomes inadequate. In the case of EKF the difficulty is further increased due to the coupling between the parameter estimation error and state estimation error.

The purpose of the analysis here is two-fold. First, it gives insight into the EKF algorithm in terms of error propagation caused by channel variations and observation noises respectively, which is the basis for the discussion of tracking performance in section 3.4. Secondly, it shows that the EKF procedure can be viewed and derived as an adaptive filter, in the sense that once the recursion of the state and parameter estimate are chosen according to a generic stochastic approximation form, the EKF update equations of the associated error covariance matrices can be readily obtained by setting the adapting gains equal to the Kalman gains.

Assume that the channel state and parameter predictions are updated as follows:

$$\hat{\mathbf{a}}_{i+1|i} = \hat{\mathbf{a}}_{i|i-1} + \mathbf{p}_{a,i}e_i \quad (3.16)$$

$$\hat{\mathbf{x}}_{i+1|i} = \hat{\mathbf{A}}_{i|i}(\hat{\mathbf{x}}_{i|i-1} + \mathbf{p}_{x,i}e_i) \quad (3.17)$$

where $\mathbf{p}_{a,i}$ and $\mathbf{p}_{x,i}$ are some adapting gain for \mathbf{a}_i and \mathbf{x}_i respectively, and $e_i \triangleq y_i - \mathbf{c}_i\hat{\mathbf{x}}_{i|i-1}$ is the signal prediction error.

First, consider the total channel estimation error. Denoting $\tilde{\mathbf{x}}_{i|i-1} \triangleq \mathbf{x}_i - \hat{\mathbf{x}}_{i|i-1}$, it follows that $e_i = \mathbf{c}_i\tilde{\mathbf{x}}_{i|i-1} + v_i$. Also denote $\tilde{\mathbf{A}}_{i|i-1} \triangleq \mathbf{A}_i - \hat{\mathbf{A}}_{i|i-1}$, $\tilde{\mathbf{a}}_{i|i-1} \triangleq \text{Vec}(\tilde{\mathbf{A}}_{i|i-1})$, $\tilde{\mathbf{A}}_{i|i} \triangleq \mathbf{A}_i - \hat{\mathbf{A}}_{i|i}$ and $\tilde{\mathbf{a}}_{i|i} \triangleq \text{Vec}(\tilde{\mathbf{A}}_{i|i})$. Then subtracting (3.16) and (3.17) from the

original parameter and state model equations in (3.2) yields

$$\tilde{\mathbf{a}}_{i+1|i} = \tilde{\mathbf{a}}_{i|i-1} + \mathbf{p}_{a,i}\mathbf{c}_i\tilde{\mathbf{x}}_{i|i-1} - \mathbf{p}_{a,i}v_i + \mathbf{u}_i \quad (3.18)$$

$$\tilde{\mathbf{x}}_{i+1|i} = [\hat{\mathbf{A}}_{i|i}(\mathbf{I}_M - \mathbf{p}_{x,i}\mathbf{c}_i)]\tilde{\mathbf{x}}_{i|i-1} + \tilde{\mathbf{A}}_{i|i}\mathbf{x}_i + \mathbf{w}_i - (\hat{\mathbf{A}}_{i|i}\mathbf{p}_{x,i})v_i \quad (3.19)$$

$$= [\hat{\mathbf{A}}_{i|i}(\mathbf{I}_M - \mathbf{p}_{x,i}\mathbf{c}_i) - \mathbf{X}_i\mathbf{p}_{a,i}\mathbf{c}_i]\tilde{\mathbf{x}}_{i|i-1} + \mathbf{X}_i\tilde{\mathbf{a}}_{i|i-1} + \mathbf{w}_i - (\hat{\mathbf{A}}_{i|i}\mathbf{p}_{x,i} + \mathbf{X}_i\mathbf{p}_{a,i})v_i \quad (3.20)$$

where $\mathbf{X}_i \triangleq \mathbf{x}_i^t \otimes \mathbf{I}_M$. The identity $\tilde{\mathbf{A}}_{i|i}\mathbf{x}_i = \mathbf{X}_i\tilde{\mathbf{a}}_{i|i}$ and the fact that $\hat{\mathbf{a}}_{i|i} = \hat{\mathbf{a}}_{i+1|i} = \hat{\mathbf{a}}_{i|i-1} + \mathbf{p}_{a,i}e_i$ have been used in deriving (3.20). \mathbf{w}_i , \mathbf{u}_i and v_i are the true noise terms whose covariance and variance are specified by the original model, independent of what are assumed by the algorithm. The assumed covariance and variance only determine the adapting gains $\mathbf{p}_{a,i}$ and $\mathbf{p}_{x,i}$.

Equations (3.18) and (3.20) show how the parameter and state estimation errors are coupled. In addition, the last term in (3.20) is associated the observation noise and would increase as the adapting gains $\mathbf{p}_{a,i}$ and $\mathbf{p}_{x,i}$ increase. The sum of the second and third terms in (3.20) may be considered as *lag error* forcing term, since they are associated with the channel variations and the estimation error of its dynamics.

In the following analysis, $\mathbf{p}_{x,i}$, $\mathbf{p}_{a,i}$ and $\hat{\mathbf{A}}_{i|i}$ are treated as nonrandom. It is then straightforward to show that taking covariance on both sides of (3.18) and letting $\mathbf{p}_{a,i} = \mathbf{k}_{a,i}$ yields an update equation for $\mathbf{P}_{\tilde{\mathbf{a}},i|i-1} \triangleq E\{\tilde{\mathbf{a}}_{i|i-1}\tilde{\mathbf{a}}_{i|i-1}^h\}$ that has the same form as (3.6) and (3.13) combined, *i.e.* the update equation for $\mathbf{P}_{\mathbf{a},i+1|i}$ from $\mathbf{P}_{\mathbf{a},i|i-1}$, the assumed parameter error covariance.

Taking covariance on both sides of (3.20) and denoting $\mathbf{P}_{\tilde{\mathbf{x}},i|i-1} \triangleq E\{\tilde{\mathbf{x}}_{i|i-1}\tilde{\mathbf{x}}_{i|i-1}^h\}$,

$\mathbf{P}_{\tilde{x}_{a,i|i-1}} \triangleq E\{\tilde{\mathbf{x}}_{i|i-1}\tilde{\mathbf{a}}_{i|i-1}^h\}$ and $\mathbf{P}_{\tilde{a}_{x,i|i-1}} \triangleq E\{\tilde{\mathbf{a}}_{i|i-1}\tilde{\mathbf{x}}_{i|i-1}^h\}$ yields

$$\begin{aligned}
\mathbf{P}_{\tilde{x},i+1|i} &= [\widehat{\mathbf{A}}_{i|i}(\mathbf{I}_M - \mathbf{p}_{x,i}\mathbf{c}_i) - \mathbf{X}_i\mathbf{p}_{a,i}\mathbf{c}_i]\mathbf{P}_{\tilde{x},i|i-1}[\widehat{\mathbf{A}}_{i|i}(\mathbf{I}_M - \mathbf{p}_{x,i}\mathbf{c}_i) - \mathbf{X}_i\mathbf{p}_{a,i}\mathbf{c}_i]^h \\
&\quad + \mathbf{X}_i\mathbf{P}_{\tilde{a},i|i-1}\mathbf{X}_i^h + [\widehat{\mathbf{A}}_{i|i}(\mathbf{I}_M - \mathbf{p}_{x,i}\mathbf{c}_i) - \mathbf{X}_i\mathbf{p}_{a,i}\mathbf{c}_i]\mathbf{P}_{\tilde{x}_{a},i|i-1}\mathbf{X}_i^h \\
&\quad + \mathbf{X}_i\mathbf{P}_{\tilde{a}_{x},i|i-1}[\widehat{\mathbf{A}}_{i|i}(\mathbf{I}_M - \mathbf{p}_{x,i}\mathbf{c}_i) - \mathbf{X}_i\mathbf{p}_{a,i}\mathbf{c}_i]^h + \mathbf{Q}_w \\
&\quad + \sigma_v^2\|\widehat{\mathbf{A}}_{i|i}\mathbf{p}_{x,i} + \mathbf{X}_i\mathbf{p}_{a,i}\|^2\mathbf{I}
\end{aligned} \tag{3.21}$$

where again the last term is the observation *noise error* forcing term and the sum of the second, third and fourth terms are the *lag error* forcing terms associated with uncertainty in dynamic parameter estimation and the channel process noise.

It can be shown that letting $\mathbf{p}_{x,i} = \mathbf{k}_{x,i}$ and replacing \mathbf{X} by $\widehat{\mathbf{X}}_{i|i}$ in (3.21) lead to (3.7) and (3.14) combined, *i.e.* the update equation for $\mathbf{P}_{x,i+1|i}$ from $\mathbf{P}_{x,i|i-1}$, the assumed channel estimation error covariance.

Reorganizing (3.16) and (3.17), it gives the following state-space form for the state and parameter prediction error propagation:

$$\begin{bmatrix} \tilde{\mathbf{x}}_{i+1|i} \\ \tilde{\mathbf{a}}_{i+1|i} \end{bmatrix} = \begin{bmatrix} \widehat{\mathbf{A}}_{i|i}(\mathbf{I}_M - \mathbf{p}_{x,i}\mathbf{c}_i) - \mathbf{X}_i\mathbf{p}_{a,i}\mathbf{c}_i & \mathbf{X}_i \\ -\mathbf{p}_{a,i}\mathbf{c}_i & \mathbf{I}_{M^2} \end{bmatrix} \begin{bmatrix} \tilde{\mathbf{x}}_{i|i-1} \\ \tilde{\mathbf{a}}_{i|i-1} \end{bmatrix} - \begin{bmatrix} \widehat{\mathbf{A}}_{i|i}\mathbf{p}_{x,i} + \mathbf{X}_i\mathbf{p}_{a,i} \\ \mathbf{p}_{a,i} \end{bmatrix} v_i + \begin{bmatrix} \mathbf{w}_i \\ \mathbf{u}_i \end{bmatrix} \tag{3.22}$$

Choosing *ad hoc* values for the state process noise covariance \mathbf{Q}_w and observation noise variance σ_v^2 in EKF is equivalent to choosing adapting gains $\mathbf{p}_{a,i}$ and $\mathbf{p}_{x,i}$ in (3.16) and (3.17) that may be different from $\mathbf{k}_{a,i}$ and $\mathbf{k}_{x,i}$ respectively, and have effects on the *lag error* and *noise error* contributions.

The channel estimation error derived above contains both the error associated with the optimal Kalman filter with perfect system knowledge as well as the excess error due to the unknown parameters in \mathbf{A}_i as well as the inaccurate noise covariances. The latter is analogous to the gradient noise in LMS and the *misadjustment noise* in RLS. However the component associated with unknown parameters in \mathbf{A}_i is unique to the current formulation.

Consider the excess error. Assuming perfect system knowledge, the Kalman filter channel estimate $\hat{\mathbf{x}}_{i+1|i}^o$, and error $\tilde{\mathbf{x}}_{i+1|i}^o$ can be written as follows:

$$\hat{\mathbf{x}}_{i+1|i}^o = \mathbf{A}_i(\hat{\mathbf{x}}_{i|i-1}^o + \mathbf{k}_i \mathbf{c}_i \tilde{\mathbf{x}}_{i|i-1}^o + \mathbf{k}_i v_i) \quad (3.23)$$

$$\tilde{\mathbf{x}}_{i+1|i}^o = \mathbf{A}_i(\mathbf{I}_M - \mathbf{k}_i \mathbf{c}_i) \tilde{\mathbf{x}}_{i|i-1}^o + \mathbf{w}_i - \mathbf{A}_i \mathbf{k}_i v_i \quad (3.24)$$

where \mathbf{k}_i is the optimal Kalman gain for the state estimates.

Denoting $\delta \tilde{\mathbf{x}}_{i|i-1}^o \triangleq \tilde{\mathbf{x}}_{i|i-1} - \tilde{\mathbf{x}}_{i|i-1}^o$ as the excess error and subtracting (3.24) from (3.20) yields

$$\begin{aligned} \delta \tilde{\mathbf{x}}_{i+1|i}^o &= [\hat{\mathbf{A}}_{i|i}(\mathbf{I}_M - \mathbf{p}_{x,i} \mathbf{c}_i)] \delta \tilde{\mathbf{x}}_{i|i-1}^o \\ &\quad + [\tilde{\mathbf{A}}_{i|i}(\mathbf{I}_M - \mathbf{k}_i \mathbf{c}_i) - \hat{\mathbf{A}}_{i|i} \delta \mathbf{p}_{x,i} \mathbf{c}_i] \tilde{\mathbf{x}}_{i|i-1}^o \\ &\quad + \tilde{\mathbf{A}}_{i|i} \mathbf{x}_i - (\hat{\mathbf{A}}_{i|i} \mathbf{p}_{x,i} - \mathbf{A}_i \mathbf{k}_i) v_i \\ &= [\hat{\mathbf{A}}_{i|i}(\mathbf{I}_M - \mathbf{p}_{x,i} \mathbf{c}_i) - \mathbf{X}_i \mathbf{p}_{a,i} \mathbf{c}_i] \delta \tilde{\mathbf{x}}_{i|i-1}^o \\ &\quad + [\tilde{\mathbf{A}}_{i|i}(\mathbf{I}_M - \mathbf{k}_i \mathbf{c}_i) - \hat{\mathbf{A}}_{i|i} \delta \mathbf{p}_{x,i} \mathbf{c}_i - \mathbf{X}_i \mathbf{p}_{a,i} \mathbf{c}_i] \tilde{\mathbf{x}}_{i|i-1}^o \\ &\quad + \tilde{\mathbf{A}}_{i|i-1} \mathbf{x}_i - (\hat{\mathbf{A}}_{i|i} \mathbf{p}_{x,i} - \mathbf{A}_i \mathbf{k}_i + \mathbf{X}_i \mathbf{p}_{a,i}) v_i \end{aligned} \quad (3.25)$$

where $\delta \mathbf{p}_{x,i} \triangleq \mathbf{p}_{x,i} - \mathbf{k}_i$. The second equality used $\tilde{\mathbf{A}}_{i|i} \mathbf{x}_i = \mathbf{X}_i \tilde{\mathbf{a}}_{i|i} = \mathbf{X}_i [\tilde{\mathbf{a}}_{i|i-1} + \mathbf{p}_{a,i}(\mathbf{c}_i \tilde{\mathbf{x}}_{i|i-1} + v_i)]$.

The second, third and last term on the right hand side of (3.25) are the error associated with the optimal Kalman filter, the error due to inaccurate parameter estimation and the observation noise error term, respectively. It can be verified that the sum of all three terms becomes zero if $\tilde{\mathbf{A}}_{i|i} = \mathbf{0}$ and $\mathbf{p}_{x,i} = \mathbf{k}_i$. Hence (3.25) makes it explicit that excess errors are caused by the parameter estimation error and the inaccurate assumption of noise covariances which causes $\mathbf{p}_{x,i}$ to deviate from \mathbf{k}_i . Note that the process noise does not contribute to excess errors directly.

3.2.3 EKF vs. MMSE and ML Estimation

In this section, EKF parameter estimation is compared with minimum mean squared prediction error (MMSE) estimation and maximum likelihood (ML) parameter estimation. It is shown that modifications to the EKF algorithm based on such comparison as proposed in [Lju79] essentially involves applying correction terms to the time-update and measurement update equations. These correction terms are the first and second-order functions of the signal prediction error. The main purpose of the analysis in this section is to establish a connecting point between the EKF algorithm and the EM algorithms. In the next chapter, it will be shown that this second-order correction also exists in the suboptimal EM algorithms.

Before venturing into comparing EKF with MMSE and ML estimation, the suboptimality of EKF can be argued intuitively as follows. One advantage of EKF is that it is recursive, hence, efficient, while most optimal implementations are iterative (see, for instance, the EM algorithm developed in the next chapter). Yet this efficiency comes at the expense of performance loss. This can be argued based on the principle of orthogonality. It is well known that the Kalman filter, applied to linear Gauss-Markov model, orthogonalizes the observation sequence into the innovation sequence. It recursively computes the optimal (filtered or predicted) state estimate at time i given \mathcal{Y}_i , the set of all available observation samples up to i . While the state estimate prior to i can be improved by smoothing over \mathcal{Y}_i , that has no effect on the (filtered or predicted) state estimate at time i given \mathcal{Y}_i , due to the orthogonality of the innovation sequence. This is not true for EKF. The sequence of prediction errors in EKF does not guarantee orthogonality. Conceivably the EKF state estimate at time n can always be improved by smoothing earlier states. Loosely speaking, the lack of orthogonality in the prediction error sequence renders the recursive EKF algorithm suboptimal.

In the following, as a parameter estimator the EKF is compared with the stochastic descent algorithms that recursively minimize the mean squared signal prediction

error or the negative log-likelihood function. The development here is mainly based on Ljung [Lju79] where two modifications of the EKF algorithms were originally proposed in a general joint estimation setting. The analysis presented here establishes the explicit connections between the descent direction (*i.e.* the negative gradient) of the stochastic gradient algorithms and the parameter Kalman gain in the EKF, while in [Lju79] it was the asymptotic ordinary differential equations (ODE) associated with each algorithm that were compared and matched.

1. The EKF vs the stochastic descent algorithm that minimizes the mean squared prediction error (MSE).

The criterion is to seek the minimization of

$$V_1(\boldsymbol{\theta}) = E\{J_i(\boldsymbol{\theta})\} \triangleq E\{|e_i(\boldsymbol{\theta})|^2\} \quad (3.26)$$

where $J_i(\boldsymbol{\theta}) \triangleq |e_i(\boldsymbol{\theta})|^2$, and $e_i(\boldsymbol{\theta}) = y_i - \mathbf{c}_i \widehat{\mathbf{x}}_{i|i-1}(\boldsymbol{\theta})$ is the prediction error assuming $\boldsymbol{\theta}$ as the model parameter. The stochastic descent direction for minimizing $V_1(\boldsymbol{\theta})$ is the complex gradient which, according to [Bra83] and [Hay96], is given by twice the conjugate derivative:

$$\begin{aligned} \nabla J_i(\boldsymbol{\theta}) &= 2 \frac{\partial J_i(\boldsymbol{\theta})}{\partial \boldsymbol{\theta}^*} \\ &= 2 \frac{\partial e_i^*(\boldsymbol{\theta})}{\partial \boldsymbol{\theta}^*} e_i(\boldsymbol{\theta}) + e_i^*(\boldsymbol{\theta}) \frac{\partial e_i(\boldsymbol{\theta})}{\partial \boldsymbol{\theta}^*} \\ &= 2 \frac{\partial e_i^*(\boldsymbol{\theta})}{\partial \boldsymbol{\theta}^*} e_i(\boldsymbol{\theta}) \\ &= -2 \left[\frac{\partial \widehat{\mathbf{x}}_{i|i-1}}{\partial \boldsymbol{\theta}} \right]^h \mathbf{c}_i^h e_i(\boldsymbol{\theta}) \end{aligned} \quad (3.27)$$

where the second equality assumes that $e_i(\boldsymbol{\theta}) = y_i - \mathbf{c}_i \mathbf{A} \widehat{\mathbf{x}}_{i-1|i-1} + \mathbf{c}_i \mathbf{w}_i + v_i = y_i - (\widehat{\mathbf{x}}_{i-1|i-1}^T \otimes \mathbf{c}_i) \boldsymbol{\theta} + \mathbf{c}_i \mathbf{w}_i + v_i$ is analytic in $\boldsymbol{\theta}$, hence $\frac{\partial e_i(\boldsymbol{\theta})}{\partial \boldsymbol{\theta}^*} = \mathbf{0}$. Details regarding complex gradient and conjugate derivatives may be found in [Bra83]

and [Hay96]. The conjugate derivative $\frac{\partial}{\partial \boldsymbol{\theta}^*}$ is defined as

$$\frac{\partial}{\partial \boldsymbol{\theta}^*} \triangleq \frac{\partial}{\partial \boldsymbol{\theta}_r} + j \frac{\partial}{\partial \boldsymbol{\theta}_i} \quad (3.28)$$

where $\boldsymbol{\theta}_r$ and $\boldsymbol{\theta}_i$ are the real and imaginary parts of $\boldsymbol{\theta}$, respectively. $j = \sqrt{-1}$.

It follows that the EKF parameter estimation would be the same as a stochastic descent algorithm minimizing the MSE if

$$\mathbf{k}_{a,i} = 2 \left[\frac{\partial \widehat{\mathbf{x}}_{i|i-1}}{\partial \boldsymbol{\theta}} \right]^h \mathbf{c}_i^h \quad (3.29)$$

$$\mathbf{P}_{ax,i|i-1} = 2 \left[\frac{\partial \widehat{\mathbf{x}}_{i|i-1}}{\partial \boldsymbol{\theta}} \right]^h R_{e_i} \quad (3.30)$$

where $\mathbf{P}_{ax,i|i-1}$ is the one-step prediction error cross-covariance and $\mathbf{k}_{a,i}$ is the parameter Kalman gain. Following the derivation given in [Lju79],

$$\begin{aligned} \frac{\partial \widehat{\mathbf{x}}_{i+1|i}}{\partial \theta_k} &= \mathbf{A}_i (\mathbf{I}_M - \mathbf{k}_{x,i} \mathbf{c}_i) \frac{\partial \widehat{\mathbf{x}}_{i|i-1}}{\partial \theta_k} + \frac{\partial \mathbf{A}_i}{\partial \theta_k} \widehat{\mathbf{x}}_{i|i} + \mathbf{A}_i \left[\frac{\partial \mathbf{k}_{x,i}(\boldsymbol{\theta})}{\partial \theta_k} \right] e_i \\ &= \mathbf{A}_i (\mathbf{I}_M - \mathbf{k}_{x,i} \mathbf{c}_i) \frac{\partial \widehat{\mathbf{x}}_{i|i-1}}{\partial \theta_k} + \frac{\partial \mathbf{A}_i}{\partial \theta_k} \widehat{\mathbf{x}}_{i|i} \\ &\quad + \left[\mathbf{A}_i (\mathbf{I}_M - \mathbf{k}_{x,i} \mathbf{c}_i) \frac{\partial \mathbf{P}_{x,i|i-1}}{\partial \theta_k} \right] \mathbf{c}_i^h R_{e_i}^{-1} e_i \end{aligned} \quad (3.31)$$

where R_{e_i} is the assumed covariance of e_i , θ_k is the k th elements of the unknown parameter vector $\boldsymbol{\theta}$.

The last term in (3.31) may be viewed as associated with the derivative of $\widehat{\mathbf{x}}_{i|i}$ with regard to $\boldsymbol{\theta}$. For the EKF, as shown in Appendix A, $\widehat{\mathbf{x}}_{i|i}$ is assumed to be independent from $\boldsymbol{\theta}$ in the EKF linearization and the last term in (3.31) is missing. It was suggested in [Lju79] that it should be included in the state transition matrix of the linearized model.

2. EKF vs stochastic descent algorithm that maximizes the log-likelihood function (ML).

The negative log-likelihood function is given as follows

$$\begin{aligned} V_2(\boldsymbol{\theta}) &= E\{e_i^*(\boldsymbol{\theta})R_{e_i}^{-1}(\boldsymbol{\theta})e_i(\boldsymbol{\theta})\} + \log(\det(R_{e_i}(\boldsymbol{\theta}))) \\ &= E\{e_i^*(\boldsymbol{\theta})R_{e_i}^{-1}(\boldsymbol{\theta})e_i(\boldsymbol{\theta})\} + \log(R_{e_i}(\boldsymbol{\theta})) \end{aligned} \quad (3.32)$$

since the assumed prediction error covariance R_{e_i} is a scalar in our case.

Then the steepest descent direction for minimizing $V_2(\boldsymbol{\theta})$ is given by (generalized from [Lju79] with complex $\boldsymbol{\theta}$):

$$\begin{aligned} \nabla V_2(\boldsymbol{\theta}) &= 2\frac{\partial V_2(\boldsymbol{\theta})}{\partial \boldsymbol{\theta}^*} \\ &= 2E\left\{\frac{\partial e_i^*(\boldsymbol{\theta})}{\partial \boldsymbol{\theta}^*}R_{e_i}^{-1}(\boldsymbol{\theta})e_i(\boldsymbol{\theta})\right\} + \\ &\quad - 2E\left\{e_i(\boldsymbol{\theta})R_{e_i}^{-1}(\boldsymbol{\theta})\frac{\partial R_{e_i}^{-1}(\boldsymbol{\theta})}{\partial \boldsymbol{\theta}^*}R_{e_i}^{-1}(\boldsymbol{\theta})e_i^*(\boldsymbol{\theta})\right\} \\ &\quad + 2\text{tr}\left(R_{e_i}^{-1}(\boldsymbol{\theta})\frac{\partial R_{e_i}^{-1}(\boldsymbol{\theta})}{\partial \boldsymbol{\theta}^*}\right) \end{aligned} \quad (3.33)$$

where the conjugate derivative is defined in (3.28) and the terms associated with $\frac{\partial e_i(\boldsymbol{\theta})}{\partial \boldsymbol{\theta}^*}$ are equal to zero due to the same reason mentioned in (3.27) and not included.

Note that the last two terms would cancel if R_{e_i} is indeed the true covariance of the prediction error. Accordingly, the measurement update equation of the parameter estimate can be modified as the stochastic gradient algorithm (*i.e.* remove the expectations in (3.33)) that minimizes $V_2(\boldsymbol{\theta})$:

$$\widehat{\boldsymbol{\theta}}_{i|i} = \widehat{\boldsymbol{\theta}}_{i|i-1} + \mathbf{k}_{\boldsymbol{\theta},i}e_i + \zeta_i \quad (3.34)$$

where

$$\mathbf{k}_{\theta,i} = 2 \frac{\partial e_i^*(\boldsymbol{\theta})}{\partial \boldsymbol{\theta}^*} R_{e_i}^{-1}(\boldsymbol{\theta}) \quad (3.35)$$

$$\zeta_i \triangleq -2e_i(\boldsymbol{\theta}) R_{e_i}^{-1}(\boldsymbol{\theta}) \frac{\partial R_{e_i}^{-1}(\boldsymbol{\theta})}{\partial \boldsymbol{\theta}^*} R_{e_i}^{-1}(\boldsymbol{\theta}) e_i^*(\boldsymbol{\theta}) + 2\text{tr}(R_{e_i}^{-1}(\boldsymbol{\theta}) \frac{\partial R_{e_i}^{-1}(\boldsymbol{\theta})}{\partial \boldsymbol{\theta}^*}) \quad (3.36)$$

Modifications as Higher-Order Innovation Terms

The modifications above effectively add first and second-order innovation terms to the time-update equation (the first modification) and the measurement-update equation (the second modification), respectively.

For the first modification, according to (3.31), $\widehat{\mathbf{X}}_{i|i}$ in (3.5)-(3.8) should be replaced by

$$\widehat{\mathbf{X}}_{i|i} \triangleq \widehat{\mathbf{X}}_{i|i} + \mathbf{L}_i e_i \quad (3.37)$$

where

$$\mathbf{L}_i \triangleq \left[(\mathbf{A}_i - \mathbf{k}_{x,i} \mathbf{c}_i) \frac{\partial \mathbf{P}_{x,i|i-1}}{\partial \boldsymbol{\theta}} \Big|_{\widehat{\boldsymbol{\theta}}} \right] \mathbf{c}_i^h R_{e_i}^{-1} \quad (3.38)$$

As a result, (3.5), (3.7) and (3.8) becomes

$$\widehat{\mathbf{x}}_{i+1|i} = \widehat{\mathbf{X}}_{i|i} \widehat{\mathbf{a}}_{i|i} + \mathbf{L}_i \widehat{\mathbf{a}}_{i|i} e_i \quad (3.39)$$

$$\begin{aligned} \mathbf{P}_{x,i+1|i} &= \widehat{\mathbf{X}}_{i|i} \mathbf{P}_{a,i|i} \widehat{\mathbf{X}}_{i|i}^h + \widehat{\mathbf{A}}_{i|i} \mathbf{P}_{x,i|i} \widehat{\mathbf{A}}_{i|i}^h \\ &\quad + \widehat{\mathbf{X}}_{i|i} \mathbf{P}_{ax,i|i} \widehat{\mathbf{A}}_{i|i}^h + \widehat{\mathbf{A}}_{i|i} \mathbf{P}_{ax,i|i}^h \widehat{\mathbf{X}}_{i|i}^h + Q_{\mathbf{w},i} \\ &\quad + \mathbf{L}_i \mathbf{P}_{a,i|i} \mathbf{L}_i^h e_i e_i^* + \mathbf{L}_i \mathbf{P}_{a,i|i} \widehat{\mathbf{X}}_{i|i}^h e_i + \\ &\quad + \widehat{\mathbf{X}}_{i|i} \mathbf{P}_{a,i|i} \mathbf{L}_i^h e_i^* + \mathbf{L}_i \mathbf{P}_{ax,i|i} \widehat{\mathbf{A}}_{i|i}^h e_i \end{aligned} \quad (3.40)$$

$$\mathbf{P}_{ax,i+1|i} = \mathbf{P}_{a,i|i} \widehat{\mathbf{X}}_{i|i}^h + \mathbf{P}_{ax,i|i} \widehat{\mathbf{A}}_{i|i}^h + \mathbf{P}_{a,i|i} \mathbf{L}_i e_i \quad (3.41)$$

respectively. The innovation terms in (3.39), (3.40) and (3.41) account for the dependency of $\widehat{\mathbf{x}}_{i|i}$ on $\boldsymbol{\theta}_i$ or \mathbf{a}_i .

In the second modification, recall $R_{e_i} = \mathbf{c}_i \mathbf{P}_{x,i|i-1} \mathbf{c}_i^h + \sigma_v^2$ is scalar, ζ_i can be

further simplified as

$$\zeta_i \triangleq \mathbf{k}_{\theta,i,2} (1 - e_i(\boldsymbol{\theta}) R_{e_i}^{-1}(\boldsymbol{\theta}) e_i^*(\boldsymbol{\theta})) \quad (3.42)$$

where the gain for the second order innovation term is given by

$$\mathbf{k}_{\theta,i,2} \triangleq 2 \frac{\partial R_{e_i}^{-1}(\boldsymbol{\theta})}{\partial \boldsymbol{\theta}^*} R_{e_i}^{-1}(\boldsymbol{\theta}) = 2 \mathbf{c}_i \frac{\partial \mathbf{P}_{x,i|i-1}}{\partial \boldsymbol{\theta}^*} \mathbf{c}_i^h R_{e_i}^{-1}(\boldsymbol{\theta}) \quad (3.43)$$

(3.42) is exactly a second-order innovation term which converts the difference between the assumed prediction error covariance and the squared prediction error into a parameter update component. It may be viewed as a second-order new innovation. It would have zero mean if the assumed prediction error covariance is the true covariance.

In Chapter 4, a second-order innovation terms identical to (3.42) will be found in the sequential suboptimal EM algorithm, which is not coincidental since this modified EKF algorithm is derived by matching the stochastic descent algorithm that minimizes the negative log-likelihood function (or ML), and EM is an approximating scheme for ML estimation.

3.3 Parameter Observability and Detectability

In this section the issue of parameter observability and detectability is considered. More specifically, it shows that when the channel is either explicitly sparse, *i.e.* there exist quiescent taps with little energy, or confined within a rank p subspace of \mathbb{C}^M with $p < M$, then the unknown parameters associated with the quiescent taps or the orthogonal subspace are not observable, and are further not detectable if their models are unstable. This has important implications on the application of EKF algorithm to estimate wideband multipath channels which usually have either explicit sparse structure or correlated tap fluctuations.

The development in this section centers around the concepts of observability

and detectability from linear system theory, for details please see, for instance, [And79][Aok67].

The main results are Theorem 1, Corollary 2 and Corollary 3, which address the issues of parameter observability and/or detectability for explicitly sparse channels and correlated channels, respectively.

Theorem 1 necessary conditions for parameter observability *Consider the linearized augmented state space model (3.3). Let $n > 0$ and $K \geq L \triangleq M^2 + M$, here M is the original state dimension. The necessary conditions for the parameter to be observable are that the sequence of state estimates, $\hat{\mathbf{x}}_{i|i}$ for $n \leq i \leq n + K - 1$, be persistently exciting and the nominal system for the original state be observable, in the sense that the matrix whose rows are vectors $\mathbf{c}_{n+m} \prod_{j=i+1}^m \hat{\mathbf{A}}_{n+j|n+j}$ for $m = 1, \dots, K - 1$ and $i = 1, \dots, m$ is full rank.*

In the following we present the proofs for Theorem 1. For notational compactness, denoting

$$\mathbf{F}_i \triangleq \begin{bmatrix} \mathbf{I}_{M^2} & \mathbf{0}_{M^2 \times M} \\ \hat{\mathbf{X}}_{i|i} & \hat{\mathbf{A}}_{i|i} \end{bmatrix} \quad (3.44)$$

$$\mathbf{h}_i \triangleq [\mathbf{0} \ \mathbf{c}_i] \quad (3.45)$$

The observability matrix of the system (3.3) for $n \leq i \leq n + K$ is given as follows:

$$\mathcal{O}_{n,n+K-1} \triangleq \begin{bmatrix} \mathbf{h}_n \\ \mathbf{h}_{n+1} \mathbf{F}_{n+1} \\ \vdots \\ \mathbf{h}_{n+K-1} \mathbf{F}_{n+K-1} \mathbf{F}_{n+K-2} \cdots \mathbf{F}_{n+1} \end{bmatrix} \quad (3.46)$$

The state \mathbf{z}_n is said to be completely observable during the time $n \leq i \leq n + K - 1$ if $\mathcal{O}_{n,n+K-1}$ has full rank. If $\mathcal{O}_{n,n+K-1}$ does not have full rank but the unobservable elements of the unknown parameters are stable, \mathbf{z}_n is said to be detectable.

Using (C.8) and (3.44), it gives

$$\mathbf{F}_{n+m}\mathbf{F}_{n+m-1}\cdots\mathbf{F}_{n+1} = \begin{bmatrix} \mathbf{I}_{M^2} & \mathbf{0}_{M^2 \times M} \\ \sum_{i=1}^m \widehat{\mathbf{x}}_{n+i|n+i}^t \otimes \left(\prod_{j=i+1}^m \widehat{\mathbf{A}}_{n+j|n+j}\right) & \prod_{i=1}^m \widehat{\mathbf{A}}_{n+i|n+i} \end{bmatrix} \quad (3.47)$$

and

$$\mathbf{h}_{n+m}\mathbf{F}_{n+m}\mathbf{F}_{n+m-1}\cdots\mathbf{F}_{n+1} = \begin{bmatrix} \sum_{i=1}^m \widehat{\mathbf{x}}_{n+i|n+i}^t \otimes \left(\mathbf{c}_{n+m} \prod_{j=i+1}^m \widehat{\mathbf{A}}_{n+j|n+j}\right) & \mathbf{c}_{n+m} \prod_{i=1}^m \widehat{\mathbf{A}}_{n+i|n+i} \end{bmatrix} \quad (3.48)$$

for $m > 1$. Substituting (3.48) into (3.46), it yields

$$\mathcal{O}_{n,n+K-1} \triangleq [\mathcal{O}_{a,n,n+K-1} \quad \mathcal{O}_{x,n,n+K-1}] \quad (3.49)$$

where

$$\mathcal{O}_{a,n,n+K-1} \triangleq \begin{bmatrix} \mathbf{0}_{1 \times M^2} \\ \widehat{\mathbf{x}}_{n+1|n+1}^t \otimes \mathbf{c}_{n+1} \\ \vdots \\ \sum_{i=1}^m \widehat{\mathbf{x}}_{n+i|n+i}^t \otimes \left(\mathbf{c}_{n+m} \prod_{j=i+1}^m \widehat{\mathbf{A}}_{n+j|n+j}\right) \\ \vdots \\ \sum_{i=1}^{K-1} \widehat{\mathbf{x}}_{n+i|n+i}^t \otimes \left(\mathbf{c}_{n+K-1} \prod_{j=i+1}^{K-1} \widehat{\mathbf{A}}_{n+j|n+j}\right) \end{bmatrix} \quad (3.50)$$

$$\mathcal{O}_{x,n,n+K-1} \triangleq \begin{bmatrix} \mathbf{c}_n \\ \mathbf{c}_{n+1} \widehat{\mathbf{A}}_{n+1|n+1} \\ \vdots \\ (\mathbf{c}_{n+m} \prod_{j=1}^m \widehat{\mathbf{A}}_{n+j|n+j}) \\ \vdots \\ (\mathbf{c}_{n+K-1} \prod_{j=1}^{K-1} \widehat{\mathbf{A}}_{n+j|n+j}) \end{bmatrix} \quad (3.51)$$

$\mathcal{O}_{a,n,n+K-1}$ and $\mathcal{O}_{x,n,n+K-1}$ are the blocks of the observability matrix associated with the parameter vector \mathbf{a} and the original state \mathbf{x} respectively. $\mathcal{O}_{x,n,n+K-1}$ in fact is the observability matrix of the original linear state-space model assuming $\mathbf{A}_n = \widehat{\mathbf{A}}_{n|n}$.

It should be noted $\mathcal{O}_{a,n,n+K-1}$ and $\mathcal{O}_{x,n,n+K-1}$ are not the observability matrices for \mathbf{a} and \mathbf{x} in the linearized model (3.3) respectively. They are used here as shorthand notations within $\mathcal{O}_{n,n+K-1}$ that indicate their respective association with \mathbf{a} and \mathbf{x} .

The proof proceeds by considering two separate cases: 1) the nominal state system is observable while the sequence of state estimates is not persistent exciting; 2) the sequence of state estimates is persistently exciting while the nominal state system is not observable. In either case, it is shown that the matrix $\mathcal{O}_{a,n,n+K-1}$ hence the observability matrix $\mathcal{O}_{n,n+K-1}$ is rank-deficient.

1. Under the assumption that the nominal state system is observable while the sequence of state estimates is not persistent exciting, *i.e.* $\widehat{\mathbf{x}}_{i|i}$ for $n \leq i \leq n + K - 1$, only span a rank p subspace of \mathbf{C}^M with $p < M$, it follows that \exists non-zero $\mathbf{v} \in \mathbf{C}^M$, such that

$$\widehat{\mathbf{x}}_{n+i|n+i}^t \mathbf{v} = 0, \text{ for } n \leq i \leq n + K - 1 \quad (3.52)$$

Then multiplying $\mathcal{O}_{n,n+K-1}$ by $\begin{bmatrix} \mathbf{v} \otimes \mathbf{e}_1 \\ \mathbf{0}_{M \times 1} \end{bmatrix}$ with \mathbf{e}_1 being any nonzero $M \times 1$

vector, it yields

$$\begin{aligned}
\mathcal{O}_{n,n+K-1}(\mathbf{v} \otimes \mathbf{e}_1) &= \mathcal{O}_{a,n,n+K-1}(\mathbf{v} \otimes \mathbf{e}_1) + \mathcal{O}_{x,n,n+K-1} \mathbf{0}_{M \times 1} \\
&= \mathcal{O}_{a,n,n+K-1}(\mathbf{v} \otimes \mathbf{e}_1) \\
&= \begin{bmatrix} \mathbf{0}_{1 \times M^2}(\mathbf{v} \otimes \mathbf{e}_1) \\ (\hat{\mathbf{x}}_{n+1|n+1}^t \otimes \mathbf{c}_{n+1})(\mathbf{v} \otimes \mathbf{e}_1) \\ \vdots \\ [\sum_{i=1}^m \hat{\mathbf{x}}_{n+i|n+i}^t \otimes (\mathbf{c}_{n+m} \prod_{j=i+1}^m \hat{\mathbf{A}}_{n+j|n+j})](\mathbf{v} \otimes \mathbf{e}_1) \\ \vdots \\ [\sum_{i=1}^{K-1} \hat{\mathbf{x}}_{n+i|n+i}^t \otimes (\mathbf{c}_{n+K-1} \prod_{j=i+1}^{K-1} \hat{\mathbf{A}}_{n+j|n+j})](\mathbf{v} \otimes \mathbf{e}_1) \end{bmatrix} \\
&= \begin{bmatrix} \mathbf{0}_{1 \times M^2} \\ (\hat{\mathbf{x}}_{n+1|n+1}^t \mathbf{v})(\mathbf{c}_{n+1} \mathbf{e}_1) \\ \vdots \\ \sum_{i=1}^m (\hat{\mathbf{x}}_{n+i|n+i}^t \mathbf{v})(\mathbf{c}_{n+m} \prod_{j=i+1}^m \hat{\mathbf{A}}_{n+j|n+j}) \mathbf{e}_1 \\ \vdots \\ \sum_{i=1}^{K-1} (\hat{\mathbf{x}}_{n+i|n+i}^t \mathbf{v})(\mathbf{c}_{n+K-1} \prod_{j=i+1}^{K-1} \hat{\mathbf{A}}_{n+j|n+j}) \mathbf{e}_1 \end{bmatrix} \\
&= \mathbf{0}_{K \times 1} \tag{3.53}
\end{aligned}$$

where in the fourth equality we have used the Kronecker product identity 4 in Appendix C and the fact that the terms inside the parentheses are scalars.

(3.53) shows that $\mathcal{O}_{n,n+K-1}$ does not have full rank. Specifically (3.53) holds for all \mathbf{v} that is orthogonal to the space spanned by the sequence of state estimates within the observation duration.

2. Under the assumption that the sequence of state estimates is persistent exciting while the nominal state system is not observable. It follows that there exists $\mathbf{u} \neq \mathbf{0}$, such that

$$(\mathbf{c}_{n+m} \prod_{j=i+1}^m \hat{\mathbf{A}}_{n+j|n+j}) \mathbf{u} = 0 \tag{3.54}$$

for $m = 1, \dots, K - 1$ and $i = 1, \dots, m$.

Then multiplying $\mathcal{O}_{n,n+K-1}$ by $\begin{bmatrix} \mathbf{e}_1 \otimes \mathbf{u} \\ \mathbf{0}_{M \times 1} \end{bmatrix}$ with \mathbf{e}_1 being any nonzero $M \times 1$ vector, it yields

$$\begin{aligned}
\mathcal{O}_{n,n+K-1}(\mathbf{e}_1 \otimes \mathbf{u}) &= \mathcal{O}_{a,n,n+K-1}(\mathbf{e}_1 \otimes \mathbf{v}) + \mathcal{O}_{x,n,n+K-1} \mathbf{0}_{M \times 1} \\
&= \mathcal{O}_{a,n,n+K-1}(\mathbf{e}_1 \otimes \mathbf{v}) \\
&= \begin{bmatrix} \mathbf{0}_{1 \times M^2}(\mathbf{e}_1 \otimes \mathbf{u}) \\ (\hat{\mathbf{x}}_{n+1|n+1}^t \otimes \mathbf{c}_{n+1})(\mathbf{e}_1 \otimes \mathbf{u}) \\ \vdots \\ [\sum_{i=1}^m \hat{\mathbf{x}}_{n+i|n+i}^t \otimes (\mathbf{c}_{n+m} \prod_{j=i+1}^m \hat{\mathbf{A}}_{n+j|n+j})](\mathbf{e}_1 \otimes \mathbf{u}) \\ \vdots \\ [\sum_{i=1}^{K-1} \hat{\mathbf{x}}_{n+i|n+i}^t \otimes (\mathbf{c}_{n+K-1} \prod_{j=i+1}^{K-1} \hat{\mathbf{A}}_{n+j|n+j})](\mathbf{e}_1 \otimes \mathbf{u}) \end{bmatrix} \\
&= \begin{bmatrix} \mathbf{0}_{1 \times M^2} \\ (\hat{\mathbf{x}}_{n+1|n+1}^t \mathbf{e}_1)(\mathbf{c}_{n+1} \mathbf{u}) \\ \vdots \\ \sum_{i=1}^m (\hat{\mathbf{x}}_{n+i|n+i}^t \mathbf{e}_1)(\mathbf{c}_{n+m} \prod_{j=i+1}^m \hat{\mathbf{A}}_{n+j|n+j}) \mathbf{u} \\ \vdots \\ \sum_{i=1}^{K-1} (\hat{\mathbf{x}}_{n+i|n+i}^t \mathbf{e}_1)(\mathbf{c}_{n+K-1} \prod_{j=i+1}^{K-1} \hat{\mathbf{A}}_{n+j|n+j}) \mathbf{u} \end{bmatrix} \\
&= \mathbf{0}_{K \times 1} \tag{3.55}
\end{aligned}$$

where in the fourth equality we have used the Kronecker product identity 4 in Appendix C and the fact that the terms inside the parentheses are scalars.

This completes the proof for Theorem 1.

Corollary 2 parameter observability/detectability for channels confined within a lower-order subspace Consider the linearized augmented state space model (3.3). Let $n > 0$ and $K \geq L \triangleq M^2 + M$, here M is the original channel state

dimension. If the sequence of state estimates $\hat{\mathbf{x}}_{i|i}$ for $n \leq i \leq n + K - 1$, span only a rank p subspace of \mathbb{C}^M with $p < M$, then the set of unknown parameters associated with the orthogonal subspace are unobservable and undetectable in (3.3) over the time period $n \leq i \leq n + K - 1$.

The proof of Corollary 2 follows directly from that of Theorem 1.

The case where the channel is explicitly sparse can be viewed as a special case of channels span a lower order subspace, hence the following corollary holds:

Corollary 3 parameter observability/detectability for explicitly sparse channels Consider the linearized augmented state space model (3.3). Let $n > 0$ and $K \geq L \triangleq M^2 + M$, here M is the original state dimension. If the sequence of state estimates $\hat{\mathbf{x}}_{i|i}$ for $n \leq i \leq n + K - 1$, has its j th element, $\hat{x}_{j,i|i}$, consistently equal to zero¹, for $n \leq i \leq n + K - 1$, then the subset of parameters associated with the j th column of \mathbf{A} are unobservable and undetectable in (3.3) over the observation time period $n \leq i \leq n + K - 1$. The same applies to the case where a fixed subset of elements of the state estimates, rather than a fixed single element, are equal to zero.

Remarks:

1. Theorem 1 and Corollaries 2, 3 explicitly connect the performance of the EKF joint channel state and parameter estimator, in terms of the parameter observability and detectability, with the characteristics of the channel physics, *i.e.* sparseness and subspace span. The observability and detectability has important implication on the stability of the EKF algorithm, the quality of the EKF parameter estimate and eventually the performance of channel estimate. For instance, without accounting for the undetectable parameters, the EKF algorithm will diverge linearly as explained later. For parameters that are

¹It may seem unrealistic to assume certain taps stay strictly zero. However, the observability/detectability results here still apply to the case where taps are quiescent rather than being zero. The observability matrix may not be strictly singular, but is still ill-conditioned in the quiescent case.

detectable but not observable, the EKF filter may be stable yet the estimate of those parameters will be conceivably poor since little information is gained from the received signal. Consequently they introduce large noise error into the channel estimation.

2. Intuitively speaking, Theorem 1 and Corollaries 2, 3 state that the problem of estimating the channel dynamics while some of its components, *e.g* tap coefficients or subspace components, have little energy is ill-defined. Essentially if a tap has no energy, then its dynamics parameter which describes how it would evolve over time is not clearly defined.
3. For the purpose of analytical tractability, the assumptions imposed by Corollaries 2 and 3 are rather strict and even unrealistic. In real channels, more often taps would fluctuate at different energy levels. Taps with small magnitude would be noisy rather than being zero. In addition, the period during which a tap keeps quiescent or a subspace stays null could be relatively short. However, the observability/detectability results of Theorem 1 and Corollaries 2, 3 can be easily extended to these cases. For instance, the ill-conditioning of the observability matrix would increase the noise sensitivity and introduce large noise error, and parameters may be effectively unobservable if on average the new information provided by the received signal flows into those parameter estimates at a negligible rate.

A Simulation Example

The consequence of parameter undetectability is the linear divergence of the assumed parameter error covariance matrix $\mathbf{P}_{a,i|i-1}$. This is a result of the fact that the Kalman gain $\mathbf{k}_{a,i}$ associated with the unobservable parameter estimate becomes zero as it obtains no new information from the observation. Thus the measurement update step does not reduce $\mathbf{P}_{a,i|i-1}$. On the other hand, assuming a random walk parameter

model, $\mathbf{P}_{a,i|i-1}$ is increased monotonically by the assumed noise covariance during the time update step.

To demonstrate this linear divergence, a simple two-tap channel is simulated. The first tap coefficient, x_1 , is generated as a Gauss-Markov process, with transition coefficient $a_1 = .998e^{-j2*\pi*10/24000}$ and process noise variance 10^{-3} . Effectively, it has steady-state variance 0.2503 and Doppler $10Hz$ at a symbol rate $24KHz$. The second tap coefficient, x_2 , is a white noise process with variance 10^{-6} . The sequence of transmitted symbols, c_i , is obtained from a sequence of zero-mean Gaussian white noise b_i , such that $c_i = 1$ if $b_i \geq 0$ and $c_i = -1$ otherwise. The received SNR is 10 dB. The received signal is generated for 5000 symbols. An EKF algorithm is then applied to jointly estimate the tap coefficients and their assumed dynamic parameters. The assumed channel process noise covariance and observation noise variance are the same as the simulation values. The parameter process noise variance is assumed as 10^{-4} for both taps. The initial values of both dynamic parameters are taken as 1. The simulated tap coefficients, the parameter error covariance, the parameter Kalman gain and parameter estimation error are given in Figure 3-1. It shows that the Kalman gain associated with the second parameter is close to zero, the error covariance of the second parameter linearly increases over time and the estimation error for the second parameter stays large (as decided by the initial value).

3.4 Two-Model EKF Parameter Estimation

Motivated by the results of Section 3.3 this section presents a modified EKF algorithm based on separately modeling the parameters associated with energetic taps and those with quiescent taps. The two parameter model is effectively a soft constraint based approach compared to hard constraint based approaches such as sparse channel estimation and multipath arrival tracking where various tap initiation and termination schemes are employed to choose explicitly the active taps while discard-

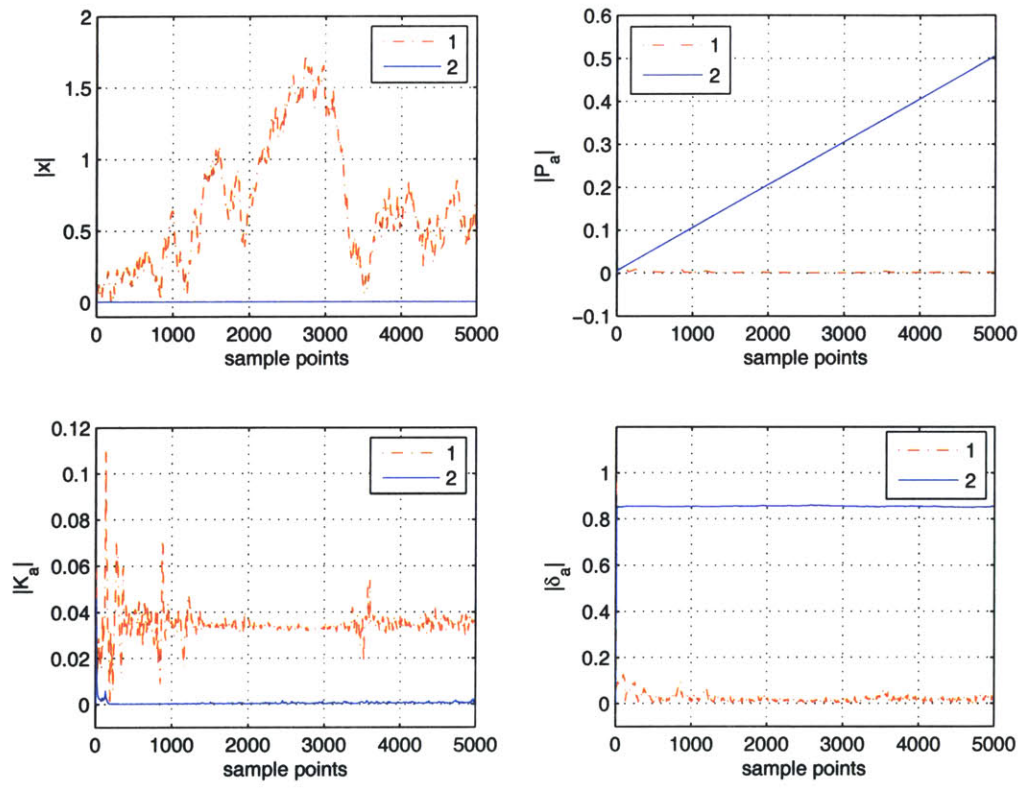


Figure 3-1: Simulation Example: Parameter Undetectability

ing others. Although still using a dynamic tap labeling scheme, the new method does not explicitly initiate and terminate taps. Instead, whether or not a tap is actively tracked is indirectly controlled by adapting its dynamic parameters based on a suitable stable model.

The approach contains three essential parts: the parameter model, the choice of model parameters and the tap labeling scheme. The details of each part and their impact on estimation performance are discussed in this section. One of the key points during the consideration, as becomes evident later, is how to trade covariance with bias, so that the overall signal prediction error is minimum.

3.4.1 Two-Model Parameter Estimation

As shown in section 3.3, the dynamic parameters associated with quiescent taps are unobservable and further undetectable if their models are unstable. In the latter case, the filter becomes unstable, in the sense that the error covariance associated with those undetectable parameters grow linearly towards infinity.

The approach proposed here is based on the result from the Kalman filter theory that detectability is the sufficient and necessary condition for filter stability, but observability is not a necessary condition [And79]. As long as the unobservable components remain stable, the filter will not diverge in the sense that the error covariance remain bounded from above. Heuristically speaking this is because the error covariance is always upper bounded by the state correlation matrix which in turn would be bounded from above if the model is stable.

The Parameter Model

Denoting \mathbf{q} as the index subset containing those quiescent taps, and \mathbf{e} containing the energetic taps, each subset of parameters are then modeled separately as follows:

$$\boldsymbol{\theta}_{\mathbf{e},i+1} = \boldsymbol{\theta}_{\mathbf{e},i} + \mathbf{u}_{\mathbf{e},i} \quad (3.56)$$

$$\boldsymbol{\theta}_{\mathbf{q},i+1} = \beta \boldsymbol{\theta}_{\mathbf{q},i} + (1 - \beta) \boldsymbol{\epsilon} + \mathbf{u}_{\mathbf{q},i} \quad (3.57)$$

where $0 < \beta < 1$, $0 < \epsilon < 1$, $\mathbf{u}_{\mathbf{e},i} \sim \mathcal{N}(\mathbf{0}, \mathbf{Q}_{u_{\mathbf{e},i}})$ and $\mathbf{u}_{\mathbf{q},i} \sim \mathcal{N}(\mathbf{0}, \mathbf{Q}_{u_{\mathbf{q},i}})$.

(3.57) is a stable system in which $\boldsymbol{\theta}_{\mathbf{q},i}$ converges exponentially in mean towards $\boldsymbol{\epsilon}$ at a rate specified by β , with a steady-state fluctuation variance specified by $\mathbf{Q}_{u_{\mathbf{q},i}}/(1 - \beta^2)$. The presence of $\mathbf{u}_{\mathbf{q},i}$ allows the associated parameter error covariance to be bounded from below so that the algorithm can maintain a certain tracking capability for these parameters after they have converged to $\boldsymbol{\epsilon}$. This is useful in scenarios where a quiescent tap is turned into an active tap by an incoming multipath arrival.

In the case where $\boldsymbol{\theta}_i = \mathbf{a}_i = \text{Vec}(\mathbf{A}_i)$, the following linearized augmented state model can be obtained following the same procedure as in Appendix A.1:

$$\begin{bmatrix} \mathbf{a}_{\mathbf{e},i+1} \\ \mathbf{a}_{\mathbf{q},i+1} \\ \mathbf{x}_{\mathbf{e},i+1} \\ \mathbf{x}_{\mathbf{q},i+1} \end{bmatrix} = \begin{bmatrix} \mathbf{I} & \mathbf{0} & \mathbf{0} & \mathbf{0} \\ \mathbf{0} & \beta \mathbf{I} & \mathbf{0} & \mathbf{0} \\ \hat{\mathbf{X}}_{\mathbf{e},i|i} & \mathbf{0} & \hat{\mathbf{A}}_{\mathbf{e},i|i} & \mathbf{0} \\ \mathbf{0} & \hat{\mathbf{X}}_{\mathbf{q},i|i} & \mathbf{0} & \hat{\mathbf{A}}_{\mathbf{q},i|i} \end{bmatrix} \begin{bmatrix} \mathbf{a}_{\mathbf{e},i} \\ \mathbf{a}_{\mathbf{q},i} \\ \mathbf{x}_{\mathbf{e},i} \\ \mathbf{x}_{\mathbf{q},i} \end{bmatrix} + \begin{bmatrix} \mathbf{u}_{\mathbf{e},i} \\ \mathbf{u}_{\mathbf{q},i} \\ \mathbf{w}_{\mathbf{e},i} \\ \mathbf{w}_{\mathbf{q},i} \end{bmatrix} + \begin{bmatrix} \mathbf{0} \\ (1 - \beta) \boldsymbol{\epsilon} \\ \mathbf{0} \\ \mathbf{0} \end{bmatrix} + \mathbf{d}_i \quad (3.58)$$

where the terms with subscripts q and e are associated with the quiescent and energetic taps respectively. \mathbf{d}_i is given in Appendix A.1.

Accordingly, the time-update equations (3.4), (3.6) (3.8) should be changed into

the following:

$$\widehat{\mathbf{a}}_{\mathbf{e},i+1|i} = \widehat{\mathbf{a}}_{\mathbf{e},i|i} \quad (3.59)$$

$$\widehat{\mathbf{a}}_{\mathbf{q},i+1|i} = \beta \widehat{\mathbf{a}}_{\mathbf{q},i|i} + (1 - \beta) \boldsymbol{\epsilon} \quad (3.60)$$

$$\mathbf{P}_{a_{\mathbf{e}},i+1|i} = \mathbf{P}_{a_{\mathbf{e}},i|i} + Q_{u_{\mathbf{e}},i} \quad (3.61)$$

$$\mathbf{P}_{a_{\mathbf{q}},i+1|i} = \beta^2 \mathbf{P}_{a_{\mathbf{q}},i|i} + Q_{u_{\mathbf{q}},i} \quad (3.62)$$

$$\mathbf{P}_{a_{\mathbf{q}a_{\mathbf{e}}},i+1|i} = \beta \mathbf{P}_{a_{\mathbf{q}a_{\mathbf{e}}},i|i} \quad (3.63)$$

$$\mathbf{P}_{a_{\mathbf{q}x_{\mathbf{e}}},i+1|i} = \beta [\mathbf{P}_{a_{\mathbf{q}},i|i} \widehat{\mathbf{X}}_{\mathbf{e},i|i}^h + \mathbf{P}_{a_{\mathbf{q}x_{\mathbf{e}}},i|i} \widehat{\mathbf{A}}_{\mathbf{q},i|i}^h] \quad (3.64)$$

$$\mathbf{P}_{a_{\mathbf{q}x_{\mathbf{q}}},i+1|i} = \beta [\mathbf{P}_{a_{\mathbf{q}},i|i} \widehat{\mathbf{X}}_{\mathbf{q},i|i}^h + \mathbf{P}_{a_{\mathbf{q}x_{\mathbf{q}}},i|i} \widehat{\mathbf{A}}_{\mathbf{q},i|i}^h] \quad (3.65)$$

$$\mathbf{P}_{a_{\mathbf{e}x_{\mathbf{e}}},i+1|i} = \mathbf{P}_{a_{\mathbf{e}},i|i} \widehat{\mathbf{X}}_{\mathbf{e},i|i}^h + \mathbf{P}_{a_{\mathbf{e}x_{\mathbf{e}}},i|i} \widehat{\mathbf{A}}_{\mathbf{e},i|i}^h \quad (3.66)$$

$$\mathbf{P}_{a_{\mathbf{e}x_{\mathbf{q}}},i+1|i} = \mathbf{P}_{a_{\mathbf{e}},i|i} \widehat{\mathbf{X}}_{\mathbf{q},i|i}^h + \mathbf{P}_{a_{\mathbf{e}x_{\mathbf{q}}},i|i} \widehat{\mathbf{A}}_{\mathbf{e},i|i}^h \quad (3.67)$$

As a result, the error covariance associated with those taps which belong to the subset \mathbf{e} increases by $Q_{u_{\mathbf{e}},i}$ at each time update, hence it is expected to maintain the active tracking capability. (Note due to the fact that these taps are observable, their error covariances are reduced in the measurement step.) On the other hand according to (3.62) the error covariance associated with those taps belonging to the subset \mathbf{q} converge exponentially to $Q_{u_{\mathbf{q}},i}/(1 - \beta^2)$ even if no reduction is obtained during the measurement step. This ensures that the filter would be stable even though these taps are not observable. The choice of β and $Q_{u_{\mathbf{q}},i}$ affects the tracking performance of the filter as discussed later.

The change in the parameter model has no effect on the measurement update equations.

Consequently, the observable parameters (associated with those energetic taps) are modeled as random walk processes to maintain active tracking capability, and the unobservable parameters (associated with those quiescent taps) are kept stable. The values of β and ϵ should be chosen carefully as discussed later. A larger ϵ would

allow the associated tap become active if an arrival moves into that tap. If ϵ is close to zero, such recovery from a quiescent tap would be difficult even in the presence of process noise. On the other hand, a larger ϵ implies that the associated taps have larger energy which might not be true for weak or quiescent taps.

Tap Labeling

The parameter model above relies on the classification of channel taps into two subsets, *i.e.* the energetic taps and the quiescent taps. The key is what criteria should be used to do this tap labeling. For the purpose of avoiding parameter undetectability, it is natural that an energy criterion should be used. That is, if $|\hat{x}_{i,j}| > \gamma$ then $j \in \mathbf{e}$, otherwise $j \in \mathbf{q}$, for some threshold level $\gamma > 0$. As a result parameters associated with taps whose magnitude is less than γ are put in the subset of quiescent taps and those having larger tap magnitude in the subset of energetic taps.

The energy criterion is simple and efficient. Yet it would have problem in cases of low SNR. In the extreme case when the ambient noise level is higher than the energy of a small arrival, such as those with multiple surface interactions, then the simple thresholding technique would mistakenly put noisy taps into energetic category while the tap associated with the small arrival is put into the quiescent category. Actively tracking noisy taps that are not associated with arrivals increases the adapting noise error. Labeling taps associated with small arrivals as quiescent tends to suppress these taps with a small ϵ being used. As a result it introduces bias into the channel estimation. This would not be a problem if all arrivals have energy larger than the background noise. When the channel fluctuates such that the mean tap energy varies over time, the threshold level should also be adaptively chosen.

In addition to the energy criterion, other criteria may be used as well, such as based on the tap phase trajectory. They are not exploited in this thesis and left for possible future work.

The performance impact of these tap labeling schemes essentially involves the tradeoff between covariance and bias. A loose labeling scheme tends to put more quiescent taps into the subset \mathbf{e} , hence increasing the adapting noise error, or variance (the stability issue is also at stake), while an over-restrictive labeling scheme puts taps associated with weak arrivals into the subset \mathbf{q} and causes large bias as these taps are not accurately estimated.

The development of a optimal criterion would have to be based on probabilistic models of the arrival distribution.

Choice of Model Parameters

The values of β , ϵ , $Q_{u_e,i}$ and $Q_{u_q,i}$ in (3.57) remain to be determined. As the subsequent analysis and experimental results show, the choice of these parameters is very important. Effectively they act as the parameters for a soft constraint on the channel taps that adaptively controls the tracking capability for each tap. The choice of these parameters involves balancing the *lag error* and the *noise error* from tracking point of view, and ultimately making trade-off between bias and covariance of the resulting channel estimate.

It is the steady-state tracking performance that should be the criterion for choosing these values. Among them the key parameter that directly impact channel tap magnitude is ϵ . According to (3.5). Qualitatively, a smaller ϵ tends to suppress exponentially the tap coefficient over time. According to (3.5), in the time update equation $\hat{\mathbf{x}}_{i+1|i}$ not only gets Doppler compensation, but also changes its magnitude as scaled by $|\hat{\mathbf{a}}_{i|i}|$. If a j th tap is labeled as quiescent and put in subset \mathbf{q} , then $a_{i,j}$ converges to ϵ_j , the j th element of ϵ , exponentially. If the j th tap is in the subset \mathbf{q} for a sufficiently long time, then ϵ_j effectively determines the rate at which $\hat{\mathbf{x}}_{i+1|i}$ is exponentially suppressed. This is desirable if there is indeed no arrival associated with the j th tap, but it also causes error. ϵ_j also affects how $\hat{\mathbf{x}}_{i+1|i}$ is being tracked. This can be observed from the error covariance time update equation (3.7).

Other values such as β and $\mathbf{Q}_{u_q,i}$ are also important, especially for those taps infrequently associated with arrivals. β determines the rate at which elements of $\hat{\mathbf{a}}$ associated with quiescent taps converge to ϵ and also the tracking ability of these elements of $\hat{\mathbf{a}}$ through \mathbf{P}_a . It also effectively controls the time constant of the parameter filter, as demonstrated in the experimental results. $\mathbf{Q}_{u_q,i}$, as mentioned early, maintains tracking capability for those elements associated with quiescent taps. For those taps infrequently associated with arrivals, it is desirable to initiate them quickly when they are energized by an arrival and terminate them when the associated arrival moves away. This would be difficult if the parameters and the coefficients of these taps are trapped in an inactive tracking mode.

Experimental Results

This section shows the results obtained by applying the EKF algorithms to the example channel in Chapter 2. Both the plain EKF algorithm and the two-model EKF algorithm are used. The results show that in both cases the signal prediction residual error is reduced comparing to that of RLS algorithm, with the two-model EKF attaining the maximum reduction. The effects of choosing β and ϵ are also demonstrated.

Figure 3-2 gives the performance comparison between the Two-Model EKF, the plain EKF and the exponentially weighted RLS, from 18 seconds to 21.5 seconds, a 3.5 second span that coincides with the wave event. The plot shows, compared to the residual error obtained by RLS, the residual error obtained by the plain EKF is about 1 ~ 2 dB less and the reduction is the largest around 20 seconds when the channel become the most dynamic. The residual error obtained by the Two-Model EKF is about 3 ~ 4 dB less than that of the RLS. At places where the channel is less dynamic, it maintains an error reduction from that of the plain EKF by approximately 2 dB. Around 20 seconds, the difference between the plain EKF and the Two-Model EKF is less significant. This is what would be expected. When the

residual error is mostly dominated by *lag error* due to the rapid channel fluctuations, the Two-Model EKF and the plain EKF both obtain significant error reduction due to their dynamic tracking capability and the noise error reduction due to separate parameter modeling is marginal, although the Two-Model EKF still has a visible improvement. When the channel is less dynamic, the Two-Model EKF algorithm can successfully apply the soft constraint to reduce the number of taps to be tracked, which effectively reduces the noise error as well as improve the tracking capability.

Note that the plain EKF does not appear to suffer from the parameter unobservability/undetectability from this plot. This is due to the fact that the divergence of the error covariance of parameters associated with the quiescent taps is linear, as shown in section 3.3. The computation did indicate the linear growth of those error covariances which implies that they will eventually diverge given a sufficiently long time.

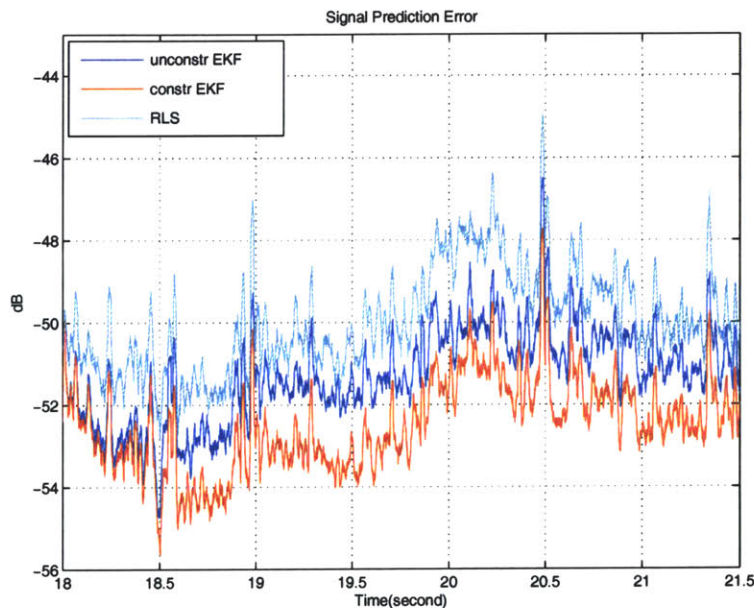


Figure 3-2: Two-Model EKF, Plain EKF and RLS, 2 ~ 4 dB performance gain.

The phase of the diagonal elements of the estimated transition matrix can be converted into the Doppler of the associated tap. The Doppler thus obtained from

the parameter estimation using the Two-Model EKF and the plain EKF algorithms are shown in Figure 3-3 and Figure 3-4 respectively. The Two-Model EKF used $\beta = 0.999998$ and $\epsilon = 0.95$. Both show the successful detection of significant Doppler values associated with the surface arrivals. The maximum Doppler values are on the order of 15 Hz, or the maximum Doppler spread at the order of 30 Hz, both closely match the results in Chapter 2. It also shows an asymmetric learning capability of the parameter filter. The shape of the Doppler pattern within the time-delay region [19.5 sec 20.5 sec 2 ms 3 ms] indicates that the filter quickly estimates the large Doppler upon its onset; however, after the arrival moves on towards other delay taps, it takes longer than 0.5 second for the Doppler to change. The asymmetry is associated with the fact that the Kalman gain for the parameter is a function of the channel impulse response estimate. When the tap coefficient has a larger magnitude as when it is associated with an arrival, the Kalman gain for the parameter tends to become larger; and when the tap coefficient is weak as no arrival is associated with it, the parameter Kalman gain is small. In this sense the EKF algorithm is itself selectively tracking the parameters. Comparing Figure 3-3 and Figure 3-4, several differences can be observed, mainly in the quiescent regions and the region associated with arrivals having multiple surface interactions. First, in the quiescent regions including between 3.5 ~ 4.5 ms and between 0.2 ~ 0.6 ms in delay, which are essentially the gaps between arrivals, the plain EKF has a noisy Doppler pattern while the Two-Model EKF has a smooth Doppler which converges towards zero, albeit slowly. Secondly, in the weak arrival region (*i.e.* the region with arrivals having multiple surface interactions) between 5.5 ~ 6.5 ms in delay, the plain EKF algorithm still picks up some Doppler patterns which are however not evident in the Two-Model EKF case. Therefore, this comparison gives a good indication of the tradeoff between covariance, associated with noise within the quiescent region, and bias, associated with the weak arrival region.

The channel impulse response estimate for the same time span is given in Figure

3-5. The correspondence between the multipath structure of the significant arrivals in Figure 3-5 closely matches the Doppler pattern in both Figures 3-3 and 3-4.

Figure 3-6 shows the scattering function estimate at time $t = 20.05747$ seconds. It connects to both Figures 3-3 and 3-3 by cutting a cross section along $t = 20.09159$ in both plots. The Doppler values associated with the dominant arrivals given in Figure 3-6 is of the same order as those in Figures 3-3 and 3-4.

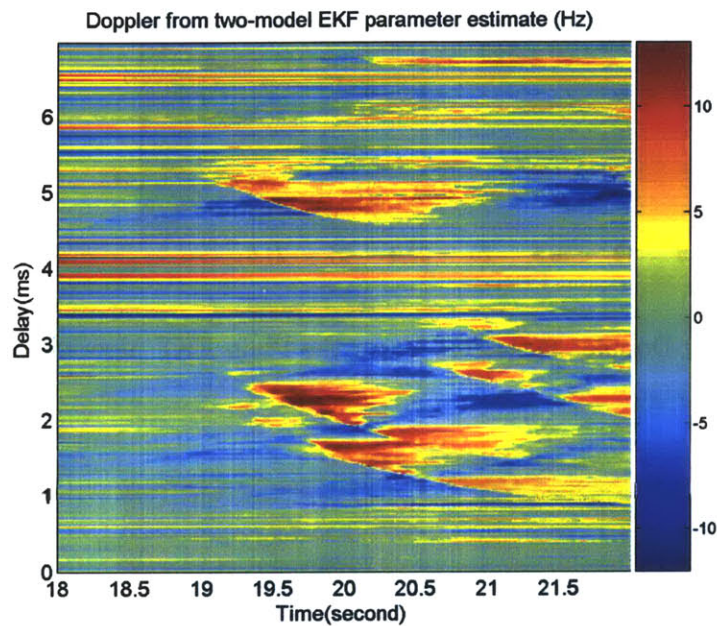


Figure 3-3: Doppler Estimates Using the Two-Model EKF algorithm

A Doppler plot obtained using the Two-Model EKF with $\beta = 0.98$ and $\epsilon = 0.96$ is shown in Figure 3-7. The difference that is evident between Figure 3-7 and Figure 3-3 is that the Doppler patterns have a much shorter tail in Figure 3-7 which corresponding to shorter memory. Note the apparent learning symmetry in Figure 3-7 is not because of an increase in the parameter Kalman gain in the absence of arrival. It is because the tap is labeled as quiescent and the parameter model (3.57) drives the parameter quickly towards ϵ which is a real quantity. Figure 3-7 also indicates both the quiescent region and the weak arrival region see little Doppler. The latter

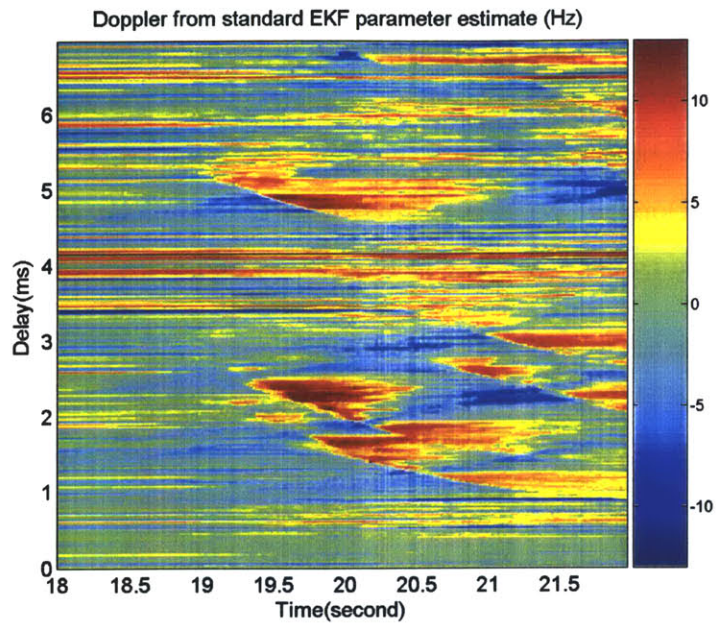


Figure 3-4: Doppler Estimates Using the Plain EKF algorithm

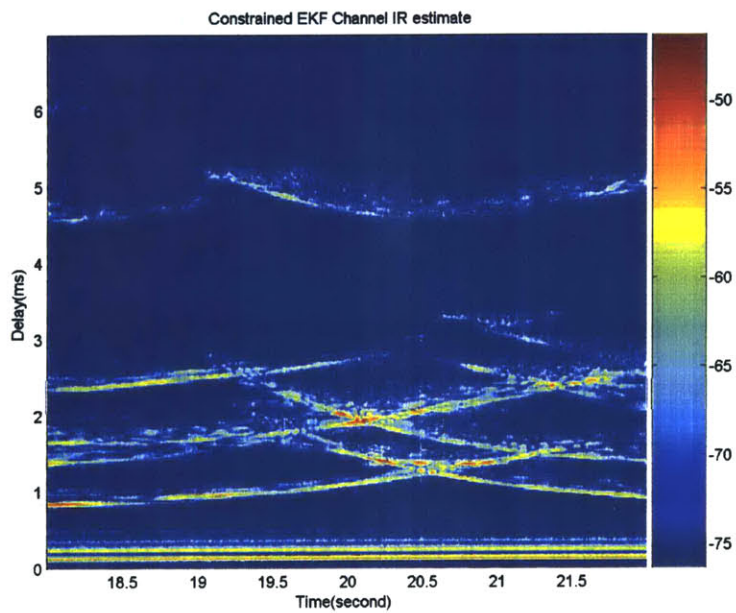


Figure 3-5: Channel Impulse Response Estimates Using the Two-Model EKF algorithm

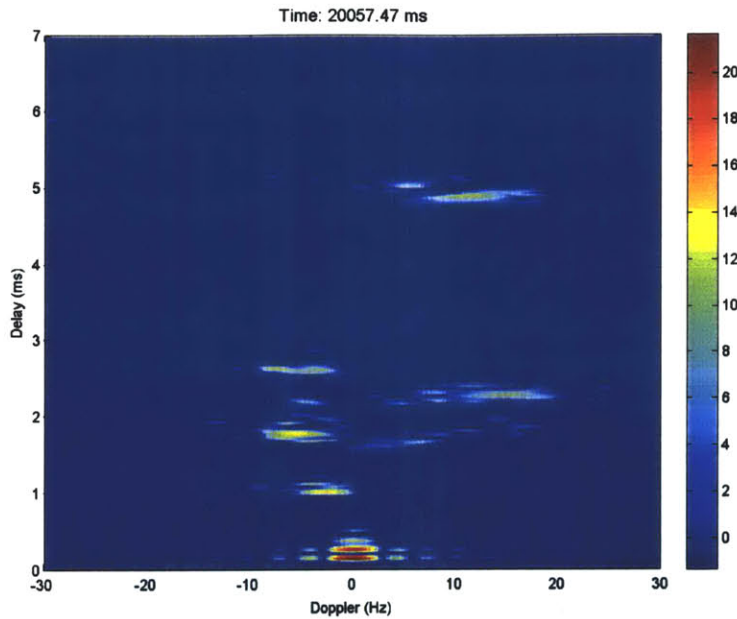


Figure 3-6: The Scattering Function Estimate at $t = 20.05747$ seconds

is a sign of parameter bias caused by over-constraining using smaller values of β and ϵ .

3.5 Concluding Remarks

To summarize, this chapter has developed channel estimation approaches based on the EKF algorithm. The EKF joint channel and dynamic parameter estimation algorithm is derived. Tracking error analysis is also given which highlights the error caused by inaccurate parameter estimation, a term analogous to the *lag error*, and the error term associated with noise. Most importantly, it is shown that for wideband shallow-water multipath channel, due to the explicit sparseness of the channel structure, or inter-path correlation, plain application of the EKF algorithm would run into the problem of parameter unobservability/undetectability which consequently cause the filter to be unstable. Based on that, a Two-Model EKF algorithm is proposed which models separately the parameters associated with energetic taps from those

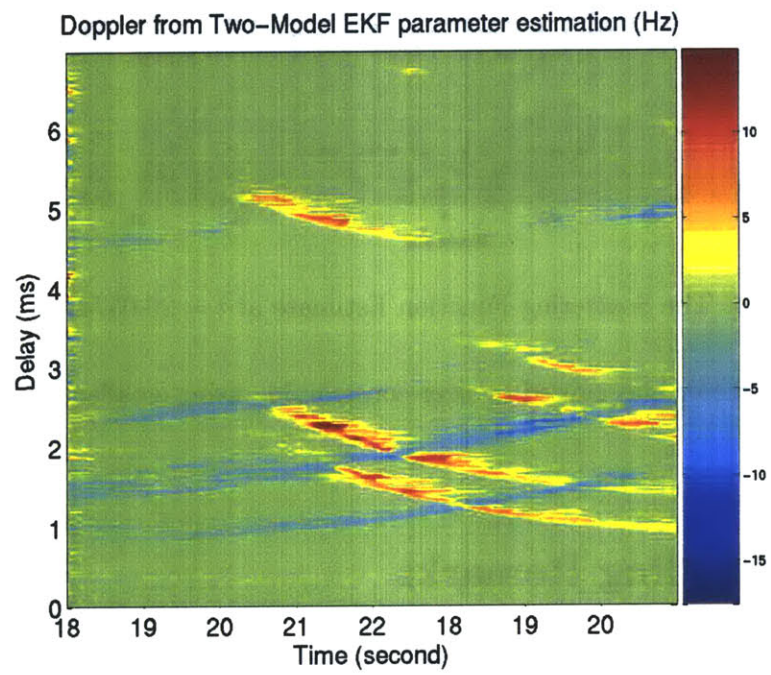


Figure 3-7: Doppler Estimates Using the Two-Model EKF algorithm, faster parameter convergence.

with quiescent taps. It thus stabilizes the parameter filter and on the other hand selectively tracks those dominant taps associated with multipath arrivals. Details of the separate modeling and the Two-Model EKF algorithm is presented. Finally as demonstrated through experimental data analysis, the dynamic model based tracking using EKF based approach significantly reduces the signal prediction residual error, and the Two-Model EKF algorithm attains further performance improvement due to its soft-constrained selective tracking.

Chapter 4

EM based Channel Impulse

Response Estimation

Dynamic channel estimation algorithms based on the Expectation Maximization (EM) approach are developed in this chapter. Applied to the state-space channel model developed in Chapter 2, the EM algorithm combined with the Kalman filter (KF) iteratively computes state estimates and ML estimates of the parameters. A new vector form recursion for computing the cumulative sum of the smoothed second-order state moments, from which the parameters are directly estimated, is derived in this chapter. By generalizing the log likelihood function into an exponentially weighted form, the new recursion motivates a class of suboptimal sequential EM algorithm with adjustable averaging memory length and state smoothing memory, whose properties are subsequently analyzed. The analysis shows a second-order innovation term in the parameter update in addition to the first-order Kalman innovation. An extended persistent excitation condition necessary for the stability of the parameter recursion is established. Extension of the EM approach towards a least squares (LS) framework is also presented.

4.1 Introduction

The EM algorithm is an approximating scheme first developed by Dempster, *et al.* [Dem77] to obtain ML parameter estimation for problems with incomplete data. It has since then been applied extensively to many problems that can be converted into an incomplete data formulation [McI97]. Parameter estimation in linear models using the EM algorithm traces back to the original paper [Dem77]. Application of the EM algorithm to estimate unknown parameters of linear dynamic systems is believed to be developed first by Shumway, *et al.* [Shu82], where the EM algorithm combined with the Kalman state smoother was proposed to compute the ML estimates of the system parameters while also providing the state estimates. Later the idea was applied to the problem of speech enhancement in [Wei94] where a suboptimal sequential algorithm is also proposed in which the state smoother is replaced by a filter, an idea which can be found in the early work of Titterton [Tit84]. More recently in [Gao03], the EM-Kalman filter structure and its suboptimal version similar to the one in [Wei94] were employed to estimate time varying multipath fading channels. In all these cases the optimal EM parameter estimator is based on sums of the second-order smoothed state moments. Upon the arrival of a new observation, these moments must be updated using new state estimate at each sample point (and in a forward-backward fashion when a state smoother is used) and stored. This requires a memory that increases with observation time. The suboptimal algorithms in [Wei94] and [Gao03] circumvented this problem by simply using the lag-one smoothed state estimation which certainly leads to performance degradation. Recently in [Ell99], a class of finite-dimensional filters were proposed to directly estimate the sums of those second-order smoothed state moments, instead of estimating the moments first and then accumulating. This greatly reduces the storage requirement and is computationally more efficient. The derivation is based on the notion of measure change. Subsequently in [Ell02], the same filters were employed in a suboptimal recursive algorithm whose convergence was proved under certain conditions. The recursion

forms proposed in [Ell99] have to be implemented element-wise for those cumulative sums and is difficult to be interpreted intuitively. In addition, despite of the convergence claim, the suboptimal algorithm in [Ell02] generally have a very slow convergence rate .

In this chapter the EM algorithm is derived which together with the Kalman filter jointly estimates the state and the ML parameter estimate. Then a new vector form recursion for computing the cumulative sum of the smoothed second-order moments is derived. The derivation is directly based on the state smoothing formula and the properties of the Kronecker product, hence, it is mathematically simpler than that in [Ell99]. More importantly, the resulting recursion form yields new insight into the structure of the problem which facilitates the stability analysis of the estimation algorithm. It leads to an intuitive interpretation of the effect of exponential forgetting on parameter estimation in terms of the parameter averaging memory and the state smoothing memory respectively. This intuition motivates a new class of suboptimal recursive algorithm which encompasses the algorithms proposed in [Ell02] and [Wei94] as special cases. In the new algorithm the parameter averaging memory and state smoothing memory are adjustable separately by two forgetting factors. Finally, the stability analysis of the suboptimal algorithm reveals the fact that the one-step recursion of the parameter matrix is rank-one. An extended persistent excitation (EPE) condition is then established for the stability of the suboptimal parameter recursion. The EPE condition requires that both the observation vector and the state estimate to be persistently exciting, a concept well known in system identification for linear regression models. This renders a geometric picture that illustrates intuitively the identifiability of the parameters which are observed indirectly through the observations. The implications of this condition are especially relevant for channel estimation in wideband transmission where the channel is generally sparse due to the resolved multipath structure hence would violate the EPE condition. As a result, dynamic parameter estimation may diverge if those quiescent taps are to be

dynamically tracked. The suboptimal EM algorithm alternates between parameter estimation based on the sequence of state estimates and state filtering via Kalman filter. An extension of this alternating structure towards the least squares framework is developed where the parameter estimation is explicitly formulated as a LS estimation problem.

Several conceptual parallels can be found between the development in this chapter and that in Chapter 3, including the extended Persistent Excitation condition of the suboptimal EM algorithm vs the parameter observability and detectability results in section 3.3; the second-order innovation term in the suboptimal EM algorithm vs the innovation correction terms for the EKF algorithm in section 3.2.3.

The content of this chapter is organized as follows: Section 4.2 formulates the problem and reviews the EM algorithm; in Section 4.3 the new recursion form of the cumulative sum of the smoothed second-order moments are derived. Section 4.4 presents the suboptimal algorithm. Analysis of the suboptimal algorithm, including its stability and convergence, is carried out in section 4.5. The analysis leads to the second-order innovation term in the suboptimal algorithm and the extended persistent excitation (EPE) condition. Section 4.6 proposes a modified EM algorithm that only estimates the parameter associated with the dominant channel tap subspace, based on eigenvalue decomposition of the cumulative sum of the smoothed state self correlation matrix. Finally Section 4.7 presents a summary of this chapter.

4.2 EM Joint Channel State and Parameter Estimation

Restate the state-space channel model (3.1):

$$\begin{cases} \mathbf{x}_{k+1} = \mathbf{A}(\boldsymbol{\theta})\mathbf{x}_k + \mathbf{w}_k & (4.1a) \\ y_k = \mathbf{c}_k\mathbf{x}_k + v_k & (4.1b) \end{cases}$$

All the model assumptions held in section 3.2, including the noise statistics, are followed here.

The derivation assumes that $\boldsymbol{\theta}$ is the only unknown parameter and there is no *a priori* structure of \mathbf{A} specified. The time-variations of $\boldsymbol{\theta}$ is not explicitly modeled, but will be dealt with later by exponentially weighting the log-likelihood function. Note that the state process noise covariance \mathbf{Q}_w and the observation noise variance σ_v^2 can be parameterized and estimated as well, as was done in [Shu82]. The basic idea and procedures of estimating \mathbf{Q}_w and σ_v^2 are very similar to those of estimating $\boldsymbol{\theta}$ in \mathbf{A} ; therefore, the development assumes that they are both known to simplify the derivation and highlight the crucial point.

The goal is to estimate the state process \mathbf{x}_n and parameter $\boldsymbol{\theta}$ based on the sequence of received signals $\mathcal{Y}_n \triangleq \{y_1, \dots, y_n\}$ assuming \mathbf{c}_k , $k = 1, \dots, n$, the sequence of transmitted symbols, are known.

The EM algorithm [Dem77], when applied to system (4.1) with observation data \mathcal{Y}_n available, consists of multiple iterations. At the l th iteration it carries out the following 'E'-step and 'M'-step:

1. E-step:

$$Q_n(\boldsymbol{\theta}, \widehat{\boldsymbol{\theta}}_n^{(l-1)}) = E\{\Lambda_n(\boldsymbol{\theta}) | \mathcal{Y}_n; \widehat{\boldsymbol{\theta}}_n^{(l-1)}\} \quad (4.2)$$

where $\Lambda_n(\boldsymbol{\theta})$ is the log likelihood function. $E\{\cdot | \mathcal{Y}_n; \widehat{\boldsymbol{\theta}}_n^{(l-1)}\}$ is the expectation taken with respect to the conditional density $p_{\Lambda_n}(\lambda_n | \mathcal{Y}_n; \widehat{\boldsymbol{\theta}}_n^{(l-1)})$. And $\widehat{\boldsymbol{\theta}}_n^{(l-1)}$ is the parameter estimate obtained from the $(l-1)$ th iteration based on \mathcal{Y}_n .

2. M-step

$$\widehat{\boldsymbol{\theta}}_n^{(l)} = \arg \max_{\boldsymbol{\theta}} Q(\boldsymbol{\theta}, \widehat{\boldsymbol{\theta}}_n^{(l-1)}) \quad (4.3)$$

EM is a batch iterative ML algorithm that deals with fixed-interval observation data

[Dem77]. The subscript n here merely indicates that the estimation is based on \mathcal{Y}_n , does not imply that EM is time recursive. When new data arrives, one needs to start the EM algorithm for the new data segment. If the total number of iterations for each data segment is L , then the EM algorithm can be initialized with $\widehat{\boldsymbol{\theta}}_{n+1}^{(1)} = \widehat{\boldsymbol{\theta}}_n^{(L)}$. When restricting $L = 1$, then the overall EM procedure becomes time-recursive and suboptimal. This is discussed in section 4.4.

The log likelihood function of the observation and state is given as

$$\begin{aligned}\Lambda_n(\boldsymbol{\theta}) &= \log[p(y_1, y_2, \dots, y_n, \mathbf{x}_0, \mathbf{x}_1, \dots, \mathbf{x}_n; \boldsymbol{\theta})] \\ &\triangleq \sum_{i=1}^n \log\left(p(\mathbf{x}_i | \mathbf{x}_{i-1}; \boldsymbol{\theta})\right) + \mathcal{C}_1\end{aligned}\quad (4.4)$$

where $\mathcal{C}_1 \triangleq \sum_{i=1}^n \log(p(y_i | \mathbf{x}_i)) + \log(p(\mathbf{x}_0))$ is not a function of $\boldsymbol{\theta}$. From the state equation (2.49a), it follows

$$\log\left(p(\mathbf{x}_i | \mathbf{x}_{i-1}; \boldsymbol{\theta})\right) = -\frac{1}{2} \|\mathbf{x}_i - \mathbf{A}(\boldsymbol{\theta})\mathbf{x}_{i-1}\|_{Q_w^{-1}}^2 + \mathcal{C}_2 \quad (4.5)$$

where $\mathcal{C}_2 = -\frac{M}{2} \log(2\pi \det(Q_w))$ and $\|\cdot\|_{Q_w^{-1}}$ is the Q_w^{-1} weighted norm. Substituting (4.4) and (4.5) into (4.2) and (4.3) yields

$$\widehat{\boldsymbol{\theta}}_n^{(l)} = \arg \max_{\boldsymbol{\theta}} J(\boldsymbol{\theta}) \quad (4.6a)$$

$$J(\boldsymbol{\theta}) \triangleq E\left\{\sum_{i=1}^n \|\mathbf{x}_i - \mathbf{A}(\boldsymbol{\theta})\mathbf{x}_{i-1}\|_{Q_w^{-1}}^2 \middle| \mathcal{Y}_n; \widehat{\boldsymbol{\theta}}_n^{(l-1)}\right\} \quad (4.6b)$$

As a generalization that will become useful later, let

$$J_\lambda(\boldsymbol{\theta}) \triangleq E\left\{\sum_{i=1}^n \lambda^{n-i} \|\mathbf{x}_i - \mathbf{A}\boldsymbol{\theta}\mathbf{x}_{i-1}\|_{Q_w^{-1}}^2 \middle| \mathcal{Y}_n; \widehat{\boldsymbol{\theta}}_n^{(l-1)}\right\} \quad (4.7)$$

where $0 < \lambda \leq 1$. Then $J_\lambda(\boldsymbol{\theta}) = J(\boldsymbol{\theta})$ when $\lambda = 1$.

Consider the case $\boldsymbol{\theta} = \text{Vec}(\mathbf{A})$. Solving $\partial J_\lambda(\boldsymbol{\theta})/\partial \boldsymbol{\theta} = \mathbf{0}$ yields

$$\widehat{\mathbf{A}}_n^{(l)} = \left[\sum_{i=1}^n \lambda^{n-i} \mathbf{R}_{x_i|n}^{(l-1)}[1] \right] \left[\sum_{i=1}^n \lambda^{n-i} \mathbf{R}_{x_{i-1}|n}^{(l-1)}[0] \right]^{-1} \quad (4.8)$$

where

$$\mathbf{R}_{x_i|n}^{(l-1)}[j] \triangleq E\{\mathbf{x}_i \mathbf{x}_{i-j}^h \mid \mathcal{Y}_n; \widehat{\mathbf{A}}_n^{(l-1)}\}, \quad j = 0, 1 \quad (4.9)$$

will be called the *smoothed state correlations*, with lag j . As shown in Appendix B.1,

$$\mathbf{R}_{x_{i-1}|n}^{(l-1)}[0] = \widehat{\mathbf{x}}_{i-1|n}^{(l-1)} (\widehat{\mathbf{x}}_{i-1|n}^{(l-1)})^h + \mathbf{P}_{i-1|n}^{(l-1)} \quad (4.10)$$

$$\mathbf{R}_{x_i|n}^{(l-1)}[1] = \widehat{\mathbf{x}}_{i|n}^{(l-1)} (\widehat{\mathbf{x}}_{i-1|n}^{(l-1)})^h + \mathbf{P}_{i|n}^{(l-1)} (\mathbf{J}_{s,i}^{(l-1)})^h \quad (4.11)$$

where $\widehat{\mathbf{x}}_{i|n}^{(l-1)}$ and $\mathbf{P}_{i|n}^{(l-1)}$ are the smoothed state estimate and the error covariance, respectively. $(\mathbf{J}_{s,i}^{(l-1)})$ is the closed-loop state transition matrix for the smoothed estimator (from $\mathbf{x}_{i|n}$ to $\mathbf{x}_{i-1|n}$) and is defined in (B.5). It also has other useful forms as given in (B.11) and (B.15). Note that the n dependency in $\mathbf{J}_{s,i}^{(l-1)}$ has been dropped for notational simplicity.

Equations (4.8)-(4.11) effectively indicate that the EM algorithm estimates the dynamic parameter, \mathbf{A}_n in this case, directly from the sequence of state estimates and their error statistics. Intuitively, this can be interpreted as the following. Assuming an initial $\widehat{\mathbf{A}}_0 \neq \mathbf{A}$, although the resulting sequence state estimates $\widehat{\mathbf{x}}_n$ may not be close to the true state \mathbf{x}_n , the trajectory $\widehat{\mathbf{x}}_n$ contains information about how the true state actually evolves over time. Hence one may estimate the true state dynamics from the sequence of state estimates and use that to improve the state estimation. Both the dynamics and state estimates can be further refined through iterations. This is illustrated by the block diagram shown in Figure 4-1. On the other hand, unlike the EKF algorithm where the uncertainties of the parameter estimation, *i.e.* the parameter estimate error covariance and the cross error covariance between the

state and parameter estimate, are available and provided to the state estimation, the EM based algorithm does not quantify this uncertainty.

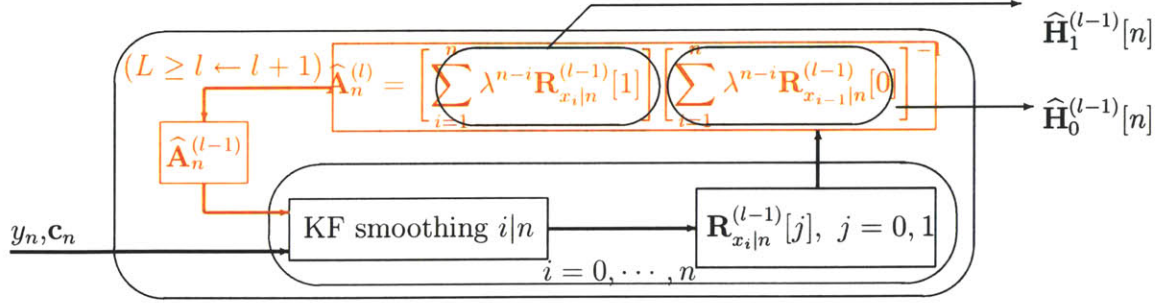


Figure 4-1: EM parameter estimation with Kalman state smoother

The derivation of (4.7)-(4.11), without the exponential weighting, can be found in [Shu82] and [Ell99] as well. The inclusion of the exponential weighting here is to favorably weight the error associated with the recent states hence allows some degree of parameter time-variability. Another effect of exponential weighting is that it also controls the smoothing memory, as explained in section 4.4.

The algorithm proposed in [Shu82] alternates between (4.8)-(4.11) and the fixed-interval Kalman state smoother (which has been included in Appendix B.2, and also see, for instance, [Jon89] and [Kai00]), and iteratively yields the parameter and state estimates. The problem is that to compute state estimates using the state smoothing recursion at the next observation data point, it needs to know all the previous smoothed state estimates and covariances. To save all these results, it requires a memory length increasing with time. In the next section a new algorithm is derived which recursively updates the sequential sums of the *smoothed state correlations* directly in vector form, thus eliminates that storage requirement.

4.3 Fast Recursion of Sums of the Second-Order Smoothed State Moments

Substituting (4.9) into (4.8) and using (4.10) and (4.11) yields

$$\widehat{\mathbf{A}}_n^{(l)} = \widehat{\mathbf{H}}_1^{(l-1)}[n] [\widehat{\mathbf{H}}_0^{(l-1)}[n]]^{-1} \quad (4.12)$$

where

$$\widehat{\mathbf{H}}_0^{(l-1)}[n] \triangleq E \left\{ \sum_{i=1}^n \lambda^{n-i} \mathbf{x}_{i-1} \mathbf{x}_{i-1}^h \middle| \mathcal{Y}_n; \widehat{\mathbf{A}}_n^{(l-1)} \right\} = \sum_{i=1}^n \lambda^{n-i} [\widehat{\mathbf{x}}_{i-1|n}^{(l-1)} (\widehat{\mathbf{x}}_{i-1|n}^{(l-1)})^h + \mathbf{P}_{i-1|n}^{(l-1)}] \quad (4.13a)$$

$$\widehat{\mathbf{H}}_1^{(l-1)}[n] \triangleq E \left\{ \sum_{i=1}^n \lambda^{n-i} \mathbf{x}_i \mathbf{x}_{i-1}^h \middle| \mathcal{Y}_n; \widehat{\mathbf{A}}_n^{(l-1)} \right\} = \sum_{i=1}^n \lambda^{n-i} [\widehat{\mathbf{x}}_{i|n}^{(l-1)} (\widehat{\mathbf{x}}_{i-1|n}^{(l-1)})^h + \mathbf{P}_{i|n}^{(l-1)} (\mathbf{J}_{s,i}^{(l-1)})^h] \quad (4.13b)$$

(4.13a)-(4.13b) are the weighted sequential sums of the *smoothed state correlations*, and will be called the *the cumulative state moments* with lag $j = 0$ and 1 , respectively. Intuitively, (4.12)-(4.13b) view the sequence of $\widehat{\mathbf{x}}_{i|n}$ as *observations* from which \mathbf{A} is estimated. The uncertainty associated with $\widehat{\mathbf{x}}_{i|n}$ is accounted for by the second terms in (4.13a) and (4.13b). (4.12) indicates that $\widehat{\mathbf{H}}_j^{(l-1)}[n]$ for $j = 0, 1$ are all that is needed to compute $\widehat{\mathbf{A}}_n^{(l)}$. Hence the basic idea of the new recursion scheme is to compute $\widehat{\mathbf{H}}_j^{(l-1)}[n]$ directly in a recursive fashion. This is similar to that of [Ell99] where a finite-dimensional filtering algorithm has been developed directly in terms of the elements of these cumulative state moments (with $\lambda = 1$). However, unlike in [Ell99] where the algorithm is derived via measure changes and the recursions of $\widehat{\mathbf{H}}_j^{(l-1)}[n]$ are elementwise, the new recursion algorithm proposed here is in vector form and the derivation follows directly from the state smoothing formula and the properties of the Kronecker product. The result is simpler from a mathematical point of view, more importantly, the resulting form of the recursion gives more insight into

the structure of the problem and leads to an intuitive interpretation of the effects of the parameter estimation averaging memory and the state smoothing memory. Note that neither [Ell99] nor [Ell02] deals with the exponential forgetting formulation. For notational simplicity, in this section the iteration index (l) is dropped. All the discussion is based on the data block \mathcal{Y}_n .

Substituting the fixed-point smoothing formulas (B.13) (see Appendix B.2) into (4.13) gives

$$\begin{aligned}\widehat{\mathbf{H}}_1[n] &= \lambda \widehat{\mathbf{H}}_1[n-1] + [\widehat{\mathbf{x}}_{n|n} \widehat{\mathbf{x}}_{n-1|n}^h + \mathbf{P}_{n|n} \mathbf{J}_{s,n}^h] \\ &\quad + \lambda \sum_{i=1}^{n-1} \lambda^{n-1-i} (\mathbf{T}_{i,n} \mathbf{M}_n \mathbf{T}_{i-1,n}^h + \widehat{\mathbf{x}}_{i|n-1} \mathbf{N}_n^h \mathbf{T}_{i-1,n}^h + \mathbf{T}_{i,n} \mathbf{N}_n \widehat{\mathbf{x}}_{i-1|n-1}^h)\end{aligned}\quad (4.14)$$

$$\begin{aligned}\widehat{\mathbf{H}}_0[n] &= \lambda \widehat{\mathbf{H}}_0[n-1] + [\widehat{\mathbf{x}}_{n-1|n} \widehat{\mathbf{x}}_{n-1|n}^h + \mathbf{P}_{n-1|n}] \\ &\quad + \lambda \sum_{i=1}^{n-1} \lambda^{n-1-i} (\mathbf{T}_{i-1,n} \mathbf{M}_n \mathbf{T}_{i-1,n}^h + \widehat{\mathbf{x}}_{i-1|n-1} \mathbf{N}_n^h \mathbf{T}_{i-1,n}^h + \mathbf{T}_{i-1,n} \mathbf{N}_n \widehat{\mathbf{x}}_{i-1|n-1}^h)\end{aligned}\quad (4.15)$$

where $\mathbf{T}_{i,n} \triangleq \prod_{j=i}^{n-1} \mathbf{J}_{s,j+1}$ for $i < n$ (and $\mathbf{T}_{n,n} = \mathbf{I}$) is the closed-loop state transition matrix from $\widehat{\mathbf{x}}_{n|n}$ to $\widehat{\mathbf{x}}_{i|n}$. In addition,

$$\mathbf{M}_n \triangleq \mathbf{P}_{n|n-1} \mathbf{c}_n^h [R_{e_n}^{-1} e_n e_n^h R_{e_n}^{-1} - R_{e_n}^{-1}] \mathbf{c}_n \mathbf{P}_{n|n-1} \quad (4.16)$$

$$\mathbf{N}_n \triangleq \mathbf{P}_{n|n-1} \mathbf{c}_n^h R_{e_n}^{-1} e_n \quad (4.17)$$

Note that \mathbf{N}_n is the measurement update term of the state estimation, *i.e.* $\mathbf{N}_n = \widehat{\mathbf{x}}_{n|n} - \widehat{\mathbf{x}}_{n|n-1}$, and $\mathbf{T}_{i,n} \mathbf{N}_n = \widehat{\mathbf{x}}_{i|n} - \widehat{\mathbf{x}}_{i|n-1}$. \mathbf{M}_n contains the cross term $\mathbf{N}_n \mathbf{N}_n^h$ coming from the state smoothing recursion and the update term of the smoothing state error covariance. Both \mathbf{M}_n and \mathbf{N}_n are zero-mean.

Based on (4.14)-(4.15) and using the properties of the Kronecker product, as shown in Appendix B.3, $\widehat{\mathbf{H}}_j[n]$ for $j = 0, 1$ can be computed recursively according to the following theorem:

Theorem 4 Consider the linear dynamical system (4.1), suppose a Kalman Filter assuming $\mathbf{A} = \widehat{\mathbf{A}}_n$ is applied to the system and at time n generates $\widehat{\mathbf{x}}_{n|n-1}$, $\widehat{\mathbf{x}}_{n|n}$, $\mathbf{P}_{n|n-1}$, $\mathbf{P}_{n|n}$, e_n , R_{e_n} , then the cumulative second-order state moments, $\widehat{\mathbf{H}}_0[n]$ and $\widehat{\mathbf{H}}_1[n]$, both defined in (4.13), can be updated recursively as follows:

$$\begin{aligned} \text{Vec}(\widehat{\mathbf{H}}_1[n]) &= \lambda \text{Vec}(\widehat{\mathbf{H}}_1[n-1]) + \text{Vec}[\widehat{\mathbf{x}}_{n|n} \widehat{\mathbf{x}}_{n-1|n}^h + \mathbf{P}_{n|n} \mathbf{J}_{s,n}^h] \\ &\quad + \lambda \{ \boldsymbol{\Omega}_{1,n} \text{Vec}(\mathbf{M}_n) + \boldsymbol{\Gamma}_{1,n} \mathbf{N}_n + \boldsymbol{\Upsilon}_{1,n} \mathbf{N}_n^* \} \end{aligned} \quad (4.18a)$$

$$\begin{aligned} \text{Vec}(\widehat{\mathbf{H}}_0[n]) &= \lambda \text{Vec}(\widehat{\mathbf{H}}_0[n-1]) + \text{Vec}[\widehat{\mathbf{x}}_{n-1|n} \widehat{\mathbf{x}}_{n-1|n}^h + \mathbf{P}_{n-1|n}] \\ &\quad + \lambda \{ \boldsymbol{\Omega}_{0,n} \text{Vec}(\mathbf{M}_n) + \boldsymbol{\Gamma}_{0,n} \mathbf{N}_n + \text{Vec}[\text{Mat}(\boldsymbol{\Gamma}_{0,n} \mathbf{N}_n)]^h \} \end{aligned} \quad (4.18b)$$

where $\boldsymbol{\Omega}_{j,n}$, $\boldsymbol{\Gamma}_{j,n}$ and $\boldsymbol{\Upsilon}_{1,n}$ for $j = 0, 1$ can be updated recursively as follows

$$\boldsymbol{\Omega}_{j,n+1} = [\mathbf{J}_{s,n}^* \otimes \mathbf{L}_{j,n} + \lambda \boldsymbol{\Omega}_{j,n}] (\mathbf{J}_{s,n+1}^* \otimes \mathbf{J}_{s,n+1}) \quad (4.19)$$

$$\boldsymbol{\Gamma}_{j,n+1} = [\widehat{\mathbf{x}}_{n-1|n}^* \otimes \mathbf{L}_{j,n} + \lambda \boldsymbol{\Gamma}_{j,n}] \mathbf{J}_{s,n+1} + \lambda \boldsymbol{\Omega}_{j,n} (\mathbf{N}_n^* \otimes \mathbf{J}_{s,n+1}) \quad (4.20)$$

$$\boldsymbol{\Upsilon}_{j,n+1} = [\mathbf{J}_{s,n}^* \otimes \widehat{\mathbf{x}}_{n-1+j|n} + \lambda \boldsymbol{\Upsilon}_{j,n}] \mathbf{J}_{s,n+1}^* + \lambda \boldsymbol{\Omega}_{j,n} (\mathbf{J}_{s,n+1}^* \otimes \mathbf{N}_n) \quad (4.21)$$

where $\mathbf{L}_{0,n} = \mathbf{J}_{s,n}$ and $\mathbf{L}_{1,n} = \mathbf{I}$. Furthermore, that $(\widehat{\mathbf{A}}_n, \mathbf{Q}_w^{1/2})$ is completely stabilisable and $(\widehat{\mathbf{A}}_n, \mathbf{c}_n)$ is completely detectable is the sufficient (and also necessary if $\lambda = 1$) conditions for (4.19)-(4.21) to be exponentially stable and hence $\boldsymbol{\Omega}_{j,n}$, $\boldsymbol{\Gamma}_{j,n}$ and $\boldsymbol{\Upsilon}_{j,n}$ all bounded.

The proof of (4.18a)-(4.21) is provided in Appendix B.3. The stability result is established in Appendix B.4.

The algorithm can be implemented as follows:

1. Get e_n , R_{e_n} from Kalman filtering then calculate \mathbf{M}_n and \mathbf{N}_n according to (4.16)-(4.17);
2. Using (B.13) with $i = n - 1$ to compute $\widehat{\mathbf{x}}_{n-1|n}$ and $\mathbf{P}_{n-1|n}$;
3. Kalman filter measurement update: calculate $\widehat{\mathbf{x}}_{n|n}$ and $\mathbf{P}_{n|n}$;

4. Update $\widehat{\mathbf{H}}_0[n]$ and $\widehat{\mathbf{H}}_1[n]$ using(4.18);
5. Kalman filter time update: calculate $\widehat{\mathbf{x}}_{n+1|n}$ and $\mathbf{P}_{n+1|n}$;
6. Calculate $\mathbf{J}_{s,n+1}$ from $\mathbf{P}_{n+1|n}$ using (B.15);
7. Update $\Omega_{1,n}$, $\Omega_{o,n}$, $\Gamma_{1,n}$, $\Gamma_{0,n}$ and $\Upsilon_{1,n}$ using (4.19)-(4.21).

where $\widehat{\mathbf{x}}_{n|n}$, $\mathbf{P}_{n|n}$ can overwrite $\widehat{\mathbf{x}}_{n-1|n-1}$, $\mathbf{P}_{n-1|n-1}$.

The block diagram for the vector form recursion for $\widehat{\mathbf{H}}_1^{(l-1)}[n]$ is given in Figure 4-2 and the EM algorithm based on this new recursion form is given in Figure 4-3. In Figure 4-2, the exponential weighting factor λ is split into λ_1 and λ_2 with each controls the averaging window length of $\widehat{\mathbf{H}}_1^{(l-1)}[n]$ and the state smoothing memory length. More details about this generalization is given in section 4.4.

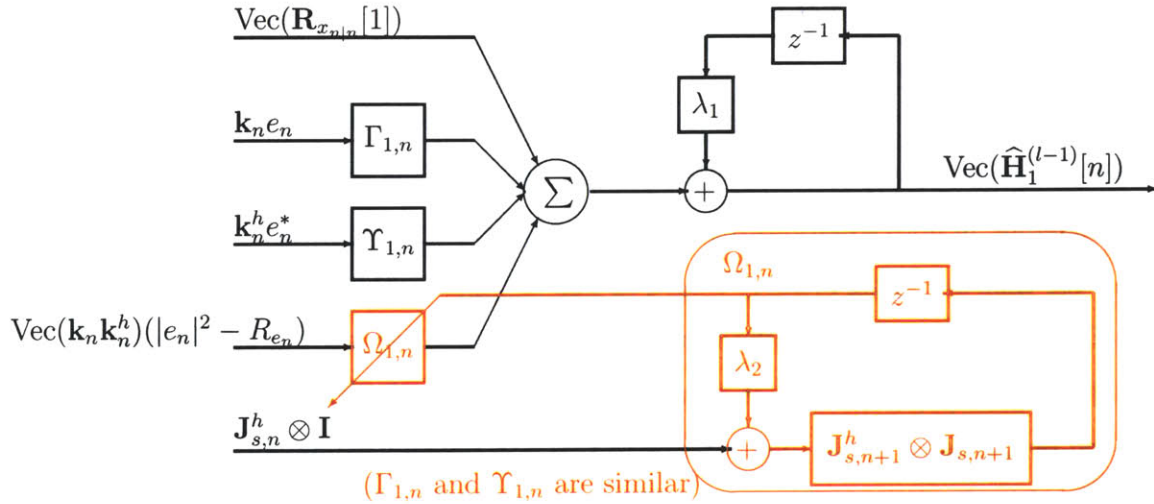


Figure 4-2: Diagram for the new vector form recursion of $\widehat{\mathbf{H}}_1^{(l-1)}[n]$. Similar for $\widehat{\mathbf{H}}_0^{(l-1)}[n]$

Note that up to this point, the new recursion form is derived solely as the computing engine for the iterative EM parameter estimator. Thus it runs once every EM iteration to calculate the parameter estimate. The EM procedure requires multiple runs of these recursions over the whole data block every time when a new data

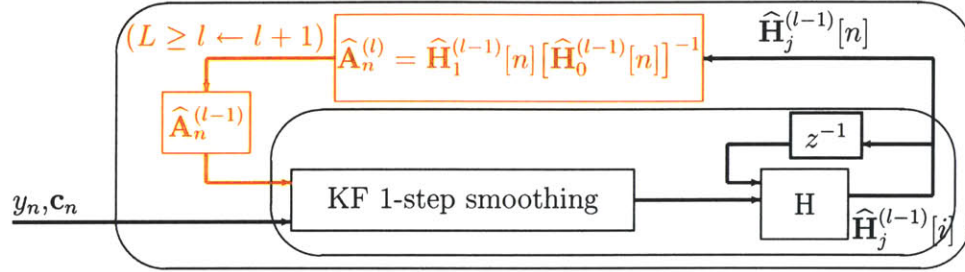


Figure 4-3: EM algorithm based on the new recursion form of the cumulative state moments

emerges. From this perspective, the advantage of the new recursion form (4.18a)-(4.21) is to provide a recursive filtering scheme at each iteration whose storage space is small and independent of the observation time.

A useful observation is that in both (4.14) and (4.15), the first terms are the averaging terms over time; the second terms are the new components associated with latest state estimates; and the terms in the summands represent the update components of the *smoothed state correlations* associated with the latest measurement data. Therefore, in both equations the exponential forgetting factor λ simultaneously controls the time averaging memory length as well as the smoothing memory length. This, of course, is the result of the formulation laid out in section 4.2, specifically by (4.7). Heuristically speaking it is not necessary to have both memory lengths controlled by the same factor. This will be reflected in the suboptimal algorithm to be developed in the next section.

4.4 Suboptimal Algorithms

The EM algorithm involves multiple iterations at each time point. In every iteration, using the parameter estimate obtained from the previous iteration, $\hat{\mathbf{H}}_j^{(l-1)}[n]$ has to be recursively computed all the way from $\hat{\mathbf{H}}_j^{(l-1)}[1]$ before being used to gen-

erate the new parameter estimate. For most on-line applications this is not feasible computationally. This section develops a class of suboptimal algorithms based on the recursion forms derived in the previous section. Specifically the new suboptimal algorithm is obtained after three modifications of the EM algorithm: 1) Limiting the number of iterations at every time point which gives the dynamic EM algorithm as discussed in [Jor99]; 2) Based on 1), further limiting the latest parameter estimate to be applied only on the current state estimate which leads to the recursive algorithm similar to the one proposed in [Tit84]; 3) Controlling separately the parameter estimate time averaging memory length and the state smoothing memory length. It will be shown that the suboptimal algorithms proposed previously in [Wei94] and [Ell02] and applied in [Gao03] are special cases of this new algorithm.

4.4.1 The Derivation of the Suboptimal Algorithm

Recall that the EM algorithm may be viewed as a solution to the quadratic minimization problem of (4.7) and an iterative approach to compute (4.13). Restate both equation as follows

$$J_\lambda(\theta) \triangleq \sum_{i=1}^n \lambda^{n-i} E\{\|\mathbf{x}_i - \mathbf{A}(\theta)\mathbf{x}_{i-1}\|_{Q_w^{-1}}^2 | \mathcal{Y}_n; \hat{\theta}_n^{(l-1)}\} \quad (4.22a)$$

$$\hat{\mathbf{H}}_j^{(l)}[n] \triangleq E\{\sum_{i=1}^n \lambda^{n-i} \mathbf{x}_{i-1+j} \mathbf{x}_{i-1}^h | \mathcal{Y}_n; \hat{\mathbf{A}}_n^{(l-1)}\} \quad (4.22b)$$

Limiting the number of iterations at each time point to be 1 effectively changes (4.22a) and (4.22b) into

$$J_\lambda(\theta) \triangleq \sum_{i=1}^n \lambda^{n-i} E\{\|\mathbf{x}_i - \mathbf{A}(\theta)\mathbf{x}_{i-1}\|_{Q_w^{-1}}^2 | \mathcal{Y}_n; \hat{\theta}_{n-1}\} \quad (4.23a)$$

$$\hat{\mathbf{H}}_j[n] \triangleq E\{\sum_{i=1}^n \lambda^{n-i} \mathbf{x}_{i-1+j} \mathbf{x}_{i-1}^h | \mathcal{Y}_n; \hat{\mathbf{A}}_{n-1}\} \quad (4.23b)$$

in which the Kalman filter assuming $\theta = \theta_{n-1}$ is applied to obtain smoothed state estimates for $i = 1, \dots, n$ with $\mathbf{A} = \hat{\mathbf{A}}_{n-1}$ from which $\hat{\mathbf{H}}_j[n]$ is calculated all the

way from $\widehat{\mathbf{H}}_j[1]$, using the recursions (4.18a)-(4.21). This is because all the state estimates are impacted by the latest parameter estimate θ_{n-1} .

The second step of simplification, replacing $\widehat{\theta}_{n-1}$ and $\widehat{\mathbf{A}}_{n-1}$ in (4.23a) and (4.23b) by $\widehat{\theta}_{i-1}$ and $\widehat{\mathbf{A}}_{i-1}$ respectively, converts the algorithm into recursive form. That is

$$J_\lambda(\theta) \triangleq \sum_{i=1}^n \lambda^{n-i} E\{\|\mathbf{x}_i - \mathbf{A}(\theta)\mathbf{x}_{i-1}\|_{Q_w^{-1}}^2 | \mathcal{Y}_n; \widehat{\theta}_{i-1}\} \quad (4.24a)$$

$$\widehat{\mathbf{H}}_j[n] \triangleq \sum_{i=1}^n \lambda^{n-i} E\{\mathbf{x}_{i-1+j}\mathbf{x}_{i-1}^h | \mathcal{Y}_n; \widehat{\mathbf{A}}_{i-1}\} \quad (4.24b)$$

in which the latest parameter estimate is applied only to the state estimates at time n and $n-1$. Consequently the resulting algorithm carries out one update step of (4.18a)-(4.21) every data point.

The next modification is motivated by the observation described at the end of the last section. That is, the parameter averaging memory and the state smoothing memory are controlled separately. Heuristically, after dropping the iteration index, (4.18a)-(4.21) can be modified directly into the following

$$\begin{aligned} \text{Vec}(\widehat{\mathbf{H}}_1[n]) &= \lambda_1 \text{Vec}(\widehat{\mathbf{H}}_1[n-1]) + \text{Vec}[\widehat{\mathbf{x}}_{n|n}\widehat{\mathbf{x}}_{n-1|n}^h + \mathbf{P}_{n|n}\mathbf{J}_{s,n}^h] \\ &\quad + \lambda_1 \{\mathbf{\Omega}_{1,n}\text{Vec}(\mathbf{M}_n) + \mathbf{\Gamma}_{1,n}\mathbf{N}_n + \mathbf{\Upsilon}_{1,n}\mathbf{N}_n^*\} \end{aligned} \quad (4.25a)$$

$$\begin{aligned} \text{Vec}(\widehat{\mathbf{H}}_0[n]) &= \lambda_1 \text{Vec}(\widehat{\mathbf{H}}_0[n-1]) + \text{Vec}[\widehat{\mathbf{x}}_{n-1|n}\widehat{\mathbf{x}}_{n-1|n}^h + \mathbf{P}_{n-1|n}] \\ &\quad + \lambda_1 \{\mathbf{\Omega}_{0,n}\text{Vec}(\mathbf{M}_n) + \mathbf{\Gamma}_{0,n}\mathbf{N}_n + \text{Vec}[\text{Mat}(\mathbf{\Gamma}_{0,n}\mathbf{N}_n)]^h\} \end{aligned} \quad (4.25b)$$

$$\mathbf{\Omega}_{j,n+1} = [\mathbf{J}_{s,n}^* \otimes \mathbf{L}_{j,n} + \lambda_2 \mathbf{\Omega}_{j,n}] (\mathbf{J}_{s,n+1}^* \otimes \mathbf{J}_{s,n+1}) \quad (4.25c)$$

$$\mathbf{\Gamma}_{j,n+1} = [\widehat{\mathbf{x}}_{n-1|n}^* \otimes \mathbf{L}_{j,n} + \lambda_2 \mathbf{\Gamma}_{j,n}] \mathbf{J}_{s,n+1} + \lambda_2 \mathbf{\Omega}_{j,n} (\mathbf{N}_n^* \otimes \mathbf{J}_{s,n+1}) \quad (4.25d)$$

$$\mathbf{\Upsilon}_{j,n+1} = [\mathbf{J}_{s,n}^* \otimes \widehat{\mathbf{x}}_{n-1+j|n} + \lambda_2 \mathbf{\Upsilon}_{j,n}] \mathbf{J}_{s,n+1}^* + \lambda_2 \mathbf{\Omega}_{j,n} (\mathbf{J}_{s,n+1}^* \otimes \mathbf{N}_n) \quad (4.25e)$$

where again $\mathbf{L}_{0,n} = \mathbf{J}_{s,n}$ and $\mathbf{L}_{1,n} = \mathbf{I}$. As a result, the parameter average memory length and the state smoothing memory length are controlled by λ_1 and λ_2 , respectively. The choices of λ_1 and λ_2 will both have effects on $\widehat{\mathbf{H}}_j[n]$ and hence on the transient as well as steady-state performance of the resulting algorithm.

Figure 4-4 shows the block diagram of the suboptimal algorithm.

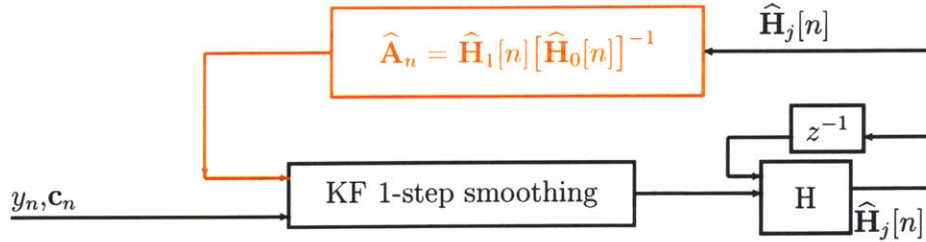


Figure 4-4: Diagram of the suboptimal EM algorithm

4.4.2 Special Cases

The algorithms given by (4.25) can be specialized by choosing specific sets of forgetting factors. In particular, two previously reported suboptimal algorithms, in [Wei94] and [Ell02] respectively, can be included as special cases of (4.25).

Letting $\lambda_1 = \lambda_2 = 1$ in (4.25) gives the recursive algorithm proposed in [Ell02], which also corresponds to (4.24) with $\lambda = 1$. Note that in [Ell02] the authors claim that their algorithm can also deal with time-varying parameter. Strictly speaking that is not true when the algorithm effectively has an infinite averaging window length, even though the parameter estimates used by the Kalman filter are time-varying. In fact, the algorithm of [Ell02] usually has a very slow convergence rate as confirmed by their own numerical results.

Another special case is when $\lambda_2 = 0$ in (4.25). This is similar to the sequential algorithm proposed in [Wei94]. Effectively, the smoothing memory is limited to lag

one. It corresponds to

$$J_\lambda(\theta) \triangleq \sum_{i=1}^n \lambda^{n-i} E\{\|\mathbf{x}_i - \mathbf{A}(\theta)\mathbf{x}_{i-1}\|_{Q_w^{-1}}^2 | \mathcal{Y}_i; \hat{\theta}_{i-1}\} \quad (4.26a)$$

$$\hat{\mathbf{H}}_j[n] \triangleq \sum_{i=1}^n \lambda^{n-i} E\{\mathbf{x}_{i-1+j} \mathbf{x}_{i-1}^h | \mathcal{Y}_i; \hat{\mathbf{A}}_{i-1}\} \quad (4.26b)$$

Consequently the computation of $\hat{\mathbf{H}}_j[n]$ has a much simpler recursion form (for $j = 0, 1$):

$$\hat{\mathbf{H}}_j[n] = \lambda \hat{\mathbf{H}}_j[n-1] + E\{\mathbf{x}_{n-1+j} \mathbf{x}_{n-1}^h | \mathcal{Y}_n; \hat{\mathbf{A}}_{n-1}\} \quad (4.27)$$

(4.27) has also been used in [Gao03] due to its reduced computation.

4.4.3 A General Parameter Recursion

The suboptimal algorithms (4.25) and its special cases can be captured by the following recursion for the parameter estimate $\hat{\mathbf{A}}_n$:

$$\hat{\mathbf{A}}_n = \hat{\mathbf{A}}_{n-1} + (\mathbf{L}_1[n] - \hat{\mathbf{A}}_{n-1} \mathbf{L}_0[n]) \hat{\mathbf{H}}_0^{-1}[n] \quad (4.28)$$

where $\mathbf{L}_1[n] - \hat{\mathbf{A}}_{n-1} \mathbf{L}_0[n]$ and $\hat{\mathbf{H}}_0^{-1}[n]$ may be viewed as the innovation and the gain respectively, more will be said on this in section 4.5. $\mathbf{L}_j[n] \triangleq \hat{\mathbf{H}}_j[n] - \lambda_1 \hat{\mathbf{H}}_j[n-1]$, $i = 0, 1$ are functions of the weighting factors:

$$\mathbf{L}_1[n] = (\hat{\mathbf{x}}_{n|n} \hat{\mathbf{x}}_{n-1|n}^h + \mathbf{P}_{n|n} \mathbf{J}_{s,n}^h) + \lambda_1 \text{Mat}\{\boldsymbol{\Omega}_{1,n} \text{Vec}(\mathbf{M}_n) + \boldsymbol{\Gamma}_{1,n} \mathbf{N}_n + \boldsymbol{\Upsilon}_{1,n} \mathbf{N}_n^*\} \quad (4.29a)$$

$$\mathbf{L}_0[n] = (\hat{\mathbf{x}}_{n-1|n} \hat{\mathbf{x}}_{n-1|n}^h + \mathbf{P}_{n-1|n}) + \lambda_1 \text{Mat}\{\boldsymbol{\Omega}_{0,n} \text{Vec}(\mathbf{M}_n) + \boldsymbol{\Gamma}_{0,n} \mathbf{N}_n + \text{Vec}[\text{Mat}(\boldsymbol{\Gamma}_{0,n} \mathbf{N}_n)]^h\} \quad (4.29b)$$

(4.28) will be the basis for the parameter convergence analysis given in the next section.

4.4.4 A Numerical Example

This section presents a numerical example of channel estimation using the suboptimal EM algorithm. The results are presented together with those of the Exponentially Weighted Recursive Least Squares (EWRLS) algorithm, the EKF, and the Kalman filter. The four-tap channel was generated according to model (4.1) such that \mathbf{A} is a 4×4 diagonal matrix with complex diagonal elements all close to the unit circle. The mean amplitude of the diagonal elements is 0.96. The process noise had a unit variance. The received signal was generated using transmitted symbols \mathbf{c}_k derived from a Gaussian pseudo-random sequence \mathbf{g}_k such that $\mathbf{c}_k = 1$ if $\mathbf{g}_k \geq 0$ and -1 otherwise. The observation noise variance was determined by the SNR values. The EWRLS had a forgetting factor .99. The EKF jointly estimated the states and the parameters. The Kalman filter, as a benchmark, knew the true value of \mathbf{A} . The suboptimal EM algorithm used different combinations of values for the two forgetting factor λ_1 and λ_2 for studying the transient parameter convergence and for steady-state error performance evaluation.

Figure 4-5 shows the parameter convergence curves using the plain EKF algorithm and the suboptimal EM with four sets of forgetting factor combinations $(\lambda_1, \lambda_2) = (0.92, 0), (0.92, 0.92), (0.98, 0), (0.98, 0.98), (0.998, 0), (0.998, 0.998)$, respectively. The data was generated as described above with $SNR = 3dB$ with 10Hz Doppler. The plot indicates that with $\lambda_1 = 0.998$ the suboptimal EM algorithm has a very slow convergence (the flat curves on the top). When λ_2 is fixed and as λ_1 decreases, effectively with a shorter parameter averaging window, the convergence speeds up. This is because the adapting gain increases as averaging memory is shortened. The effects of λ_2 which controls the length of the smoothing memory, is in opposite. As λ_2 decreases while fixing λ_1 , the convergence slows down. This is due to the smaller amount of data used to update the parameter at each recursion when the smoothing window is shortened. Note that the simulation is based on a constant \mathbf{A} . In the case of a time-varying \mathbf{A}_i , it would be desirable to use smaller values for both forgetting

factors to obtain a good tracking ability. In addition, by choosing a smaller λ_1 , the suboptimal algorithm parameter estimate converges faster than the EKF estimate.

Figure 4-6 shows the steady-state channel prediction errors obtained using the EWRLS, the suboptimal EM algorithm with two sets of $(\lambda_1, \lambda_2) = (0.92, 0), (0.92, 0.92)$, the EKF algorithm and a Kalman filter respectively. The comparison is made at six different receiver SNR levels with a fixed 5 Hz Doppler. The Kalman filter is the optimal benchmark as it assumes perfect knowledge of the system. At the lower SNR region, i.e. $SNR = -10 \sim -5\text{dB}$, the suboptimal EM algorithm performs better than the EWRLS and the EKF. As the SNR level increases, the EWRLS has a significantly larger error than the suboptimal EM. On the other hand, the EKF gradually approaches and eventually outperforms the suboptimal EM. This could be explained by decomposing the error into the noise error and the lag error. At the lower SNR region, it is expected that the noise error dominates the total prediction error. The effect of dynamics which causes the lag error is less important. As a result, the EWRLS, even though does not account for the channel variations explicitly, still has a marginally larger error. In addition, the suboptimal EM uses a smoother with a limited smoothing memory, is expected to perform better than the EKF which only provides filtered estimates. In the higher SNR region, the lag error caused by channel dynamics becomes more important as the noise effect diminishes. Thus the lack of dynamic modeling of the EWRLS causes substantial performance loss. Both the suboptimal EM and EKF are able to estimate the channel as well as its dynamics. However, as the noise level lowered, the advantage of smoothing become less important. Furthermore, the suboptimal EM with a small λ_1 has a fixed adapting gain that does not diminish in steady-state. Since the parameter used is constant, this causes the EKF to perform better in the steady-state.

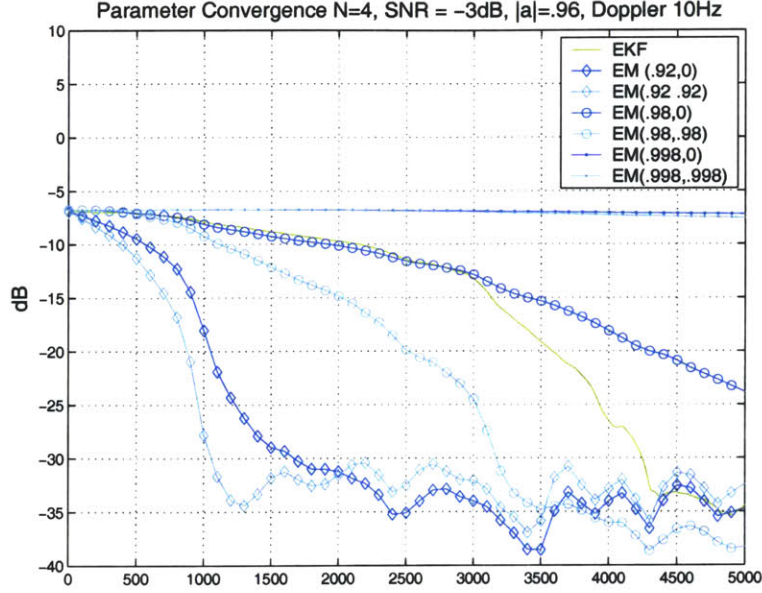


Figure 4-5: Parameter convergence of the suboptimal EM algorithms. A four-tap channel with $\text{SNR} = -3\text{dB}$ and 10Hz Doppler. \mathbf{A} is a diagonal matrix. The mean amplitude of its diagonal elements is 0.96 .

4.5 Properties of the Suboptimal Algorithm

4.5.1 The Innovation Form of the Parameter Recursion

This section considers the stability of parameter recursion, using the suboptimal algorithm (4.25) with $\lambda_2 = 0$. More specifically, consider the recursion

$$\hat{\mathbf{A}}_n = \hat{\mathbf{A}}_{n-1} + (\mathbf{L}_1[n] - \hat{\mathbf{A}}_{n-1}\mathbf{L}_0[n])\hat{\mathbf{H}}_0^{-1}[n] \quad (4.30)$$

$$\mathbf{L}_j[n] = E\{\mathbf{x}_{n-1+j}\mathbf{x}_{n-1}^h | \mathcal{Y}_n; \hat{\mathbf{A}}_{n-1}\}, \quad j = 0, 1 \quad (4.31)$$

where the parameter estimate obtained at time n , $\hat{\mathbf{A}}_n$, is a matrix.

According to (B.34) derived in Appendix B.5,

$$\mathbf{L}_1[n] - \hat{\mathbf{A}}_{n-1}\mathbf{L}_0[n] = \mathbf{k}_n(y_n\hat{\mathbf{x}}_{n-1|n}^h - \mathbf{c}_n\hat{\mathbf{A}}_{n-1}\mathbf{L}_0[n]) \quad (4.32)$$

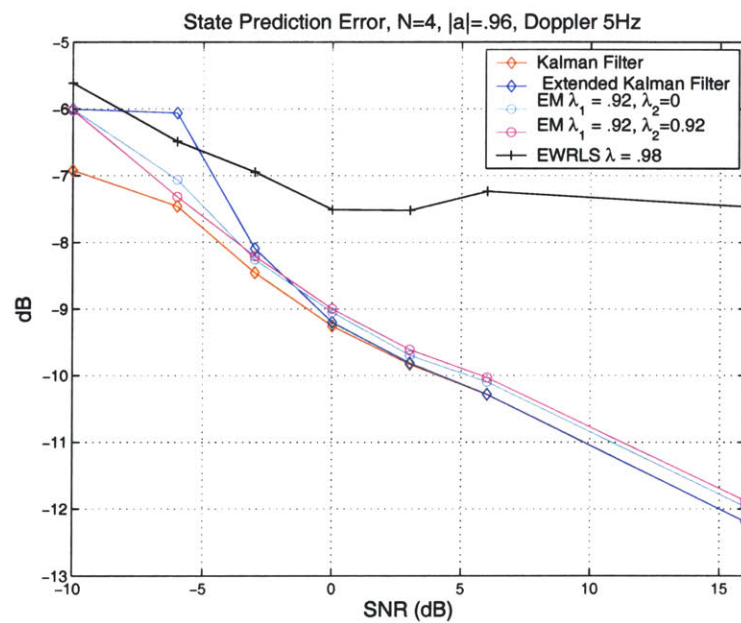


Figure 4-6: Steady-state channel prediction errors of Suboptimal EM algorithm, the EWRLS, the EKF, and the KF knowing the model parameters. A four-tap channel with 10Hz Doppler. \mathbf{A} is a diagonal matrix. The mean amplitude of its diagonal elements is 0.96

where $\mathbf{k}_n = (\mathbf{c}_n \mathbf{Q}_w \mathbf{c}_n^h + \sigma_v^2)^{-1} \mathbf{Q}_w \mathbf{c}_n^h$.

Denoting $s_n \triangleq (\mathbf{c}_n \mathbf{Q}_w \mathbf{c}_n^h + \sigma_v^2)^{-1}$, then $\mathbf{k}_n = s_n \mathbf{Q}_w \mathbf{c}_n^h$.

Substituting (4.32) into (4.30) yields

$$\widehat{\mathbf{A}}_n = \widehat{\mathbf{A}}_{n-1} + \mathbf{k}_n (y_n \widehat{\mathbf{x}}_{n-1|n}^h - \mathbf{c}_n \widehat{\mathbf{A}}_{n-1} \mathbf{L}_0[n]) \widehat{\mathbf{H}}_0^{-1}[n] \quad (4.33)$$

(4.33) is essentially a matrix recursion in $\mathcal{C}^{N \times N}$. However, it is clear that the second term on the right hand side of (4.33) is of rank one. In other words, the one-step update of the matrix is only of rank one along a particular direction. Hence intuitively one would expect that at least $N \times N$ steps will be needed to completely update the whole parameter space. Later this will become more evident.

Now letting $\widehat{\mathbf{a}}_n = \text{Vec}(\widehat{\mathbf{A}}_n)$, following (B.39) derived in Appendix B.5 yields:

$$\begin{aligned} \widehat{\mathbf{a}}_n &= \widehat{\mathbf{a}}_{n-1} + (\widehat{\mathbf{H}}_0^{-t}[n] \otimes \mathbf{Q}_w) (\widehat{\mathbf{x}}_{n-1|n-1}^t \otimes \mathbf{c}_n)^h R_{e_n}^{-1} e_n \\ &+ [(\widehat{\mathbf{H}}_0^{-t}[n] \otimes \mathbf{Q}_w) (\mathbf{P}_{n-1|n-1}^t \otimes \mathbf{c}_n^h \mathbf{c}_n)] \widehat{\mathbf{a}}_{n-1} R_{e_n}^{-1} (R_{e_n}^{-1} e_n e_n^* - 1) \end{aligned} \quad (4.34)$$

in which the parameter is updated by two innovation terms. The first order term is similar to that of EKF update hence an equivalent Kalman gain may be defined as $\mathbf{L}_n \triangleq [(\widehat{\mathbf{H}}_0^{-t}[n] \widehat{\mathbf{x}}_{n-1|n-1}^* \otimes \mathbf{Q}_w) \mathbf{c}_n^h R_{e_n}^{-1}]$. The second term is of second order in e_n . Specifically, it is an update term based on the error $R_{e_n}^{-1} e_n e_n^* - 1$, the mismatch between R_{e_n} , the predicted innovation variance, and $e_n e_n^*$, the residual error energy.

A connection between the suboptimal EM algorithm and the EKF modification in section 3.2.3 can be established at this point. The second-order innovation term in (4.34) is in an identical form as in (3.42). This is not accidental. (3.42) is obtained by matching EKF with the stochastic gradient algorithm that minimizes the negative log-likelihood function, or equivalently computes the ML parameter estimate, while the suboptimal EM is a sequential version of the EM algorithm which also tries to find the ML parameter estimate. This extra second-order term is effectively a result of data smoothing which is required to obtain the ML parameter estimate for this

nonlinear problem.

Another important consequence of (4.34) is computational. It can be seen that except $\widehat{\mathbf{H}}_0^{-t}[n]$, all terms in the update equation have been computed from the Kalman filtering and the previous parameter estimation. Thus an efficient and relatively accurate approximation of $\widehat{\mathbf{H}}_0[n]$ will lead to a fast version of the suboptimal EM algorithm.

4.5.2 The Extended Persistent Excitation Condition

Now define $\tilde{\mathbf{A}}_n \triangleq \widehat{\mathbf{A}} - \mathbf{A}$ as the parameter error matrix; $\tilde{\mathbf{g}}_n \triangleq z_n \widehat{\mathbf{x}}_{n-1|n}^h - E\{z_n \widehat{\mathbf{x}}_{n-1|n}^h\} + \mathbf{c}_n \mathbf{A} \tilde{\mathbf{x}}_{n-1|n} \widehat{\mathbf{x}}_{n-1|n}^h$, a zero-mean random row vector and $\mathbf{\Gamma}_n \triangleq \mathbf{k}_n \tilde{\mathbf{g}}_n \widehat{\mathbf{H}}_0^{-1}[n]$. Here $z_n = \mathbf{c}_n \mathbf{w}_{n-1} + v_n$. Denote the parameter error vector by $\tilde{\mathbf{a}}_n = \text{Vec}(\tilde{\mathbf{A}}_n)$, and let $\gamma_n = \text{Vec}(\mathbf{\Gamma}_n)$, the following has been shown in Appendix B.5,

$$\widehat{\mathbf{A}}_n = \widehat{\mathbf{A}}_{n-1} + [\mathbf{k}_n (-\mathbf{c}_n \tilde{\mathbf{A}}_{n-1} \widehat{\mathbf{x}}_{n-1|n} \widehat{\mathbf{x}}_{n-1|n}^h + \tilde{\mathbf{g}}_n)] \widehat{\mathbf{H}}_0^{-1}[n] \quad (4.35a)$$

$$\tilde{\mathbf{A}}_n = \tilde{\mathbf{A}}_{n-1} - \mathbf{k}_n \mathbf{c}_n \tilde{\mathbf{A}}_{n-1} \widehat{\mathbf{x}}_{n-1|n} \widehat{\mathbf{x}}_{n-1|n}^h \widehat{\mathbf{H}}_0^{-1}[n] + \mathbf{\Gamma}_n \quad (4.35b)$$

$$\begin{aligned} \tilde{\mathbf{a}}_n &= [\mathbf{I} - (\widehat{\mathbf{x}}_{n-1|n} \widehat{\mathbf{x}}_{n-1|n}^h \widehat{\mathbf{H}}_0^{-1}[n])^t \otimes (\mathbf{k}_n \mathbf{c}_n)] \tilde{\mathbf{a}}_{n-1} + \gamma_n \\ &= \{\mathbf{I} - [(\|\widehat{\mathbf{x}}_{n-1|n}\|^2 \widehat{\mathbf{H}}_0^{-t}[n]) \otimes (\mathbf{Q}_w \|\mathbf{c}_n\|^2 (\mathbf{c}_n \mathbf{Q}_w \mathbf{c}_n^h + \sigma_v^2)^{-1})] (\mathbf{b}_n \mathbf{b}_n^h)\} \tilde{\mathbf{a}}_{n-1} + \gamma_n \end{aligned} \quad (4.35c)$$

$$\triangleq [\mathbf{I} - \mathbf{S}_n \mathbf{b}_n \mathbf{b}_n^h] \tilde{\mathbf{a}}_{n-1} + \gamma_n \quad (4.35d)$$

where $\mathbf{S}_n \triangleq [(\|\widehat{\mathbf{x}}_{n-1|n}\|^2 \widehat{\mathbf{H}}_0^{-t}[n]) \otimes (\mathbf{Q}_w \|\mathbf{c}_n\|^2 (\mathbf{c}_n \mathbf{Q}_w \mathbf{c}_n^h + \sigma_v^2)^{-1})]$ and

$$\mathbf{b}_n \triangleq \left(\frac{\widehat{\mathbf{x}}_{n-1|n}^t}{\|\widehat{\mathbf{x}}_{n-1|n}\|} \otimes \frac{\mathbf{c}_n}{\|\mathbf{c}_n\|} \right)^h \quad (4.36)$$

is a $N^2 \times 1$ unit vector along the direction of $\widehat{\mathbf{x}}_{n-1|n}^t \otimes \mathbf{c}_n$.

Remarks on (4.35c)-(4.36):

- (4.35c) is a time-varying stochastic difference equation in the parameter estimation error $\tilde{\mathbf{a}}_n$. It specifies convergence behavior as well as the stability of the

parameter estimation. The exponential stability of (4.35c) is decided by the maximum singular value of the sequential products of its coefficient matrices. In this case, it is $\sigma_{max}[\prod_{m=n}^{n+M-1}(\mathbf{I} - \mathbf{S}_m \mathbf{b}_m \mathbf{b}_m^h)]$ for some $M \geq N^2$ and any $n > 0$. If $\sigma_{max} < 1$ deterministically or in probability 1, then given a bounded stochastic input, (4.35c) will be exponentially stable and the parameter estimation converges. In this case, that is largely dependent on the sequences of \mathbf{S}_m and \mathbf{b}_m .

2. The coefficient matrix $\mathbf{I} - \mathbf{S}_n \mathbf{b}_n \mathbf{b}_n^h$ has a very interesting structure. if $\mathbf{S}_n = 2\mathbf{I}$, then it corresponds to the Householder transform matrix with $(\mathbf{I} - \mathbf{S}_n \mathbf{b}_n \mathbf{b}_n^h) \mathbf{b}_n = -\mathbf{b}_n$. If $\mathbf{S}_n = \eta \mathbf{I}$ for some $0 < \eta < 1$, then $\mathbf{I} - \mathbf{S}_n \mathbf{b}_n \mathbf{b}_n^h$ acts like a filter, such that vectors orthogonal to \mathbf{b}_n pass through the system intact while all others will be compressed, *i.e.* $\|(\mathbf{I} - \eta \mathbf{b}_n \mathbf{b}_n^h) \mathbf{e}\| = \|\mathbf{e}\|$ if $\mathbf{b}_n^h \mathbf{e} = 0$, and $\|(\mathbf{I} - \eta \mathbf{b}_n \mathbf{b}_n^h) \mathbf{e}\| < \|\mathbf{e}\|$ if $\mathbf{b}_n^h \mathbf{e} \neq 0$. When \mathbf{S}_n is not a scaled identity matrix, it is easy to show that all eigenvalues of $\mathbf{I} - \mathbf{S}_n \mathbf{b}_n \mathbf{b}_n^h$ are on or within the unit circle. But the singular values, which decides the stability as mentioned early, are not necessarily confined by the unit circle. This makes the stability analysis of (4.35c) very difficult. As shown in Appendix B.6, the singular values of $\prod_{m=n}^{n+M-1}(\mathbf{I} - \mathbf{S}_m \mathbf{b}_m \mathbf{b}_m^h)$ are decided by the eigenvalue distribution of \mathbf{S}_m as well as the degree of persistent excitation of the sequence \mathbf{b}_m .
3. The expression (B.51c) is similar to the error recursion equation for parameter estimation in linear regression models, as reviewed in Chapter 1. According to the stability results developed in [Bit84][Cam94][Guo95a], that $\hat{\mathbf{x}}_{n-1|n}^t \otimes \mathbf{c}_n$ satisfies the persistent excitation (PE) condition is necessary for the stability of (4.35c), which in turn requires both $\hat{\mathbf{x}}_{n-1|n}^t$ and \mathbf{c}_n be persistently exciting.

The above persistent excitation result can be interpreted from a slightly different perspective. The recursive algorithm that alternatively estimates the state and the parameter, using one to get the other, can equivalently be viewed as formulating the

problem into two steps:

- Step I: State estimation, using $\mathbf{A} = \widehat{\mathbf{A}}_{n-1}$ and the model:

$$\begin{cases} \mathbf{x}_{k+1} = \widehat{\mathbf{A}}_{n-1}(\theta)\mathbf{x}_k + \mathbf{w}_k & (4.37a) \\ y_k = \mathbf{c}_k\mathbf{x}_k + v_k & (4.37b) \end{cases}$$

- Step II: Parameter estimation, assuming $\mathbf{x}_k = \mathbf{A}\widehat{\mathbf{x}}_{k-1|k} + \widehat{\mathbf{w}}_{k-1|k}$, from

$$y_k = \mathbf{c}_k\mathbf{A}\widehat{\mathbf{x}}_{k-1|k} + \mathbf{c}_k\widehat{\mathbf{w}}_{k-1|k} + v_k \quad (4.38)$$

taking Vec on both sides yields

$$y_k = (\widehat{\mathbf{x}}_{k-1|k}^t \otimes \mathbf{c}_k)\text{Vec}(\mathbf{A}) + \mathbf{c}_k\widehat{\mathbf{w}}_{k-1|k} + v_k \quad (4.39)$$

which is a linear regression model with unknown parameter $\mathbf{a} \triangleq \text{Vec}(\mathbf{A})$. The condition of persistent excitation then is in terms of $\widehat{\mathbf{x}}_{k-1|k}^t \otimes \mathbf{c}_k$.

As remarked early, the stability of (4.35c) is determined by $\|\Pi_{m=n}^{n+M-1}(\mathbf{I} - \mathbf{S}_m\mathbf{b}_m\mathbf{b}_m^h)\|$ for some $M \geq N^2$ and any $n > 0$ and the boundedness of γ_n . The difficulty is that $\mathbf{I} - \mathbf{S}_m\mathbf{b}_m\mathbf{b}_m^h$ may have singular value greater than 1 even though all its eigenvalues are all less than 1. Appendix B.6 provided analytical results concerning the singular values of $\Pi_{m=n}^{n+M-1}(\mathbf{I} - \mathbf{S}_m\mathbf{b}_m\mathbf{b}_m^h)$ for special cases, and for general case, conjectures via numerical investigation that assuming $\mathbf{S}_m = \mathbf{S}$ and if \mathbf{S} is well conditioned, then $\lim_{M \rightarrow \infty} \Pi_{m=n}^{n+M-1}(\mathbf{I} - \mathbf{S}_m\mathbf{b}_m\mathbf{b}_m^h) = \mathbf{0}$; otherwise, $\lim_{M \rightarrow \infty} \Pi_{m=n}^{n+M-1}(\mathbf{I} - \mathbf{S}_m\mathbf{b}_m\mathbf{b}_m^h) = r\mathbf{e}\mathbf{f}^h$ with $r \geq 1$ and \mathbf{e}, \mathbf{f} are some unit vectors. In both cases \mathbf{S} is assumed Hermitian and $\|\mathbf{S}\| \leq 1$ which holds in this case. Therefore if \mathbf{S}_m is slowly time-varying compared with \mathbf{b}_m , it is possible to establish stability only if \mathbf{S}_m is well conditioned. Since $\mathbf{S}_n \triangleq [(\|\widehat{\mathbf{x}}_{n-1|n}\|^2\widehat{\mathbf{H}}_0^{-t}[n]) \otimes (\mathbf{Q}_w\|\mathbf{c}_n\|^2(\mathbf{c}_n\mathbf{Q}_w\mathbf{c}_n^h + \sigma_v^2)^{-1})]$, it follows that the stability of parameter estimation requires that both $\widehat{\mathbf{H}}_0^{-t}[n]$ and \mathbf{Q}_w are well conditioned, in addition to the PE condition mentioned above. The following conjecture

summarizes the stability results concerning (4.35c) :

Conjecture 1 *The parameter estimation error of the suboptimal EM algorithm is specified by equation (4.35c). If \mathbf{S}_m is slowly time-varying compared with \mathbf{b}_m , then the exponential stability of (4.35c), hence the stability of parameter estimation, requires that both $\widehat{\mathbf{H}}_0^{-t}[n]$ and \mathbf{Q}_w are well conditioned, and both sequences $\widehat{\mathbf{x}}_{n-1|n}^t$ and \mathbf{c}_n are persistently exciting.*

4.5.3 Convergence of the Parameter Recursion

Stability is a steady-state behavior and as mentioned above, is determined by the singular values of $\lim_{M \rightarrow \infty} \prod_{m=n}^{n+M-1} (\mathbf{I} - \mathbf{S}_m \mathbf{b}_m \mathbf{b}_m^h)$. The convergence rate describes the transient behavior of the algorithm. However they both are decided by the same factors. Appendix B.6 shows that assuming that \mathbf{b}_n are persistently exciting, the convergence rate of (4.35c) is essentially determined by the eigenstructure of \mathbf{S}_n .

Since $\mathbf{S}_n \triangleq [(\|\widehat{\mathbf{x}}_{n-1|n}\|^2 \widehat{\mathbf{H}}_0^{-t}[n]) \otimes (\mathbf{Q}_w \|\mathbf{c}_n\|^2 (\mathbf{c}_n \mathbf{Q}_w \mathbf{c}_n^h + \sigma_v^2)^{-1})]$, the eigen-spread of \mathbf{S}_n is determined by those of $\widehat{\mathbf{H}}_0^{-t}[n]$, the conditional state correlation, and \mathbf{Q}_w , the state noise covariance. More specifically,

$$\frac{\lambda_{max}(\mathbf{S}_n)}{\lambda_{min}(\mathbf{S}_n)} = \frac{\lambda_{max}(\mathbf{Q}_w) \lambda_{max}(\widehat{\mathbf{H}}_0[n])}{\lambda_{min}(\mathbf{Q}_w) \lambda_{min}(\widehat{\mathbf{H}}_0[n])} \quad (4.40)$$

The eigen-spread of $\widehat{\mathbf{H}}_0[n]$ is related to the energy distribution of the true system over state components.

In addition, $\|\mathbf{S}_n\|$ is related to $\|\widehat{\mathbf{x}}_{n-1|n}\|^2 \|\widehat{\mathbf{H}}_0^{-t}[n]\|$ which is a function of the exponential weighting factor λ_1 , and $\|\mathbf{Q}_w\| \|\mathbf{c}_n\|^2 (\mathbf{c}_n \mathbf{Q}_w \mathbf{c}_n^h + \sigma_v^2)^{-1}$ which depends on the signal noise ratio (SNR) and the eigen-spread of \mathbf{Q}_w .

Therefore, if the true system is such that either $\widehat{\mathbf{H}}_0[n]$ or \mathbf{Q}_w is ill-conditioned so that their eigen-spread is considerably large, then the parameter estimation may well diverge. For certain applications such as broadband acoustic communication where

the channel is often sparse or not well populated, this indicates that the suboptimal algorithm may lead to parameter divergence.

In the case where both $\widehat{\mathbf{H}}_0[n]$ and \mathbf{Q}_w are well-conditioned, then the convergence rate is controlled by λ_1 and SNR. Large value of λ_1 leads to long averaging window hence $\|\widehat{\mathbf{x}}_{n-1|n}\|^2 \|\widehat{\mathbf{H}}_0^{-t}[n]\|$ is small which gives a small $\|\mathbf{S}_n\|$. Low SNR level leads to small $\|\mathbf{Q}_w\| \|\mathbf{c}_n\|^2 (\mathbf{c}_n \mathbf{Q}_w \mathbf{c}_n^h + \sigma_v^2)^{-1}$ which also reduces $\|\mathbf{S}_n\|$. Hence according to Appendix B.6, small $\|\mathbf{S}_n\|$ leads to a slow rate at which $\prod_{m=n}^{n+M-1} (\mathbf{I} - \mathbf{S}_m \mathbf{b}_m \mathbf{b}_m^h)$ approaches $\mathbf{0}$, therefore large λ_1 value or low SNR level will result a slow parameter convergence rate, and vice versa.

In general, however, due to the fact that the parameter recursion is only a rank-one update in the \mathcal{C}^{N^2} space, the rate of convergence is slow relative to that of linear regression problems and decreases as the state dimension increases.

4.6 EM Parameter Estimation Within Subspace

The Extended Persistent Excitation condition (EPE) indicates that if the sequence $\widehat{\mathbf{x}}_{n-1|n}^t \otimes \mathbf{c}_n$ is not persistently exciting then the parameter recursion will diverge, a phenomenon often called *wind up* or *parameter drift* in system identification and control literature [Ast95] [Bit90] [Kul87] [Par90] [Par92] [Cao00] [Set86] [Set88]. In communication applications, in general the sequence of transmitted symbols can be assumed as persistently exciting, especially if the symbols are modulated using an M-Sequence. Hence the limitation mainly comes from sparsity in the channel estimates.

Consider the original EM parameter estimation form (c.f (4.12) after dropping off the iteration index):

$$\widehat{\mathbf{A}}_n = \widehat{\mathbf{H}}_1[n] [\widehat{\mathbf{H}}_0[n]]^{-1} \quad (4.41)$$

Clearly the quality of the estimate $\widehat{\mathbf{A}}_n$ heavily depends on the conditioning of the matrix $\widehat{\mathbf{H}}_0[n]$. If the channel is sparse and $\widehat{\mathbf{H}}_0[n]$ is ill-conditioned, then $\widehat{\mathbf{A}}_n$ would

be very sensitive to noise.

Equivalently, viewed from the parameter recursion form (c.f. (4.34)),

$$\begin{aligned} \hat{\mathbf{a}}_n &= \hat{\mathbf{a}}_{n-1} + (\hat{\mathbf{H}}_0^{-t}[n] \otimes \mathbf{Q}_w) (\hat{\mathbf{x}}_{n-1|n-1}^t \otimes \mathbf{c}_n)^h R_{e_n}^{-1} e_n \\ &+ [(\hat{\mathbf{H}}_0^{-t}[n]) \otimes \mathbf{Q}_w] (\mathbf{P}_{n-1|n-1}^t \otimes \mathbf{c}_n^h \mathbf{c}_n) \hat{\mathbf{a}}_{n-1} R_{e_n}^{-1} (R_{e_n}^{-1} e_n e_n^* - 1) \end{aligned} \quad (4.42)$$

this means an ill-conditioned or singular $\hat{\mathbf{H}}_0[n]$ will lead to large or unbounded adapting gains for both the first and the second-order innovations. As mentioned in Chapter 1, large adapting gain yields large noise error and unbounded adapting gain leads to divergence.

In the context of system identification with a linear regression model, several *ad hoc* approaches have been proposed to deal with this insufficient excitation problem [Kul87] [Par90] [Par92] [Cao00]. Most of them are based on the so-called *directional forgetting* method in which only the parameter subspace that's been persistently excited is constantly updated (a detailed exposition on subspaces with different levels of persistent excitation may be found in [Set86]). More specifically, with RLS, the forgetting factor is applied selectively to different parameters [Kul87][Par90] [Par92]. Recently directional forgetting based on subspace decomposition of the information matrix is developed in [Cao00].

The subspace EM approach in this section is similar to the information matrix subspace decomposition method in [Cao00].

Consider the eigen-decomposition of the matrix $\hat{\mathbf{H}}_0[n]$:

$$\hat{\mathbf{H}}_0[n] = \mathbf{U}_n \boldsymbol{\Sigma}_n \mathbf{U}_n^h \quad (4.43)$$

where $\boldsymbol{\Sigma}_n = \text{diag}(\lambda_1, \lambda_2, \dots, \lambda_N)$ with $\lambda_1 \geq \lambda_2 \geq \dots, \geq \lambda_N$. \mathbf{U}_n is orthonormal. Assume that only the first P ($P < N$) eigenvalues of $\hat{\mathbf{H}}_0[n]$ are significant, and denote $\bar{\boldsymbol{\Sigma}}_n \triangleq \text{diag}(\lambda_1, \lambda_2, \dots, \lambda_P)$, $\bar{\mathbf{U}}_n$ and $\tilde{\mathbf{U}}_n$ are the first P columns of \mathbf{U}_n and the

remaining $N - P$ columns of \mathbf{U}_n . The following approximation

$$\widehat{\mathbf{H}}_0^{-1}[n] \approx \bar{\mathbf{U}}_n \bar{\boldsymbol{\Sigma}}_n^{-1} \bar{\mathbf{U}}_n^h \quad (4.44)$$

effectively projects the parameter onto the subspace spanned by the first P eigenvectors as (4.41) becomes:

$$\widehat{\mathbf{A}}_n \bar{\mathbf{U}}_n = (\widehat{\mathbf{H}}_1[n] \bar{\mathbf{U}}_n) \bar{\boldsymbol{\Sigma}}_n^{-1} \quad (4.45)$$

Using $\text{Vec}(\widehat{\mathbf{A}}_n \bar{\mathbf{U}}_n) = (\bar{\mathbf{U}}_n^t \otimes \mathbf{I}_M) \widehat{\mathbf{a}}_n$, left multiplying both sides of (4.42) by $(\bar{\mathbf{U}}_n^t \otimes \mathbf{I}_M)$, it yields:

$$\begin{aligned} \widehat{\mathbf{a}}_n &= \widehat{\mathbf{a}}_{n-1} + (\bar{\boldsymbol{\Sigma}}_n^{-t} \otimes \mathbf{Q}_w) (\bar{\mathbf{x}}_{n-1|n-1}^t \otimes \mathbf{c}_n)^t R_{e_n}^{-1} e_n \\ &+ \{ (\bar{\boldsymbol{\Sigma}}_n^{-t} \otimes \mathbf{Q}_w) [(\bar{\mathbf{P}}_{n-1|n-1}^t \otimes \mathbf{c}_n^h \mathbf{c}_n) \widehat{\mathbf{a}}_{n-1} \\ &+ (\tilde{\mathbf{P}}_{n-1|n-1}^t \otimes \mathbf{c}_n^h \mathbf{c}_n) \widehat{\mathbf{a}}_{n-1}] \} R_{e_n}^{-1} (R_{e_n}^{-1} e_n e_n^* - 1) \end{aligned} \quad (4.46)$$

where

$$\widehat{\mathbf{a}}_n \triangleq (\bar{\mathbf{U}}_n^t \otimes \mathbf{I}_M) \widehat{\mathbf{a}}_n \quad (4.47)$$

$$\widehat{\mathbf{a}}_n \triangleq (\bar{\mathbf{U}}_n^t \otimes \mathbf{I}_M) \widehat{\mathbf{a}}_n \quad (4.48)$$

$$\bar{\mathbf{P}}_{n-1|n-1} \triangleq \bar{\mathbf{U}}_n^h \mathbf{P}_{n-1|n-1} \bar{\mathbf{U}}_n \quad (4.49)$$

$$\tilde{\mathbf{P}}_{n-1|n-1} \triangleq \bar{\mathbf{U}}_n^h \mathbf{P}_{n-1|n-1} \bar{\mathbf{U}}_n \quad (4.50)$$

The parameter recursion in (4.46) is stable. The extra step involved in the subspace EM parameter estimation is the eigen-decomposition of $\widehat{\mathbf{H}}_0[n]$.

4.7 Concluding Remarks

This chapter develops joint channel state and dynamics parameter estimation algorithm based on the EM formulation. Optimal and suboptimal EM algorithms are both developed. A fast recursion form for the sums of the second-order smoother state moments is derived. The properties of the suboptimal algorithm are analyzed which lead to the extended persistent excitation (EPE) condition. The EPE condition indicates that if the channel is sparse then the parameter estimation is not persistently excited.

1. The optimal EM algorithm is derived. The algorithm combined with the Kalman filter iteratively computes state estimates and the ML estimates of the parameters. It can be viewed intuitively an iterative scheme in which the parameter estimated directly from the sequence of state estimates obtained from the previous iteration is used in the state estimation for the next iteration. Through multiple iterations, both the parameter estimates and the state estimates are refined. The uncertainties associated with the parameter estimates are not quantified;
2. A fast vector form recursion for the sums of the second-order smoother state moments is derived. The new recursion reduces the memory requirement and motivates the development of a class of sequential suboptimal EM algorithms;
3. Suboptimal EM algorithms are derived which sequentially computes the parameter estimates and state estimates as new data arrives. It is point out that in the suboptimal EM algorithm the parameter averaging window length and the state smoothing memory length can be adjusted separately, to achieve desirable convergence rate and steady-state performance, as demonstrated in a numerical example;
4. The properties of the suboptimal algorithm is analyzed which leads to the

extended persistent excitation (EPE) condition. The EPE condition indicates that if the channel is sparse then the parameter estimation is not persistently excited. the Subspace EM algorithm is proposed to obtain a stable parameter recursion within the dominant channel subspace.

Chapter 5

Sparse Estimation of the Delay-Doppler Spread Function

This chapter develops algorithms that find explicitly sparse channel estimates. Comparing to the state-space model based channel estimation algorithms developed in Chapter 3 and Chapter 4, the approach taken in this chapter is not based on such an explicit channel dynamic model. Instead it accounts for the channel variations by using the discrete *delay-Doppler spread function* representation. Sparse estimation of the *delay-Doppler spread function* is then obtained using several modified Matching Pursuit (MP) algorithms.

5.1 Introduction

As shown in Chapter 2, in addition to the highly dynamic channel fluctuations, another evident feature of the broadband shallow-water surface scattering channel is the sparse channel structure, as reflected in both the *time-varying channel impulse response* and the *delay-Doppler spread function*. This sparse structure is formed by the delay-resolved multipath arrivals, as the delay spread of each arrival, proportional to the inverse of the the transmission bandwidth, is smaller than the delay separation

between these arrivals.

The advantage of sparse adaptive channel estimation is the potential of reducing the number of taps to be tracked. As a result, the tracking algorithms have a reduced computational complexity and memory, and more importantly, a smaller noise error and an increased rate of channel fluctuations that it is capable of tracking [Sto99][Stoed].

There are mainly two categories of sparse estimation techniques that have been used in adaptive filtering and recently in channel estimation. Algorithms falling in the first category are effectively approximation schemes for solving the nonlinear optimization problem of minimizing the squared prediction residual error as a function of the gain and the delay location of all the dominant taps. Among them are the sparse DFE [Ron05], the adaptive delay filter [Che89], the adaptive echo canceller [Yip90] and the thresholding RLS algorithm [Stoed] [Koc95] [Sto99] [Oze02]. The common strategy of these algorithms is to break down the original optimization problem over the whole gains-delays space into a sequence of optimization problems over a smaller parameter space. In [Ron05] a sparse DFE algorithm is derived by optimizing over the gains first and then finding the optimal delays. The adaptive delay filter [Che89] approximates the original problem by sequentially optimizing over the gain/delay of each tap. The adaptive echo canceller [Yip90] and the threshold RLS are similar, in the sense that a full-tap adaptive filter is used as an auxiliary filter to provide tap location and then transfer the detected delay locations to a set of lower order filters to adapt those identified taps. The adaptive echo canceller uses a combination of various criteria to pick the dominant taps while the threshold RLS uses simple energy criterion.

The second group includes algorithms that find the sparsest representation of the received signal, using the transmitted symbol sequence as basis vectors (or often called as dictionary). Explicit sparse estimation mainly includes L_p norm regularized method [Don03] [Mal03][Fuc00] and greedy method such as the MP [Mal93] and its

orthogonal version (OMP)[Kar04]. MP is computationally more efficient, yet, until the recent work by Tropp [Tro04], has been analytically less tractable. These methods originated from the signal representation literature where the dictionary subset that provides the the most compact signal representation is sought. Applications to sparse channel estimation and equalization, mostly using MP or its orthogonalized variant, have noticeably increased recently, see for instance [Cot00, Cot02] [Kar04] [Cet05]. Some of these works are developed for the high definition television (HDTV) terrestrial broadcast channel which, similar to wideband acoustic channel, also has very sparse structure. Cotter, *et al.* in [Cot00] applied adaptive MP algorithm for slowly time-varying channel tracking which according to the authors performs favorably over both LMS and RLS algorithms. In [Cot02] the same authors showed that MP also outperforms the thresholded LS algorithms in dealing with slowly varying channels. In [Cet05], Cetin, *et al.* compared MP with LS and L_1 norm constrained algorithm for channel estimation. It was shown, in terms of locating the nonzero taps, MP performs better than LS and is close to the L_1 constrained algorithm. In [Kar04], the authors proposed an orthogonal MP (OMP) algorithm which twas shown to perform better than the basic MP algorithm in a decision feedback equalizer. However, these applications of MP algorithms to channel estimation were preliminary and rarely provide performance analysis. Comparison between these algorithms has not been done extensively. The main limitation of these sparsing methods, is that they require the sparse structure of the channel impulse response to be stable over a certain time scale, which could be easily violated for the type of channel considered in this thesis as illustrated in Chapter 2.

Following the line of development in Chapters 3 and 4, conceivably one would expect to combine dynamic model based channel tracking with sparse processing. An explicit formulation of this can be carried out by first generalizing the quadratic minimization formulation of the Kalman filter [Jaz70] to the EKF algorithm and then modifying that quadratic cost function by adding some sparse penalty terms.

Although such formulation seems analytically appealing, its implementation and analysis are nevertheless nontrivial. Hence it is left for the future development.

This chapter develops explicit sparse estimation algorithms for the delay-Doppler spread function. As illustrated in Chapter 2, although the channel impulse response has a very fast fluctuating rate, mainly due to Doppler, the variations of the scattering function, although still significant, are much slower at a comparable time scale.

In section 5.2, various explicit sparse estimation algorithms are reviewed. Sensitivity of these algorithms to channel variations are investigated through a numerical example. Section 5.3 derives a sequential least squares modification of the MO algorithm (SLSMP). While the MP algorithm sequentially maximizes the cross-correlation between the transmitted symbol and the residual vector, the SLSMP algorithm minimizes the LS error at each iteration. A recursive procedure is derived using the Shur formula. Section 5.4 formulates the sparse estimation of the delay-Doppler spread function, develops MP, OMP and SLSMP based channel estimation algorithms. An efficient two-stage sparse estimation procedure is also proposed which finds the sparse channel estimate first and then estimates a reduced set of the delay-Doppler spread components on the identified delays. Experimental results are presented in section 5.5.

5.2 Explicit Sparse Channel Estimation

Consider the general least squares (LS) problem

$$\mathbf{y} = \mathbf{C}\mathbf{x} \tag{5.1}$$

where \mathbf{C} is a $N \times M$ matrix, \mathbf{y} and \mathbf{x} are $N \times 1$ and $M \times 1$ vectors respectively. A solution $\hat{\mathbf{x}}$ may be viewed as coefficients of the representation of \mathbf{y} in terms of the columns of \mathbf{C} . Therefore the problem of finding the sparsest solution for the original LS problem becomes finding the most compact representation of \mathbf{y} in terms

of the columns of \mathbf{C} , in the sense that it has the least number of nonzero coefficients. In that context, the columns of \mathbf{C} are often called the dictionaries instead of basis vectors since they may or may not be orthogonal.

Two major approaches for solving the sparse LS problem are the L_p norm constrained LS or the Basis Pursuit (BP) method [Che01][Don03] and the Matching Pursuit (MP) algorithm and its orthogonal variants. The MP algorithm was originally introduced into the signal processing literature by Mallat, *et al.* [Mal93].

5.2.1 Basis Pursuit With L_1 Norm Constraint

The degree of sparseness of a given vector, *i.e.*, its number of nonzero elements, is naturally quantified by its L_0 norm:

$$\|\mathbf{x}\|_0 \triangleq \sum_{m=1}^M f(x_m) \quad (5.2)$$

with $f(x_m) = 0$ if $x_m = 0$ and $f(x_m) = 1$ otherwise .

Finding the sparsest solution for (5.1), or equivalently the L_0 norm constrained solution, is NP-Hard [Don03]. It has a complexity growing exponentially with M . To simplify the problem, L_p constrained approach, for $0 < p \leq 1$ and most often $p = 1$, is used as a convex relaxation of the original L_0 constrained LS problem. The L_1 constrained problem is analytically more tractable since it can be solved by convex optimization, although the amount of computation it involves is still intensive. In [Don03], the conditions for solution uniqueness and the equivalence between L_0 and L_1 constrained problems are established for general dictionaries.

The Basis Pursuit principle is based on reformulating the L_1 norm constrained LS problem into the following optimization problem [Che01, Don03]

$$\min_x \|\mathbf{x}\|_1, \quad \text{subject to: } \mathbf{y} = \mathbf{C}\mathbf{x} \quad (5.3)$$

Or

$$\min_x \|\mathbf{y} - \mathbf{C}\mathbf{x}\|^2 + \lambda \|\mathbf{x}\|_1 \quad (5.4)$$

where λ is a scalar parameter that can be chosen to balance the degree of sparseness in the resulting solution with the LS error. (5.4) basically includes a L_1 norm penalty term in addition to the LS cost function so that the resulting solution would achieve the minimal LS error under certain sparse condition.

In [Cet05], the formulation (5.4) was used to find the sparse channel impulse response estimate. both (5.3) and (5.4) can be solved using either Simplex or Interior Point method [Che01]. The BP is a global optimization principle and its implementations are in general computationally intensive.

5.2.2 Matching Pursuit (MP)

A more efficient alternative for solving the sparse representation problem is the so-called Matching Pursuit (MP) algorithm. The MP algorithm is an iterative *greedy* procedure that selects at each iteration the column of \mathbf{C} that correlates best with the residual of the approximation at the previous iteration [Mal93]. The Orthogonal Matching Pursuit (OMP) algorithm is a variant of of MP with an additional step that projects \mathbf{y} onto all the selected columns of \mathbf{C} . It has been shown that for finite dimensional problem, MP converges exponentially and OMP converges in finite steps (see [Tro04] and its references).

At each iteration, the MP algorithm finds the column of \mathbf{C} onto which the residual vector \mathbf{r}_i (with $\mathbf{r}_0 = \mathbf{y}$) has the maximal projection:

$$\mathbf{c}_{s,i} = \arg \max_{\mathbf{c}_j \neq \mathbf{c}_{s,1}, \dots, \mathbf{c}_{s,i-1}} \frac{|\mathbf{c}_j^h \mathbf{r}_{i-1}|^2}{\|\mathbf{c}_j\|^2} \quad (5.5)$$

where $\mathbf{c}_{s,1}, \dots, \mathbf{c}_{s,i-1}$ are the columns chosen at previous iterations. The residual

vector is computed iteratively as

$$\mathbf{r}_i = \mathbf{r}_{i-1} - \frac{\mathbf{c}_{s,i}^h \mathbf{r}_{i-1}}{\mathbf{c}_{s,i}^h \mathbf{c}_{s,i}} \mathbf{c}_{s,i} \quad (5.6)$$

and $\mathbf{r}_0 = \mathbf{y}$.

Then \hat{x}_i , the i th element of $\hat{\mathbf{x}}$, is found as the coefficient associated with $\mathbf{c}_{s,i}$:

$$\hat{x}_i = \frac{\mathbf{c}_{s,i}^h \mathbf{r}_{i-1}}{\|\mathbf{c}_{s,i}\|^2} \quad (5.7)$$

Note that according to (5.5) and (5.7), there is no need to compute the residual vector \mathbf{r}_i recursively. Instead it is only necessary to compute $b_{i,j} \triangleq \mathbf{c}_j^h \mathbf{r}_i$ for $j = 1, \dots, M$, which can be recursively computed as

$$b_{i,j} = b_{i-1,j} - \hat{x}_i \mathbf{c}_j^h \mathbf{c}_{s,i} = b_{i-1,j} - \frac{\mathbf{c}_j^h \mathbf{c}_{s,i}}{\|\mathbf{c}_{s,i}\|^2} b_{i-1,s_i} \quad (5.8)$$

which is just a scalar update for each j . Here $b_{i-1,s_i} \triangleq \mathbf{c}_{s,i}^h \mathbf{r}_{i-1}$.

The MP algorithm is summarized in Table 5.1.

The major amount of computation involved in the MP algorithm is computing the inner product between each pair of columns and recursively compute $b_{i,j}$ according to (5.8). Suppose that there are maximum K nonzero taps to be identified, then the overall computations are: K divisions for \hat{x}_i , $2MK$ multiplications and MK subtractions for $b_{i,j}$ with $j = 1, \dots, M$ and $i = 1, \dots, K$. The computation of inner products between columns, *i.e.* $\mathbf{C}^h \mathbf{C}$, for a fixed block of data is NM^2 . In the case when data arrives sequentially, and the transmitted symbols are shifted symbol by symbol, $\mathbf{C}^h \mathbf{C}$ can be computed recursively, only involving $2M^2$ multiplications and additions. In summary, the amount of computation involved in the BMP algorithm working in recursive data processing is of the order $\mathcal{O}(K + 2MK + 2M^2)$, which is independent of the averaging window length N .

It can be shown that each MP iteration is equivalent to solving the following

<i>initialization</i>	$\mathbf{r}_0 = \mathbf{y}$	(5.9)
	$b_{0,j} = \mathbf{c}_j^h \mathbf{r}_0, \text{ for } j = 1, \dots, M$	(5.10)
	$k_1 = \arg \max_{j=1, \dots, M} \frac{ b_{0,j} ^2}{\ \mathbf{c}_j\ ^2}$	(5.11)
	$\mathbf{c}_{s,1} = \mathbf{c}_{k_1}$	(5.12)
	$\mathbf{C}_{s,1} = [\mathbf{c}_{s,1}], \quad I_{s,1} = \{k_1\}$	(5.13)
	$\hat{x}_1 = \frac{b_{0,k_1}}{\ \mathbf{c}_{k_1}\ ^2}$	(5.14)
	$b_{1,j} = b_{0,j} - \frac{\mathbf{c}_j^h \mathbf{c}_{s,1}}{\ \mathbf{c}_{s,1}\ ^2} b_{0,k_1}$	(5.15)
<i>the ith iteration, $i > 1$</i>	$k_i = \arg \max_{j=1, \dots, M, j \notin I_{s,i-1}} \frac{ b_{i-1,j} ^2}{\ \mathbf{c}_j\ ^2}$	(5.16)
	$\mathbf{c}_{s,i} = \mathbf{c}_{k_i}$	(5.17)
	$\mathbf{C}_{s,i} = [\mathbf{C}_{s,i-1}; \mathbf{c}_{s,i}], \quad I_{s,i} = \{I_{s,i-1}; k_i\}$	(5.18)
	$\hat{x}_i = \frac{b_{i-1,k_i}}{\ \mathbf{c}_{k_i}\ ^2}$	(5.19)
	$b_{i,j} = b_{i-1,j} - \frac{\mathbf{c}_j^h \mathbf{c}_{s,i}}{\ \mathbf{c}_{s,i}\ ^2} b_{i-1,k_i}$	(5.20)

Table 5.1: The Basic Matching Pursuit Algorithm (MP).

optimization problem:

$$\mathbf{c}_{s,i} = \arg \min_{\mathbf{c}_j \notin \mathbf{C}_{s,i-1}} \left(\min_x \|\mathbf{r}_{i-1} - \mathbf{c}_j \mathbf{x}\|^2 \right) \quad (5.21)$$

This leads to a representation of \mathbf{y} as follows:

$$\mathbf{y} = \sum_{i=1}^M \frac{\mathbf{c}_{s,i}^h \mathbf{r}_{i-1}}{\mathbf{c}_{s,i}^h \mathbf{c}_{s,i}} \mathbf{c}_{s,i} + \mathbf{r}_M = \sum_{i=1}^M \hat{x}_i \mathbf{c}_{s,i} + \mathbf{r}_M \quad (5.22)$$

and as $\mathbf{c}_{s,i}$ is orthogonal to \mathbf{r}_i , it follows that

$$\|\mathbf{y}\|^2 = \sum_{i=1}^M \|\hat{x}_i \mathbf{c}_{s,i}\|^2 + \|\mathbf{r}_M\|^2 \quad (5.23)$$

Equation (5.23) essentially expands \mathbf{y} in terms of the columns $\mathbf{c}_{s,i}$, with coefficients given by $\frac{\mathbf{c}_{s,i}^h \mathbf{r}_{i-1}}{\mathbf{c}_{s,i}^h \mathbf{c}_{s,i}}$.

When the chosen set of columns are not orthogonal, the obtained set of coefficients \hat{x}_i at the end of MP iteration may not give the minimal LS residual error, hence an Orthogonal Matching Pursuit algorithm was proposed to correct this by adding an extra step in which the coefficients are computed by projecting \mathbf{y} over the set of all chose columns. However, the selected columns stay the same.

The MP algorithm is a greedy algorithm for finding the sparse solution. It solves the original sparse problem by a sequence of one-dimensional projections. It does not try to find the minimum LS error hence the resulting estimate is not guaranteed to give a small LS error. However, when the transmitted symbols are white, it is optimal in the sense that it provides a sparsest solution that has the smallest LS error. In fact, the algorithm obtained in [Ron05] by minimizing the LS error over the gains first and then find the optimal delays and assuming the transmitted symbols are white, is exactly the MP algorithm, although the authors did not make the explicit connection.

Note that although \mathbf{r}_i is orthogonal to $\mathbf{c}_{s,i}$, \mathbf{r}_i is not necessarily orthogonal to $\mathbf{c}_{s,j}$

for $j < i$.

5.2.3 Sensitivity to Channel Time-Variations

Although both the BP and the MP algorithms have increasingly been used for channel estimation, some times even for time-varying channels, very little has been done to find out what effect channel variations may have on the resulting estimate and the LS error. Here a numerical example is used to investigate the sensitivity of the BP and MP algorithms to channel variations.

The main results are:

1. For both algorithms, the mean square channel estimation error is less sensitive to variations in the tap gain provided that the tap delay locations are fixed, but is very sensitive to variations in tap delay variations even though the tap gains are kept constant.
2. For both algorithms, the number of correctly identified taps is very sensitive to all channel variations, including variations in tap gain with delays being fixed and fluctuations in delay with constant gains.

Figure 5-1 shows a constant sparse channel with 10 nonzero taps over a span of 120 taps. For the purpose of comparison, the channel impulse response is the same as that used in [Cet05] and [Cot02]. The number of correctly identified taps and the mean square channel estimation error are given in Figure 5-2 and Figure— 5-3 respectively, as functions of SNR. Each plot contains results obtained using LS, BMP and BP. Results with three different averaging window lengths $L = 40, 80, 130$ are shown separately. Both figures show an increased performance, *i.e.* increased number of correctly identified taps and smaller MSE, as SNR increases. In addition, as the averaging window length increases, the performance also increases, both in terms of the number of correctly identified taps and the resulting MSE. Comparatively speaking for short averaging window, the results of the BP and the MP algorithms

are superior than that of the LS algorithm, with the BP algorithm slightly outperform the MP algorithm. The performance difference is less significant with sufficiently long averaging window.

The channel is then set to vary in two different ways.

First, the delay location of all taps is fixed while the tap gains fluctuates according to a state-space model with different Doppler values. The channel impulse response snapshots are plotted in Figure 5-4 which shows the fluctuations as the snapshots overlap. Then the LS, the MP and the BP algorithms are applied and the resulting number of correctly identified taps and the mean square channel estimation errors are shown in Figure 5-5 and Figure 5-6. Figure 5-5 shows the number of correctly identified taps is reduced significantly (by about a half) when a long averaging window is used while it is approximately the same if a short window is used. On the other hand, Figure 5-6 shows that the channel MSE appear less sensitive to gain fluctuations alone. This indicates that when tap gains fluctuate significantly, the sparse structure becomes more difficult to maintain over a long averaging window. A relatively small MSE can still be attained by a less sparse solution (aka, smearing of the sparseness).

The next step is to fix the tap gains while let the tap delay locations to vary randomly, with a small variance, as shown in Figure 5-7 (an overlap plot of channel impulse response snapshots). In this case the number of correctly identified taps and the channel MSE both deteriorate drastically, for all values of averaging window length. With a long averaging window, essentially the sparse structure is lost in all estimates.

While rigorous analysis is not presented here. It can be point out here that the sparse channel estimation algorithms are similarly subject to the dilemma of reducing *lag error* at the cost of increased *noise error*. On the other hand, due to the explicit sparse constraint, it also tries to maintain the sparseness in the estimates which would be severely smeared when the channel fluctuates significantly. The impact of

the loss of sparseness on MSE needs further analysis.

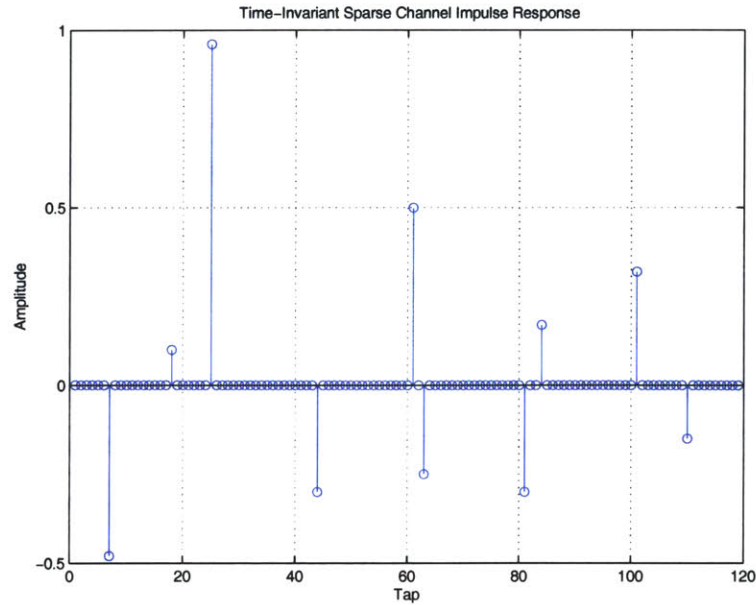


Figure 5-1: A Constant Sparse Channel

5.3 Sequential Least Squares Matching Pursuit

In general the set of columns selected by the MP algorithm does not necessarily lead to a representation of \mathbf{y} that has the smallest LS error. This can be demonstrated through a simple example in the three-dimensional space. Figure 5-10 shows various MP algorithms that try to find a sparse representation for the vector \mathbf{y} , plotted in red, in terms of the vectors c_1, \dots, c_6 which are labeled in the upper left plot. The LS, the BMP, and the OMP and the sequential LS Matching Pursuit (SLSMP, which will be presented later in this section) methods are applied to find the two vectors out of c_1, \dots, c_6 to represent \mathbf{y} . The upper left plot shows that c_1 and c_2 are the best LS fit, which is simply because among all the 2D plane spanned by any two of these vectors the one spanned by c_1 and c_2 has the largest projection of \mathbf{y} . The BMP algorithm, however, picks up c_5 first and then c_1 . This is because among any of those

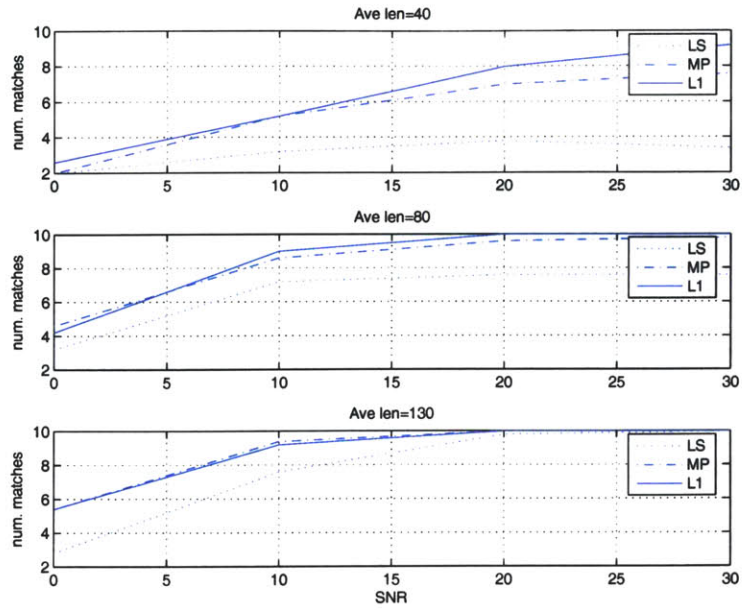


Figure 5-2: Tap Identification in Sparse Estimation of A Constant Sparse Channel

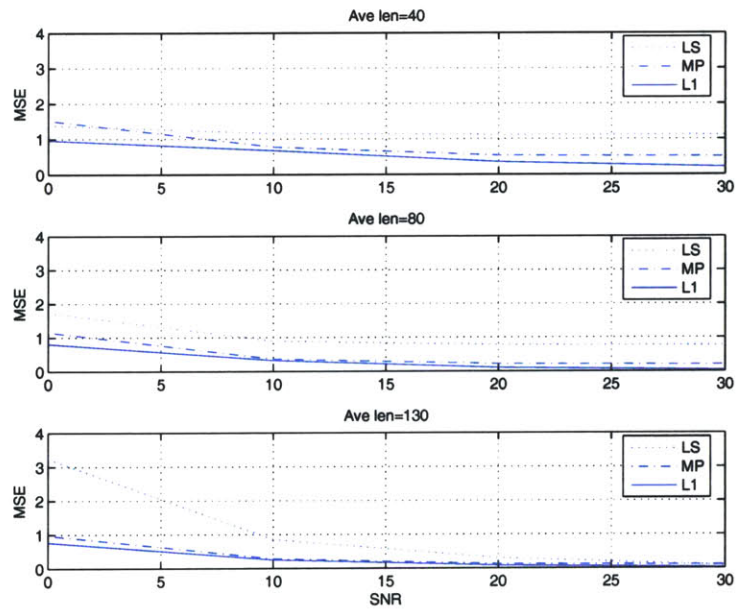


Figure 5-3: MSE of Sparse Estimation of A Constant Sparse Channel

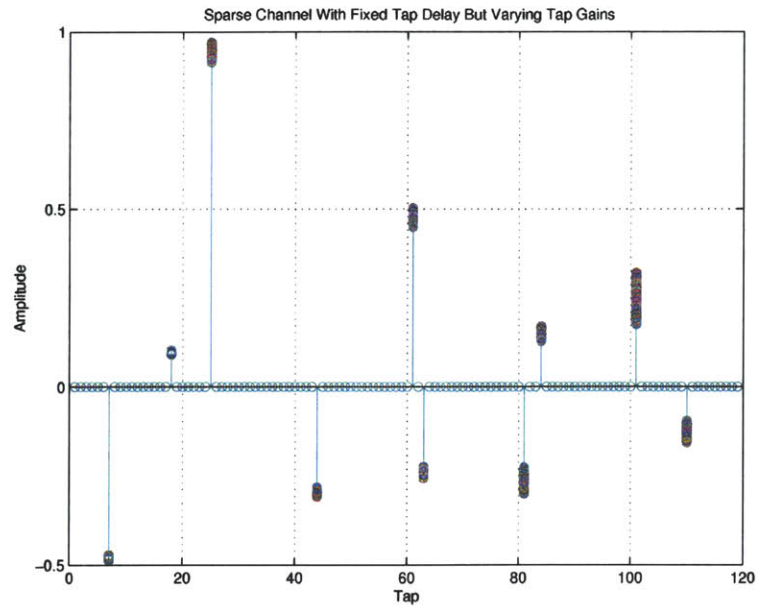


Figure 5-4: A Time-Varying Sparse Channel with Fixed Tap Delays and Varying Gains

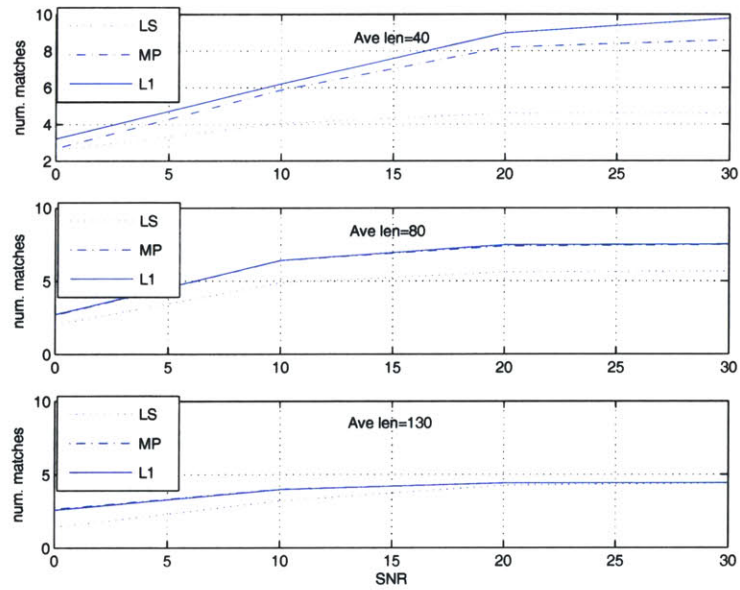


Figure 5-5: Tap Identification in Sparse Estimation of A Time-Varying Sparse Channel with Fixed Tap Delays and Varying Gains

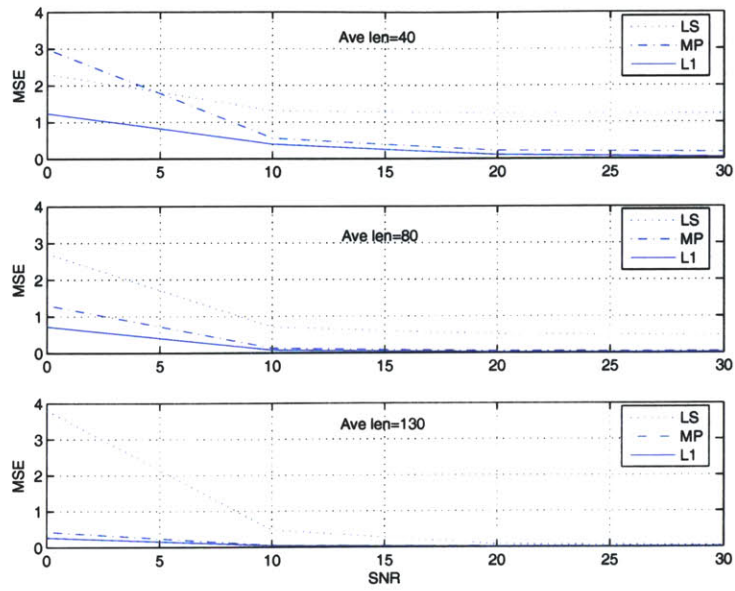


Figure 5-6: MSE of Sparse Estimation of A Time-Varying Sparse Channel with Fixed Tap Delays and Varying Gains

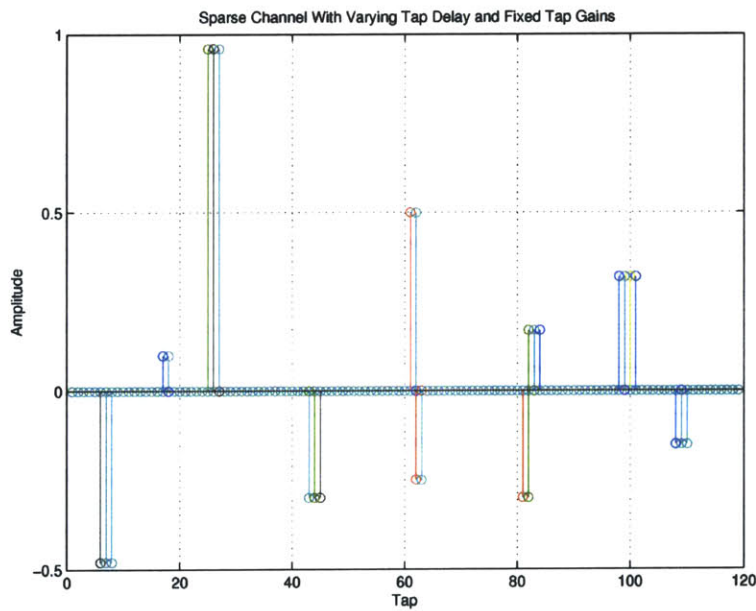


Figure 5-7: A Time-Varying Sparse Channel with Varying Tap Delays and Fixed Gains

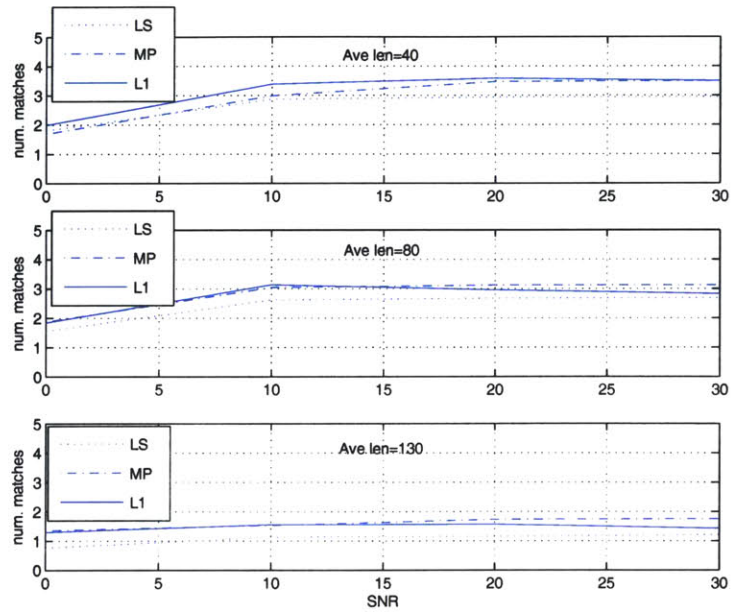


Figure 5-8: Tap Identification in Sparse Estimation of A Time-Varying Sparse Channel with Varying Tap Delays and Fixed Gains

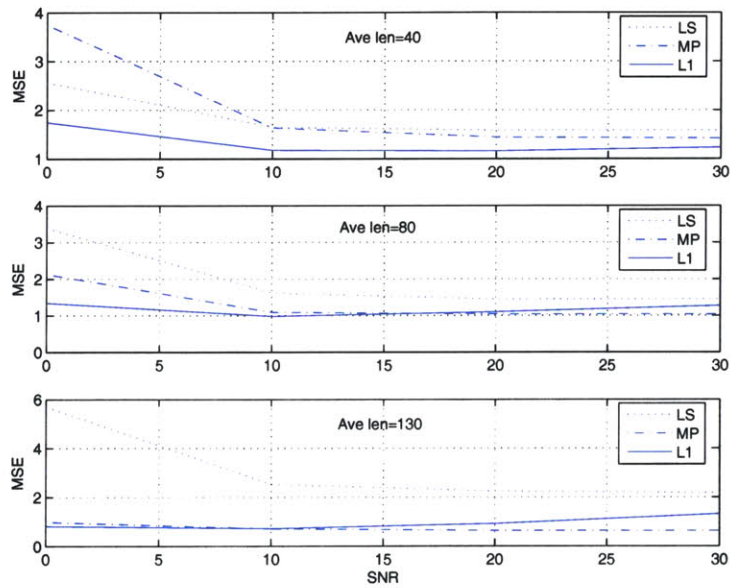


Figure 5-9: MSE of Sparse Estimation of A Time-Varying Sparse Channel with Varying Tap Delays and Fixed Gains

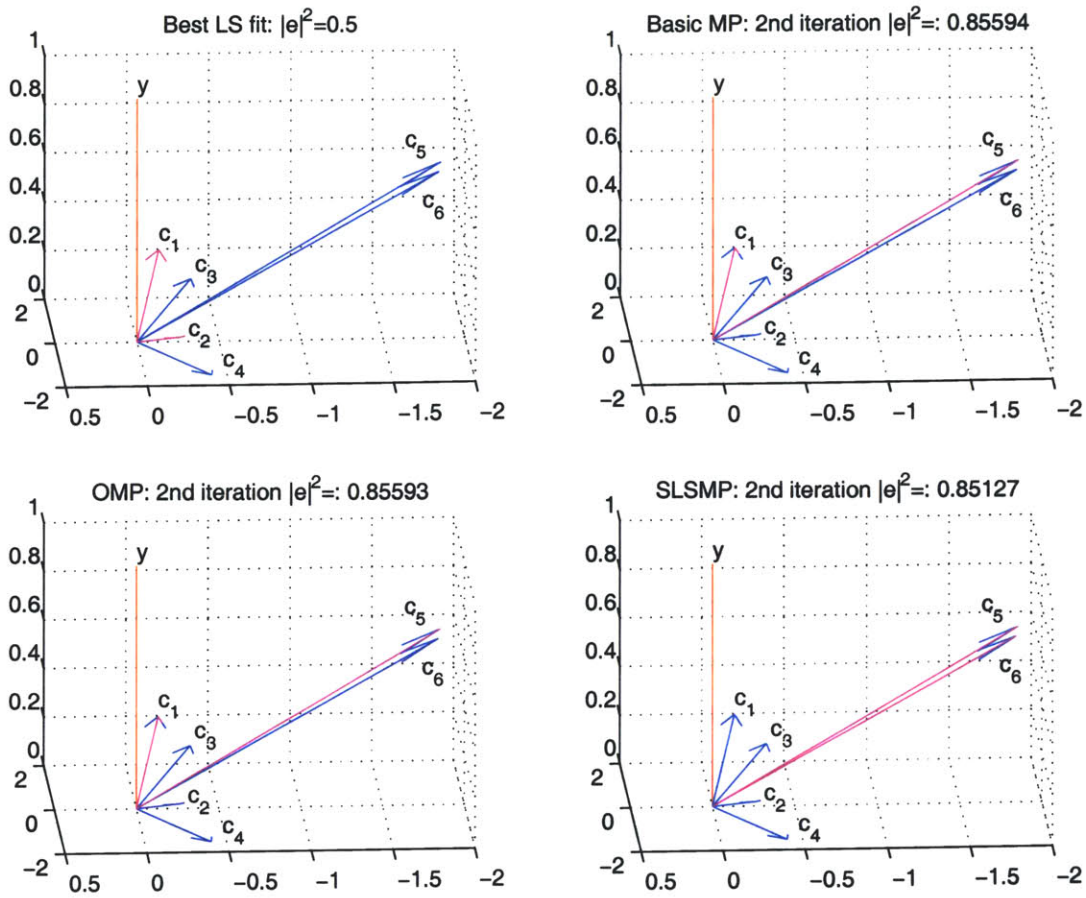


Figure 5-10: Comparison of Matching Pursuit algorithms, A simple Example

vectors c_5 has the largest projection of y . Then because c_6 is almost affine with c_5 and nearly orthogonal to the residual error vector thus is not selected as the second vector. As a result, BMP has a much larger residual error. OMP essentially has the same vector selection but coefficients are recomputed, which does not reduce the error significantly. The SLSMP has a different column vector selection criterion, as is discussed in this section, and chooses c_5 and c_6 despite that these two are highly non-orthogonal. The resulting residual error is still larger than the LS case, but is better than those of the BMP and the OMP.

At each iteration of the MP or the OMP algorithm, a new column vector is selected such that the projection of the residual vector onto the selected column is

maximized. In the context of channel estimation, an important measure is the LS residual error, *i.e.* $\|\mathbf{y} - \mathbf{C}_{s,i}\mathbf{x}_i\|^2$ which needs to be minimized. Now suppose $\mathbf{C}_{s,i}$ is the set of columns identified after i th iteration, from minimizing the LS error point of view, $\mathbf{c}_{s,i+1}$, the new column to be selected at the $i + 1$ st iteration, should form a subspace together with $\mathbf{C}_{s,i}$ to which \mathbf{y} has the minimal distance. The column selected by MP or OMP, as described above, does not necessarily lead to such a subspace expansion. This is because geometrically a subspace spanned by a set of vectors is invariant to the rotation of those vectors within the subspace, as long as the rank stays the same (even though the vectors are nearly affine to each other). The projection onto a vector as done in MP/OMP is very sensitive to vector location within the subspace. Hence as suggested by the counterexample in Figure 5-10, it is quite possible that MP/OMP chooses a set of vectors that have the largest normalized cross-correlation with the residual vector but form a subspace to which the residual vector is not minimal. In addition, MP/OMP will not simultaneously select columns nearly affine to each other due to the subtraction of the signal component along the first selected vector, even though the subspace spanned by those vectors has a smaller distance.

Motivated by these observations, a new algorithm is developed in this section which, instead of choosing columns based on the normalized cross-correlation, it chooses columns based on minimizing the LS error at each iteration.

More specifically, assume that after the i th iteration, the set of identified columns are $\mathbf{C}_{s,i} \triangleq [\mathbf{c}_{s,1} \ \mathbf{c}_{s,2} \ \cdots \ \mathbf{c}_{s,i}]$; the associated coefficients, contained in the vector \mathbf{x}_i , are obtained using the LS method, *i.e.*

$$\hat{\mathbf{x}}_i = \mathbf{R}_i^{-1}\mathbf{z}_i \quad (5.24)$$

where

$$\mathbf{R}_i = \mathbf{C}_{s,i}^h \mathbf{C}_{s,i} \quad (5.25)$$

$$\mathbf{z}_i = \mathbf{C}_{s,i}^h \mathbf{y} \quad (5.26)$$

and \mathbf{R}_i is assumed invertible.

The associated residual vector, \mathbf{r}_i , and the squared residual error, $\|\mathbf{r}_i\|^2$, can be calculated as

$$\mathbf{r}_i = \mathbf{y} - \mathbf{C}_{s,i} \hat{\mathbf{x}}_i \quad (5.27)$$

$$\|\mathbf{r}_i\|^2 = \|\mathbf{y}\|^2 - \mathbf{z}_i^h \mathbf{R}_i^{-1} \mathbf{z}_i \quad (5.28)$$

The second equality follows from the Orthogonality Principle and (5.25).

Now at the $i + 1$ st iteration, the algorithm finds a new column out of the set of remaining columns, denoted by $\mathbf{c}_{s,i+1}$, which gives the minimum squared residual error, that is

$$\mathbf{c}_{s,i+1} = \arg \min_{\mathbf{c}_j \notin \mathbf{C}_{s,i}} \|\mathbf{r}_{i+1,j}\|^2 \quad (5.29)$$

where

$$\mathbf{r}_{i+1,j} = \mathbf{y} - [\mathbf{C}_{s,i} \ \mathbf{c}_j] \mathbf{x}_{i+1,j} \quad (5.30)$$

and $\mathbf{x}_{i+1,j}$ is the associated LS coefficients and is given by:

$$\mathbf{x}_{i+1,j} = \mathbf{R}_{i+1,j}^{-1} \mathbf{z}_{i+1,j} \quad (5.31)$$

where

$$\begin{aligned}\mathbf{R}_{i+1,j} &= [\mathbf{C}_{s,i} \ \mathbf{c}_j]^h [\mathbf{C}_{s,i} \ \mathbf{c}_j] \\ &= \begin{bmatrix} \mathbf{R}_i & \mathbf{C}_{s,i}^h \mathbf{c}_j \\ \mathbf{c}_j^h \mathbf{C}_{s,i} & \|\mathbf{c}_j\|^2 \end{bmatrix}\end{aligned}\quad (5.32)$$

$$\mathbf{z}_{i+1,j} = \begin{bmatrix} \mathbf{z}_i \\ \mathbf{c}_j^h \mathbf{y} \end{bmatrix}\quad (5.33)$$

Using the Shur formula for block matrix inversion [Har97], it yields

$$\mathbf{R}_{i+1,j}^{-1} = \begin{bmatrix} \mathbf{R}_i^{-1} & \mathbf{0} \\ \mathbf{0} & 0 \end{bmatrix} + \Delta_{i,j}^{-1} \begin{bmatrix} -\mathbf{R}_i^{-1} \mathbf{C}_{s,i}^h \mathbf{c}_j \\ 1 \end{bmatrix} \begin{bmatrix} -\mathbf{R}_i^{-1} \mathbf{C}_{s,i}^h \mathbf{c}_j \\ 1 \end{bmatrix}^h\quad (5.34)$$

where

$$\begin{aligned}\Delta_{i,j} &= \|\mathbf{c}_j\|^2 - [\mathbf{C}_{s,i}^h \mathbf{c}_j]^h \mathbf{R}_i^{-1} [\mathbf{C}_{s,i}^h \mathbf{c}_j] \\ &= \mathbf{c}_j^h [\mathbf{I} - \mathbf{C}_{s,i} \mathbf{R}_i^{-1} \mathbf{C}_{s,i}^h] \mathbf{c}_j \\ &\triangleq \mathbf{c}_j^h \mathbf{Q}_i \mathbf{c}_j\end{aligned}\quad (5.35)$$

where $\mathbf{Q}_i \triangleq \mathbf{I} - \mathbf{C}_{s,i} \mathbf{R}_i^{-1} \mathbf{C}_{s,i}^h$ is a projection matrix associated with the nullspace of $\mathbf{C}_{s,i}$. $\Delta_{i,j}$ is the Shur complement of \mathbf{R}_i and has the geometric meaning as the LS distance between the vector \mathbf{c}_j and the subspace spanned by $\mathbf{C}_{s,i}$ (or analogously the variance of the estimate of \mathbf{c}_j based on $\mathbf{C}_{s,i}$). $\Delta_i = \|\mathbf{c}_j\|^2$ if \mathbf{c}_j is orthogonal to $\mathbf{C}_{s,i}$.

Combining (5.31)-(5.36) yields the following recursion form for the residual vector

:

$$\mathbf{r}_{i+1,j} = \mathbf{r}_i - \frac{\mathbf{Q}_i \mathbf{c}_j^h \mathbf{r}_i}{\Delta_{i,j}} \mathbf{c}_j\quad (5.36)$$

Suppose at $i + 1$ st iteration, the k_{i+1} th column is chosen, i.e. $\mathbf{c}_{s,i+1} = \mathbf{c}_{k_{i+1}}$, then

$$\mathbf{r}_{i+1} = \mathbf{r}_i - \frac{\mathbf{Q}_i \mathbf{c}_{k_{i+1}}^h \mathbf{r}_i}{\Delta_{i,k_{i+1}}} \mathbf{c}_{k_{i+1}} \quad (5.37)$$

where $\mathbf{r}_{i+1} \triangleq \mathbf{r}_{i+1,k_{i+1}}$. (5.38) is analogous to (5.6) and is the same if \mathbf{Q}_i is an identity matrix. It can be shown that \mathbf{r}_{i+1} is orthogonal to $\mathbf{c}_{s,j}$ for all $j < i + 1$.

Denoting $b_{i,j} \triangleq \mathbf{c}_j^h \mathbf{r}_i$, it follows from (5.38) that

$$\begin{aligned} b_{i+1,j} &= b_{i,j} - [\mathbf{c}_j^h \mathbf{Q}_i \mathbf{c}_{k_{i+1}}] \Delta_{i,k_{i+1}}^{-1} \mathbf{c}_{k_{i+1}}^h \mathbf{r}_i \\ &\triangleq b_{i,j} - [\mathbf{c}_j^h \mathbf{Q}_i \mathbf{c}_{k_{i+1}}] \hat{\mathbf{x}}_{i+1} \end{aligned} \quad (5.38)$$

where

$$\hat{\mathbf{x}}_{i+1} \triangleq \Delta_{i,k_{i+1}}^{-1} \mathbf{c}_{k_{i+1}}^h \mathbf{r}_i \quad (5.39)$$

Combining (5.32)-(5.35) and (5.40) yields

$$\begin{aligned} \hat{\mathbf{x}}_{i+1} &= \begin{bmatrix} \hat{\mathbf{x}}_i \\ 0 \end{bmatrix} + \begin{bmatrix} -\mathbf{R}_i^{-1} \mathbf{C}_{s,i}^h \mathbf{c}_{k_{i+1}} \\ 1 \end{bmatrix} \Delta_{i,k_{i+1}}^{-1} \mathbf{c}_{k_{i+1}}^h \mathbf{r}_i \\ &= \begin{bmatrix} \hat{\mathbf{x}}_i \\ 0 \end{bmatrix} + \begin{bmatrix} -\mathbf{R}_i^{-1} \mathbf{C}_{s,i}^h \mathbf{c}_{k_{i+1}} \\ 1 \end{bmatrix} \hat{\mathbf{x}}_{i+1} \end{aligned} \quad (5.40)$$

Using the orthogonality principle and the idempotent property of the projection matrix, i.e. $\mathbf{Q}_i \mathbf{Q}_i = \mathbf{Q}_i$, the squared residual error associated with the set of columns $[\mathbf{C}_{s,i} \ \mathbf{c}_j]$ is given by

$$\begin{aligned} \|\mathbf{r}_{i+1,j}\|^2 &= \|\mathbf{y}\|^2 - \mathbf{z}_{i+1,j}^h \mathbf{R}_{i+1,j}^{-1} \mathbf{z}_{i+1,j} \\ &= \|\mathbf{y}\|^2 - \mathbf{z}_i^h \mathbf{R}_i^{-1} \mathbf{z}_i - \Delta_{i,j}^{-1} \|\mathbf{y}^h [\mathbf{I} - \mathbf{C}_{s,i} \mathbf{R}_i^{-1} \mathbf{C}_{s,i}^h] \mathbf{c}_j\|^2 \\ &= \|\mathbf{r}_i\|^2 - \Delta_{i,j}^{-1} \|\mathbf{r}_i^h \mathbf{c}_j\|^2 \end{aligned} \quad (5.41)$$

Consequently, the newly chosen column should maximize the second term in (5.42):

$$\mathbf{c}_{s,i+1} = \arg \max_{\mathbf{c}_j \notin \mathbf{C}_{s,i}} \frac{\|\mathbf{c}_j^h \mathbf{r}_i\|^2}{\Delta_{i,j}} \quad (5.42)$$

For notational convenience, assume $\mathbf{c}_{s,i+1}$ is the k_{i+1} th column in \mathbf{C} .

Equations (5.43) and (5.5) differ only in the denominator. Recall that $\Delta_{i,j} = \|\mathbf{c}_j\|^2 - [\mathbf{C}_{s,i}^h \mathbf{c}_j]^h \mathbf{R}_i^{-1} [\mathbf{C}_{s,i}^h \mathbf{c}_j]$, (5.43) and (5.5) become identical if all columns are orthogonal, since then $\mathbf{C}_{s,i}^h \mathbf{c}_j = \mathbf{0}$ and $\Delta_{i,j} = \|\mathbf{c}_j\|^2$.

In (5.5) the cross-correlation between the residual vector and a column is normalized by the L_2 norm of the column while in (5.43) the cross-correlation is normalized by the squared distance between the new column and the previous column set $\mathbf{C}_{s,i}$. This change of normalization in (5.43) may be viewed geometrically as an orthogonalization step at each iteration, so that if a new column is affine to any columns in $\mathbf{C}_{s,i}$, it may still be selected by the new algorithm due to its smaller distance to the space spanned by $\mathbf{C}_{s,i}$, while it will not be selected by the MP or OMP algorithm.

On the other hand, the sequential LS basis selection algorithm is not globally optimal as it approximates the original NP hard optimization problem by a set of successive lower dimension LS minimization problem, although that is one-step further than the MP algorithm which approximates the original problem by a set of successive one dimensional projections. A globally optimal $i + 1$ dimension subspace is not necessarily a simple augmentation from the optimal subspace of dimension i .

The net increase of computation involved in the SLSMP algorithm is mainly in (5.35) and (5.39). Other than that, it involves computing the inner products between columns of \mathbf{C} and between \mathbf{y} and columns of \mathbf{C} all of which, similar to the MP algorithm, only need to be computed once for a given block of data and can be computed recursively if data arrives sequentially. The algorithm is summarized in Table 5.2.

<i>initialization</i>	$\mathbf{r}_0 = \mathbf{y}$	(5.43)
	$b_{0,j} = \mathbf{c}_j^h \mathbf{r}_0, \quad \text{for } j = 1, \dots, M$	(5.44)
	$\Delta_{0,j} = \ \mathbf{c}_j\ ^2, \quad \text{for } j = 1, \dots, M$	(5.45)
	$k_1 = \arg \max_{j=1, \dots, M} \frac{ b_{0,j} ^2}{\Delta_{0,j}}$	(5.46)
	$\mathbf{C}_{s,1} = \mathbf{c}_{k_1}, \quad I_{s,1} = \{k_1\}$	(5.47)
	$R_1^{-1} = \ \mathbf{c}_{k_1}\ ^2$	(5.48)
	$\hat{\mathbf{x}}_1 = R_1^{-1} b_{0,k_1}$	(5.49)
	$b_{1,j} = b_{0,j} - \mathbf{c}_j^h \mathbf{c}_{k_1} \hat{\mathbf{x}}_1, \quad \text{for } j = 1, \dots, M$	(5.50)
	$\mathbf{Q}_1 = \mathbf{I} - \mathbf{C}_{s,1} R_1^{-1} \mathbf{C}_{s,1}^h$	(5.51)
	$\Delta_{1,j} = \mathbf{c}_j^h \mathbf{Q}_1 \mathbf{c}_j, \quad \text{for } j = 1, \dots, M$	(5.52)
<i>the ith iteration</i>	$k_i = \arg \max_{j=1, \dots, M, j \notin I_{s,i-1}} \frac{ b_{i-1,j} ^2}{\Delta_{i-1,j}}$	(5.53)
$i > 1$	$\mathbf{C}_{s,i} = [\mathbf{C}_{s,i-1}; \mathbf{c}_{k_i}], \quad I_{s,i} = \{I_{s,i-1}; k_i\}$	(5.54)
	$\mathbf{R}_i^{-1} = \begin{bmatrix} \mathbf{R}_{i-1}^{-1} & \mathbf{0} \\ \mathbf{0}^t & 0 \end{bmatrix} + \Delta_{i-1,k_i}^{-1} \begin{bmatrix} -\mathbf{R}_{i-1}^{-1} \mathbf{C}_{s,i-1}^h \mathbf{c}_{k_i} \\ 1 \end{bmatrix} \begin{bmatrix} -\mathbf{R}_{i-1}^{-1} \mathbf{C}_{s,i-1}^h \mathbf{c}_{k_i} \\ 1 \end{bmatrix}^h$	(5.55)
	$\hat{\mathbf{x}}_i = \Delta_{i-1,k_i}^{-1} b_{i-1,k_i}$	(5.56)
	$\hat{\mathbf{x}}_i = \begin{bmatrix} \hat{\mathbf{x}}_{i-1} \\ 0 \end{bmatrix} + \begin{bmatrix} -\mathbf{R}_{i-1}^{-1} \mathbf{C}_{s,i-1}^h \mathbf{c}_{k_i} \\ 1 \end{bmatrix} \hat{\mathbf{x}}_i$	(5.57)
	$b_{i,j} = b_{i-1,j} - \mathbf{c}_j^h \mathbf{Q}_{i-1} \mathbf{c}_{k_i} \hat{\mathbf{x}}_i, \quad \text{for } j = 1, \dots, M$	(5.58)
	$\mathbf{Q}_i = \mathbf{I} - \mathbf{C}_{s,i} \mathbf{R}_i^{-1} \mathbf{C}_{s,i}^h$	(5.59)
	$\Delta_{i,j} = \mathbf{c}_j^h \mathbf{Q}_i \mathbf{c}_j, \quad \text{for } j = 1, \dots, M$	(5.60)

Table 5.2: The Sequential Least Squares Matching Pursuit Algorithm (SLSMP).

5.4 Sparse Estimation of the Delay-Doppler Spread Function

In terms of the *discrete delay-Doppler spread function*, the received signal can be represented as sums of delayed and Doppler shifted copies of the transmitted sequence. Restating the equation (2.6) in Chapter 2 (with noise term dropped off),

$$r_i = \mathbf{u}_i^t(\mathbf{z}_i \otimes \boldsymbol{\phi}_i) \quad (5.61)$$

where \otimes is the Kronecker product, $r_i = r(i\delta t)$ is the sampled received signal, $\mathbf{z}_i = [z(i\delta t - \tau_0) z(i\delta t - \tau_0 - \delta\tau) \cdots z(i\delta t - \tau_0 - M\delta\tau)]^t$ is the transmitted symbol sequence. Here τ_0 is the reference delay, δt and $\delta\tau$ are the sample interval in time and delay respectively and M is the number of delay-taps. The delay-Doppler components \mathbf{u}_i and the Doppler phase vector $\boldsymbol{\phi}_i$ are given by:

$$\begin{aligned} \mathbf{u}_i = & [u(\nu_0, \tau_0) u(\nu_0 + \delta\nu, \tau_0) \cdots u(\nu_0 + P\delta\nu, \tau_0) \\ & u(\nu_0, \tau_0 + \delta\tau) u(\nu_0 + \delta\nu, \tau_0 + \delta\tau) \cdots u(\nu_0 + P\delta\nu, \tau_0 + \delta\tau) \\ & \dots \dots \dots \\ & u(\nu_0, \tau_0 + M\delta\tau) u(\nu_0 + \delta\nu, \tau_0 + M\delta\tau) \cdots u(\nu_0 + P\delta\nu, \tau_0 + M\delta\tau)]^t \end{aligned} \quad (5.62)$$

$$\boldsymbol{\phi}_i = [e^{j2\pi\nu_0 i\delta t} e^{j2\pi(\nu_0 + \delta\nu)i\delta t} \dots e^{j2\pi(\nu_0 + P\delta\nu)i\delta t}]^t \quad (5.63)$$

where P is the maximum number of Doppler shifts. \mathbf{u}_i and $\boldsymbol{\phi}_i$ are MP and $P \times 1$ respectively.

Let

$$\mathbf{y}_i \triangleq [r_i r_{i-1} \cdots r_{i-N+1}]^t \quad (5.64)$$

where N is the window length. Assuming that \mathbf{u}_i is sufficiently slowly varying so

that it may be viewed as constant during the window period, it follows that

$$\mathbf{y}_i = \begin{bmatrix} \mathbf{u}_i^t(\mathbf{z}_i \otimes \boldsymbol{\phi}_i) \\ \mathbf{u}_i^t(\mathbf{z}_{i-1} \otimes \boldsymbol{\phi}_{i-1}) \\ \vdots \\ \mathbf{u}_i^t(\mathbf{z}_{i-N+1} \otimes \boldsymbol{\phi}_{i-N+1}) \end{bmatrix} \quad (5.65)$$

$$\triangleq \mathbf{C}_i \mathbf{u}_i \quad (5.66)$$

where

$$\mathbf{C}_i \triangleq \begin{bmatrix} (\mathbf{z}_i \otimes \boldsymbol{\phi}_i)^t \\ (\mathbf{z}_{i-1} \otimes \boldsymbol{\phi}_{i-1})^t \\ \vdots \\ (\mathbf{z}_{i-N+1} \otimes \boldsymbol{\phi}_{i-N+1})^t \end{bmatrix} \quad (5.67)$$

is $N \times (MP)$. It consists of M horizontal blocks each is of size $N \times P$ and is associated with a particular delay. It can be shown that the columns of \mathbf{C}_i are not orthogonal.

Equation (5.67) is a typical sparse LS problem in which \mathbf{u}_i has a very sparse structure that only a limited elements are significant. Therefore the sparse estimation approaches, including the BP, the BMP and the SLSMP algorithms, can be applied. It is expected that the SLSMP algorithm would perform better than the BMP algorithm due to the nonorthogonality of columns of \mathbf{C}_i .

5.4.1 Suboptimal Two-Stage Sparse Estimation Algorithms

Direct application of the BMP or the SLSMP algorithm to (5.67) requires large memory space as well as a significant amount of computation, especially in the case of the SLSMP algorithm. Recall from Chapter 2 that the scattering function is sparse in both delay and Doppler. This motivates a two-stage suboptimal algorithm which in the first stage identifies the dominant delay taps from a fast sparse channel estimation and then the second stage estimates the delay-Doppler spread function

on these identified delay locations using sparse algorithms.

5.5 Experimental Results

Both the Orthogonal Matching Pursuit (OMP) algorithm and the Sequential Least Squares Matching Pursuit (SLSMP) algorithm are applied to the example channel presented in Chapter 2. An averaging window of 800 samples was used for both the OMP and the SLSMP algorithms and a total of 200 delay-Doppler components were estimated. Figure 5-11 shows the signal prediction residual error obtained by both algorithms, compared with the residual error obtained from channel impulse response estimation using exponentially weighted RLS algorithm with $\lambda = 0.98$. The residual error of both the OMP and the SLSMP algorithms are lower than that of the RLS algorithm by about 2dB.

Figure 5-12 shows snapshots of both the nonsparse estimate and sparse estimate of the delay-Doppler spread function using SLSMP algorithm, respectively, both at time $t = 20.05747$ seconds. It shows that the sparse estimate picks up the dominant delay-Doppler components. It also picks up some slightly larger Doppler components compared with the nonsparse estimate.

5.6 Concluding Remarks

Sparse channel estimation algorithms are developed in this chapter. Several existing sparse estimation algorithms are reviewed and their sensitivity to channel variations are investigated through a numerical example. Based on the Matching Pursuit algorithm, a new Sequential Least Squares Matching Pursuit (SLSMP) algorithm is developed and applied to estimate the channel delay-Doppler function. Experimental results show a 2dB reduction in the signal prediction residual error compared with the RLS channel impulse response estimation.

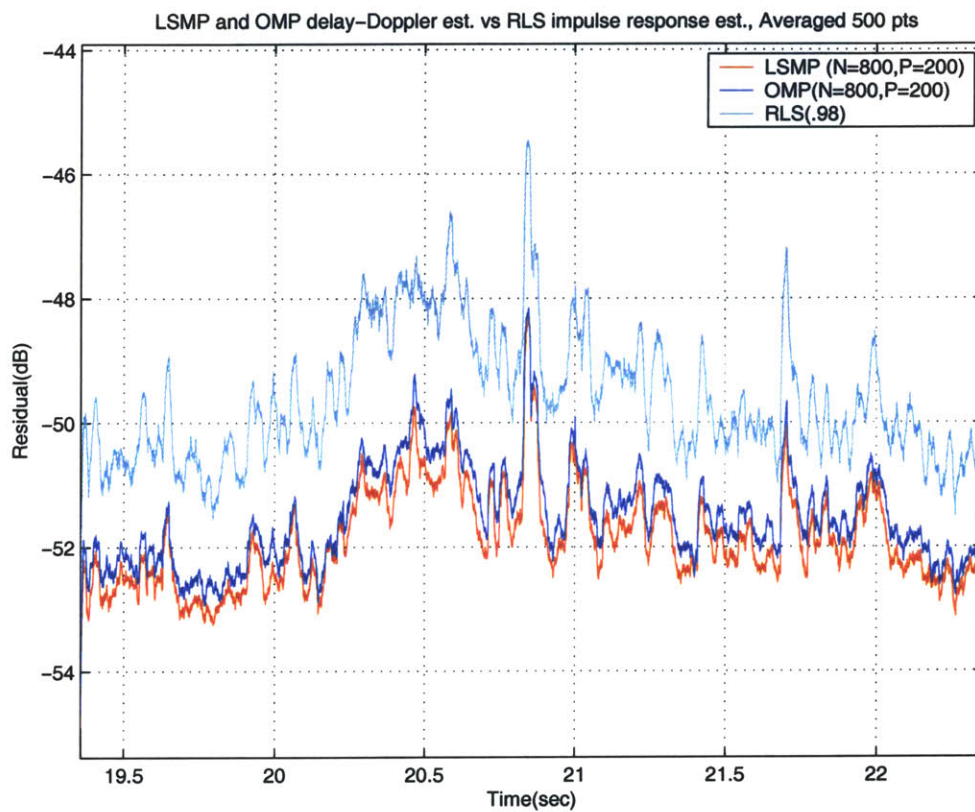


Figure 5-11: Sparse Estimation of the Discrete Delay-Doppler Spread Function

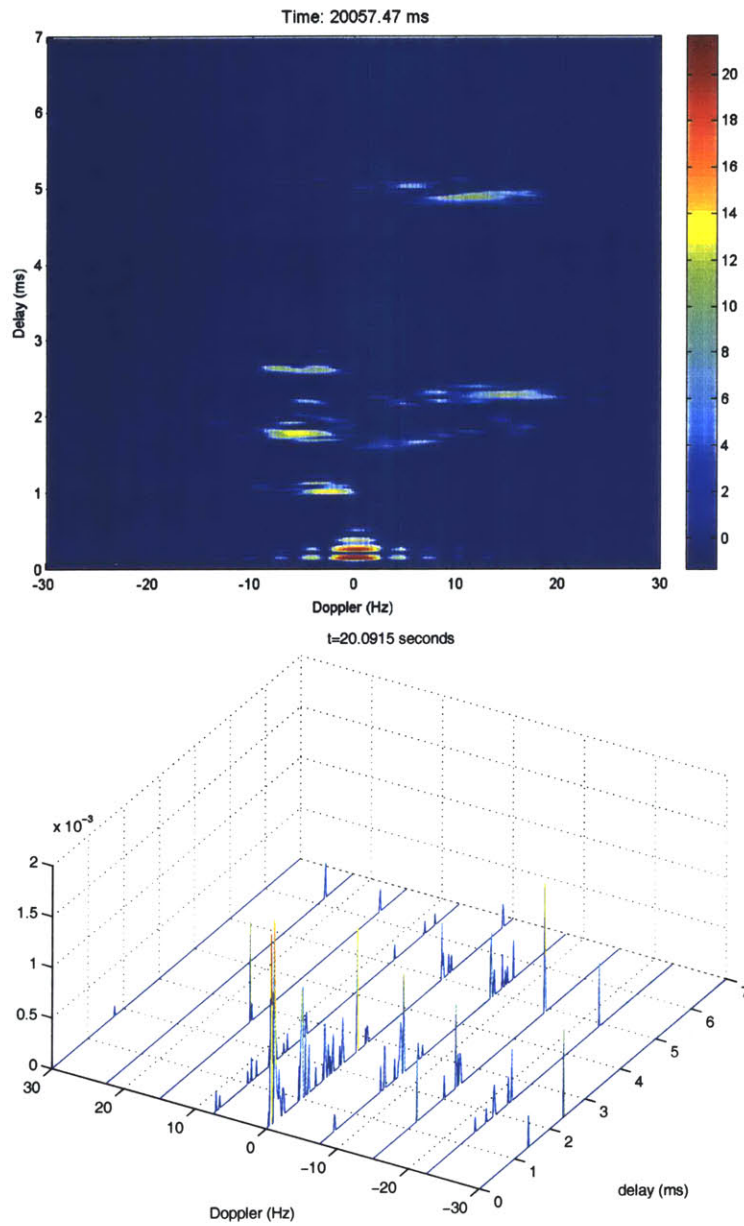


Figure 5-12: Nonsparse (the upper plot) and sparse (the lower plot) delay-Doppler spread function estimate via the SLSMP algorithm

Chapter 6

Summary and Future Work

6.1 Summary

In this thesis, channel estimation and tracking algorithms are developed for broadband shallow-water acoustic communications. The problem of estimating and tracking rapidly fluctuating channel that also has very sparse structure is approached from two different paths.

First, a state-space channel model is derived based on the dynamics of moving point scatterers for wideband transmission. Based on this model, two types of dynamic channel estimation algorithms are developed based on the Extended Kalman Filter (EKF) and the Expectation Maximization (EM) approach, respectively. These algorithms jointly estimate the channel impulse response and the dynamic parameters of the channel fluctuations. Parameter identifiability associated with the sparse channel structure is analyzed for both types of algorithms, which reveals that: i) in the EKF algorithm the dynamic parameters associated with those quiescent taps are unobservable and, if in addition the model is unstable, are undetectable; ii) in the EM based algorithms the dynamic parameter estimation is not persistently exciting if the channel is very sparse. In either case it will lead to unstable parameter estimation and eventually cause divergence, linearly in the EKF algorithm

and exponentially in the EM based algorithms. Base on these analysis, separate parameter models are proposed for the EKF algorithm in which parameters associated with quiescent tap are modeled as stable. The resulting algorithm can selectively tracks the dominant taps while avoiding the instability associated with those quiescent taps. For EM based approach a subspace EM algorithm is proposed so that the parameter is only updated recursively within the dominant subspace. Performance gains of both algorithms are demonstrated via experimental results. Additionally, the analysis has established several important conceptual parallels between the EKF algorithm and the sequential suboptimal EM algorithm, such as the second-order innovation representation.

The development in this first part effectively transforms the physical properties of the channel, *i.e.* large fluctuation dynamics and very sparse structures, through modeling, into model theoretical concepts such as the parameter observability/detectability and the Extended Persistent Excitation conditions, which can be directly used for tracking algorithm design and performance evaluation.

In the second part of the thesis, algorithms for explicit sparse estimation of the channel delay-Doppler spread function are developed. Based on the Matching Pursuit algorithm, a Sequential Least Squares Matching Pursuit (SLSMP) algorithm is proposed which successively find the best subspace to which the residual vector has the shortest distance hence yields the minimum LS error, instead of the best vector to which the residual vector has the maximum correlation. The algorithm is then applied to estimate the discrete delay-Doppler spread function. A suboptimal two-stage algorithm is also proposed which identifies the dominant delays via sparse channel impulse response estimation and then estimates the delay-Doppler components on those identified delays. The performance gains of the sparse estimation algorithms are demonstrated via experimental results.

The focus of the thesis study has been on how to reconcile the rapid channel fluctuations and the sparse channel structures. The approaches described above

provide not only algorithms having improved performance, but more importantly, a framework that allows the physical channel constraints be incorporated effectively in receiver algorithm development. The approaches developed here should also be useful to other applications where similar conflicting constraints exists, such as in array processing where it is typical to have large data dimension, a limited number of actual targets and fast time-variations due to target maneuvering.

6.2 Future Work

The current development in the thesis opens up several interesting fronts for future study.

1. More rigorous study of stochastic channel modeling.

The state-space channel model in Chapter 2 is derived based on deterministic dynamic behavior of the point scatterers. The stochastic properties attached to the model are rather *ad hoc*. As mentioned in Chapter 2, a natural continuation would be to look at the stochastic and dynamic properties of the scattering amplitude of the surface patches and combine them with the state-space model. The existing theory and results of acoustic surface scattering would then be directly helpful.

2. Explicit formulation of dynamic tracking with sparse constraints.

Considering the problem of dynamic tracking with sparse constraints, a natural extension of current work would be to explicitly modify the associated cost function of the Kalman filter in both the EKF and the EM algorithms, in such a way that explicit sparse constraints are included as penalty terms, similar to the L_1 norm constrained optimization. Although the amount of computation involved in that development would be understandably intensive, it would provide a more coherent framework within which dynamic tracking capability and

estimate sparseness can be analyzed and evaluated.

3 Efficient Implementations.

Modifications of the proposed algorithms are needed for real-time implementations. This can be achieved through several suboptimal modifications, such as using two loosely coupled Kalman Filter instead of an EKF for joint parameter and state estimation, and simplified LS implementations of the EM algorithm.

4. Detailed study of impact of various channel estimation methods on equalization performance.

One important goal of channel estimation is to provide channel estimates for subsequent equalization. The performance of various channel estimator, currently evaluated in terms of signal prediction residual error, would have important impact on the equalization performance which heavily relies on the channel estimation error.

5. Extension towards channels in more hybrid environmental conditions.

So far the thesis has been limited to the broadband shallow-water short-range channels of which the issues addressed in this thesis are the most dominant features. In a sense these channels are extreme cases with mostly discrete arrivals. In other environment conditions, such as deep-water long-range channels, the multipath structure would consist of both discrete-arrivals (normal modes or boundary reflected arrivals) and continuous arrivals (refracted arrivals). It would be of practical importance to study how the approaches developed in this thesis would perform under those conditions, and what modifications should be made.

Appendix A

EKF Channel Estimation

A.1 The Extended Kalman Filter Channel Estimation Algorithm

Restate the augmented state-space model((3.2) in section 3.2):

$$\begin{cases} \boldsymbol{\theta}_{i+1} = \boldsymbol{\theta}_i + \mathbf{u}_i & \text{(A.1a)} \\ \mathbf{x}_{i+1} = \mathbf{A}(\boldsymbol{\theta}_i)\mathbf{x}_i + \mathbf{w}_i & \text{(A.1b)} \\ y_i = \mathbf{c}_i\mathbf{x}_i + v_i & \text{(A.1c)} \end{cases}$$

We first assume that all elements of \mathbf{A} are unknown and mathematically independent. Thus $\boldsymbol{\theta}_i = \mathbf{a}_i \triangleq \text{Vec}(\mathbf{A}_i)$. \mathbf{a}_i is an $M^2 \times 1$ column vector formed by orderly stacking all columns of the matrix \mathbf{A}_i . Special cases where some elements of \mathbf{A} are known to be zero are discussed later.

The EKF procedure basically consists of i) state augmentation, ii) linearization and iii) applying the Kalman filter to the linearized model [Jaz70, And79, Lju79]. In the following we briefly state each step as applied to the model (3.2).

1 State Augmentation.

Define the $(M^2 + M) \times 1$ augmented state \mathbf{z}_i as:

$$\mathbf{z}_i^t \triangleq (\mathbf{a}_i^t \ \mathbf{x}_i^t) \quad (\text{A.2})$$

based on which the augmented system model, in terms of \mathbf{z}_i , is given as follows:

$$\begin{cases} \mathbf{z}_{i+1} = f(\mathbf{z}_i) + \mathbf{v}_i & (\text{A.3a}) \\ y_i = (\mathbf{0} \ \mathbf{c}_i)\mathbf{z}_i + \nu_i & (\text{A.3b}) \end{cases}$$

where $\mathbf{v}_i^t \triangleq (\mathbf{u}_i^t \ \mathbf{w}_i^t)$ is $(M^2 + M) \times 1$, and

$$f(\mathbf{z}_i) \triangleq \begin{pmatrix} \mathbf{a}_i \\ \mathbf{A}_i \mathbf{x}_i \end{pmatrix} \quad (\text{A.4})$$

2. Linearization

The state equation in the system model (A.3) becomes nonlinear. Linearizing $f(\mathbf{z}_i)$ around $\widehat{\mathbf{z}}_{i|i}$:

$$f(\mathbf{z}_i) \approx \mathbf{F}_i \mathbf{z}_i + \mathbf{d}_i \quad (\text{A.5})$$

where $\mathbf{d}_i \triangleq f(\widehat{\mathbf{z}}_{i|i}) - \mathbf{F}_i \widehat{\mathbf{z}}_{i|i}$, and

$$\mathbf{F}_i \triangleq f'(\widehat{\mathbf{z}}_{i|i}) = \left(\frac{\partial f(\mathbf{z}_i)}{\partial \mathbf{z}_i} \right)_{\mathbf{z}_i = \widehat{\mathbf{z}}_{i|i}} \quad (\text{A.6})$$

It leads to the following approximating linear model:

$$\begin{cases} \mathbf{z}_{i+1} \approx \mathbf{F}_i \mathbf{z}_i + \mathbf{d}_i + \mathbf{v}_i & (\text{A.7a}) \\ y_i = [\mathbf{0} \ \mathbf{c}_i]\mathbf{z}_i + \nu_i & (\text{A.7b}) \end{cases}$$

The observation equation is not affected by the linearization.

Using the $\text{Vec}(\cdot)$ property of the Kronecker product given in Appendix C, we

could write

$$\mathbf{A}_i \mathbf{x}_i = \text{Vec}(\mathbf{A}_i \mathbf{x}_i) = (\mathbf{x}_i^t \otimes \mathbf{I}_M) \mathbf{a}_i \triangleq \mathbf{X}_i \mathbf{a}_i \quad (\text{A.8})$$

where $\mathbf{X}_i \triangleq \mathbf{x}_i^t \otimes \mathbf{I}_M$ is $M \times M^2$.

Taking the derivation in (A.6), then \mathbf{F}_i can be obtained explicitly as follows:

$$\mathbf{F}_i = \begin{bmatrix} \mathbf{I}_{M^2} & \mathbf{0}_{M^2 \times M} \\ \widehat{\mathbf{X}}_{i|i} & \widehat{\mathbf{A}}_{i|i} \end{bmatrix} \quad (\text{A.9})$$

where $\widehat{\mathbf{X}}_{i|i} \triangleq \widehat{\mathbf{x}}_{i|i}^t \otimes \mathbf{I}_M$. Note (A.9) is obtained assuming $\widehat{\mathbf{X}}_{i|i}$ or equivalently $\widehat{\mathbf{x}}_{i|i}$ is independent of \mathbf{a}_i .

Substituting (A.9) back into (A.5), it becomes clear that the linearization essentially carries out the following approximation:

$$\mathbf{A}_i \widehat{\mathbf{x}}_{i|i} + \widehat{\mathbf{A}}_{i|i} \mathbf{x}_i - \widehat{\mathbf{A}}_{i|i} \widehat{\mathbf{x}}_{i|i} \approx \mathbf{A}_i \mathbf{x}_i \quad (\text{A.10})$$

in which the second order estimation error term, $\widetilde{\mathbf{A}}_{i|i} \widetilde{\mathbf{x}}_{i|i}$ has been neglected. Here $\widetilde{\mathbf{A}}_{i|i} \triangleq \mathbf{A}_i - \widehat{\mathbf{A}}_{i|i}$, and $\widetilde{\mathbf{x}}_{i|i} \triangleq \mathbf{x}_i - \widehat{\mathbf{x}}_{i|i}$.

3. Kalman Filtering on the Linearized Model

Applying the standard Kalman Filter to the model (A.7) is straightforward. Expanded in terms of state and parameters estimation separately, both the time-update and measurement update steps are summarized in Table A.1.

It is clear that the first term on the right hand side of (A.21), the time update of state error covariance, consumes the major amount of computation and the number of complex multiplications and additions involved are of $\mathcal{O}(M^5)$. Hence without any structural constraints, the estimation of a general \mathbf{A}_i will be computationally very intensive and requires prohibitive amount of storage space even for a moderate state dimension M .

$$\text{Measurement} \quad e_i = y_i - \mathbf{c}_i \widehat{\mathbf{x}}_{i|i-1} \quad (\text{A.11})$$

$$\text{Update:} \quad R_{e,i} = \mathbf{c}_i \mathbf{P}_{x,i|i-1} \mathbf{c}_i^h + \sigma_{\nu,i}^2 \quad (\text{A.12})$$

$$\widehat{\mathbf{a}}_{i|i} = \widehat{\mathbf{a}}_{i|i-1} + \mathbf{k}_{a,i} e_i \quad (\text{A.13})$$

$$\widehat{\mathbf{x}}_{i|i} = \widehat{\mathbf{x}}_{i|i-1} + \mathbf{k}_{x,i} e_i \quad (\text{A.14})$$

$$\mathbf{P}_{a,i|i} = \mathbf{P}_{a,i|i-1} - \mathbf{k}_{a,i} R_{e,i} \mathbf{K}_{a,i}^h \quad (\text{A.15})$$

$$\mathbf{P}_{x,i|i} = \mathbf{P}_{x,i|i-1} - \mathbf{k}_{x,i} R_{e,i} \mathbf{k}_{x,i}^h \quad (\text{A.16})$$

$$\mathbf{P}_{ax,i|i} = \mathbf{P}_{ax,i|i-1} - \mathbf{k}_{a,i} R_{e,i} \mathbf{k}_{x,i}^h \quad (\text{A.17})$$

$$\text{Time} \quad \widehat{\mathbf{a}}_{i+1|i} = \widehat{\mathbf{a}}_{i|i} \quad (\text{A.18})$$

$$\text{Update:} \quad \widehat{\mathbf{x}}_{i+1|i} = \widehat{\mathbf{A}}_{i|i} \widehat{\mathbf{x}}_{i|i} = \widehat{\mathbf{X}}_{i|i} \widehat{\mathbf{a}}_{i|i} \quad (\text{A.19})$$

$$\mathbf{P}_{a,i+1|i} = \mathbf{P}_{a,i|i} + Q_{u,i} \quad (\text{A.20})$$

$$\begin{aligned} \mathbf{P}_{x,i+1|i} = & \widehat{\mathbf{X}}_{i|i} \mathbf{P}_{a,i|i} \widehat{\mathbf{X}}_{i|i}^h + \widehat{\mathbf{A}}_{i|i} \mathbf{P}_{x,i|i} \widehat{\mathbf{A}}_{i|i}^h \\ & + \widehat{\mathbf{X}}_{i|i} \mathbf{P}_{ax,i|i} \widehat{\mathbf{A}}_{i|i}^h + \widehat{\mathbf{A}}_{i|i} \mathbf{P}_{ax,i|i}^h \widehat{\mathbf{X}}_{i|i}^h + Q_{w,i} \end{aligned} \quad (\text{A.21})$$

$$\mathbf{P}_{ax,i+1|i} = \mathbf{P}_{a,i|i} \widehat{\mathbf{X}}_{i|i}^h + \mathbf{P}_{ax,i|i} \widehat{\mathbf{A}}_{i|i}^h \quad (\text{A.22})$$

Table A.1: EKF algorithm for the joint estimation of state and state transition matrix. $\mathbf{P}_{a,\cdot}$ and $\mathbf{P}_{x,\cdot}$ are the error covariance matrices of the state and parameter estimates respectively, and $\mathbf{P}_{ax,\cdot}$ is their error cross-covariance matrix. Subscript $\cdot_{i+1|i}$ corresponds to one-step prediction and $\cdot_{i|i}$ refers to filtering. $\mathbf{k}_{a,i} \triangleq \mathbf{P}_{ax,i|i-1} \mathbf{c}_i^h R_{e,i}^{-1}$ and $\mathbf{k}_{x,i} \triangleq \mathbf{P}_{x,i|i-1} \mathbf{c}_i^h R_{e,i}^{-1}$ are the Kalman gains for the parameter and state estimates, respectively. The portion highlighted as red corresponds to the standard Kalman filtering assuming known \mathbf{A}_i .

A.2 Special Cases: Diagonal and Tridiagonal State Transition Matrix

We now consider two special cases: i) \mathbf{A}_i is diagonal and ii) \mathbf{A}_i is tridiagonal. In both cases one could get the algorithm by repeating the procedure in last section with the new parameterization. Alternatively, one could derive the same results by specializing the EKF algorithm obtained in last section according to the new parameterization, as presented in the following:

1. Diagonal \mathbf{A}_i :

Letting \mathbf{A}_i be diagonal, we effectively assume that channel fluctuations are not coupled across taps. As a result, there are only M unknown parameters. Denote the diagonal elements as $\mathbf{a}^d \triangleq [a_1^d, a_2^d, \dots, a_M^d]^t = \text{diag}(\mathbf{A})$, then for $\mathbf{a} = \text{Vec}(\mathbf{A})$ (for notational simplicity, we have temporally dropped the time index),

$$\mathbf{a}^t = (a_1^d \underbrace{0 \dots 0}_{M+1} a_2^d \underbrace{0 \dots 0}_{M+1} \dots \dots a_{M-1}^d \underbrace{0 \dots 0}_{M+1} a_N^d) \quad (\text{A.23})$$

The same applies to \mathbf{u} . Denote \mathbf{P}_{a^d} and $\mathbf{P}_{a^d x}$ as the error covariance of estimate of \mathbf{a}^d and cross error covariance between estimates of \mathbf{a}^d and \mathbf{x} , It then can be verified that

$$\mathbf{X}\mathbf{P}_a\mathbf{X}^h = \text{Diag}(\mathbf{x})\mathbf{P}_{a^d}\text{Diag}(\mathbf{x})^h \quad (\text{A.24})$$

$$\mathbf{X}\mathbf{P}_{ax}\mathbf{A}^h = \text{Diag}(\mathbf{x})\mathbf{P}_{a^d x}\text{Diag}(\mathbf{a}^d)^h \quad (\text{A.25})$$

$$S(\mathbf{P}_a\mathbf{X}^*) = \mathbf{P}_{a^d}\text{Diag}(\mathbf{x})^h \quad (\text{A.26})$$

$$S(\mathbf{P}_{ax}\mathbf{A}^h) = \mathbf{P}_{a^d x}\text{Diag}(\mathbf{a}^d)^h \quad (\text{A.27})$$

$$S(\mathbf{P}_{ax}\mathbf{c}^h) = \mathbf{P}_{a^d x}\mathbf{c}^h \quad (\text{A.28})$$

hold for both one-step prediction as well as filtering. Here the operator $\text{Diag}(\mathbf{p})$ is a diagonal matrix whose diagonal elements are given by the vector \mathbf{p} ; the

operator $S(\mathbf{G})$ squeezes out all the elements in \mathbf{G} known to be zero. It also follows that

$$S(\mathbf{a}) = \mathbf{a}^d \quad (\text{A.29})$$

$$S(\mathbf{K}_a) = \mathbf{K}_{a^d} \quad (\text{A.30})$$

$$S(\mathbf{P}_a) = \mathbf{P}_{a^d} \quad (\text{A.31})$$

$$S(\mathbf{P}_{ax}) = \mathbf{P}_{a^d x} \quad (\text{A.32})$$

We now recover the time index i in the presentation.

Applying the operator S on both sides of (A.13), (A.15), (A.17), (A.18), (A.20) and (A.22) and using (A.24)-(A.32), it follows that the algorithm corresponding to a diagonal \mathbf{A}_i would simply be the EKF algorithm in Table A.1 with its elements appearing on left hand side of (A.24)-(A.32) replaced by their right hand counterparts.

The reduction in both computation and storage space is significant. With diagonal \mathbf{A}_i , the involved number of complex multiplications and additions are of $\mathcal{O}(M^2)$.

2. Tridiagonal \mathbf{A}_i :

The case of a tridiagonal \mathbf{A}_i is similar to the diagonal case. However, by including the first upper and first lower off-diagonal elements, the channel fluctuations are allowed to be correlated with those of the immediate neighboring taps.

Denote the main diagonal elements, the first upper diagonal elements and the first lower diagonal elements of \mathbf{A} as (the time index are dropped off again temporally) $\mathbf{a}^d \triangleq [a_1^d, a_2^d, \dots, a_M^d]^t$, $\mathbf{a}^+ \triangleq [a_2^+, a_3^+, \dots, a_M^+]^t$ and $\mathbf{a}^- \triangleq$

and similarly

$$S(\mathbf{K}_a) = \mathbf{K}_{a^s} \tag{A.41}$$

$$S(\mathbf{P}_a) = \mathbf{P}_{a^s} \tag{A.42}$$

$$S(\mathbf{P}_{ax}) = \mathbf{P}_{a^s x} \tag{A.43}$$

Due to the sparse structure of \mathcal{X} , (A.35)-(A.37) can be computed efficiently and only involve $\mathcal{O}(M^2)$ number of complex multiplications and additions.

Appendix B

EM Channel Estimation

B.1 Derivation of the smoothed state correlation equations

The derivation of the autocorrelation $\mathbf{R}_{x_i|n}^{(l-1)}[0]$ directly follows from the orthogonality principle. Since $\mathbf{x}_i = \hat{\mathbf{x}}_{i|n}^{(l-1)} + \tilde{\mathbf{x}}_{i|n}^{(l-1)}$, here $\hat{\mathbf{x}}_{i|n}^{(l-1)}$ and $\tilde{\mathbf{x}}_{i|n}^{(l-1)}$, the smoothed state estimate and error conditioned on $\hat{\mathbf{A}}_n^{(l-1)}$ respectively, are orthogonal to each other, it yields

$$\begin{aligned}\mathbf{R}_{x_i|n}^{(l-1)}[0] &\triangleq E\{\mathbf{x}_i^{(l-1)}(\mathbf{x}_i^{(l-1)})^h|\mathcal{Y}_n; \hat{\mathbf{A}}_n^{(l-1)}\} \\ &= \hat{\mathbf{x}}_{i|n}^{(l-1)}(\hat{\mathbf{x}}_{i|n}^{(l-1)})^h + E\{\tilde{\mathbf{x}}_{i|n}^{(l-1)}(\tilde{\mathbf{x}}_{i|n}^{(l-1)})^{(l-1)}|\mathcal{Y}_n; \hat{\mathbf{A}}_n^{(l-1)}\} \\ &= \hat{\mathbf{x}}_{i|n}^{(l-1)}(\hat{\mathbf{x}}_{i|n}^{(l-1)})^h + \mathbf{P}_{i|n}^{(l-1)}\end{aligned}\tag{B.1}$$

The lag-1 cross-correlation $\mathbf{R}_{x_i|n}^{(l-1)}[1]$ can be derived using the so-called *the law of iterative projection*: given two sets of observations $\mathcal{Z}_1 \subset \mathcal{Z}_2$, the following equality holds

$$E\{\mathbf{X}|\mathcal{Z}_1\} = E\{E\{\mathbf{X}|\mathcal{Z}_2\}|\mathcal{Z}_1\}\tag{B.2}$$

Applying (B.2) with $\mathbf{X} = \mathbf{x}_i \mathbf{x}_{i-1}^h$, $\mathcal{Z}_1 = \mathcal{Y}_n$ and $\mathcal{Z}_2 = \{\mathbf{x}_i, \mathcal{Y}_n\}$, it yields

$$\mathbf{R}_{x_i|n}^{(l-1)}[1] \triangleq E\{\mathbf{x}_i \mathbf{x}_{i-1}^h | \mathcal{Y}_n; \widehat{\mathbf{A}}_n^{(l-1)}\} = E\{E\{\mathbf{x}_i \mathbf{x}_{i-1}^h | \mathbf{x}_i, \mathcal{Y}_n; \widehat{\mathbf{A}}_n^{(l-1)}\} | \mathcal{Y}_n; \widehat{\mathbf{A}}_n^{(l-1)}\} \quad (\text{B.3})$$

Since

$$E\{\mathbf{x}_i \mathbf{x}_{i-1}^h | \mathbf{x}_i, \mathcal{Y}_n; \widehat{\mathbf{A}}_n^{(l-1)}\} = \mathbf{x}_i E\{\mathbf{x}_{i-1}^h | \mathbf{x}_i, \mathcal{Y}_{i-1}; \widehat{\mathbf{A}}_n^{(l-1)}\} = \mathbf{x}_i [\widehat{\mathbf{x}}_{i-1|i-1}^{(l-1)} + \mathbf{J}_{s,i}^{(l-1)} (\mathbf{x}_i - \widehat{\mathbf{x}}_{i|i-1}^{(l-1)})]^h \quad (\text{B.4})$$

where the gain factor associated with the state prediction error

$$\mathbf{J}_{s,i}^{(l-1)} \triangleq \mathbf{P}_{i-1|i-1}^{(l-1)} (\widehat{\mathbf{A}}_n^{(l-1)})^h (\mathbf{P}_{i|i-1}^{(l-1)})^{-1} \quad (\text{B.5})$$

is also the closed-loop state matrix for the smoothed estimator [Kai00]. Substituting (B.4) into (B.3), it yields

$$\begin{aligned} \mathbf{R}_{x_i|n}^{(l-1)}[1] &= E\{\mathbf{x}_i [\widehat{\mathbf{x}}_{i-1|i-1}^{(l-1)} + \mathbf{J}_{s,i}^{(l-1)} (\mathbf{x}_i - \widehat{\mathbf{x}}_{i|i-1}^{(l-1)})]^h | \mathcal{Y}_n; \widehat{\mathbf{A}}_n^{(l-1)}\} \\ &= E\{\mathbf{x}_i \mathbf{x}_i^h (\mathbf{J}_i^{(l-1)})^h | \mathcal{Y}_n; \widehat{\mathbf{A}}_n^{(l-1)}\} + E\{\mathbf{x}_i [\widehat{\mathbf{x}}_{i-1|i-1}^{(l-1)} - \mathbf{J}_{s,i}^{(l-1)} \widehat{\mathbf{x}}_{i|i-1}^{(l-1)}]^h | \mathcal{Y}_n; \widehat{\mathbf{A}}_n^{(l-1)}\} \\ &= [\widehat{\mathbf{x}}_{i|n}^{(l-1)} (\widehat{\mathbf{x}}_{i|n}^{(l-1)})^h + \mathbf{P}_{i|n}^{(l-1)}] (\mathbf{J}_i^{(l-1)})^h + \widehat{\mathbf{x}}_{i|n}^{(l-1)} (\widehat{\mathbf{x}}_{i-1|i-1}^{(l-1)} - \mathbf{J}_{s,i}^{(l-1)} \widehat{\mathbf{x}}_{i|i-1}^{(l-1)})^h \\ &= \widehat{\mathbf{x}}_{i|n}^{(l-1)} \{ \mathbf{J}_{s,i}^{(l-1)} (\widehat{\mathbf{x}}_{i|n}^{(l-1)} - \widehat{\mathbf{x}}_{i|i-1}^{(l-1)}) + \widehat{\mathbf{x}}_{i-1|i-1}^{(l-1)} \}^h + \mathbf{P}_{i|n}^{(l-1)} (\mathbf{J}_{s,i}^{(l-1)})^h \end{aligned} \quad (\text{B.6})$$

Using the fixed-interval state smoothing formula (B.16)

$$\widehat{\mathbf{x}}_{i-1|n}^{(l-1)} = \mathbf{J}_{s,i}^{(l-1)} (\widehat{\mathbf{x}}_{i|n}^{(l-1)} - \widehat{\mathbf{x}}_{i|i-1}^{(l-1)}) + \widehat{\mathbf{x}}_{i-1|i-1}^{(l-1)} \quad (\text{B.7})$$

Substituting (B.7) into (B.6), it yields

$$\mathbf{R}_{x_i|n}^{(l-1)}[1] = \widehat{\mathbf{x}}_{i|n}^{(l-1)} (\widehat{\mathbf{x}}_{i-1|n}^{(l-1)})^h + \mathbf{P}_{i|n}^{(l-1)} (\mathbf{J}_{s,i}^{(l-1)})^h \quad (\text{B.8})$$

B.2 Kalman smoothing formula

B.2.1 Fixed-point Kalman smoothing

The fixed-point smoothing formula follows directly from the innovation representation ([Kai00]):

$$\begin{cases} \hat{\mathbf{x}}_{i|n} = \hat{\mathbf{x}}_{i|n-1} + \mathbf{P}_{i,n} \mathbf{c}_n^h R_{e_n}^{-1} e_n & \text{(B.9a)} \\ \mathbf{P}_{i|n} = \mathbf{P}_{i|n-1} - \mathbf{P}_{i,n} \mathbf{c}_n^h R_{e_n}^{-1} \mathbf{c}_n \mathbf{P}_{i,n}^h & \text{(B.9b)} \end{cases}$$

where $n \geq i$; e_n , R_{e_n} are the innovation and its variance at time n ; the cross error covariance $\mathbf{P}_{i,n} = E[\tilde{\mathbf{x}}_{i|i-1} \tilde{\mathbf{x}}_{n|n-1}^h]$ is given by

$$\mathbf{P}_{i,n} = \mathbf{P}_{i|i-1} [\mathbf{F}_{p,n-1} \mathbf{F}_{p,n-2} \cdots \mathbf{F}_{p,i}]^h \quad \text{(B.10a)}$$

$$\mathbf{F}_{p,i} = \hat{\mathbf{A}}_n [\mathbf{I} - \mathbf{P}_{i|i-1} \mathbf{c}_i^h R_{e_i}^{-1} \mathbf{c}_i] \quad \text{(B.10b)}$$

for $n > i$, and $\mathbf{P}_{i,n} = \mathbf{P}_{n|n-1}$ for $i = n$. $\hat{\mathbf{A}}_n$ is the latest estimate of \mathbf{A} ; $\mathbf{F}_{p,i}$ denotes the transition matrix of the one-step state prediction. The iteration index is dropped in this appendix to simplify the notation, and is understood to be $(l-1)$ unless otherwise specified.

Since $\mathbf{P}_{i|i} \hat{\mathbf{A}}_n^h = (\mathbf{P}_{i|i-1} - \mathbf{P}_{i|i-1} \mathbf{c}_i^h R_{e_i}^{-1} \mathbf{c}_i \mathbf{P}_{i|i-1}) \hat{\mathbf{A}}_n^h = \mathbf{P}_{i|i-1} \mathbf{F}_{p,i}^h$, as defined in appendix B.1,

$$\mathbf{J}_{s,i+1} \triangleq \mathbf{P}_{i|i} \hat{\mathbf{A}}_n^h (\mathbf{P}_{i+1|i})^{-1} = \mathbf{P}_{i|i-1} \mathbf{F}_{p,i}^h \mathbf{P}_{i+1|i}^{-1} \quad \text{(B.11)}$$

Combining (B.11) with (B.10a), and denoting $\mathbf{T}_{i,n} \triangleq \prod_{j=i}^{n-1} \mathbf{J}_{s,j+1}$, it is easy to show that for $i < n$

$$\mathbf{P}_{i,n} = \left(\prod_{j=i}^{n-1} \mathbf{J}_{s,j+1} \right) \mathbf{P}_{n|n-1} \triangleq \mathbf{T}_{i,n} \mathbf{P}_{n|n-1} \quad \text{(B.12)}$$

For $i = n$, one may let $\mathbf{T}_{i,n} = \mathbf{I}$. Substituting (B.12) into (B.9) yields the following

recursions

$$\begin{cases} \widehat{\mathbf{x}}_{i|n} = \widehat{\mathbf{x}}_{i|n-1} + \mathbf{T}_{i,n} \mathbf{P}_{n|n-1} \mathbf{c}_n^h R_{e_n}^{-1} e_n & \text{(B.13a)} \\ \mathbf{P}_{i|n} = \mathbf{P}_{i|n-1} - \mathbf{T}_{i,n} \mathbf{P}_{n|n-1} \mathbf{c}_n^h R_{e_n}^{-1} \mathbf{c}_n \mathbf{P}_{n|n-1}^h \mathbf{T}_{i,n}^h & \text{(B.13b)} \end{cases}$$

which are the base for the new recursion form derived in section 4.3 and appendix B.3.

Note there is another useful expression for $\mathbf{J}_{s,i}$. Right multiplying both sides of the error covariance measurement update equation $\mathbf{P}_{i+1|i} = \mathbf{A}_i \mathbf{P}_{i|i} \widehat{\mathbf{A}}_n^h + \mathbf{Q}_i$ by $\mathbf{P}_{i+1|i}^{-1}$ yields

$$\mathbf{I} - \mathbf{Q}_i \mathbf{P}_{i+1|i}^{-1} = \widehat{\mathbf{A}}_n \mathbf{P}_{i|i} \mathbf{A}_i^h \mathbf{P}_{i+1|i}^{-1} \quad \text{(B.14)}$$

Assuming $\widehat{\mathbf{A}}_n$ invertible, it follows

$$\mathbf{J}_{s,i+1} \triangleq \mathbf{P}_{i|i} \widehat{\mathbf{A}}_n^h \mathbf{P}_{i+1|i}^{-1} = \widehat{\mathbf{A}}_n^{-1} [\mathbf{I} - \mathbf{Q}_i \mathbf{P}_{i+1|i}^{-1}] \quad \text{(B.15)}$$

B.2.2 Fixed-interval Kalman smoothing

Following [Kai00], the fixed-interval smoothing formula is

$$\begin{cases} \widehat{\mathbf{x}}_{i-1|n} = \mathbf{J}_{s,i} (\widehat{\mathbf{x}}_{i|n} - \widehat{\mathbf{x}}_{i|i-1}) + \widehat{\mathbf{x}}_{i-1|i-1} & \text{(B.16a)} \\ \mathbf{P}_{i-1|n} = \mathbf{P}_{i-1|i-1} + \mathbf{J}_{s,i} (\mathbf{P}_{i|n} - \mathbf{P}_{i|i-1}) \mathbf{J}_{s,i}^h & \text{(B.16b)} \end{cases}$$

In [Shu82][Wei94], the fixed-interval smoothing formula was used to recursively compute the smoothed state estimate and its error covariance, starting from $\widehat{\mathbf{x}}_{n|n}$ and $\mathbf{P}_{n|n}$ backwards to $\widehat{\mathbf{x}}_{1|n}$ and $\mathbf{P}_{1|n}$, after the Kalman filter has generated the filtered state estimate and the 1-step prediction for $i = 1, \dots, n$. From that the smoothed state correlations were computed and summed up to obtain the parameter estimate according to (4.10), (B.8) and (4.8).

B.3 Derivation of the new vector form recursions

The following identities are crucial to the derivation of the vector recursion form [Gra81]:

$$Vec(\mathbf{ABC}) = (\mathbf{C}^t \otimes \mathbf{A})Vec(\mathbf{B}) \quad (\text{B.17})$$

$$(\mathbf{AB}) \otimes (\mathbf{CD}) = (\mathbf{A} \otimes \mathbf{C})(\mathbf{B} \otimes \mathbf{D}) \quad (\text{B.18})$$

Taking Vec on both sides of (4.14) and (4.15), and applying (B.17), it yields

$$\begin{aligned} Vec(\widehat{\mathbf{H}}_1[n]) &= \lambda Vec(\widehat{\mathbf{H}}_1[n-1]) + Vec[\widehat{\mathbf{x}}_{n|n}\widehat{\mathbf{x}}_{n-1|n}^h + \mathbf{P}_{n|n}\mathbf{J}_{s,n}^h] \\ &\quad + \lambda[\boldsymbol{\Omega}_{1,n}Vec(\mathbf{M}_n) + \boldsymbol{\Upsilon}_{1,n}\mathbf{N}_n^* + \boldsymbol{\Gamma}_{1,n}\mathbf{N}_n] \end{aligned} \quad (\text{B.19})$$

$$\begin{aligned} Vec(\widehat{\mathbf{H}}_0[n]) &= \lambda Vec(\widehat{\mathbf{H}}_0[n-1]) + Vec[\widehat{\mathbf{x}}_{n-1|n}\widehat{\mathbf{x}}_{n-1|n}^h + \mathbf{P}_{n-1|n}] \\ &\quad + \lambda[\boldsymbol{\Omega}_{0,n}Vec(\mathbf{M}_n) + \boldsymbol{\Upsilon}_{0,n}\mathbf{N}_n^* + \boldsymbol{\Gamma}_{0,n}\mathbf{N}_n] \end{aligned} \quad (\text{B.20})$$

where \mathbf{M}_n and \mathbf{N}_n are defined in section 4.3. \mathbf{N}_n is a column vector so $Vec(\mathbf{N}_n) = \mathbf{N}_n$ and $Vec(\mathbf{N}_n^h) = \mathbf{N}_n^*$. In addition for $j = 0, 1$,

$$\boldsymbol{\Omega}_{j,n} \triangleq \sum_{i=1}^{n-1} \lambda^{n-1-i} \mathbf{T}_{i-1,n}^* \otimes \mathbf{T}_{i-1+j,n} \quad (\text{B.21})$$

$$\boldsymbol{\Gamma}_{j,n} \triangleq \sum_{i=1}^{n-1} \lambda^{n-1-i} \widehat{\mathbf{x}}_{i-1|n-1}^* \otimes \mathbf{T}_{i-1+j,n} \quad (\text{B.22})$$

$$\boldsymbol{\Upsilon}_{j,n} \triangleq \sum_{i=1}^{n-1} \lambda^{n-1-i} \mathbf{T}_{i-1,n}^* \otimes \widehat{\mathbf{x}}_{i-1+j|n-1} \quad (\text{B.23})$$

which can all be calculated recursively as shown below.

First consider $\Omega_{1,n}$,

$$\begin{aligned}
\Omega_{1,n+1} &= \sum_{i=1}^n \lambda^{n-i} \mathbf{T}_{i-1,n+1}^* \otimes \mathbf{T}_{i,n+1} \\
&= \mathbf{T}_{n-1,n+1}^* \otimes \mathbf{T}_{n,n+1} + \sum_{i=1}^{n-1} \lambda^{n-i} \mathbf{T}_{i-1,n+1}^* \otimes \mathbf{T}_{i,n+1} \\
&= (\mathbf{J}_{s,n}^* \mathbf{J}_{s,n+1}^*) \otimes \mathbf{J}_{s,n+1} + \sum_{i=1}^{n-1} \lambda^{n-i} (\mathbf{T}_{i-1,n} \mathbf{J}_{s,n+1})^* \otimes (\mathbf{T}_{i,n} \mathbf{J}_{s,n+1}) \\
&= (\mathbf{J}_{s,n}^* \otimes \mathbf{I})(\mathbf{J}_{s,n+1}^* \otimes \mathbf{J}_{s,n+1}) + \lambda \sum_{i=1}^{n-1} \lambda^{n-1-i} (\mathbf{T}_{i-1,n}^* \otimes \mathbf{T}_{i,n}) (\mathbf{J}_{s,n+1}^* \otimes \mathbf{J}_{s,n+1}) \\
&= [(\mathbf{J}_{s,n}^* \otimes \mathbf{I}) + \lambda \Omega_{1,n}] (\mathbf{J}_{s,n+1}^* \otimes \mathbf{J}_{s,n+1}) \tag{B.24}
\end{aligned}$$

where we used $\mathbf{T}_{i,n+1} = \mathbf{T}_{i,n} \mathbf{J}_{s,n+1}$ in the second equality and applied the property (B.18) in the third equality. Now consider $\Upsilon_{1,n+1}$,

$$\begin{aligned}
\Upsilon_{1,n+1} &= \sum_{i=1}^n \lambda^{n-i} \mathbf{T}_{i-1,n+1}^* \otimes \hat{\mathbf{x}}_{i|n} \\
&= \mathbf{T}_{n-1,n+1}^* \otimes \hat{\mathbf{x}}_{n|n} + \sum_{i=1}^{n-1} \lambda^{n-i} \mathbf{T}_{i-1,n+1}^* \otimes \hat{\mathbf{x}}_{i|n} \\
&= (\mathbf{J}_{s,n}^* \mathbf{J}_{s,n+1}^*) \otimes \hat{\mathbf{x}}_{n|n} + \sum_{i=1}^{n-1} \lambda^{n-i} (\mathbf{T}_{i-1,n}^* \mathbf{J}_{s,n+1}^*) \otimes (\hat{\mathbf{x}}_{i|n-1} + \mathbf{T}_{i,n} \mathbf{N}_n) \\
&= (\mathbf{J}_{s,n}^* \mathbf{J}_{s,n+1}^*) \otimes \hat{\mathbf{x}}_{n|n} + \lambda \sum_{i=1}^{n-1} \lambda^{n-1-i} (\mathbf{T}_{i-1,n}^* \mathbf{J}_{s,n+1}^*) \otimes \hat{\mathbf{x}}_{i|n-1} \\
&\quad + \lambda \sum_{i=1}^{n-1} \lambda^{n-1-i} (\mathbf{T}_{i-1,n}^* \mathbf{J}_{s,n+1}^*) \otimes (\mathbf{T}_{i,n} \mathbf{N}_n) \\
&= (\mathbf{J}_{s,n}^* \otimes \hat{\mathbf{x}}_{n|n}) \mathbf{J}_{s,n+1}^* + \lambda \sum_{i=1}^{n-1} \lambda^{n-1-i} (\mathbf{T}_{i-1,n}^* \otimes \hat{\mathbf{x}}_{i|n-1}) \mathbf{J}_{s,n+1}^* \\
&\quad + \lambda \sum_{i=1}^{n-1} \lambda^{n-1-i} (\mathbf{T}_{i-1,n}^* \otimes \mathbf{T}_{i,n}) (\mathbf{J}_{s,n+1}^* \otimes \mathbf{N}_n) \\
&= [\mathbf{J}_{s,n}^* \otimes \hat{\mathbf{x}}_{n|n} + \lambda \Upsilon_{1,n}] \mathbf{J}_{s,n+1}^* + \lambda \Omega_{1,n} (\mathbf{J}_{s,n+1}^* \otimes \mathbf{N}_n) \tag{B.25}
\end{aligned}$$

The recursions for the remaining terms can be derived similarly. To summarize, for $j = 0, 1$

$$\mathbf{\Omega}_{j,n+1} = [\mathbf{J}_{s,n}^* \otimes \mathbf{L}_{j,n} + \lambda \mathbf{\Omega}_{j,n}] (\mathbf{J}_{s,n+1}^* \otimes \mathbf{J}_{s,n+1}) \quad (\text{B.26})$$

$$\mathbf{\Gamma}_{j,n+1} = [\widehat{\mathbf{x}}_{n-1|n}^* \otimes \mathbf{L}_{j,n} + \lambda \mathbf{\Gamma}_{j,n}] \mathbf{J}_{s,n+1} + \lambda \mathbf{\Omega}_{j,n} (\mathbf{N}_n^* \otimes \mathbf{J}_{s,n+1}) \quad (\text{B.27})$$

$$\mathbf{\Upsilon}_{j,n+1} = [\mathbf{J}_{s,n}^* \otimes \widehat{\mathbf{x}}_{n-1+j|n} + \lambda \mathbf{\Upsilon}_{j,n}] \mathbf{J}_{s,n+1}^* + \lambda \mathbf{\Omega}_{j,n} (\mathbf{J}_{s,n+1}^* \otimes \mathbf{N}_n) \quad (\text{B.28})$$

where $\mathbf{L}_{0,n} = \mathbf{J}_{s,n}$ and $\mathbf{L}_{1,n} = \mathbf{I}$.

B.4 Proof of the stability of the new vector form recursions

Grouping (B.26)-(B.28) yields the following state equations for $\Omega_{j,n}$, $\Gamma_{j,n}$ and $\Upsilon_{j,n}$ (for $j = 0, 1$):

$$\begin{bmatrix} \Omega_{j,n+1}^t \\ \Gamma_{j,n+1}^t \\ \Upsilon_{j,n+1}^t \end{bmatrix} = \lambda \begin{bmatrix} \mathbf{G}_{n+1}^t & \mathbf{0} & \mathbf{0} \\ \mathbf{U}_{n+1}^t & \mathbf{J}_{s,n+1}^t & \mathbf{0} \\ \mathbf{V}_{n+1}^t & \mathbf{0} & \mathbf{J}_{s,n+1}^h \end{bmatrix} \begin{bmatrix} \Omega_{j,n}^t \\ \Gamma_{j,n}^t \\ \Upsilon_{j,n}^t \end{bmatrix} + \begin{bmatrix} \mathbf{G}_{n+1}^t & \mathbf{0} & \mathbf{0} \\ \mathbf{0} & \mathbf{J}_{s,n+1}^t & \mathbf{0} \\ \mathbf{0} & \mathbf{0} & \mathbf{J}_{s,n+1}^h \end{bmatrix} \begin{bmatrix} \mathbf{J}_{s,n}^h \otimes \mathbf{L}_{j,n}^t \\ \widehat{\mathbf{x}}_{n-1|n}^h \otimes \mathbf{L}_{j,n}^t \\ \mathbf{J}_{s,n}^h \otimes \widehat{\mathbf{x}}_{n-1+j|n}^t \end{bmatrix} \quad (\text{B.29})$$

where $\mathbf{L}_{0,n} = \mathbf{J}_{s,n}$, $\mathbf{L}_{1,n} = \mathbf{I}$. And $\mathbf{G}_{n+1} = \mathbf{J}_{s,n+1}^* \otimes \mathbf{J}_{s,n+1}$, $\mathbf{U}_{n+1} = \mathbf{N}_n^* \otimes \mathbf{J}_{s,n+1}$, $\mathbf{V}_{n+1} = \mathbf{J}_{s,n+1}^* \otimes \mathbf{N}_n$.

Equation (B.29) has a block lower tridiagonal transition matrix hence it is stable if and only if (iff) all the eigenvalues of $\lambda \mathbf{G}_{n+1}$ and $\lambda \mathbf{J}_{s,n+1}$ are inside the unit circle. Since the eigenvalues of \mathbf{G}_{n+1} are the set of all products between those of $\mathbf{J}_{s,n+1}^*$ and $\mathbf{J}_{s,n+1}$, (B.29) is stable iff all the eigenvalues of $\lambda \mathbf{J}_{s,n+1}$ are inside the unit circle. For $\lambda = 1$ this is equivalent to saying that the KF assuming $\mathbf{A} = \widehat{\mathbf{A}}_n^{(l-1)}$ is stable (equivalently $(\widehat{\mathbf{A}}_n^{(l-1)}, \mathbf{Q}_w^{1/2})$ and $(\widehat{\mathbf{A}}_n^{(l-1)}, \mathbf{c}[n])$ are completely stabilisable and completely detectable, respectively). This follows from the fact that the KF state estimates admit the following recursion [Kai00]

$$(\mathbf{P}_{n|n}^{-1} \widehat{\mathbf{x}}_{n|n}) = \mathbf{J}_{s,n}^h (\mathbf{P}_{n-1|n-1}^{-1} \widehat{\mathbf{x}}_{n-1|n-1}) + \mathbf{c}_{n-1}^h \mathbf{Q}_v^{-1} y_n \quad (\text{B.30})$$

which is stable iff all the eigenvalues of $\mathbf{J}_{s,n}$ are inside the unit circle.

Therefore, the complete stabilizability and complete detectability of the Kalman filter assuming $\mathbf{A} = \widehat{\mathbf{A}}_n^{(l-1)}$ is the sufficient condition (and also necessary if $\lambda = 1$) for the stability of the recursion (B.29).

B.5 Some Proofs for Section 4.5

B.5.1 Derivation of (4.32)

Consider the matrix recursion (4.30) where $\mathbf{L}_j[n]$ and $\widehat{\mathbf{H}}_0^{-1}[n]$ are computed using (4.25) with $\lambda_2 = 0$. Denote $\delta\mathbf{L}[n] \triangleq \mathbf{L}_1[n] - \widehat{\mathbf{A}}_{n-1}\mathbf{L}_0[n]$, then

$$\begin{aligned}\delta\mathbf{L}[n] &= E\{\mathbf{x}_n\mathbf{x}_{n-1}^h - \widehat{\mathbf{A}}_{n-1}\mathbf{x}_{n-1}\mathbf{x}_{n-1}^h | \mathcal{Y}_n; \widehat{\mathbf{A}}_{n-1}\} \\ &= E\{(\mathbf{x}_n - \widehat{\mathbf{A}}_{n-1}\mathbf{x}_{n-1})\mathbf{x}_{n-1}^h | \mathcal{Y}_n; \widehat{\mathbf{A}}_{n-1}\} \\ &= E\{\mathbf{w}_{n-1}\mathbf{x}_{n-1}^h | \mathcal{Y}_n; \widehat{\mathbf{A}}_{n-1}\}\end{aligned}\quad (\text{B.31})$$

where the last equality used the state equation $\mathbf{x}_n = \mathbf{A}\mathbf{x}_{n-1} + \mathbf{w}_{n-1}$ with $\mathbf{A} = \widehat{\mathbf{A}}_{n-1}$.

Using the law of iterative projection

$$\begin{aligned}E\{\mathbf{w}_{n-1}\mathbf{x}_{n-1}^h | \mathcal{Y}_n; \widehat{\mathbf{A}}_{n-1}\} &= E\{E\{\mathbf{w}_{n-1}\mathbf{x}_{n-1}^h | \mathbf{x}_{n-1}, \mathcal{Y}_n; \widehat{\mathbf{A}}_{n-1}\} | \mathcal{Y}_n; \widehat{\mathbf{A}}_{n-1}\} \\ &= E\{E\{\mathbf{w}_{n-1} | \mathbf{x}_{n-1}, \mathcal{Y}_n; \widehat{\mathbf{A}}_{n-1}\}\mathbf{x}_{n-1}^h | \mathcal{Y}_n; \widehat{\mathbf{A}}_{n-1}\}\end{aligned}\quad (\text{B.32})$$

Conditioned on $\mathbf{A} = \widehat{\mathbf{A}}_{n-1}$, using the observation equation $y_n = \mathbf{c}_n\mathbf{x}_n + v_n$ and the state equation, denoting $z_n \triangleq y_n - \mathbf{c}_n\widehat{\mathbf{A}}_{n-1}\mathbf{x}_{n-1}$, it follows that $z_n = \mathbf{c}_n\mathbf{w}_{n-1} + v_n$. Consequently,

$$E\{\mathbf{w}_{n-1} | \mathbf{x}_{n-1}, \mathcal{Y}_n; \widehat{\mathbf{A}}_{n-1}\} = \langle \mathbf{w}_{n-1}, z_n \rangle \langle z_n, z_n \rangle^{-1} z_n = \mathbf{Q}_w \mathbf{c}_n^h (\mathbf{c}_n \mathbf{Q}_w \mathbf{c}_n^h + \sigma_v^2)^{-1} z_n \triangleq \mathbf{k}_n z_n \quad (\text{B.33})$$

where $\mathbf{k}_n = \mathbf{Q}_w \mathbf{c}_n^h (\mathbf{c}_n \mathbf{Q}_w \mathbf{c}_n^h + \sigma_v^2)^{-1}$.

Substituting (B.33) into (B.32) and (B.31) yields

$$\begin{aligned}
\delta\mathbf{L}[n] &= E\{\mathbf{w}_{n-1}\mathbf{x}_{n-1}^h|\mathcal{Y}_n; \widehat{\mathbf{A}}_{n-1}\} \\
&= E\{\mathbf{k}_n(y_n - \mathbf{c}_n\widehat{\mathbf{A}}_{n-1}\mathbf{x}_{n-1})\mathbf{x}_{n-1}^h|\mathcal{Y}_n; \widehat{\mathbf{A}}_{n-1}\} \\
&= \mathbf{k}_n(y_n\widehat{\mathbf{x}}_{n-1|n}^h - \mathbf{c}_n\widehat{\mathbf{A}}_{n-1}\mathbf{L}_0[n])
\end{aligned} \tag{B.34}$$

which gives (4.32).

The term inside the parenthesis can be expressed in terms of the first-order and the second-order innovation terms. To show that, first note the following identities:

$$\widehat{\mathbf{x}}_{n-1|n} = \widehat{\mathbf{x}}_{n-1|n-1} + \mathbf{P}_{n-1|n-1}\widehat{\mathbf{A}}_{n-1}^h\mathbf{c}_n^h R_{e_n}^{-1}e_n \tag{B.35}$$

$$\mathbf{P}_{n-1|n} = \mathbf{P}_{n-1|n-1} - \mathbf{P}_{n-1|n-1}\widehat{\mathbf{A}}_{n-1}^h\mathbf{c}_n^h R_{e_n}^{-1}\mathbf{c}_n\widehat{\mathbf{A}}_{n-1}\mathbf{P}_{n-1|n-1}^h \tag{B.36}$$

$$R_{e_n} = \mathbf{c}_n\widehat{\mathbf{A}}_{n-1}\mathbf{P}_{n-1|n-1}\widehat{\mathbf{A}}_{n-1}^h\mathbf{c}_n^h + (\mathbf{c}_n\mathbf{Q}_w\mathbf{c}_n^h + \sigma_v^2) \tag{B.37}$$

where (B.35) and (B.36) directly follow from the smoothing formula in Appendix B.2.

Using (B.36) and (B.37) it can be shown that

$$\begin{aligned}
\mathbf{c}_n\widehat{\mathbf{A}}_{n-1}\mathbf{P}_{n-1|n} &= (\mathbf{c}_n\mathbf{Q}_w\mathbf{c}_n^h + \sigma_v^2)R_{e_n}^{-1}\mathbf{c}_n\widehat{\mathbf{A}}_{n-1}\mathbf{P}_{n-1|n-1} \\
&\triangleq s_n R_{e_n}^{-1}\mathbf{c}_n\widehat{\mathbf{A}}_{n-1}\mathbf{P}_{n-1|n-1}
\end{aligned} \tag{B.38}$$

where $s_n \triangleq (\mathbf{c}_n\mathbf{Q}_w\mathbf{c}_n^h + \sigma_v^2)$ contains the total noise contribution in the residual error.

Now consider the term inside the parenthesis in (B.34),

$$\begin{aligned}
y_n \widehat{\mathbf{x}}_{n-1|n}^h - \mathbf{c}_n \widehat{\mathbf{A}}_{n-1} \mathbf{L}_0[n] &= y_n \widehat{\mathbf{x}}_{n-1|n}^h - \mathbf{c}_n \widehat{\mathbf{A}}_{n-1} (\widehat{\mathbf{x}}_{n-1|n} \widehat{\mathbf{x}}_{n-1|n}^h + \mathbf{P}_{n-1|n}) \\
&= (y_n - \mathbf{c}_n \widehat{\mathbf{A}}_{n-1} \widehat{\mathbf{x}}_{n-1|n}) \widehat{\mathbf{x}}_{n-1|n}^h - \mathbf{c}_n \widehat{\mathbf{A}}_{n-1} \mathbf{P}_{n-1|n} \\
&= (y_n - \mathbf{c}_n \widehat{\mathbf{A}}_{n-1} \widehat{\mathbf{x}}_{n-1|n-1}) \widehat{\mathbf{x}}_{n-1|n}^h - \mathbf{c}_n \widehat{\mathbf{A}}_{n-1} \mathbf{P}_{n-1|n-1} \widehat{\mathbf{A}}_{n-1}^h \mathbf{c}_n^h R_{e_n}^{-1} e_n \widehat{\mathbf{x}}_{n-1|n}^h \\
&\quad - s_n R_{e_n}^{-1} \mathbf{c}_n \widehat{\mathbf{A}}_{n-1} \mathbf{P}_{n-1|n-1} \\
&= (\mathbf{I} - \mathbf{c}_n \widehat{\mathbf{A}}_{n-1} \mathbf{P}_{n-1|n-1} \widehat{\mathbf{A}}_{n-1}^h \mathbf{c}_n^h R_{e_n}^{-1}) e_n \widehat{\mathbf{x}}_{n-1|n}^h - s_n R_{e_n}^{-1} \mathbf{c}_n \widehat{\mathbf{A}}_{n-1} \mathbf{P}_{n-1|n-1} \\
&= s_n R_{e_n}^{-1} (e_n \widehat{\mathbf{x}}_{n-1|n}^h - \mathbf{c}_n \widehat{\mathbf{A}}_{n-1} \mathbf{P}_{n-1|n-1}) \\
&= s_n R_{e_n}^{-1} (e_n \widehat{\mathbf{x}}_{n-1|n-1}^h + s_n (R_{e_n}^{-1} e_n e_n^* - 1) R_{e_n}^{-1} \mathbf{c}_n \widehat{\mathbf{A}}_{n-1} \mathbf{P}_{n-1|n-1}) \quad (\text{B.39})
\end{aligned}$$

where the third equality used (B.35) and (B.36), the fourth equality used $e_n = y_n - \mathbf{c}_n \widehat{\mathbf{A}}_{n-1} \widehat{\mathbf{x}}_{n-1|n-1}$, the fifth equality used (B.37) and the last equality used (B.35). Note that $e_n = y_n - \mathbf{c}_n \widehat{\mathbf{A}}_{n-1} \widehat{\mathbf{x}}_{n-1|n-1}$. (B.39) essentially consists of a first-order and a second-order innovation terms. This will be used in section 4.5.1 to derive the innovation form of the parameter recursion.

B.5.2 Derivation of (4.35)

Following (B.34),

$$\begin{aligned}
\delta \mathbf{L}[n] &= \mathbf{k}_n (\mathbf{c}_n \mathbf{A} \mathbf{x}_{n-1} \widehat{\mathbf{x}}_{n-1|n}^h + z_n \widehat{\mathbf{x}}_{n-1|n}^h - \mathbf{c}_n \widehat{\mathbf{A}}_{n-1} \mathbf{L}_0[n]) \\
&= \mathbf{k}_n (-\mathbf{c}_n \tilde{\mathbf{A}}_{n-1} \mathbf{L}_0[n] + \mathbf{c}_n \mathbf{A} (\mathbf{x}_{n-1} \widehat{\mathbf{x}}_{n-1|n}^h - \mathbf{L}_0[n]) + z_n \widehat{\mathbf{x}}_{n-1|n}^h) \quad (\text{B.40})
\end{aligned}$$

Substituting (B.40) into (4.30) gives

$$\widehat{\mathbf{A}}_n = \widehat{\mathbf{A}}_{n-1} + [\mathbf{k}_n (-\mathbf{c}_n \tilde{\mathbf{A}}_{n-1} \mathbf{L}_0[n] + \mathbf{c}_n \mathbf{A} (\mathbf{x}_{n-1} \widehat{\mathbf{x}}_{n-1|n}^h - \mathbf{L}_0[n]) + z_n \widehat{\mathbf{x}}_{n-1|n}^h)] \widehat{\mathbf{H}}_0^{-1}[n] \quad (\text{B.41})$$

Since $\mathbf{L}_0[n] = \widehat{\mathbf{x}}_{n-1|n} \widehat{\mathbf{x}}_{n-1|n}^h + \mathbf{P}_{n-1|n}$, (B.41) may be rewritten as

$$\widehat{\mathbf{A}}_n = \widehat{\mathbf{A}}_{n-1} + [\mathbf{k}_n (-\mathbf{c}_n \widetilde{\mathbf{A}}_{n-1} \mathbf{L}_0[n] + \mathbf{c}_n \mathbf{A} (\widetilde{\mathbf{x}}_{n-1|n} \widehat{\mathbf{x}}_{n-1|n}^h - \mathbf{P}_{n-1|n}) + z_n \widehat{\mathbf{x}}_{n-1|n}^h) \widehat{\mathbf{H}}_0^{-1}[n]] \quad (\text{B.42})$$

It is clear that $E\{\mathbf{c}_n \mathbf{A} \widetilde{\mathbf{x}}_{n-1|n} \widehat{\mathbf{x}}_{n-1|n}^h\} = 0$. Now consider $-\mathbf{c}_n \mathbf{A} \mathbf{P}_{n-1|n} + z_n \widehat{\mathbf{x}}_{n-1|n}^h$. Since

$$\widehat{\mathbf{x}}_{n-1|n} = \widehat{\mathbf{x}}_{n-1|n-1} + \mathbf{J}_{s,n} \mathbf{P}_{n|n-1} \mathbf{c}_n^h R_{e_n}^{-1} e_n \quad (\text{B.43a})$$

$$\langle e_n, v_n \rangle = \sigma_v^2, \quad \langle e_n, \mathbf{w}_{n-1} \rangle = \mathbf{c}_n \mathbf{Q}_w \quad (\text{B.43b})$$

it follows that

$$\langle \widetilde{\mathbf{x}}_{n-1|n}, \mathbf{w}_{n-1} \rangle = \mathbf{J}_{s,n} \mathbf{P}_{n|n-1} \mathbf{c}_n^h R_{e_n}^{-1} \mathbf{c}_n \mathbf{Q}_w \quad (\text{B.44a})$$

$$\langle \widetilde{\mathbf{x}}_{n-1|n}, v_n \rangle = \mathbf{J}_{s,n} \mathbf{P}_{n|n-1} \mathbf{c}_n^h R_{e_n}^{-1} \sigma_v^2 \quad (\text{B.44b})$$

Therefore,

$$\begin{aligned} E\{z_n \widehat{\mathbf{x}}_{n-1|n}^h\} &= \mathbf{c}_n \langle \mathbf{w}_{n-1}, \widehat{\mathbf{x}}_{n-1|n} \rangle + \langle v_n, \widehat{\mathbf{x}}_{n-1|n} \rangle \\ &= (\mathbf{c}_n \mathbf{Q}_w \mathbf{c}_n^h + \sigma_v^2) R_{e_n}^{-1} \mathbf{c}_n \widehat{\mathbf{A}}_{n-1} \mathbf{P}_{n-1|n-1} \end{aligned} \quad (\text{B.45a})$$

where $\mathbf{P}_{n|n-1} \mathbf{J}_{s,n}^h = \widehat{\mathbf{A}}_{n-1} \mathbf{P}_{n-1|n-1}$ has been used in the last equality.

Also recall

$$\mathbf{P}_{n-1|n} = \mathbf{P}_{n-1|n-1} - \mathbf{P}_{n-1|n-1} \widehat{\mathbf{A}}_{n-1}^h \mathbf{c}_n^h R_{e_n}^{-1} \mathbf{c}_n \widehat{\mathbf{A}}_{n-1} \mathbf{P}_{n-1|n-1} \quad (\text{B.46a})$$

$$\begin{aligned} R_{e_n} &= \mathbf{c}_n \mathbf{P}_{n|n-1} \mathbf{c}_n^h + \sigma_v^2 \\ &= \mathbf{c}_n (\widehat{\mathbf{A}}_{n-1} \mathbf{P}_{n-1|n-1} \widehat{\mathbf{A}}_{n-1}^h + \mathbf{Q}_w) \mathbf{c}_n^h + \sigma_v^2 \\ &= \mathbf{c}_n \widehat{\mathbf{A}}_{n-1} \mathbf{P}_{n-1|n-1} \widehat{\mathbf{A}}_{n-1}^h \mathbf{c}_n^h + (\mathbf{c}_n \mathbf{Q}_w \mathbf{c}_n^h + \sigma_v^2) \end{aligned} \quad (\text{B.46b})$$

Hence

$$\begin{aligned}
\mathbf{c}_n \mathbf{A} \mathbf{P}_{n-1|n} &= -\mathbf{c}_n \tilde{\mathbf{A}}_{n-1} \mathbf{P}_{n-1|n} + \mathbf{c}_n \hat{\mathbf{A}}_{n-1} [\mathbf{P}_{n-1|n-1} - \mathbf{P}_{n-1|n-1} \hat{\mathbf{A}}_{n-1}^h \mathbf{c}_n^h R_{e_n}^{-1} \mathbf{c}_n \hat{\mathbf{A}}_{n-1} \mathbf{P}_{n-1|n-1}] \\
&= -\mathbf{c}_n \tilde{\mathbf{A}}_{n-1} \mathbf{P}_{n-1|n} + \mathbf{c}_n \hat{\mathbf{A}}_{n-1} \mathbf{P}_{n-1|n-1} - \mathbf{c}_n \hat{\mathbf{A}}_{n-1} \mathbf{P}_{n-1|n-1} \hat{\mathbf{A}}_{n-1}^h \mathbf{c}_n^h R_{e_n}^{-1} \mathbf{c}_n \hat{\mathbf{A}}_{n-1} \mathbf{P}_{n-1|n-1} \\
&= -\mathbf{c}_n \tilde{\mathbf{A}}_{n-1} \mathbf{P}_{n-1|n} + \mathbf{c}_n \hat{\mathbf{A}}_{n-1} \mathbf{P}_{n-1|n-1} \\
&\quad - [R_{e_n} - (\mathbf{c}_n \mathbf{Q}_w \mathbf{c}_n^h + \sigma_v^2)] R_{e_n}^{-1} \mathbf{c}_n \hat{\mathbf{A}}_{n-1} \mathbf{P}_{n-1|n-1} \\
&= -\mathbf{c}_n \tilde{\mathbf{A}}_{n-1} \mathbf{P}_{n-1|n} + E\{z_n \hat{\mathbf{x}}_{n-1|n}^h\}
\end{aligned} \tag{B.47}$$

Denoting $\tilde{\mathbf{g}}_n \triangleq z_n \hat{\mathbf{x}}_{n-1|n}^h - E\{z_n \hat{\mathbf{x}}_{n-1|n}^h\} + \mathbf{c}_n \mathbf{A} \tilde{\mathbf{x}}_{n-1|n} \hat{\mathbf{x}}_{n-1|n}^h$, which is a zero-mean fluctuation component, consequently

$$\mathbf{c}_n \mathbf{A} (\tilde{\mathbf{x}}_{n-1|n} \hat{\mathbf{x}}_{n-1|n}^h - \mathbf{P}_{n-1|n}) + z_n \hat{\mathbf{x}}_{n-1|n}^h = \mathbf{c}_n \tilde{\mathbf{A}}_{n-1} \mathbf{P}_{n-1|n} + \tilde{\mathbf{g}}_n \tag{B.48}$$

Substituting (B.48) into (B.42) gives

$$\begin{aligned}
\hat{\mathbf{A}}_n &= \hat{\mathbf{A}}_{n-1} + [\mathbf{k}_n (-\mathbf{c}_n \tilde{\mathbf{A}}_{n-1} \mathbf{L}_0[n] + \mathbf{c}_n \tilde{\mathbf{A}}_{n-1} \mathbf{P}_{n-1|n} + \tilde{\mathbf{g}}_n)] \hat{\mathbf{H}}_0^{-1}[n] \\
&= \hat{\mathbf{A}}_{n-1} + [\mathbf{k}_n (-\mathbf{c}_n \tilde{\mathbf{A}}_{n-1} \hat{\mathbf{x}}_{n-1|n} \hat{\mathbf{x}}_{n-1|n}^h + \tilde{\mathbf{g}}_n)] \hat{\mathbf{H}}_0^{-1}[n]
\end{aligned} \tag{B.49}$$

Subtracting both sides of (B.49) by the true parameter \mathbf{A} yields

$$\tilde{\mathbf{A}}_n = \tilde{\mathbf{A}}_{n-1} - \mathbf{k}_n \mathbf{c}_n \tilde{\mathbf{A}}_{n-1} \hat{\mathbf{x}}_{n-1|n} \hat{\mathbf{x}}_{n-1|n}^h \hat{\mathbf{H}}_0^{-1}[n] + \Gamma_n \tag{B.50}$$

where $\Gamma_n \triangleq \mathbf{k}_n \tilde{\mathbf{g}}_n \hat{\mathbf{H}}_0^{-1}[n]$. Denoting $\tilde{\mathbf{a}}_n = \text{Vec} \tilde{\mathbf{A}}_n$ and $\gamma_n = \text{Vec} \Gamma_n$, then taking Vec on both sides of (B.50) and using the identity $\text{Vec}(\mathbf{ABC}) = (\mathbf{C}^t \otimes \mathbf{A}) \text{Vec} \mathbf{B}$, it

follows

$$\tilde{\mathbf{a}}_n = [\mathbf{I} - (\hat{\mathbf{x}}_{n-1|n} \hat{\mathbf{x}}_{n-1|n}^h \hat{\mathbf{H}}_0^{-1}[n])^t \otimes (\mathbf{k}_n \mathbf{c}_n)] \tilde{\mathbf{a}}_{n-1} + \gamma_n \quad (\text{B.51a})$$

$$= \{\mathbf{I} - [(\|\hat{\mathbf{x}}_{n-1|n}\|^2 \hat{\mathbf{H}}_0^{-t}[n]) \otimes (\mathbf{Q}_w \|\mathbf{c}_n\|^2 (\mathbf{c}_n \mathbf{Q}_w \mathbf{c}_n^h + \sigma_v^2)^{-1})] (\mathbf{b}_n \mathbf{b}_n^h)\} \tilde{\mathbf{a}}_{n-1} + \gamma_n \quad (\text{B.51b})$$

$$\triangleq [\mathbf{I} - \mathbf{S}_n \mathbf{b}_n \mathbf{b}_n^h] \tilde{\mathbf{a}}_{n-1} + \gamma_n \quad (\text{B.51c})$$

where $\mathbf{S}_n \triangleq [(\|\hat{\mathbf{x}}_{n-1|n}\|^2 \hat{\mathbf{H}}_0^{-t}[n]) \otimes (\mathbf{Q}_w \|\mathbf{c}_n\|^2 (\mathbf{c}_n \mathbf{Q}_w \mathbf{c}_n^h + \sigma_v^2)^{-1})]$ and

$$\mathbf{b}_n \triangleq \left(\frac{\hat{\mathbf{x}}_{n-1|n}^t}{\|\hat{\mathbf{x}}_{n-1|n}\|} \otimes \frac{\mathbf{c}_n}{\|\mathbf{c}_n\|} \right)^h \quad (\text{B.52})$$

is a $N^2 \times 1$ unit vector along the direction of $\hat{\mathbf{x}}_{n-1|n}^t \otimes \mathbf{c}_n$.

B.6 $\|\Pi_{i=n}^{n+m-1}(\mathbf{I} - \mathbf{S}_i \mathbf{b}_i \mathbf{b}_i^h)\|$

According to section 4.5, the maximum singular value of the sequential matrix product $\Pi_{i=n}^{n+m-1}(\mathbf{I} - \mathbf{S}_i \mathbf{b}_i \mathbf{b}_i^h)$ is crucial to the stability of the parameter estimate error equation (4.35c). This section consider the properties of this important product. First analysis is carried out for several special cases. Then numerical investigation is implemented for the general case which leads to a conjecture concerning the dependency of the singular values of $\Pi_{i=n}^{n+m-1}(\mathbf{I} - \mathbf{S}_i \mathbf{b}_i \mathbf{b}_i^h)$ on the eigen-structure of the matrices \mathbf{S}_i and the excitation properties of the sequence \mathbf{b}_i .

According to Appendix B.5, in particular (B.51c) and (B.52),

$$\mathbf{S}_n \triangleq [(\|\widehat{\mathbf{x}}_{n-1|n}\|^2 \widehat{\mathbf{H}}_0^{-t}[n]) \otimes (\mathbf{Q}_w \|\mathbf{c}_n\|^2 (\mathbf{c}_n \mathbf{Q}_w \mathbf{c}_n^h + \sigma_v^2)^{-1})] \quad (\text{B.53})$$

$$\mathbf{b}_n \triangleq \left(\frac{\widehat{\mathbf{x}}_{n-1|n}^t}{\|\widehat{\mathbf{x}}_{n-1|n}\|} \otimes \frac{\mathbf{c}_n}{\|\mathbf{c}_n\|} \right)^h \quad (\text{B.54})$$

from which several observations are immediate:

1. \mathbf{S}_i is nonnegative Hermitian. This is because both $\widehat{\mathbf{H}}_0[n]$ and \mathbf{Q}_w are nonnegative Hermitian;
2. All eigenvalues of \mathbf{S}_i are less than 1. This is follows from the property 7 of the Kronecker product (eigenvalue decomposition of a Kronecker product) together with that all the eigenvalues of $\|\widehat{\mathbf{x}}_{n-1|n}\|^2 \widehat{\mathbf{H}}_0^{-t}[n]$ are less than 1 (assuming that $\widehat{\mathbf{H}}_0^T[n]$ is invertible), and the same is for $\mathbf{Q}_w \|\mathbf{c}_n\|^2 (\mathbf{c}_n \mathbf{Q}_w \mathbf{c}_n^h + \sigma_v^2)^{-1}$;
3. \mathbf{b}_n have unit norm.

It can also be shown that the matrix $(\mathbf{I} - \mathbf{S}_i \mathbf{b}_i \mathbf{b}_i^h)$ only has one nonzero eigenvalue and this nonzero eigenvalue has absolute value less than 1. However, the eigenvalue distribution of $(\mathbf{I} - \mathbf{S}_i \mathbf{b}_i \mathbf{b}_i^h)$ is not relevant to the stability analysis of interest here.

Instead, it is the singular values of the sequential product directly matter in this case. A reasonable assumption, to simplify the problem, is that \mathbf{S}_i changes slower

than \mathbf{b}_i does. This is in general true in communications where the transmitted symbols change faster than the channel does.

Hence replace \mathbf{S}_i by a constant \mathbf{S} with all the previously mentioned properties. Consider $\prod_{i=n}^{n+m-1}(\mathbf{I} - \mathbf{S}\mathbf{b}_i\mathbf{b}_i^h)$. It can be converted into a more accessible format using the following eigenvalue decomposition of \mathbf{S} :

$$\mathbf{S} = \mathbf{U}\mathbf{\Lambda}\mathbf{U}^h \quad (\text{B.55})$$

where \mathbf{U} is orthonormal and $\mathbf{\Lambda}$ is diagonal. Since orthonormal transformation does not change singular values, it follows

$$\begin{aligned} \|\prod_{i=n}^{n+m-1}(\mathbf{I} - \mathbf{S}\mathbf{b}_i\mathbf{b}_i^h)\| &= \|\mathbf{U}^h [\prod_{i=n}^{n+m-1}(\mathbf{I} - \mathbf{S}\mathbf{b}_i\mathbf{b}_i^h)] \mathbf{U}\| \\ &= \|\prod_{i=n}^{n+m-1} \mathbf{U}^h (\mathbf{I} - \mathbf{S}\mathbf{b}_i\mathbf{b}_i^h) \mathbf{U}\| \\ &= \|\prod_{i=n}^{n+m-1} (\mathbf{I} - \mathbf{U}^h \mathbf{S} \mathbf{U} \mathbf{b}_i \mathbf{b}_i^h) \mathbf{U}\| \\ &= \|\prod_{i=n}^{n+m-1} (\mathbf{I} - \mathbf{\Lambda} \mathbf{d}_i \mathbf{d}_i^h)\| \end{aligned} \quad (\text{B.56})$$

where $\mathbf{d}_i \triangleq \mathbf{U}^h \mathbf{b}_i$ still has unit norm, and $\mathbf{\Lambda}$ is diagonal matrix containing eigenvalues of \mathbf{S} .

(B.56) reveals, explicitly, the dependency of the maximum singular value of the sequential matrix product on the eigenvalues of \mathbf{S} and the sequence \mathbf{b}_i .

Consider the following special cases first:

1. $\mathbf{\Lambda} = \alpha \mathbf{I}$, i.e. \mathbf{S} has equal eigenvalues.

As mentioned before, $0 \leq \alpha < 1$. In this case, since $\mathbf{I} - \alpha \mathbf{d}_i \mathbf{d}_i^h$ is Hermitian, its singular values are squares of its eigenvalues. On the other hand, $\mathbf{I} - \alpha \mathbf{d}_i \mathbf{d}_i^h$ has one eigenvalue less than one, all others equal to one. Then it can shown that if the sequence \mathbf{d}_i is persistently exciting, $\|\prod_{i=n}^{n+M-1}(\mathbf{I} - \alpha \mathbf{d}_i \mathbf{d}_i^h)\| < 1$.

2. The sequence \mathbf{b}_i are orthogonal, for $i = n, \dots, n + N^2 - 1$.

So are the sequence \mathbf{d}_i . Denoting $\mathbf{D} \triangleq [\mathbf{d}_n, \dots, \mathbf{d}_{n+N^2-1}]$, \mathbf{D} is orthonormal. Then it follows that

$$\begin{aligned}
\|\Pi_{i=n}^{n+N^2-1}(\mathbf{I} - \Lambda \mathbf{d}_i \mathbf{d}_i^h)\| &= \|\mathbf{I} - \Lambda \sum_{i=n}^{n+N^2-1} \mathbf{d}_i \mathbf{d}_i^h\| \\
&= \|\mathbf{I} - \Lambda \mathbf{D} \mathbf{D}^h\| \\
&= \|\mathbf{I} - \mathbf{D}^h \Lambda \mathbf{D}\| \\
&= \|\mathbf{I} - \Lambda\| \leq 1 \quad (\text{B.57})
\end{aligned}$$

Strict inequality holds if \mathbf{S} is not singular.

The above two cases both lead to stability of the parameter estimation using the suboptimal EM algorithm.

For the general case, however, the proof is more difficult. In fact, the problem is essentially in the same form as that of establishing the stability of RLS parameter identification in linear regression models see, for instance, [Hay96][Cam94][Guo95a], where \mathbf{S}_i is usually the (weighted) averaging of $\mathbf{b}_i \mathbf{b}_i^h$. The typical approaches there has been i) to invoke the so-called *direct averaging* method [Hay96] which replaces both \mathbf{S}_i and $\mathbf{b}_i \mathbf{b}_i^h$ by their expectations; or ii) to show that the error propagation is well approximated by its expectation version for which the stability would hold when the regressor satisfies certain conditions such as ϕ -mixing [Cam94][Guo95a]. Effectively the *direct averaging* method approximates $\mathbf{S}_i \mathbf{b}_i \mathbf{b}_i^h$ with $\mu \mathbf{I}$ for some $0 < \mu < 1$. Yet that approximation is not accurate in general since $\|\mathbf{I} - \mathbf{S}_i \mathbf{b}_i \mathbf{b}_i^h\|$ may be greater than or equal to 1 while $\|\mathbf{I} - \mu \mathbf{I}\|$ is always less than 1 for $0 < \mu < 1$.

In the following a numerical investigation is implemented, leaving rigorous proof for possible future work. The goal is to gain some insights on which factors have dominant influence on $\|\Pi_{i=n}^{n+m-1}(\mathbf{I} - \mathbf{S}_i \mathbf{b}_i \mathbf{b}_i^h)\|$. That \mathbf{S}_i is slowly varying compared with \mathbf{b}_i is still assumed, thus $\mathbf{S}_i = \mathbf{S}$.

The experiment generates $\Pi_{i=n}^{n+m-1}(\mathbf{I} - \mathbf{S} \mathbf{b}_i \mathbf{b}_i^h)$ for some constant \mathbf{S} with different

eigenvalue distribution and a sequence of random unit vectors \mathbf{b}_i , and then computes the distribution of its singular values. The main discovery is the following Conjecture:

Conjecture 2 *Suppose \mathbf{S} is nonnegative Hermitian with eigenvalues less than or equal to 1, and \mathbf{b}_i are a sequence of randomly generated unit vectors, then dependent on the eigen-spread of the matrix \mathbf{S} , the matrix $\prod_{i=n}^{n+m-1}(\mathbf{I} - \mathbf{S}\mathbf{b}_i\mathbf{b}_i^h)$, denoted by \mathbf{A}_m , converges either to a zero matrix (for moderate eigen-spread) or to a rank one matrix with singular value greater than or equal to 1 (for large eigen-spread). Here the eigen-spread of \mathbf{S} is the ratio between its maximum and minimum eigenvalues. In addition, $\|\mathbf{S}\|$ controls the rate of that convergence: the closer is it to 1, the faster is the convergence.*

Figure B-1 and B-2 show the 2-dimensional case where the singular values of $\mathbf{A}_m = \prod_{i=n}^{n+m-1}(\mathbf{I} - \mathbf{S}\mathbf{b}_i\mathbf{b}_i^h)$ can be visualized by plotting $\|\mathbf{A}_m\mathbf{x}\|$ for all unit vectors x . Figure B-1 depicts the case where \mathbf{S} has a moderate eigen-spread equal to 10. The four plots corresponding to $m = 1, 2, 10, 60$ respectively. It clearly shows that while \mathbf{A}_1 has a dominant singular value larger than 1, \mathbf{A}_m gradually converges to a zero matrix. Figure B-2 shows that case where \mathbf{S} has a large eigen-spread equal to 10^4 . As it shows, \mathbf{A}_m converges to a rank-one matrix with singular value larger than 1.

For higher dimensional case, $N = 5$, Figure B-3 and B-4 have plotted the distribution of the singular values of \mathbf{A}_m for several values of m , as well as the distribution of its eigenvalues. In each figure, the small plots on the right column is the enlarged display of the dominant singular value or eigenvalue. Figure B-3 shows the results with moderate eigen-spread (10) in \mathbf{S} where all the singular values, including the dominant one, converge toward 0. while Figure B-4 correspond to the case with large eigen-spread (10^4) in \mathbf{S} where it shows that all singular values, except the dominant one, converge to 0. The dominant singular value stays larger than 1. In all cases, however, the eigenvalues are less than or equal to 1.

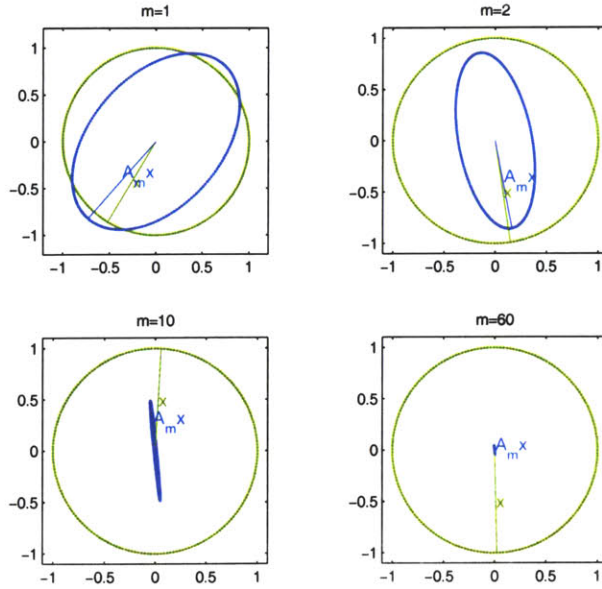


Figure B-1: Singular values of $\mathbf{A}_m = \prod_{i=n}^{n+m-1} (\mathbf{I} - \mathbf{S} \mathbf{b}_i \mathbf{b}_i^h)$, m is the number of products, $\lambda_{max}(\mathbf{S}) = 10\lambda_{min}(\mathbf{S})$, \mathbf{S} is 2×2 .

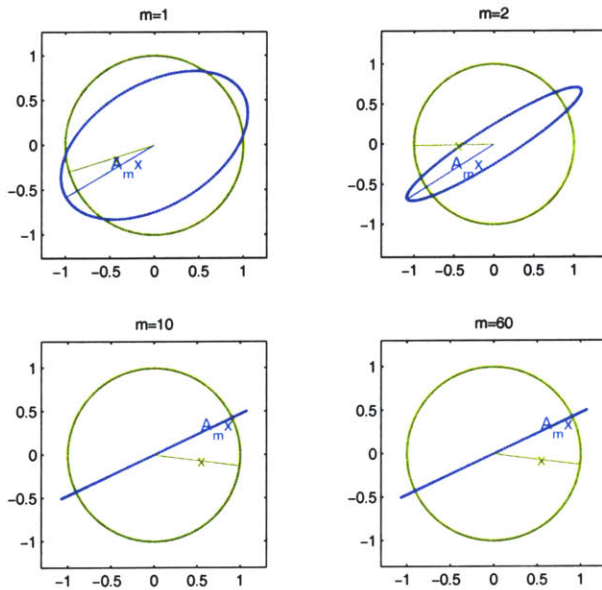


Figure B-2: Singular values of $\mathbf{A}_m = \prod_{i=n}^{n+m-1} (\mathbf{I} - \mathbf{S} \mathbf{b}_i \mathbf{b}_i^h)$, m is the number of products, $\lambda_{max}(\mathbf{S}) = 10^4\lambda_{min}(\mathbf{S})$, \mathbf{S} is 2×2 .

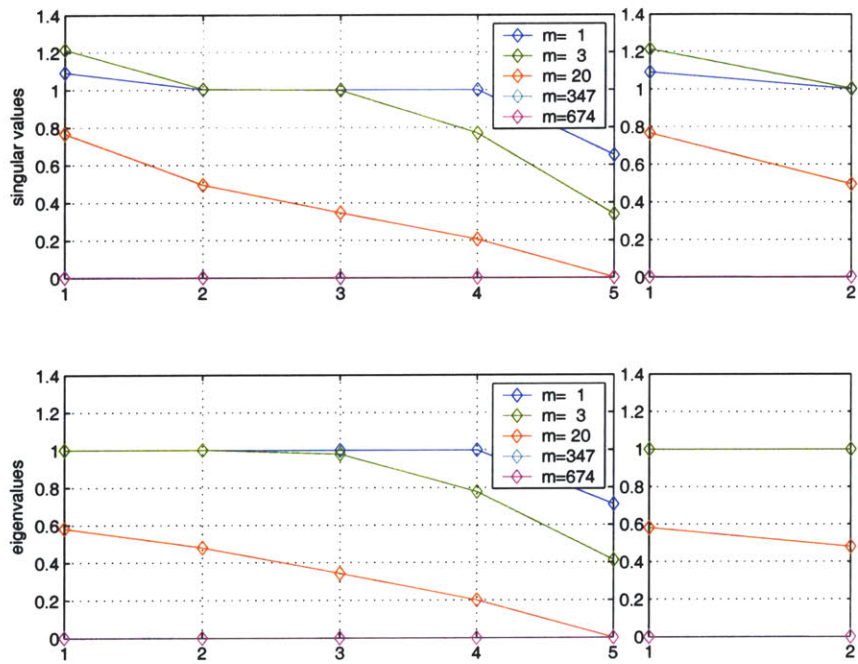


Figure B-3: Singular values and eigenvalues of $\prod_{i=n}^{n+m-1}(\mathbf{I} - \mathbf{S}\mathbf{b}_i\mathbf{b}_i^h)$, $\lambda_{max}(\mathbf{S}) = 10\lambda_{min}(\mathbf{S})$, \mathbf{S} is 5×5

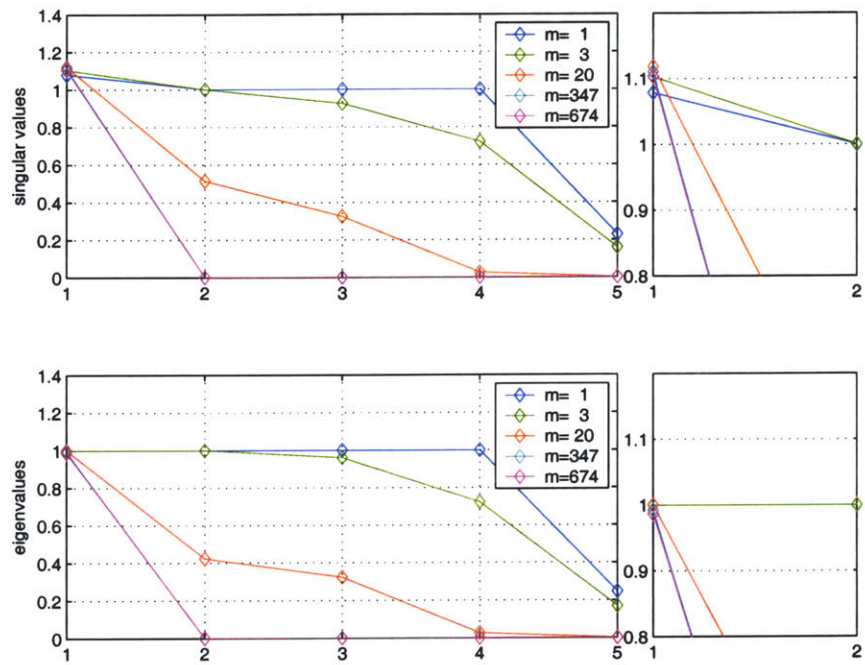


Figure B-4: Singular values and eigenvalues of $\prod_{i=n}^{n+m-1} (\mathbf{I} - \mathbf{S} \mathbf{b}_i \mathbf{b}_i^h)$ $\lambda_{max}(\mathbf{S}) = 10^4 \lambda_{min}(\mathbf{S})$, \mathbf{S} is 5×5

Appendix C

The Kronecker Product

Kronecker product and its properties have been extensively used in this thesis, especially in Chapters 3 and 4 where matrix calculus and equations are involved in derivations. Some of the materials present here were taken from [Gra81] but can also be found in many matrix analysis books. We also prove some new properties in this appendix.

C.1 The $Vec(\cdot)$ Operator

Definition 1 $Vec(\mathbf{M})$ is a vector valued function of matrix \mathbf{M} obtained as an ordered stack of columns of \mathbf{M} . i.e. if \mathbf{M} is $k \times l$,

$$Vec(\mathbf{M}) = \begin{bmatrix} \mathbf{M}_{\cdot,1} \\ \mathbf{M}_{\cdot,2} \\ \vdots \\ \mathbf{M}_{\cdot,l} \end{bmatrix} \quad (\text{C.1})$$

where $\mathbf{M}_{\cdot,j}$ is the j th column of \mathbf{M} , for $j = 1, \dots, l$.

From the definition it follows that $Vec(\mathbf{a}) = \mathbf{a}$ for any column vector \mathbf{a} .

C.2 The Kronecker Product and Its Properties

Definition 2 The kronecker product between matrices \mathbf{A} ($k \times l$) and \mathbf{B} ($p \times q$), denoted by $\mathbf{A} \otimes \mathbf{B}$, is a $kp \times lq$ matrix given as follows:

$$\mathbf{A} \otimes \mathbf{B} = \begin{bmatrix} a_{1,1}\mathbf{B} & a_{1,2}\mathbf{B} & \cdots & a_{1,l}\mathbf{B} \\ a_{2,1}\mathbf{B} & a_{2,2}\mathbf{B} & \cdots & a_{2,l}\mathbf{B} \\ & & \vdots & \\ a_{k,1}\mathbf{B} & a_{k,2}\mathbf{B} & \cdots & a_{k,l}\mathbf{B} \end{bmatrix} \quad (\text{C.2})$$

where $a_{k,l}$ is the element of \mathbf{A} on the k th row and l th column.

The following properties and rules of the Kronecker product hold (c.f. [Gra81]):

1. Scalar multiplication: $\mathbf{A} \otimes (\alpha\mathbf{B}) = \alpha\mathbf{A} \otimes \mathbf{B}$ for scalar α ;
2. Distributivity: $(\mathbf{A} + \mathbf{B}) \otimes \mathbf{C} = \mathbf{A} \otimes \mathbf{C} + \mathbf{B} \otimes \mathbf{C}$; $\mathbf{A} \otimes (\mathbf{B} + \mathbf{C}) = \mathbf{A} \otimes \mathbf{B} + \mathbf{A} \otimes \mathbf{C}$.
Associativity: $\mathbf{A} \otimes (\mathbf{B} \otimes \mathbf{C}) = (\mathbf{A} \otimes \mathbf{B}) \otimes \mathbf{C}$;
3. Hermitian: $(\mathbf{A} \otimes \mathbf{B})^h = \mathbf{A}^h \otimes \mathbf{B}^h$;
4. Product of two Kronecker products: $(\mathbf{A} \otimes \mathbf{B})(\mathbf{C} \otimes \mathbf{D}) = (\mathbf{AC}) \otimes (\mathbf{BD})$;
5. Inverse: $(\mathbf{A} \otimes \mathbf{B})^{-1} = \mathbf{A}^{-1} \otimes \mathbf{B}^{-1}$ assume both \mathbf{A} and \mathbf{B} invertible;
6. *Vec* of matrix products: $\text{Vec}(\mathbf{ABC}) = (\mathbf{C}^t \otimes \mathbf{A})\text{Vec}(\mathbf{B})$;
7. Eigenvalue decomposition: The (eigenvalue, eigenvector) pairs of $\mathbf{A} \otimes \mathbf{B}$ are $(\lambda_i\mu_j, \mathbf{u}_i \otimes \mathbf{v}_j)$. Here $(\lambda_i, \mathbf{u}_i)$ and (μ_j, \mathbf{v}_j) are the (eigenvalue, eigenvector) pairs of \mathbf{A} and respectively;
8. Determinant: $\det(\mathbf{A} \otimes \mathbf{B}) = (\det(\mathbf{A}))^m (\det(\mathbf{B}))^n$ for $n \times n$ \mathbf{A} and $m \times m$ \mathbf{B} ;
9. The trace: $\text{tr}(\mathbf{A} \otimes \mathbf{B}) = \text{tr}(\mathbf{A})\text{tr}(\mathbf{B})$.

The following properties can be proved directly from the definition or the above rules.

1. Kronecker product of column and row vectors:

$$\mathbf{a} \otimes \mathbf{b}^t = \mathbf{b}^t \otimes \mathbf{a} \quad (\text{C.3})$$

directly follows from the definition.

2. Kronecker product of vectors and a matrix:

$$\mathbf{a}^t \otimes (\mathbf{c}^t \mathbf{B}) = \mathbf{c}^t (\mathbf{a}^t \otimes \mathbf{B}) \quad (\text{C.4})$$

$$(\mathbf{c}^t \mathbf{B}) \otimes \mathbf{a} = (\mathbf{c}^t \otimes \mathbf{a}) \mathbf{B} \quad (\text{C.5})$$

where \mathbf{a} , \mathbf{c} and \mathbf{B} are $n \times 1$, $k \times 1$ and $n \times m$ respectively. **Proof:**

$$\begin{aligned} \mathbf{c}^t (\mathbf{a}^t \otimes \mathbf{B}) &= \mathbf{c}^t (a_1 \mathbf{B} \ a_2 \mathbf{B} \ \cdots \ a_n \mathbf{B}) \\ &= (a_1 \mathbf{c}^t \mathbf{B} \ a_2 \mathbf{c}^t \mathbf{B} \ \cdots \ a_n \mathbf{c}^t \mathbf{B}) \\ &= \mathbf{a}^t \otimes (\mathbf{c}^t \mathbf{B}) \end{aligned} \quad (\text{C.6})$$

$$\begin{aligned} (\mathbf{c}^t \otimes \mathbf{a}) \mathbf{B} &= (c_1 \mathbf{a} \ c_2 \mathbf{a} \ \cdots \ c_k \mathbf{a}) \mathbf{B} \\ &= \begin{bmatrix} a_1 \mathbf{c}^t \mathbf{B} \\ a_2 \mathbf{c}^t \mathbf{B} \\ \vdots \\ a_n \mathbf{c}^t \mathbf{B} \end{bmatrix} \\ &= \mathbf{a} \otimes (\mathbf{c}^t \mathbf{B}) \\ &= (\mathbf{c}^t \mathbf{B}) \otimes \mathbf{a} \end{aligned} \quad (\text{C.7})$$

where the last equality uses (C.3).

3. Kronecker product of matrices and a vector:

$$\mathbf{a}^t \otimes (\mathbf{CB}) = \mathbf{C}(\mathbf{a}^t \otimes \mathbf{B}) \quad (\text{C.8})$$

$$(\mathbf{CB}) \otimes \mathbf{a} = (\mathbf{C} \otimes \mathbf{a})\mathbf{B} \quad (\text{C.9})$$

where \mathbf{a} , \mathbf{B} and \mathbf{C} are $n \times 1$, $k \times m$ and $l \times k$ respectively.

Proof: Directly follow from (C.4) and (C.5) respectively.

3. *Vec* of vector outer-product: $\text{Vec}(\mathbf{ab}^t) = \mathbf{b} \otimes \mathbf{a}$ which directly follows from the definitions of *Vec* and the Kronecker product.

Bibliography

- [And79] Anderson, B. D. O. and Moore, J. B. *Optimal Filtering*. Prentice-Hall, 1979.
- [Aok67] Aoki, M. *Optimization of Stochastic Systems*. Academic Press, 1967.
- [Ast95] Astrom, K. J. and Wittenmark, B. *Adaptive Control*. Addison-Wesley, 2nd edition, 1995.
- [Bag81] Baggeroer, A. B. A Survey of Acoustic Telemetry. *Proceedings of Oceans*, pages 48–55, 1981.
- [Bag84] Baggeroer, A. B. Acoustic Telemetry, An Overview. *IEEE Journal of Oceanic Engineering*, OE-9(4):229–235, Oct. 1984.
- [Bec63] Beckmann, P. and Spizzichino, A. *The scattering of electromagnetic waves from rough surfaces*. Pergamon Press , Oxford, 1963.
- [Bel63] Bello, P.A. Characterization of Randomly Time-Variant Linear Channels. *IEEE Trans. Communications Systems*, CS-11(4):360–393, Dec 1963. Classical on LTV channel.
- [Bel69] Bello, P. Measurement of random time-variant linear channels. *Information Theory, IEEE Transactions on*, 15(4):469–475, 1969.
- [Bel74] Belanger, Pierre R. Estimation of noise covariance matrices for a linear time-varying stochastic process. *Automatica*, 10(3):267–275, May 1974.
- [Ben87] Benveniste, A. Design of Adaptive Algorithms for the Tracking of Time-Varying Systems. *International Journal of Adaptive Control and Signal Processing*, 1:3–29, 1987.
- [Bit84] Bitmead, R. R. Persistence of Excitation Conditions and the Convergence of Adaptive Schemes. *IEEE Trans. Information Theory*, IT-30(2):183–191, March 1984.

- [Bit90] Bittanti, S. and Bolzern, P. and Campi, M. Recursive Least-Square Identification Algorithms with Incomplete Excitation: Convergence Analysis and Application to Adaptive Control. *IEEE Trans. Automatic Control*, 35(12):1371–1373, Dec 1990.
- [Bra83] Brandwood, D. H. A complex gradient operator and its application in adaptive array theory. *IEE Proceedings*, 130, Parts F and H(1):11–16, Feb 1983.
- [Bre1] Brekhovskikh, L. M. and Lysanov, Y. P. *Fundamentals of Ocean Acoustics*. Springer-Verlag , New York, 2nd edition, 1991 .
- [Bro74] Brown, M. V. and Frisk, G. V. Frequency smearing of sound forward-scattering from the ocean surface. *Journal of the American Statistical Association*, 55:744–749, 1974.
- [Bro97] Broschat, S. L. and Thorsos, E. I. An investigation of the small slope approximation for scattering from rough surfaces. Part II. Numerical studies . *Journal of the American Statistical Association*, 101(5), 1997.
- [Bun81] Bunn, Derek W. Recursive estimation of the observation and process noise covariances in online Kalman filtering. *European Journal of Operational Research*, 6(3):302–308, March 1981.
- [Cam94] Campi, M. Performance of RLS Identification Algorithms with Forgetting Factor: A Φ -Mixing Approach. *Journal of Mathematical Systems, Estimation, and Control*, 4(3):1–25, 1994.
- [Cao00] Cao, L. and Schwartz, H. M. A directional forgetting algorithm based on the decomposition of the information matrix. *Automatica*, 36:1725–1731, 2000.
- [Cet05] Cetin, M. and Sadler, B. Semi-blind sparse channel estimation with constant modulus symbols. In *ICASSP*, volume III, pages 561–564, March 2005.
- [Che89] Cheng, Yung-Fu and Etter, D.M. Analysis of an adaptive technique for modeling sparse systems. *Acoustics, Speech, and Signal Processing, IEEE Transactions on*, 37(2):254–264, 1989.
- [Che01] Chen, Scott Shaobing and Donoho, David L. Atomic Decomposition by Basis Pursuit. *SIAM Review*, 43(1):129–150, 2001.
- [Cot00] Cotter, S.F. and Rao, B.D. The adaptive matching pursuit algorithm for estimation and equalization of sparse time-varying channels. In *Signals, Systems and Computers, 2000. Conference Record of the Thirty-Fourth Asilomar Conference on*, volume 2, pages 1772–1776 vol.2, 2000.

- [Cot01] Cotter, S. F. *Subset Selection Algorithms with Applications*. PhD thesis, University of California, San Diego, 2001.
- [Cot02] Cotter, S.F. and Rao, B.D. Sparse channel estimation via matching pursuit with application to equalization. *Communications, IEEE Transactions on*, 50(3):374–377, 2002.
- [Dah96] Dahl, P. H. On the spatial coherence and angular spreading of sound forward scattered from the sea surface: Measurements and interpretive model. *J. Acoust. Soc. Am.* , 100(2), 1996.
- [Dah99] Dahl, P. H. On bistatic sea surface scattering: Field measurements and modeling. *Journal of the American Statistical Association*, 105(4), 1999.
- [Dah01] Dahl, P. H. High-Frequency Forward Scattering from the Sea Surface: The Characteristic Scales of Time and Angle Spreading. *IEEE Journal of Oceanic Engineering*, 26(1), Jan 2001.
- [Dem77] Dempster, A. P. and Laird, N. M. and Rubin, D. B. Maximum Likelihood from Incomplete Data via the EM algorithm. *Journal of the Royal Statistical Society*, 39, series B(Methodological)(1):1–38, 1977.
- [Don03] Donoho, D. L. and Elad, M. Optimally sparse representation in general (nonorthogonal) dictionaries via L1 minimization. *Proc. Nat. Acad. Sci.*, 100(5):2197–2202, Mar. 2003.
- [Eck53] Eckart, C. The Scattering of Sound from the Sea Surface . *Journal of the American Statistical Association*, 25:566–570, 1953.
- [Egg97] Eggen, T. *Underwater acoustic communication over Doppler spread channels*. PhD thesis, Massachusetts Institute of Technology, 1997.
- [Egg00] Eggen, T. H. and Baggeroer, A. B. and Preisig, J. C. Communication Over Doppler Spread Channels, Part I: Channel and Receiver Presentation. *IEEE Journal of Oceanic Engineering*, 25(1):62–72, Jan 2000.
- [Egg01] Eggen, T. H. and Preisig, J. C. and Baggeroer, A. B. Communication Over Doppler Spread Channels, II:Receiver Characterization and Practical Results. *IEEE Journal of Oceanic Engineering*, 26(4):612–622, Oct. 2001.
- [Ele86] Eleftheriou, E. and Falconer, D. D. Tracking Properties and Steady-State Performance of RLS Adaptive Filter Algorithms. *IEEE, Trans. ASSP*, ASSP-34(5):1097–1110, Oct 1986.
- [Ell99] Elliott, R. J. and Krishnamurthy, V. New Finite-Dimensional Filters for Parameter Estimation of Discrete-Time Linear Gaussian Models. *IEEE Trans. Automatic Control*, 44(5):938–951, May 1999.

- [Eli02] Elliott, R. J. and Ford, J. J. and Moore, J. B. On-line almost-sure parameter estimation for partially observed discrete-time linear systems with known noise characteristics. *International Journal of Adaptive Control and Signal Processing*, 16:435–453, 2002.
- [For70] Fortuin, L. Survey of literature on Reflection and scattering of sound waves at the sea surface. *Journal of the American Statistical Association*, 47(5):1209–1228, October 1970.
- [Fuc00] Fuchs, J. J. and Delyon, B. Minimal L1-norm reconstruction function for oversampled signals: applications to time-delay estimation. *IEEE Trans. Information Theory*, 46(4):1666–1673, Jul 2000.
- [Gao03] Gao, W. and Tsai, S. and Lehnert, S. Diversity Combining for DS/SS Systems With Time-Varying, Correlated Fading Branches. *IEEE Transactions on Communications*, 51(2):284–295, Feb 2003.
- [Gra81] Graham, A. *Kronecker Products and Matrix Calculus: With Applications* . Wiley, 1981.
- [Guo95a] Guo, L. and Ljung, L. Exponential Stability of General Tracking Algorithms. *IEEE Trans. Automatic Control*, 40(8):1376–1387, August 1995.
- [Guo95b] Guo, L. and Ljung, L. Performance Analysis of General Tracking Algorithms. *IEEE Trans. Automatic Control*, 40(8):1388–1402, August 1995.
- [Hag85] Hagglund, T. Recursive estimation of slowly time-varying parameters. In *Proceedings of the seventh IFAC symposium on identification and system parameter estimation*, pages 1137–1142, 1985.
- [Har97] Harville, David. *Matrix Algebra from a Statistician's Perspective*. Springer, 1997.
- [Hay96] Haykin, S. *Adaptive Filter Theory*. Prentice Hall, 3rd edition, 1996.
- [Ilt90] Iltis, R.A. Joint estimation of PN code delay and multipath using the extended Kalman filter. *Communications, IEEE Transactions on*, 38(10):1677–1685, 1990.
- [Ilt91] Iltis, R.A. and Fuxjaeger, A.W. A digital DS spread-spectrum receiver with joint channel and Doppler shift estimation. *Communications, IEEE Transactions on*, 39(8):1255–1267, 1991.
- [Ilt94] Iltis, R.A. An EKF-based joint estimator for interference, multipath, and codedelay in a DS spread-spectrum receiver. *Communications, IEEE Transactions on*, 42(234):1288–1299, 1994.

- [Ilt01] Iltis, R.A. A DS-CDMA tracking mode receiver with joint channel/delay estimation and MMSE detection. *Communications, IEEE Transactions on*, 49(10):1770–1779, 2001.
- [Jaz70] Jazwinski, A. H. *Stochastic Processes and Filtering Theory*. Academic Press, 1970.
- [Jon89] Jong, P. d. Smoothing and Interpolation with the State-Space Model. *Journal of the American Statistical Association*, 84(408):1085–1088, Dec 1989.
- [Jor99] Jorgensen, M. A dynamic EM algorithm for estimating mixture proportions. *Statistics and Computing*, 9:299–302, 1999.
- [Kai59] Kailath, T. Sampling Models For Linear Time-Variant Filters. Technical report, MIT Research Lab, 1959.
- [Kai00] Kailath, T. and Sayed, A. H. and Hassibi, B. *Linear Estimation*, chapter A.6, pages 740–742. Prentice Hall, 2000.
- [Kar04] Karabulut, G.Z. and Yongacoglu, A. Sparse channel estimation using orthogonal matching pursuit algorithm. In *Vehicular Technology Conference, 2004. VTC2004-Fall. 2004 IEEE 60th*, volume 6, pages 3880–3884 Vol. 6, 2004.
- [Kay03] Kay, S. M. and Doyle, S. B. Rapid Estimation of the Range-Doppler Scattering Function. *IEEE Trans. Signal Processing*, 51(1):255–268, Jan 2003.
- [Ken68] Kennedy, R. S. *Fading Dispersive Communication Channels*. Wiley, 1968.
- [Kil00] Kilfoyle, D.B. and Baggeroer, A.B. The state of the art in underwater acoustic telemetry. *Oceanic Engineering, IEEE Journal of*, 25(1):4–27, 2000.
- [Koc95] Kocic, M. and Brady, D. and Stojanovic, M. Sparse equalization for real-time digital underwater acoustic communications. In *OCEANS '95. MTS/IEEE. 'Challenges of Our Changing Global Environment'. Conference Proceedings.*, volume 3, pages 1417–1422 vol.3, 1995.
- [Kul87] Kulhavy, R. . Restricted exponential forgetting in real-time identification. *Auomatica*, 23:589–600, 1987.
- [Kus78] Kushner, H. J. and Clark, D. S. *Stochastic approximation methods for constrained and unconstrained systems*. New York : Springer-Verlag, 1978.

- [Lak03] Lakhzouri, A. and Iohan, E. S. and Hamila, R. and Renfors, M. Extended Kalman Filter Channel Estimation for Line-of-Sight Detection in WCDMA Mobile Positioning. *EURASIP Journal on Applied Signal Processing*, 13:1268–1278, 2003.
- [Li,05] Li, W. and Preisig, J. Identification of rapidly time-varying wideband acoustic communication channels. *J. Acoust. Soc. Am.*, 118(3):2014–2014, September 2005.
- [Lju79] Ljung, L. Asymptotic Behavior of the Extended Kalman Filter as a Parameter Estimator for Linear Systems. *IEEE Trans. Automatic Control*, AC-24(1):36–50, Feb 1979.
- [Lju90] Ljung, L. and Gunnarsson, S. Adaptation and tracking in system identification—A survey. *Automatica*, 26(1):7–21, Jan 1990.
- [Mac86] Macchi, O. Optimization of adaptive identification for time-varying filters. *Automatic Control, IEEE Transactions on*, 31(3):283–287, 1986.
- [Mal93] Mallat, S.G. and Zhang, Zhifeng. Matching pursuits with time-frequency dictionaries. *Signal Processing, IEEE Transactions on*, 41(12):3397–3415, 1993.
- [Mal03] Malioutov, D. A Sparse Signal Reconstruction Perspective for Source Localization with Sensor Arrays. Master’s thesis, Massachusetts Institute of Technology, 2003.
- [McD75] McDonald, J. and Tuteur, F. B. Calculation of the range-Doppler plot for a doubly spread surface-scatter channel at high Rayleigh parameters. *Journal of the American Statistical Association*, 70(5):1025–1029, May 1975.
- [McI97] McLachlan, G. J. and Krishnan, T. *The EM Algorithm and Extensions*. Wiley, 1997.
- [Med70] Medwin, H. and Clay, C. S. Dependence of spatial and temporal correlation of forward-scattered underwater sound on the surface statistics. II. Experiment. *Journal of the American Statistical Association*, 65(5(part 2)):1419–1429, 1970.
- [Meh70] Mehra, R. On the identification of variances and adaptive Kalman filtering. *Automatic Control, IEEE Transactions on*, 15(2):175–184, 1970.
- [Meh72] Mehra, R. Approaches to adaptive filtering. *Automatic Control, IEEE Transactions on*, 17(5):693–698, 1972.

- [Mil03] Miles, D. A. and Hewitt, R. N. and Donnelly, M. K. and Clarke, T. Forward scattering of pulses from a rough sea surface by Fourier synthesis of parabolic equation solutions. *Journal of the American Statistical Association*, 114(3):1266–1280, 2003.
- [Nie91] Niedzwiecki, M. and Guo, L. Nonasymptotic Results for Finite-Memory WLS Filters. *IEEE Trans. Automatic Control*, 36(2):198–206, Feb 1991.
- [Ogi1] Ogilvy, J. A. *Theory of waves scattering from random rough surfaces*. Institute of Physics Publishing , Bristol and Philadelphia , 1991 .
- [Oze02] Ozen, S. and Hillery, W. and Zoltowski, M. and Nereyanuru, S.M. and Fimoff, M. Structured channel estimation based decision feedback equalizers for sparse multipath channels with applications to digital TV receivers. In *Signals, Systems and Computers, 2002. Conference Record of the Thirty-Sixth Asilomar Conference on*, volume 1, pages 558–564 vol.1, 2002.
- [Par90] Parkum, J. E. and Poulsen, N. K. and Holst, J. Selective Forgetting In Adaptive Procedures. In *Proceedings of the 11th Triennial World Congress of the IFAC*, number 2 in 1, pages 137–142, 1990.
- [Par92] Parkum, J. E. and Poulsen, N. K. and Holst, J. Recursive Forgetting Algorithms. *Int. J. Control*, 55(1):109–128, 1992.
- [Pre04] Preisig, J. C. and Deane, G. B. Surface wave focusing and acoustic communications in the surf zone. *Journal of Acoustical Society of America*, 116(3):2067–2080, Sept 2004.
- [Pre05] Preisig, James C. Performance analysis of adaptive equalization for coherent acoustic communications in the time-varying ocean environment. *J. Acoust. Soc. Am.*, 118(1):263–278, July 2005.
- [Pri58] Price, R. and Green, P. E. A Communication technique for multipath channels. *Proc. IRE* , 46, 1958.
- [Pro01a] J. G. Proakis. *Digital Communications*. McGraw-Hill, 4 edition, 2001.
- [Pro01b] Proakis, J.G. and Sozer, E.M. and Rice, J.A. and Stojanovic, M. Shallow water acoustic networks. *Communications Magazine, IEEE*, 39(11):114–119, 2001.
- [Ron05] Rontogiannis, A.A. and Berberidis, K. Bandwidth efficient transmission through sparse channels using a parametric channel-estimation-based DFE [decision-feedback equaliser]. *Communications, IEE Proceedings-*, 152(2):251–256, 2005.

- [Ros99] Rosenberg, A. P. A new rough surface parabolic equation program for computing low-frequency acoustic forward scattering from the ocean surface. *Journal of the American Statistical Association*, 105(1):144–153, 1999.
- [Say03] Sayed, Ali H. *Fundamentals of Adaptive Filtering*, chapter 2.B, pages 105–107. John Wiley & Sons, 2003.
- [Set86] Sethares, W. A. and Lawrence, D. A. and Johnson, C. R. and Bitmead, R. R. Parameter Drift in LMS Adaptive Filters. *IEEE Trans. Acoustics, Speech, and Signal Processing*, ASSP-34(4):868–879, August 1986.
- [Set88] Sethares, W. A. and Mareels, I. M. Y. and Anderson, B. O. and Johnson, C. R. and Bitmead, R. R. . Excitation Conditions for Signed Regressor Least Mean Squares Adaptation. *IEEE Trans. Circuits and Systems*, 35(6):613–624, June 1988.
- [Shu82] Shumway, R. H. and Stoffer, D. S. An Approach to Time Series Smoothing and Forecasting Using the EM Algorithm . *Journal of Time Series Analysis*, 3(4):253–264, 1982.
- [Shu91] Shukla, P.K. and Turner, L.F. Channel-estimation-based adaptive DFE for fading multipath radio channels. *Communications, Speech and Vision, IEE Proceedings I*, 138(6):525–543, Dec 1991.
- [Spi72] Spindel, R. C. and Schultheiss, P. M. Acoustic Surface-Reflection Channel Characterization through Impulse Response Measurements . *Journal of the American Statistical Association*, 51(6):1812–1824, 1972.
- [Sto95] Stojanovic, M. and Proakis, J.G. and Catipovic, J.A. Analysis of the impact of channel estimation errors on the performance of a decision-feedback equalizer in fading multipath channels. *Communications, IEEE Transactions on*, 43(234):877–886, 1995.
- [Sto96] Stojanovic, M. Recent advances in high-speed underwater acoustic communications. *Oceanic Engineering, IEEE Journal of*, 21(2):125–136, 1996.
- [Sto99] Stojanovic, M. and Freitag, L. and Johnson, M. Channel-estimation-based adaptive equalization of underwater acoustic signals. In *OCEANS '99 MTS/IEEE. Riding the Crest into the 21st Century*, volume 2, pages 985–990 vol.2, 1999.
- [Stoed] Stojanovic, M. Efficient acoustic signal processing based on channel estimation for high rate underwater information. *Journal of the American Statistical Association*, submitted.

- [Tho88] Thorsos, E. I. The validity of the Kirchhoff approximation for the rough surface scattering using a Gaussian roughness spectrum . *Journal of the American Statistical Association*, 83(1):78–92, January 1988.
- [Tho89] Thorsos, E. I. The validity if the perturbation approximation for the rough surface scattering using a Gaussian roughness spectrum . *Journal of the American Statistical Association*, 86(1):261–277, July 1989.
- [Tho95] Thorsos, E. I. and Broschat, S. L. An investigation of the small slope approximation for scattering from rough surfaces. Part I. Theory . *Journal of the American Statistical Association*, 97(4), 1995.
- [Tit84] Titterton, D. M. Recursive Parameter Estimation Using Incomplete Data. *Journal of the Royal Statistical Society*, 46:257–267, 1984.
- [Tro04] Tropp, J.A. Greed is good: algorithmic results for sparse approximation. *Information Theory, IEEE Transactions on*, 50(10):2231–2242, 2004.
- [Tsa05] Tsai, S. and Lehnert, J. S. and Bell, M. R. Convergence of a ML Parameter-Estimation Algorithm for DS/SS Systems in Time-Varying Channels With Strong Interference. *IEEE Transactions on Communications*, 53(1):142–151, Jan 2005.
- [Van71] Van Trees, H. L. *Detection, Eestimation and Modulation Theory, Part III* . New York: Wiley , 1971.
- [Ven71] Venetsanopoulos, A. N. and Tuteur, F. B. Stochastic Filter Modeling for the Sea-Surface Scattering Channel. *Journal of the American Statistical Association*, 49(4):1100–1107, 1971.
- [Vor9] Voronovich, A. G. *Wave scattering from rough surfaces*. Springer-Verlag , New York, 2nd, Updated Edition edition, 1999 .
- [Wei94] Weinstein, E. and Oppenheim, A. V. and Feder, M. and Buck, J. Iterative and Sequential Algorithms for Multisensor Signal Enhancement. *IEEE Trans. Signal Processing*, 42(4):846–859, Apr 1994.
- [Yip90] Yip, P.C.-W. and Etter, D.M. An adaptive multiple echo canceller for slowly time-varying echo. *Communications, IEEE Transactions on*, 38(10):1693–1698, 1990.
- [Zio82a] Ziomek, L. J. Genralized Kirchhoff approach to the ocean surface-scatter communication channel. Part I. Transfer function of the ocean surface . *Journal of the American Statistical Association*, 71(1):116–126, January 1982.

[Zio82b] Ziomek, L. J. Generalized Kirchhoff approach to the ocean surface-scatter communication channel. Part II. Second-order functions . *Journal of the American Statistical Association*, 71(6):1487–1495, June 1982.